Mechanical Properties of Materials at Low Temperatures

Springer

MECHANICAL PROPERTIES OF MATERIALS AT LOW TEMPERATURES

THE INTERNATIONAL CRYOGENICS MONOGRAPH SERIES

MECHANICAL PROPERTIES OF MATERIALS AT LOW TEMPERATURES

D. A. Wigley
Engineering Laboratories
The University of Southampton
Southampton, England

PLENUM PRESS • NEW YORK–LONDON • 1971

The author acknowledges with gratitude the permission granted by the following publishers and societies to make use of figures which have appeared in their publications:

American Institute of Mining, Mechanical, and Petroleum Engineers *(Transactions of the Metallurgical Society).*
American Institute of Physics *(Physical Review, Soviet Physics—Solid State, Journal of Applied Physics).*
American Society for Metals *(Transactions).*
American Society for Testing and Materials *(Special Technical Publications, Bulletin, Materials Research and Standards, Journal of Materials).*
American Welding Society *(Welding Journal, Welding Research Supplement).*
Business Communications, Inc. *(Cryogenic Engineering News).*
Clarendon Press, Oxford.
Marcel Dekker, Inc.
Heywood and Co. Ltd. *(Progress in Applied Materials Research).*
Institute of Metals *(Journal).*
Institute of Physics and Physical Society.
Instrument Society of America *(Industrial Laboratory).*
Interscience Publishing Corp. *(Journal of Polymer Science).*
Iron and Steel Institute *(Journal).*
Macmillan (Journals) Ltd. *(Nature).*
National Bureau of Standards *(Monographs, Cryogenics Materials Data Handbook).*
National Research Council of Canada *(Canadian Journal of Physics).*
Plenum Press *(Advances in Cryogenic Engineering).*
Pergamon Press Ltd. *(Acta Metallurgica, Transactions of the Plastics Institute).*
The Royal Society *(Proceedings).*
Springer-Verlag *(Zeitschrift für Metallkunde).*
Taylor and Francis Ltd. *(Philosophical Magazine).*
The Welding Institute *(British Welding Journal).*
J. Wiley and Sons, Inc.

Library of Congress Catalog Card Number 70-157929

ISBN-13: 978-1-4684-1889-7 e-ISBN-13: 978-1-4684-1887-3
DOI: 10.1007/978-1-4684-1887-3

Softcover reprint of the hardcover 1st edition 1971

A Division of Plenum Publishing Corporation
227 West 17th Street, New York, N.Y. 10011

United Kingdom edition published by Plenum Press, London
A Division of Plenum Publishing Company, Ltd.
Davis House (4th Floor), 8 Scrubs Lane, Harlesden, NW10 6SE, England

To Jill, Michael, and Carolyn

Preface

In writing this monograph, the aim has been to consider the mechanical properties of the wide range of materials now available in such a way as to start with the fundamental nature of these properties and to follow the discussion through to the point at which the reader is able to comprehend the significance or otherwise of the large amounts of data now available in design manuals and other compilations. In short, it is hoped that this volume will be used as a companion to these data compilations and as an aid to their interpretation.

In attempting to cover such a wide field, a large degree of selection has been necessary, as complete volumes have been written on topics which here have had to be covered in a few pages or less. It is inevitable that not everyone will agree with the choice made, especially if it is his own subject which has been discussed rather briefly, and the author accepts full responsibility for the selection made. The book is written at a level which should be easily followed by a university graduate in science or engineering, although, if his background has not included a course in materials science, some groundwork may be lacking. This omission can easily be corrected by the use of one of the excellent texts now available,[1,2] in particular, experience in teaching a one-year master's degree course in cryogenics has shown that volumes 1 and 3 of the series edited by Wulff[1] are particularly suitable for this purpose.*

Although this book is entitled "The Mechanical Properties of Materials at Low Temperatures," it is in fact impossible to discuss the low-temperature properties in isolation, as in most cases they must be considered over the whole range of temperatures below ambient. For example, much equipment designed for use at low temperatures has to be built and tested at room temperature, and furthermore, the allowable stresses laid down by most design codes are based on the room-temperature properties of the materials concerned. Most of the materials likely to be of use in cryogenic engineering have been included but, despite the superiority of nonmetals for certain applications, it is a reflection of the major importance of metals that about 70% of the book is devoted to their deformation and fracture characteristics. Most plastics suffer from the fundamental disadvantage of

* The references cited in the Preface will be found at the end of Chapter 1.

undergoing a glass transition at some temperature below which they are relatively brittle; a few varieties such as PTFE are, however, less seriously affected and they have proved very valuable in certain applications. Although the science of low-temperature physics developed by using apparatus made of glass, its brittleness made it too delicate for general engineering use and the major use of glass is now in the form of finely divided fibers which reinforce plastics to produce composites. Such composites are already finding widespread application, especially in situations where their high strength/weight ratio is advantageous, and the recent availability of high-modulus carbon fibers is likely to accelerate the transition to this class of material.

Some indication of the mature state of the science of metallurgy may be gained from the large number of books which have been written on almost every aspect of the subject and from the almost overwhelming amount of data which has been generated. Many metallurgy textbooks[6-7,8] include sections on the behavior of metals at low temperatures, particularly on the effect of temperature on the fundamental mechanism of plastic deformation in crystalline solids.[9-11] There are also a number of excellent reviews on this aspect of the subject.[41-46] Fracture is also well documented in books[12,13] and reviews,[47] the work by Tetelman and McEvily[13] being particularly worthy of note, as it attempts to bridge the gap which so often exists between the fundamental, microscopic aspects of the problem and the practical considerations which must be understood if structures are to be designed and built free from the risks of catastrophic brittle failure.

Most textbooks and reviews on the properties of plastics[4] and composites[5,40] deal mainly with their properties at room temperature and above, although some[4] have sections on low-temperature properties. Most of the available data on the low-temperature mechanical properties of all of these materials is to be found in specialist monographs, conference proceedings, and review articles. These include some of the special Technical Publications of the American Society for Testing and Materials,[14,15] while the proceedings of the annual Cryogenic Engineering Conferences, published as "Advances in Cryogenic Engineering",[16] are a particularly rich source of information on all aspects of cryogenic engineering. There are also a number of valuable reviews on the more technological aspects of the cryogenic properties of materials,[3,48-55] although many of them are rather heavily biased toward aerospace applications. Information on the more general facets of cryogenic engineering is to be found in a number of textbooks,[17-21,35,36] the theoretical and practical aspects of low-temperature physics are covered in further volumes and journals,[22-26,37,38] while individual topics of particular interest are to be found in other monographs in this series.[27,28] A recent bibliographical guide to cryogenics and refrigeration[39] is also of considerable value.

It is, however, in the "Cryogenic Materials Data Handbook",[32] the UCRL "Cryogenic Data Book",[33] the manufacturers' data manuals,[34] and in a series of excellent monographs[21,29-31] published by the National Bureau of Standards that specific data are to be found. These cover most of the available alloys in a range of conditions, purities, and heat treatments but, as we shall attempt to demonstrate in the coming chapters, there are an extremely large number of variables which can influence the strength, ductility, and toughness of materials. It is, therefore, often necessary to carry out tests to measure the required properties of a particular material, and in chapter 3 the most important methods of determining toughness are discussed, while in chapter 5 a brief indication is given of the experimental arrangements used to carry out tensile tests at low temperatures.

In conclusion, I would like to extend my thanks to all those who have helped in the preparation of this monograph, to Dr. R. A. Farrar for reading the whole of the manuscript and for many helpful comments and criticisms, to Messrs. A. Monroe, F. P. Grimshaw and P. Halford for advice and criticism on certain of its sections. All sources of figures have been acknowledged as they occur and I would like to thank all those authors and publishers who have assisted in this way and to apologize to anyone whose work has been drawn upon and used without specific acknowledgment. I would especially like to thank the editor, Dr. K. Mendelssohn, F.R.S., for his patience in awaiting the completion of this volume, which took considerably longer than either of us had anticipated, Mrs. B. Smith for her efficient typing, my wife, Jill, for her valued assistance in the preparation of the manuscript, and finally my family for accepting the inconveniences caused by my involvement in this task.

D. A. WIGLEY

Engineering Materials Laboratory
Southampton University
June 1970

Contents

Chapter 1

Deformation Processes in Pure Metals

When a metal is loaded, the resultant deformation is initially elastic and the metal returns to its original state as the load is removed. If, however, the applied load exceeds the yield strength of the metal, it deforms plastically and the strain so produced is not recoverable when the load is released. In most metals, the stress necessary to cause plastic deformation increases with the strain because the material work-hardens, and for over 5000 years man has used this property to strengthen metals and make them more suitable for his needs. It is, however, only in the last few decades that the fundamental mechanisms responsible for these properties have begun to be understood, and even now there are a number of important details which remain to be elucidated. For example, the phenomenon of work-hardening is not yet fully explained.

Much of our present knowledge of the mechanical properties of metals stems from the study of the microscopic aspects of plastic deformation, which have revealed its essentially crystalline nature. Perhaps the most significant advances have come from an understanding of the ways in which dislocations move, multiply, and interact with each other and with other features of the crystal lattice, such as impurity atoms, point defects, grain boundaries, and the free surface of the material. In particular, it is possible to explain many of the effects of temperature on the deformation and failure characteristics of metals by its influence on the ease with which dislocations may move through the various lattice structures. Although some knowledge of these mechanisms should form the basis of any thorough comprehension of the mechanical properties of metals, bulk engineering materials are not specified by their dislocation densities but by parameters such as their yield and tensile strengths, elongation, and reduction in area. It is therefore important to be able to correlate these two approaches if the fullest use is to be made of the wide range of materials which is now available to a designer. The properties of pure metals will be considered in this chapter, while impure metals and alloys will be covered in chapter 2.

The present chapter starts with an introduction to the terminology used

in describing the various features of the deformation of a specimen in the uniaxial tensile test, as this is one of the most universal methods of determining the mechanical properties of a material. Elastic deformation is then considered briefly before the general aspects of plastic deformation are discussed, firstly in terms of the microscopic mechanisms involved, and then in relation to the yield and flow of single crystals and polycrystals. The effect of temperature on these properties is then considered separately for metals with the three common crystal structures, face-centered cubic, body-centered cubic, and hexagonal close-packed. In each case, the behavior of single crystals is considered first and this is then compared with the characteristics shown by polycrystals. The dislocation structures developed during deformation are then described, and this section could, if desired, be omitted by those readers less interested in the fundamental aspects of the problem. Each section is completed by a short discussion on the effect of temperature on the familiar parameters used to describe the characteristics of engineering materials, while in section 1.7 the main characteristics of these three classes of metal are compared and summarized.

Although creep is only important as a mode of failure at high temperatures, its study at low temperatures reveals details of the fundamental processes which control plastic deformation in metals and these are discussed in section 1.8. The chapter concludes with a brief indication of the relevance of recovery processes to the deformation of metals at low temperatures.

1.1. GLOSSARY OF TERMS RELEVANT TO THE TENSILE TEST

Many specialized tests have been devised to measure the suitability of a material for service under particular combinations of applied stress, temperature, strain rate, and other relevant variables. The uniaxial tensile test is still, however, the most widely used measurement of the mechanical properties of a material. There are a number of ways in which the results of these tests may be presented, and confusion can arise if the meanings of the various terms involved are not clearly understood: it is hoped that this short section will help to clarify the situation.

The *engineering stress* σ is the ratio of the instantaneous load on the specimen P to its original cross-sectional area A_0, i.e.,

$$\sigma = \frac{P}{A_0} \tag{1.1}$$

The central uniform portion of a specimen between two reference marks is the *gauge length* l_0, and the *engineering strain* ε is the ratio of the

instantaneous increase in length of this section, $\Delta l = l - l_0$, to the original length l_0, i.e.,

$$\varepsilon = \frac{\Delta l}{l_0} \tag{1.2}$$

A typical engineering stress–strain curve for a ductile metal is shown in Fig. 1.1. The relation between stress and strain is linear up to the *elastic limit*, the constant of proportionality being *Young's modulus*, $E = \sigma/\varepsilon$.

Up to the elastic limit, the strain is fully recoverable on removal of the applied stress; beyond this point, permanent plastic deformation occurs. In some metals, the transition between elastic and plastic deformation occurs quite sharply and it is possible to define a unique *yield stress* σ_y. In many cases, including the one illustrated in Fig. 1.1, transition from elastic to plastic deformation takes place so smoothly that it is impossible to define a unique yield stress from macroscopic strain readings. On a microscopic scale and with sensitive strain-measuring equipment, it is, however, possible to detect the onset of plastic yielding at the *microyield stress*, which is the stress required for a strain of 10^{-5}.

For practical purposes, we require a less-sophisticated and more readily reproducible value for the yield process, and this need is satisfied by the definition of the "*proof*" stress (also known as the "*offset yield*" stress). Defined as the stress required to produce a certain degree of permanent plastic strain, usually 0.1, 0.2, or 0.5%, it is often determined in practice as shown in Fig. 1.2. A line is drawn from the relevant strain, say 0.2%, parallel to the elastic loading line until it intercepts the stress–strain curve. The 0.2% proof stress is then read off from the ordinate.

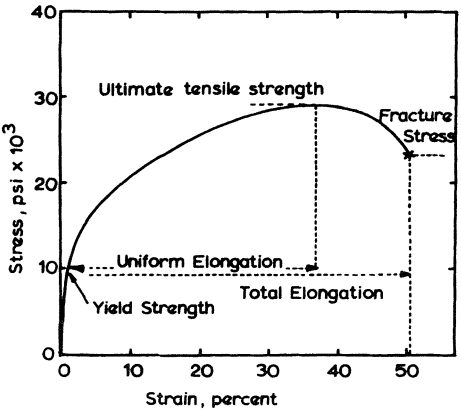

Fig. 1.1. Engineering stress–strain curve for a typical ductile metal such as copper.

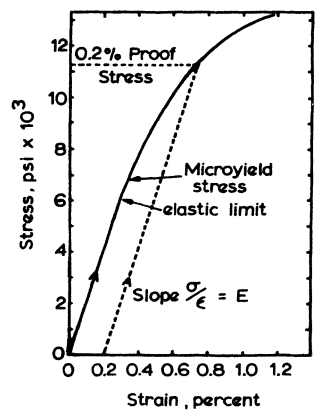

Fig. 1.2. Elastic and initial stages of plastic deformation shown enlarged to illustrate the method of determining the 0.2% proof stress.

In most tensile tests, the crosshead is driven at a constant strain rate and the stress developed in the specimen is measured as the dependent variable. Most metals have the capacity to *work-* or *strain-harden* and the stress needed to produce further plastic deformation increases as the plastic strain increases. The strain-hardening rate decreases with increasing strain until it is zero at the *ultimate tensile strength* (UTS, sometimes called simply the *tensile strength* TS), where the engineering stress is at a maximum. At this point, a neck starts to develop in the specimen because the metal can no longer strain-harden rapidly enough to compensate for the decrease in cross-sectional area. Further plastic deformation becomes concentrated in this localized region and the engineering stress decreases with increasing strain.

Fracture occurs at the *fracture stress* σ_f, which is lower than the ultimate tensile stress. The *reduction in area* RA is defined as the ratio of the minimum cross-sectional area at fracture, A_f, to the original cross-sectional area, A_0, i.e.,

$$\text{RA} = \frac{A_f}{A_0} \tag{1.3}$$

The *fracture strain, ductility,* or *fracture elongation* is the amount of *plastic* strain produced before fracture and is thus the total strain measured at the instant of fracture minus the elastic strain. As, however, the elastic strain is typically a few tenths of 1%, while the plastic strain is a few tens per cent, the elastic strain is usually neglected and the total strain is used to represent the ductility. This is often measured by fitting together the two fracture halves and comparing the final value of the gauge length l_f, to the original value l_0. Until necking starts, plastic deformation usually occurs uniformly along the specimen, and the *uniform elongation* is the amount of plastic strain occurring prior to the ultimate tensile stress.

During elastic deformation, there is a small change in volume of the specimen, but during plastic deformation, the volume remains constant. Thus, $A_0 l_0 = A_i l_i$, where A_i and l_i are the instantaneous values of cross-sectional area and gauge length, respectively. In the definition of engineering stress, this decrease in cross-sectional area is neglected and a more exact description of the stresses developed in a sample is obtained from the definition of the *true stress* σ_T. This is defined as the ratio of the load to the instantaneous minimum cross-sectional area supporting the load, i.e.,

$$\sigma_T = \frac{P}{A_i} \tag{1.4}$$

This definition of true stress accurately describes the stress in the necked region of the specimen, and it can be seen from Fig. 1.3 that the true stress increases right up to the instant of fracture, when its value is the *true fracture stress.*

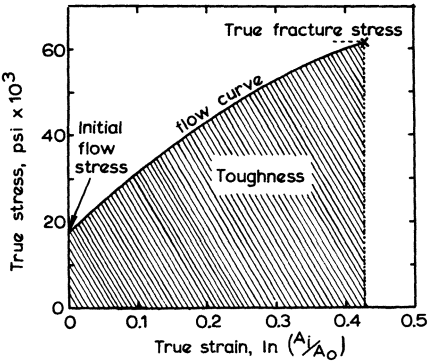

Fig. 1.3. True stress–strain curve for a ductile metal such as copper, showing true stress increasing continuously to fracture.

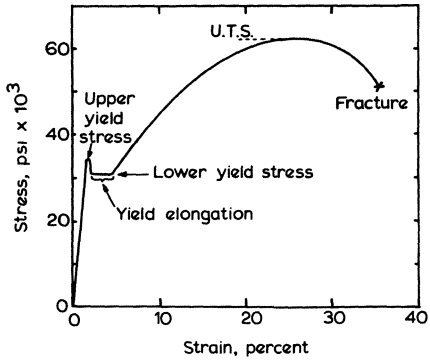

Fig. 1.4. Schematic stress–strain curve for mild steel, illustrating sharp yield phenomena.

True strain, sometimes known as *natural elongation*, may be defined in two ways. In the first, it is the definite integral of the ratio of an incremental change in length to the instantaneous length of the sample,

$$\varepsilon = \int_{l_0}^{l_i} \frac{dl}{l} \tag{1.5}$$

On integration, this gives

$$\varepsilon = \ln\left(\frac{l_i}{l_0}\right) \tag{1.6}$$

where l_i is the instantaneous length minus the small amount of elastic strain present. This definition is not valid after necking commences, and the second definition of true strain is needed, viz.

$$\varepsilon = \ln\left(\frac{A_i}{A_0}\right) \tag{1.7}$$

A_i being the instantaneous minimum cross-sectional area. As the second definition of true strain is valid over the period of plastic deformation from yield to fracture, it is generally preferred.

The true-stress–true-strain curve shown in Fig. 1.3 is known as a *flow* curve and the stress for a particular strain is the *flow strees*. The *initial flow stress* is that stress required to initiate plastic deformation and is thus a synonym for yield stress. An important quantity also shown in this figure is the *toughness* of the material. This is a measure of the energy absorbed prior to fracture,

$$\int_{\varepsilon_0}^{\varepsilon_f} \sigma_T \, d\varepsilon$$

and is given by the area under the flow curve.

As we shall see later in this chapter, plastic deformation in crystalline materials occurs by a shear mechanism and many results are presented in terms of *shear-stress–shear-strain* curves. Occasionally, materials are tested in such a way that values of shear stress and shear strain are obtained directly by measurement. In many cases, however, single crystalline specimens are tested in tension or compression and then the *resolved* shear stresses and strains are calculated from the geometry of the slip processes. Plastic yield occurs when the critical resolved shear stress is first exceeded on one of the possible slip systems. In the elastic region, the shear modulus G is the ratio of shear stress to shear strain.

In some metals, e.g., mild steel, yield occurs so suddenly that there is a sharp *yield drop* in the stress–strain curve as shown in Fig. 1.4. A small amount of plastic strain precedes the *upper yield* stress but macroscopic strains only occur after the stress has dropped to the *lower yield* stress. A period of *yield elongation* usually follows in which plastic deformation occurs at a more or less constant stress. This inhomogeneous deformation starts at a point of stress concentration, often near the grips, and propagates through the rest of the specimen. Its progress is accompanied by the formation of striations on the surface known as *Lüders bands* or *stretcher strains*, and once the deformation has propagated completely through the specimen, normal strain-hardening commences. The occurrence of sharp yield phenomena usually depends on the locking of dislocations by impurities and is discussed in more detail in section 2.4.

1.2. ELASTIC DEFORMATION

In metals and other crystalline solids, elasticity has its basis in the interatomic forces which act to restore displaced atoms to their equilibrium positions, and, as these forces are derived from strong primary bonds, the elastic moduli are high. In contrast, weaker, secondary bonds are responsible for the restoring forces in noncrystalline solids, the moduli are correspondingly lower, and there is often a nonlinear relationship between stress and strain.

A perfect crystal should theoretically show recoverable elastic strains of up to a few per cent, values of $\sim 5\%$ having in fact been found for whiskers which are minute, almost perfect, single crystals. In most metals, however, elastic behavior is limited to strains of about 0.1% by the onset of permanent plastic deformation. A further consequence of the crystalline nature of metals is that atoms are more closely packed in some directions than others: for example, the interatomic spacing along the body diagonal ($\langle 111 \rangle$ direction) of a fcc lattice is smaller than that along a cube edge ($\langle 100 \rangle$ direction). As stronger restoring forces act at smaller interatomic spacings, Young's modulus is largest along the most closely packed direc-

tions, and hence in single crystals elastic moduli are anisotropic, e.g., in fcc lead crystals, $E_{\langle 111\rangle}/E_{\langle 100\rangle} \simeq 3$. In asymmetrical lattices, such as the hexagonal-close-packed structure, this ratio can be even larger, e.g., $E_{\perp \text{hexagonal axis}}/E_{\parallel \text{hexagonal axis}} \simeq 4$ for zinc crystals. In a polycrystal, the experimentally determined modulus represents an average of the moduli of the individual grains, and if these are small and have completely random orientations, the metal behaves isotropically. The measured moduli and those calculated from an average of the values obtained from single crystals usually agree to within about 10%. The exact degree of agreement depends, however, on the assumptions made in the averaging process, in particular, whether the stresses or the strains are assumed to be equal in all grains,[60] and on the practical difficulties involved in ensuring a completely random distribution of orientations.

There are three main factors which influence the elastic constants of metals: temperature,[61] chemical purity,[62] and the degree of prior cold-working.[63] The effect of temperature on the moduli is closely related to its influence on the expansion coefficient. A metal contracts as the temperature falls because the anharmonic vibration of its atoms about their mean positions causes a decrease in the interatomic spacing: this in turn strengthens the restoring forces and leads to an increase in the moduli. In general, it is found that most of this increase occurs as the temperature falls to $\sim\theta/3$ (θ is the Debye characteristic temperature) and that, as absolute zero is approached, the moduli become independent of temperature as required by the third law of thermodynamics. As θ for many common metals is above 200°K, it follows that their moduli vary little below liquid-

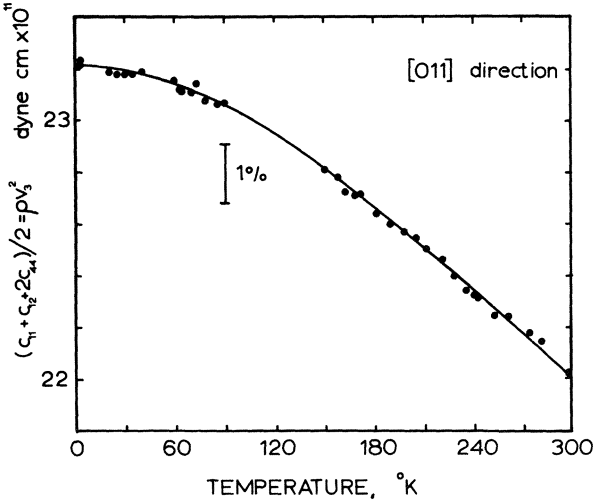

Fig. 1.5. Temperature dependence of the combined adiabatic elastic constants of a copper single crystal (Overton and Gaffney[64]).

nitrogen temperature. This behavior is illustrated for single crystals of copper in Fig. 1.5, where the combined adiabatic elastic constants $(c_{11} + c_{12} + 2c_{44})/2$ are shown[64] as a function of temperature in the range 0–300°K. Between 300 and 120°K, the moduli increase by about 0.03%/deg and, as this value is typical of many metals, it may be used for the rough calculation of low-temperature moduli if only their room-temperature values are known.

There are two important mechanisms by which cold-work can reduce the elastic moduli of metals. They may develop an oriented structure which favors one of the low-modulus crystallographic directions, such as the ⟨111⟩ in fcc metals, this effect being strongest in heavily rolled sheets, while a further 1% of the decrease can be ascribed to the presence of the point defects produced during deformation. These defects increase the effective equilibrium spacing of the atoms, thus reducing the strength of the atomic restoring forces and lowering the moduli. Impurity atoms can either increase or decrease the moduli, depending upon the relative importance of the following three factors:

(1) Solute atoms can alter the interatomic spacings and this can affect the moduli as described above.

(2) As dislocations that are free to move through a crystal lower its moduli, solute atoms that can pin these mobile dislocations prevent this reduction.

(3) The atomic bonds between solvent and solute atoms may be stronger than those between like atoms and, under these circumstances, alloying will increase the moduli.

On a macroscopic scale, the presence of hard second-phase particles in aluminum alloys has been found[65] to increase their moduli by up to 30% and one explanation for this increase is based on the barriers to dislocation movement caused by the hard particles. It is, however, also possible that the effective modulus is a weighted average of the moduli of the hard particles and the softer matrix, a situation analogous to that found in the fiber-reinforced composites discussed in section 4.5. In contrast, the presence of second-phase particles or precipitate zones in aluminum–copper and aluminum–silver alloys seems to have no effect on the temperature dependence of their moduli, which is the same as that found for pure aluminum.[66]

So far, we have assumed that maximum elastic strain is developed at the instant of maximum applied stress. In some cases, this is not true and the strain lags behind the stress, and under these conditions the deformation is said to be anelastic. Furthermore, if the material is subjected to cyclic loading, the lag of strain behind stress leads to a dissipation of energy and damping known generally as "internal friction." One of the most important dissipative processes in metals is due to the vibration of short lengths of dislocation whose ends are pinned by impurity atoms or other defects, and

it is, in principle, possible to obtain from internal-friction measurements an important insight into the interactions between the crystal lattice and impurities, dislocations, and other defects. In practice, however, the value of such experiments is reduced because of the difficulty frequently found in obtaining an unambiguous interpretation of the experimental results.

Accurate values of the elastic constants over a wide range of temperatures are often needed, as they enter into theoretical expressions for the specific heat and other physical properties (see section 6.5). For practical purposes, the rule of thumb that a 1°K decrease in temperature increases the moduli by about 0.03% is usually adequate for obtaining low-temperature values when only room-temperature data are available, while if more accurate values are needed they are best obtained by direct measurement on the metal to be used, as it is possible that differences in purity or texture could cause the moduli to deviate from the published values.[32,67]

1.3. GENERAL ASPECTS OF PLASTIC DEFORMATION IN METALS

1.3.1. Microplasticity

Once the elastic limit of a metal has been exceeded, permanent plastic deformation takes place. One of the most important characteristics possessed by ductile metals is the ability to undergo considerable plastic deformation before failure and this enables applied stresses to be redistributed evenly over the whole of a structure, with the consequent avoidance of the localized stress concentrations which are conducive to failure. Metals in general, ductile ones in particular, are weaker in shear than in tension or compression, and yield takes place by plastic shear, or slip of one crystal plane over another. This slip does not occur randomly but takes place most readily on certain planes and in specific directions. The combination of a particular slip plane and direction is called a slip system and the most common systems are those which require the lowest stress to produce slip. These are given in Table I for the common lattice structures.

Slip is found to occur preferentially on the most closely packed planes and in the most closely packed directions, but if slip on these planes is constrained, other, less closely packed planes become active. Thus, for example, in hcp zinc, slip occurs most readily on the basal plane (a) and less readily on the prismatic (b) or pyramidal planes (c). Once slip on the basal planes is restricted, either the other slip systems must function, or further modes of plastic deformation such as twinning must operate if plastic deformation is to continue. If such alternative modes of deformation are not available, the flow stress rises above the cleavage stress and brittle fracture follows.

Table I. Slip Planes and Direction for the Common Lattice Structures

Lattice	Slip plane	Slip direction	Number of systems	Examples
fcc	{111}	$\langle 1\bar{1}0 \rangle$	$4 \times 3 = 12$	Cu, Ag, Al, etc.
hcp	(a) {0001}	$\langle 11\bar{2}0 \rangle$	$1 \times 3 = 3$	Zn, Mg, Ti
	(b) $\{10\bar{1}0\}$	$\langle 11\bar{2}0 \rangle$	$3 \times 1 = 3$	Ti
	(c) $\{10\bar{1}1\}$	$\langle 11\bar{2}0 \rangle$	$6 \times 1 = 6$	Ti, Mg
bcc	(a) {110}	$\langle \bar{1}11 \rangle$	$6 \times 2 = 12$	Fe, Mo
	(b) {211}	$\langle \bar{1}11 \rangle$	$12 \times 1 = 12$	Fe
	(c) {321}	$\langle \bar{1}11 \rangle$	$24 \times 1 = 24$	Fe

Slip in fcc lattices always takes place on one of the twelve $\{111\}\ \langle 1\bar{1}0 \rangle$ systems. In bcc metals, the most important system is the $\{110\}\ \langle \bar{1}11 \rangle$, but wavy slip lines are also commonly observed on the {211} and {321} planes, suggesting that slip either occurs simultaneously on several $\{110\}\ \langle \bar{1}11 \rangle$ systems or that the other slip systems are active. In contrast to the wavy slip observed in bcc lattices, slip lines are usually straight in hcp and fcc metals. Although slip is the most common mode of plastic deformation in metals, twinning becomes important in bcc and hcp metals, especially at low temperatures. Twinning, which is always preceded by some slip, is a discontinuous process whose occurrence is usually indicated by load drops on the stress–strain curve and sometimes by an audible "clicking."

The distinctive yield, flow, and fracture characteristics of fcc, bcc, and hcp metals can be attributed basically to the different microscopic deformation systems which operate in the various lattice structures. One common factor is that deformation commences when the resolved shear stress for a slip system first exceeds a critical value τ_0 (the critical resolved shear stress, crss), and it has been found[11] that τ_0 is more or less constant for a given metal tested under reproducible experimental conditions. It may therefore be considered as a fundamental mechanical property reflecting the basic mode of plastic deformation by shear of one plane of atoms over another. A study of the influence on τ_0 of such parameters as purity, temperature, strain rate, and other testing variables might thus be expected to yield important information on the mechanical properties of metals. Typical values for the critical resolved shear stress of the three main metallic crystal structures over the temperature range 0–500°K are shown in Fig. 1.6: the exact values of τ_0 depend on the physical and chemical purity of the material, and banded values are therefore given. The large difference between the critical resolved shear stresses of, say, the fcc and bcc metals are, however, of a much more fundamental nature.

If the theoretical shear stress of a metal is calculated by finding the stress needed to shear one plane of atoms over another, a value of approximately 1/30 shear modulus is obtained. As the shear modulus of the fcc

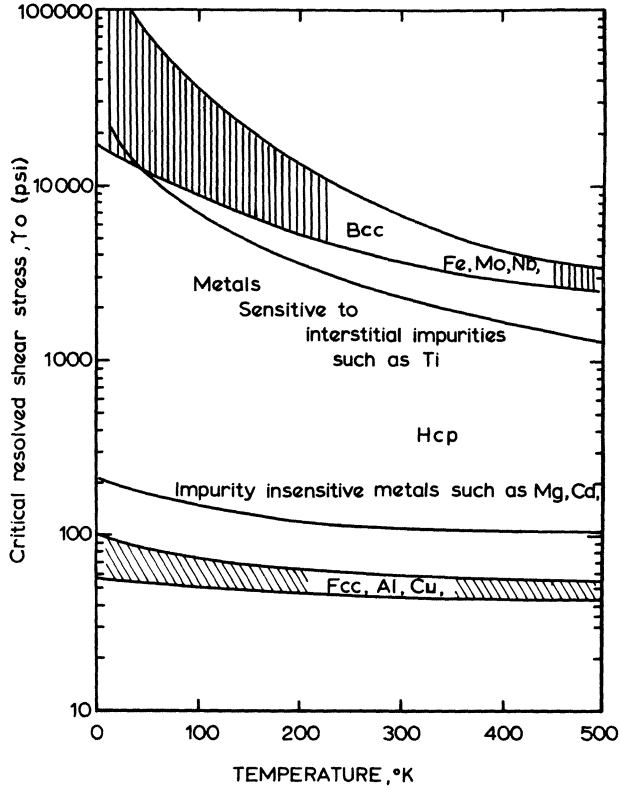

Fig. 1.6. Typical values for the critical resolved shear stresses of metals with the three principal crystal structures.

metals whose crss is shown in Fig. 1.6 is of the order of 6 to 10×10^4 psi, their theoretical shear strengths are about 2×10^3 psi. However, their measured shear strengths can be seen from Fig. 1.6 to be closer to 40 psi, and thus the observed strength of metals fall considerably short of the theoretical predictions. The concept of dislocations in a crystalline solid was originally proposed independently by Orowan,[68] Polanyi,[69] and Taylor[70] to resolve this discrepancy—much lower stresses being required to move these line defects through a crystal than to shear one plane of atoms over another—and the characteristic properties of dislocations have since been used to explain many of the mechanical and physical properties of crystalline materials. Modern theories of the deformation of metals are based on the movement of dislocations and their interaction with other dislocations, impurity atoms, grain boundaries, etc., and more or less detailed treatments of their properties can be found in the textbooks on materials listed at the end of this chapter.[6–11]

The movement of one dislocation along its slip plane and out of the crystal produces a slip step about 3×10^{-8} cm high on its surface, but to produce experimentally observed amounts of strain, which are typically many per cent, a vast number of such movements are required—far more than can be produced by the motion of dislocations preexisting in the crystal. A source of new dislocations is needed, and this is thought to be provided by sources such as that described by Frank and Read[71] in which a short length of edge dislocation is pinned at either end and able to generate a series of fresh dislocation loops once the applied stress exceeds a certain value.

One of the most important characteristics possessed by metals is their ability to strain-harden, or become stronger as they deform. Although the detailed theory of strain-hardening is not yet complete, it is clear that the movement and interaction of dislocations play a fundamental role in this process. If the dislocations generated by a source are unable to move freely along their slip plane, a higher stress is necessary to produce and move further dislocations. As the stress increases, more sources come into operation, the dislocation density gets higher, and an increasing number of interactions occur to form sessile dislocations. These in turn act as barriers to the motion of other dislocations and, as the density of dislocations increases, their movement becomes more difficult and higher applied stresses are needed to continue deformation.

Modern metallographic techniques, in particular electron microscopy, have made it possible to observe and identify many of the dislocation mechanisms occurring during the deformation of metals. Furthermore, it has been found possible to correlate these mechanisms quite closely with the main stages of strain hardening shown by single crystals of metals of all three common lattice structures.

1.3.2. The Generic Tensile Stress–Strain Curve for Single Crystals

It is now recognized that the most general form of shear-stress–shear-strain curve generated during the tensile deformation of single crystals has three distinct stages of strain hardening. The extent and importance of each of the three stages varies with the crystal structure, temperature, purity, strain rate, and other testing conditions, and under certain circumstances one or more of these basic stages may be completely suppressed. Figure 1.7 shows[41] schematically a typical three-stage curve for a pure fcc single crystal and defines the relevant work-hardening parameters. Although the exact nature of the dislocation processes responsible for the various stages of deformation depend on the lattice structure of the metal concerned, it is possible to make a few generalizations.

In suitably oriented crystals, slip initially takes place when the crss, τ_0, is exceeded on a single slip system. Sources needing the lowest applied

stress operate first and their dislocations glide over large distances before becoming obstructed. Many are, in fact, able to reach the free surface and form slip steps. During this "easy glide" or stage I hardening region, the dislocation density is low ($\sim 10^7$ lines/cm) and the strain-hardening rate θ_I has a constant value of about $10^{-4}\,G$ (G is the shear modulus). The actual value of θ_I depends on the crystal orientation, some orientations being "harder" than others. (See, for example, the variation in initial strain-hardening rates of the copper single crystals in Fig. 1.8).

Seeger[72] attributes stage I hardening to long-range interactions between dislocation loops on separated primary slip planes. These interactions reduce the average distance moved by dislocations before becoming obstructed, and increase the stress needed to move them. A second factor which increases the applied stress necessary to continue deformation is the rotation of the crystal axes and a consequent reduction in the resolved shear stress.

Eventually, the crss is exceeded on a second slip system and multiple slip commences. Dislocations moving on intersecting slip systems are now able to react and form barriers, such as Lomer–Cottrell locks,[73,74] which hinder the passage of further dislocations down the intersecting slip planes. This leads to a much more rapid rate of strain-hardening known as stage II or the "linear hardening" region, with θ_{II} having a value of $\sim 3 \times 10^{-3} G$. The dislocation density also increases rapidly during stage II hardening, reaching values of about 10^{11}–10^{12} lines/cm.

At the end of stage II, the flow stress has risen to such a high value that dislocations are able to bypass obstacles on their slip plane by cross-slip onto other, parallel slip planes. Two processes thus occur simultane-

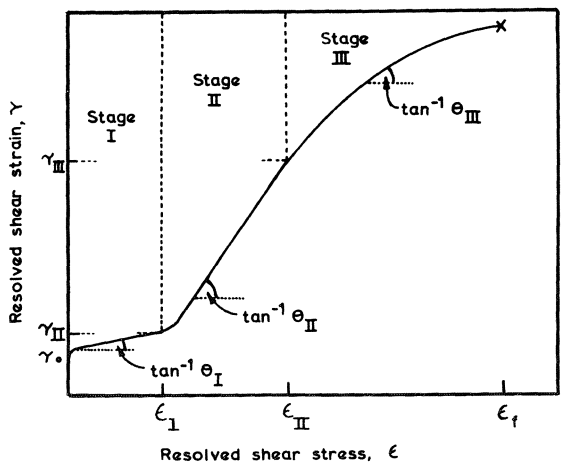

Fig. 1.7. Idealized stress-strain curve for a pure fcc single crystal, showing the three basic stages of work-hardening (after Mitchell[41]).

ously during stage III deformation; strain hardening due to the pile up of dislocations behind barriers, and recovery due to cross-slip past these barriers. The resultant strain-hardening rate reflects a balance between these two processes: θ_{III} decreases continuously with increasing strain and tends to zero unless fracture intervenes. Stage III is often known as the parabolic hardening region, from the shape of the stress–strain curve.

1.3.3. Yield and Plastic Deformation in Polycrystals

Although the fundamental processes occurring during plastic deformation are most readily identified in single crystals, structural materials are invariably polycrystalline and it is important to see how well the results obtained from single crystals can be applied to polycrystals. In a polycrystalline matrix, the grains have a range of orientations with respect to the tensile axis, and the elastic anisotropy mentioned in section 1.2 causes the stress to be concentrated in those grains that have their maximum elastic modulus parallel to the tensile axis. Dislocation sources operate first in these grains, but the dislocations produced are unable to move far before they are obstructed by nearby grain boundaries. Other sources needing higher applied stress then become effective until their dislocations in turn become blocked. This sequence of production and grain boundary obstruction of dislocations results in an extremely rapid form of strain-hardening which occurs during the microstrain region of plastic deformation. Yield in polycrystals thus takes place successively in one grain after another and, in the absence of one of the impurity-locking mechanisms to be considered in section 2.4, it is difficult to define a unique yield stress, there apparently being a smooth transition from elastic to plastic deformation. (For practical purposes, this ambiguity is removed by the definition of proof stress as described in section 1.1).

As the yield process is strongly affected by the distance a dislocation moves before it is blocked by a grain boundary, it is reasonable to expect the yield stress to be some function of the grain size. The Hall–Petch equation[75,76] gives such a relationship,

$$\sigma = \sigma_i + Kd^{-1/2} \tag{1.8}$$

where σ is the yield or proof stress; σ_i is the friction stress, which is constant for a given metal, purity, and temperature; K is a further constant; and d is the grain diameter. This relationship, which holds for a number of ferrous and nonferrous metals and alloys, indicates that a fine-grained metal will have a higher yield stress than a coarse-grained one, with the limiting case being that of a single crystal.

In addition to their strong influence on the initial yield, grain boundaries also play a decisive part in the subsequent plastic deformation and

strain hardening of polycrystals. Von Mises[77] has shown that a minimum of five independent slip systems are required for a crystalline solid to deform without change in volume, a condition necessary in a polycrystal in order that each grain remains coherent with its neighbors. *Thus, multiple slip has to occur right from the onset of plastic deformation and there can be no easy glide region in polycrystals.* (Yield elongation, in which there is a large plastic strain at constant stress, is due to a different mechanism and is considered in section 2.4).

A further example of the influence of grain boundaries in enforcing multiple slip is found in the variation of initial strain-hardening rate with grain size, the finest-grained material having the highest strain-hardening rate. These effects are illustrated in Fig. 1.8,[6] where true-stress–true-strain curves are shown for single crystals and polycrystals of copper deformed at room temperature. It can be seen that the yield stress of the fine-grained polycrystal is higher than that of the coarse-grained one, which is in turn higher than that of the single crystals. The initial linear strain-hardening rate of the polycrystals is slightly higher than that of stage II deformation in single crystals, probably because slip is more complex in polycrystals.

Once deformation by multiple slip becomes well-established, the pile up of dislocations behind Lomer-Cottrell barriers becomes the controlling factor in determining the strain-hardening rate, the effect of the grain boundaries diminishes, and *the strain-hardening rates of single crystals and polycrystals become very similar.* After a few per cent plastic deformation, the strain-hardening rate starts to decrease and the true stress–strain curve assumes a characteristic parabolic shape. This is analogous to stage III

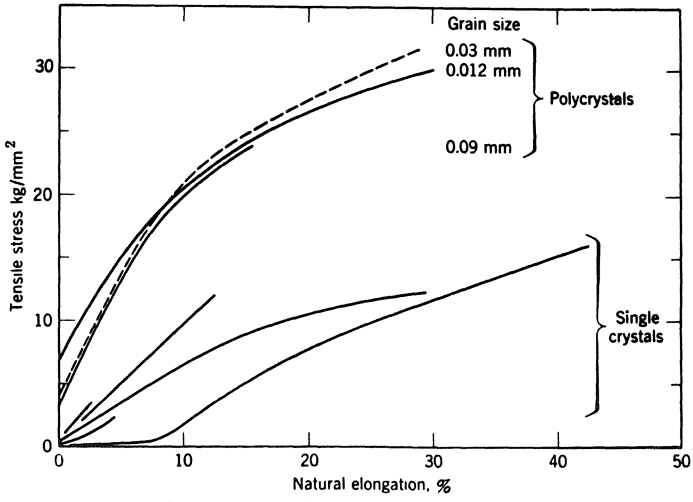

Fig. 1.8. True stress–strain curves for single crystals of various orientations and polycrystals with a range of grain sizes (McLean[6]).

deformation in single crystals, which, as we saw in the previous section, is controlled by dislocation cross-slip. Cross-slip, especially in fcc metals, is a thermally activated process which occurs more readily at high than at low temperatures, and thus the temperature of deformation is an important factor in determining the extent of strain-hardening in metals.

The three principal stages in the response of a metal to an applied stress are the initial yield, the subsequent strain-hardening, and the final mode of fracture. The first two of these will be considered in detail in the rest of this chapter and chapter 2, the third in chapter 3.

1.4. THE EFFECT OF TEMPERATURE ON THE YIELD AND FLOW OF PURE FACE-CENTERED-CUBIC METALS

1.4.1. Single Crystals

The three distinct strain-hardening stages discussed generally in section 1.3.2 are most readily shown by single crystals of pure fcc metals tested at, or below, room temperature. The effect of temperature on the various stages of deformation is illustrated in Fig. 1.9 for single crystals of copper[78] and nickel[79] favorably oriented for single slip. Between them, these two metals demonstrate the most important changes which result from a decrease in temperature. They may be summarized thus: As the temperature is lowered, the following occur:

(a) *The Critical Resolved Shear Stress τ_0 Increases Slightly.* It is a fundamental characteristic of all pure metals with an fcc lattice structure that the yield stress is only slightly influenced by the temperature. In general, a decrease in temperature increases the yield stress, but some metals show no change and others even a slight decrease.

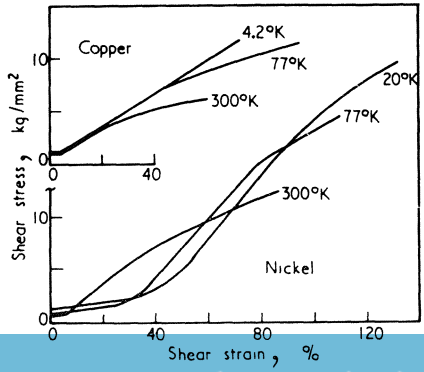

Fig. 1.9. Shear stress–strain curves for single crystals of copper and nickel, showing the effect of temperature on the three stages of strain hardening (after Blewitt *et al.*[78] and Hassen[79]).

(b) *Stage I Is Increased in Extent while the Strain-Hardening Rate θ_I Remains Unchanged.* The increase in extent of stage I, which is most noticeable in the case of nickel, is associated with the increase in critical shear stress mentioned above and τ_0 is not only raised on the primary slip system but also on the various secondary systems. As θ_I is unchanged, larger strains are necessary to raise the flow stress to a value high enough for the critical shear stress to be exceeded on a secondary slip system. Thus, the multiple slip which characterizes stage II commences at higher strains.

(c) *The Strain-Hardening Rate of Stage II, θ_{II}, Is Unchanged.* The high value of θ_{II} is believed to be caused by a rapid increase in the stress needed to move dislocations down the primary slip planes once they start to become obstructed by obstacles. The temperature independence of θ_{II} indicates that neither the rate of formation of these barriers nor the rate at which dislocations pile up against them is dependent on temperature.

(d) *The Onset of Stage III Is Raised to Higher Stresses and the Strain Hardening Rate θ_{III} Is Increased.* The decrease in θ_{III} below the value of θ_{II} is due to a recovery mechanism which allows the barriers formed in stage II to be broken or avoided in stage III. It is generally agreed that the recovery mechanism involved is cross-slip, a thermally activated process which becomes more difficult as the temperature is decreased: hence, the delayed onset of stage III and higher strain-hardening rate θ_{III} at low temperatures.

Another factor which has a strong influence on cross-slip is the stacking-fault energy of the metal. The higher the stacking-fault energy, the smaller the separation of the two partial dislocations and the easier it is for them to recombine and allow cross-slip. Thus, at a given temperature, a lower stress is needed for recombination in a metal with a high stacking-fault energy: according to Seeger,[72] the necessary shear stress τ is given by the equation

$$\tau = \frac{1}{n}\left(\frac{G}{\pi\sqrt{2}} - \frac{2\gamma}{b}\right) \tag{1.9}$$

where b is the Burgers vector, n is the number of dislocations in the pile-up, and γ is the stacking-fault energy. Furthermore, the higher the stacking fault energy, the lower the temperature at which cross-slip is possible and the lower the temperature at which stage III hardening commences. This is illustrated in Fig. 1.9. In the case of copper deformed at 4.2°K, stage II continues until fracture, while in nickel, which has a higher stacking fault energy than copper, there is a stage III region at 20°K. Similarly, stage II is more extensive at room temperature in copper than in nickel due to the earlier onset of cross-slip and stage III in nickel, while in aluminum, which has a still higher stacking-fault energy, stage II is almost completely suppressed and stage I merges into stage III.

1.4.2. Polycrystals

In section 1.3.3, the correlation between the various stages of plastic deformation in single crystals and polycrystals was discussed in general terms without reference to any specific lattice structure. If the linear strain-hardening in polycrystals is identified with stage II deformation in single crystals and parabolic hardening with stage III, we find the influence of temperatures and stacking-fault energy shown by single crystals of fcc metals to be followed in their polycrystals. Metals with high stacking-fault energy, such as aluminum, exhibit parabolic strain-hardening throughout plastic deformation at room temperature, linear strain-hardening only becoming significant as the temperature is lowered toward 77°K. In contrast, a period of linear strain-hardening precedes parabolic hardening at room temperature in metals of lower stacking-fault energy, such as copper.

Despite the strong influence of grain boundaries on the yield stress and the initial stages of plastic deformation, it is the creation and relief of dislocation pile-ups which mainly determine the nature and extent of strain-hardening in metals. Thus, much information on the dislocation process occurring during plastic deformation can be obtained from polycrystalline specimens and the extra effort involved in the preparation and handling of single crystals can often be avoided.

1.4.3. Dislocation Structures

During the last two decades, much effort has been expended in trying to understand the detailed nature of the dislocation mechanisms and structures developed during the plastic deformation of metals. There is now fairly general agreement on the main outlines of a theory, especially for fcc metals, although there is still a considerable amount of dissension on many points of detail.

Much of the information on dislocation structures has been obtained using the technique of thin-film transmission electron microscopy. Qualitatively, it has been found that, after about 1% strain, dislocations start to tangle and arrange themselves into a cellular structure with the majority of the dislocations lying in the walls of the cells. With increasing deformation, the cell structure becomes more pronounced, the dislocation density increases, and the cell size decreases; typical cell sizes are about 1–2 μm after 10% strain. In metals of low stacking-fault energy, cells tend to be smaller than in those where such energy is high, while for a given strain, the cell size decreases as the deformation temperature is lowered.

Quantitatively, it has been found that there is a linear relationship between dislocation density ρ and strain ε: $\rho \simeq 2 \times 10^{11}\varepsilon$. The given constant of proportionality is that for polycrystals of Cu and Ag; for single

crystals, it is two or three orders of magnitude lower. It has also been found that the dependence of flow stress on dislocation density is of the form

$$\tau = \alpha G b \rho^{-1/2}$$

where G is the shear modulus, b the Burgers vector, and α is a constant which has the value 0.5 for many metals.[41] Similar relationships have been shown to exist connecting flow stress, cell size, and dislocation density.

It thus appears that the flow stress in fcc metals depends principally on the dislocation density, the shear modulus and the size of the cell structure developed by the dislocations after a certain amount of strain, and the temperature. It is important to separate the two main factors which control the flow stress, and these are (a) the effect of temperature, etc. on the flow stress of a given strained structure, and (b) the different structures produced by a given strain at various temperatures. To assist in isolating these two effects, it is convenient to separate the flow stress into three components: (1) a thermal component τ^* which is a function of the temperature T and strain rate ε, (2) an athermal component τ_G which depends on temperature only through the shear modulus G,† and (3) the grain size component $Kd^{-1/2}$ of the Hall–Petch relationship, equation (1.8).

Thus, we have effectively split the friction stress τ_i into thermal and athermal components τ^* and τ_G. In terms of dislocation theory it is presumed that the thermal component τ^* is associated with short-range obstacles or stress fields less than $\sim$10 Burgers vectors in extent, where thermal fluctuations can provide the energy to overcome these obstacles. In relatively pure, metals, these include the Peierls–Nabarro stress, forest dislocations, resistance to cross-slip of screw dislocations, and impurity atoms. The athermal component τ_G is presumed to relate to long-range obstacles or stress fields, and thermal fluctuations are unable to provide enough energy to overcome these barriers. Typically, they include large precipitates, dislocations on intersecting or parallel slip planes, and large jogs.

A convenient way of separating the thermal and athermal stress components is to carry out differential tensile tests in which the temperature or strain rate is changed during deformation. Typically, a specimen is strained at one temperature T_1. The temperature is then changed, and after thermal equilibrium has been established, the flow stress τ_2 is determined by a small deformation at the new temperature T_2. The temperature is then returned to T_1, the specimen restrained, and the flow stress τ_1 redetermined. These measurements determine the flow stresses at temperatures T_1 and T_2 for the same strain and hence the same dislocation structure. By repeated cycling between T_1 and T_2, the temperature dependence of the flow stress can be obtained for a range of dislocation structures.

---

† Some authors use μ for the shear modulus and τ_μ for the athermal component of the flow stress.

Cottrell and Stokes[80] first showed that for fcc metals the ratio of the flow stresses at two temperatures is almost independent of strain after the first few per cent of plastic deformation, i.e., $\tau_{T_1}/\tau_{T_2} = K$. It also follows that τ^*/τ_G is also constant and independent of the strain, which illustrates that there is a close relationship between the densities of short-range and long-range obstacles. Subsequent investigations have shown that the Cottrell–Stokes "law" is obeyed for many fcc metals in both single-crystal and polycrystalline form, and that it holds for changes in strain rate ε as well as in temperature. As even the athermal part of the flow stress depends slightly on temperature through the temperature dependence of the shear modulus, it is usual to divide the flow stress by the appropriate value of the shear modulus. The temperature dependence of this modulus-corrected flow stress is then shown by referring the flow stress to its extrapolated value at 0°K and plotting this ratio $(\tau_T/G_T)/(\tau_0/G_0)$ as a function of T as shown in Fig. 1.10.[41]

Two important features are shown in this diagram. First, the flow stress ratio is relatively insensitive to changes in temperature and thus the athermal component of the flow stress τ_G is larger than the thermal component τ^*. The almost complete temperature independence of the flow stress ratio above ~200°K indicates that the short-range obstacles which give rise to τ^* have been completely overcome and the flow stress is controlled entirely by the long-range obstacles responsible for τ_G. Below ~200°K, it becomes increasingly difficult for thermal fluctuations to provide enough energy to enable dislocations to overcome the short-range obstacles and τ^* becomes more significant.

Second, the temperature sensitivity of the flow stress ratio increases in the order Ag, Cu, Ni, Al, which is also the order of increasing stacking-fault

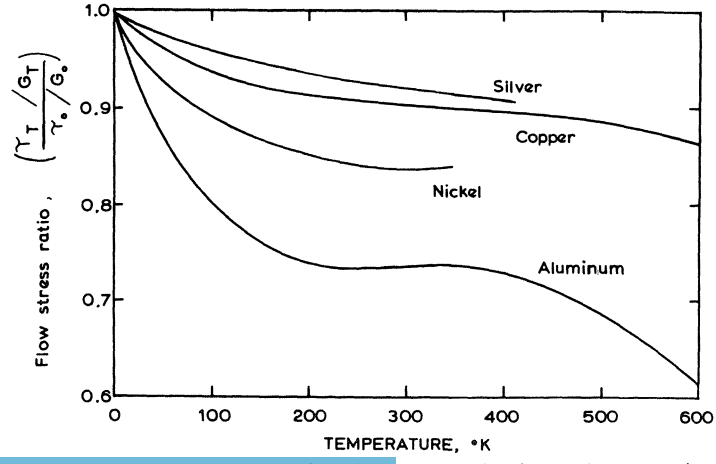

Fig. 1.10. Temperature dependence of the flow stress ratio of some fcc metals (Mitchell[41]).

energy. We saw earlier when considering stage III deformation in single crystals that the higher the stacking-fault energy, the easier it was for cross-slip to occur and the lower the flow stress associated with a given strain [see equation (1.9)]. Both of these effects follow from the fact that cross-slip is a stress-aided, thermally activated process in metals.

Once it is recognized that plastic flow is a thermally activated process at low temperatures, it is possible to determine the rate-controlling mechanisms from the temperature and strain-rate dependence of the thermal component of flow stress τ^*. It can be shown[82,83] that the strain rate ε is given by $\varepsilon \propto \nu e^{-H/kT}$, where ν is the frequency factor, H the activation energy, and T the absolute temperature. By carrying out creep tests in which the stress or temperature is changed during deformation, or tensile tests in which the strain rate or temperature is changed, it is possible to obtain experimental values of H, ν, and a further derived quantity V, known as the activation volume. These experimental values may then be compared with the values calculated for different dislocation mechanisms. The detailed mechanisms responsible for τ^* and τ_G have not yet, however, been resolved. This is partially a result of the difficulty in making the theoretical calculations but is also due to the fact that the experimental results are often compatible with several different dislocation mechanisms.

1.4.4. Engineering Parameters

Having considered in some detail the microscopic mechanisms responsible for plastic yield and flow in pure fcc metals, it is appropriate to see how far these are reflected by the parameters obtained from conventional tensile tests. In Fig. 1.11,[30] a series of simple engineering stress-strain curves are shown for annealed polycrystalline O.F.H.C. copper tested in tension at 300, 195, 76, and 20°K. The following points should be noted.

(a) The yield strength is virtually unaffected by a change in deformation temperature.

(b) The ultimate tensile stress (UTS) increases significantly as the temperature falls.

(c) The uniform elongation increases at low temperatures and failure is always ductile.

The higher values of tensile strength and uniform elongation arise from the thermal nature of cross-slip. At low temperatures, cross-slip becomes more difficult and high work-hardening rates extend to greater strains. The material is thus able to strain-harden enough to compensate for a greater decrease in cross-sectional area, the formation of a neck is postponed, and the uniform elongation increases. Furthermore, the improved values of UTS reflect both the increased rate and extent of strain-hardening at low temperatures.

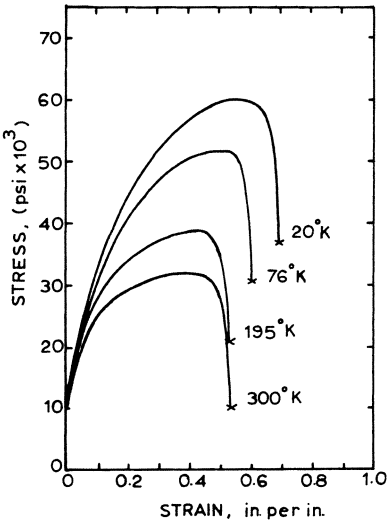

Fig. 1.11. Engineering stress-strain curves for polycrystalline copper tested at 300, 195, 76, and 20°K (Warren and Reed[30]).

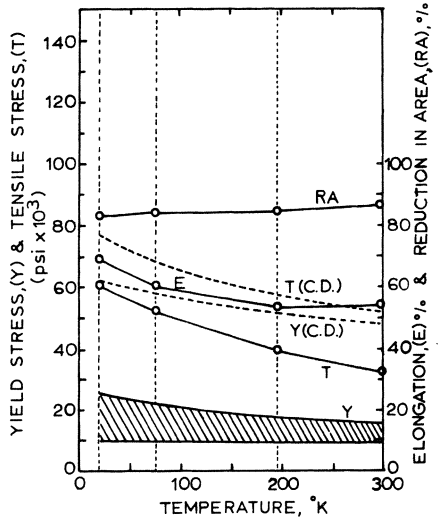

Fig. 1.12. Summary of the effect of temperature on the mechanical properties of annealed and cold-drawn copper (after Warren and Reed[30] and Carrekar and Hibbard[81]).

A common method of summarizing such results is that used in Fig. 1.12, where the yield and tensile stresses, the percentage elongation, and the reduction in area are plotted as a function of temperature. As the yield strength of the annealed metal depends on a number of factors, including its physical and chemical purity and its grain size,[81] the measured results taken from Fig. 1.12 are included in a band covering typical values. The tensile strength is, however, less influenced by these variables. The combination of a temperature-insensitive yield stress with a rapidly increasing tensile stress leads to high tensile/yield stress ratios at low temperatures. This implies that fcc metals are able to accommodate a large amount of plastic deformation before fracture, and also accounts for their extreme reliability at low temperatures.

An important practical point where load-bearing capacity is required is the large increase in yield stress of the cold-worked metal. Its yield stress increases with decrease in temperature, but not so rapidly as does the tensile stress. Thus, once again the ratio of UTS to yield stress improves at low temperatures, although its value is lower than that for the annealed metal. The percentage elongation also increases as the temperature falls, although in some metals, such as aluminum, there is often a reversal of this trend below $\sim$100°K.

It is more difficult to generalize about the variation of reduction in area with testing temperature. The reduction in area prior to fracture in

the necked region of a tensile specimen occurs under the influence of a triaxial tensile stress system and is very sensitive to the presence of inclusions in the metal. For example, at room temperature, the RA is almost 100% for zone-refined aluminum, 90–95% for normal high-purity material, but can drop as low as 25–35% for some commercial-purity aluminum.[84] Thus, the reduction in area is intimately associated with the type of fracture mechanism, and this topic will be dealt with in detail in chapter 3. Such trends as exist point, however, to a smaller reduction in area at low temperature than at high, with the decrease being more apparent in impure than pure metals.

In summary, pure fcc metals are inherently reliable for use at low temperatures, as all of the important engineering parameters improve as the temperature decreases. Their main disadvantage lies in their low yield stresses in the annealed condition, although this difficulty can be overcome if they are obtainable and usable in the cold-worked state. In many applications, their low strength is not a serious drawback and the high thermal and electrical conductivities possessed by commercially available grades of copper and aluminum are highly beneficial.

1.5. THE EFFECT OF TEMPERATURE ON THE YIELD AND FLOW OF PURE BODY-CENTERED-CUBIC METALS

Body-centered-cubic crystal structures occur in two main regions of the periodic table: the alkali metals of group I and the transition metals of groups Va, VIa, and VIII. The alkali metals, lithium, sodium, potassium, rubidium, and cesium, are characteristically soft, ductile, and chemically reactive. They are, therefore, of little practical use at low temperatures, but, because their electronic structures approximate closely to those of ideal metals, they are of considerable theoretical interest. Potassium[85] retains its bcc structure down to the lowest temperatures, but sodium[86,87] and lithium[86,88] undergo spontaneous and stress-induced martensitic transformations to hcp and fcc phases. These transformations, which are of interest in their own right,[89] complicate the interpretation of mechanical property investigations and further reduce their practical potential. Accordingly, little further attention will be given to the alkali metals.

The bcc transition metals are hard, have high melting points, and so have considerable potential for use at elevated temperatures. Their low-temperature properties have also received much attention and, due to the intractable nature of the problem, there is probably more effort still being devoted to the study of pure and impure transition metals than to all other metals and alloys combined.

The root cause of the problem is the extreme sensitivity of the mechanical properties of bcc transition metals to the presence of very small concentrations of impurity atoms, especially interstitials. Whereas fcc metals are, in general, little affected by impurity concentrations of less than about 1%, a decrease in impurity content of a few tens of ppm can transform some bcc metals from a hard, brittle condition into a relatively soft, ductile one. Consequently, there is often a large disparity between the properties of commercial-purity bcc metals and their higher-purity laboratory counterparts. This susceptibility to brittle behavior makes commercial-purity bcc metals generally unsuitable for cryogenic applications.

On a fundamental level, there is as yet no general agreement on the basic mechanisms responsible for yield and flow in these metals. The recent availability of very-high-purity single crystals of the refractory metals has produced results which differ significantly from those previously obtained in normal-purity metals. This poses the question of whether the characteristic mechanical properties of the bcc transition metals result from the interaction of dislocations with interstitial impurity atoms or from fundamental properties of the bcc lattice structure.

The basic experimental results described in the following section are unlikely to be rendered obsolete by future theoretical advances, but their interpretation must be regarded as somewhat tentative.

1.5.1. Single Crystals

Stress–strain curves showing the three characteristic stages of strain-hardening can be obtained for bcc single crystals, but they are much less common and are only found for favorable combinations of temperature, purity, orientation, and strain rate. A very instructive series of curves which demonstrate this effect are shown[90] in Fig. 1.13 for zone-refined niobium. These curves show three distinct hardening stages in the temperature range 300–400°K which resemble those found in fcc crystals. A detailed examination of the slip mechanisms involved reveals, however, differences between the behavior of the two lattice structures. A more important difference concerns the effect of temperature on the strain-hardening rate. Not only is the rate low compared to stage II in fcc crystals, but in niobium, lowering the temperature decreases both the rate and the extent of strain-hardening. This contrasts strongly with the behavior of fcc metals, where the extent of stage II, and rate in stage III, increases at low temperatures. Another point shown by these curves is the decrease in failure strain of niobium with decrease in temperature, again the reverse of that found in fcc metals.

The most important effect demonstrated by these curves is undoubtedly

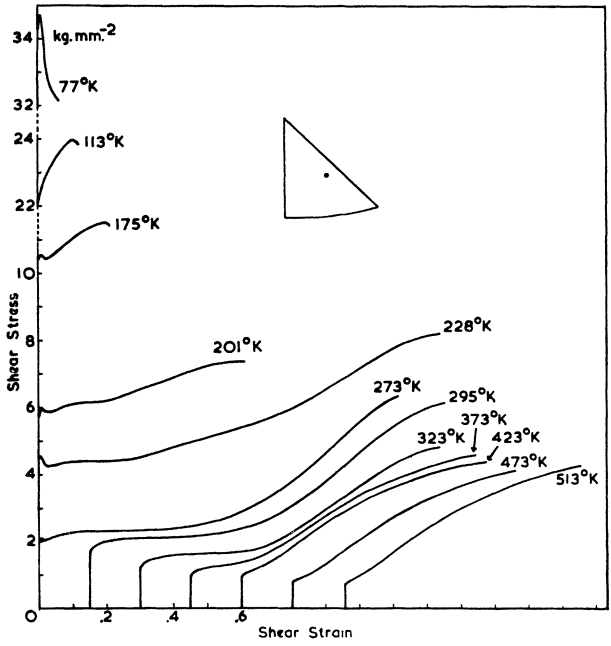

Fig. 1.13. Series of stress–strain curves for zone-refined niobium tested at temperatures between 77 and 513°K (Mitchell *et al.*[90]).

the extremely large increase in the yield stress with decrease in temperature below ~250°K. This, above all other properties, distinguishes bcc metals from the fcc's, which are characterized by the insensitivity of their yield stresses to changes in temperature. The mechanisms responsible for the temperature dependence of the yield and flow stresses in bcc metals will be discussed shortly. There are two other effects commonly found in bcc crystals which are not shown in these curves but which are worth mentioning briefly. First, sharp yield points are often shown in the stress–strain curves of bcc crystals. These yield points are probably due to the pinning of dislocations by interstitial impurities such as carbon and nitrogen, and they can be eliminated by careful purification of the metal. Second, plastic deformation by slip in bcc metals at low temperatures is often very limited in extent and is augmented by deformation by twinning, which occurs in bursts and shows up as serrations in the stress–strain curves. The onset of twinning can be delayed by testing in compression instead of tension, and almost completely avoided by prestraining at room temperature prior to deformation at low temperature. Both yield drops and twinning are considered further in section 2. 4.

1.5.2. Polycrystals

In Fig. 1.14, a series of stress–strain curves for polycrystalline, vacuum-melted Armco iron are shown[91] for temperatures in the range below 300°K. These confirm the features shown by the single crystals of niobium; namely, a low, temperature-insensitive strain-hardening rate, a large increase in yield stress as the temperature is decreased, and an almost complete loss of ductility at the lowest temperatures. The exact degree of ductility and the final mode of fracture depend strongly on the purity of the metal; the smaller the impurity concentration, the greater the ductility and the smaller the likelihood of brittle fracture. Twinning[92] is a very common mode of deformation, especially at and below 77°K, while the abrupt yield effects found in single crystals are more common in polycrystals, being sharpest in very-fine-grained material.

The Hall–Petch relationship between yield stress and grain size is generally found[93,94] to be more applicable to the lower yield stress $\sigma_{y_{\text{Lower}}}$ than to the upper. In the expression

$$\sigma_{y_{\text{Lower}}} = \sigma_i + Kd^{-1/2} \tag{1.10}$$

the constant K is virtually independent of temperature, indicating that the interactions between dislocations and the impurities which pin them are not affected by temperature. In contrast, the friction stress σ_i is highly temperature-dependent.

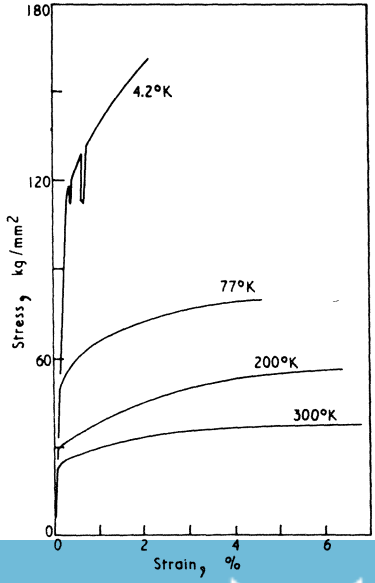

Fig. 1.14. Stress-strain curves for polycrystalline Armco iron tested at various temperatures (after Smith and Rutherford[91]).

The mechanical properties of the refractory bcc metals of groups Va (vanadium,[95–97] niobium, [90,95,98–100] and tantalum[95,101–105]) and VIa (chromium,[106] molybdenum,[107] and tungsten[110–112]) show many similarities to those of iron[113–117] at low temperatures. In particular, the yield stresses of all these metals are extremely temperature-dependent below about $0.2T_m$ (the melting point). The main differences between them arise in the degree to which the extent of plastic deformation is shortened by the onset of brittle fracture, the group Va metals generally showing a larger amount of plastic deformation than the more brittle metals in group VIa. A further important difference between these two groups is the much greater solid solubilities of the common interstitial impurities carbon, nitrogen, oxygen, and hydrogen in metals of group Va compared with those of VIa.

1.5.3. Dislocation Structures

In general, the dislocation structures developed by bcc metals after deformation at room temperature and below are similar to those of fcc metals. Cells and tangles form during the earlier stages of deformation, the cells becoming smaller and more pronounced as the strain increases. At low temperatures and in higher-purity metals, the dislocation distribution tends, however, to become more uniform and to consist of elongated loops which lie along the close-packed $\langle 111 \rangle$ directions. This results in the dislocations having a predominantly screw character, and it is one of the reasons why cross-slip is easier in bcc metals.

As in the fcc metals, there is an approximately linear relationship between dislocation density and strain in bcc metals, but the flow stress is no longer simply proportional to the square root of the dislocation density. Instead of the flow stress extrapolating to zero for a dislocation density of zero, it intercepts the stress axis at a value which depends on temperature and strain rate. This indicates that the thermal and athermal components of flow stress are not proportional to each other and that the Cottrell–Stokes law is not obeyed in bcc metals. Instead of the *ratio* of the flow stresses at two temperatures being independent of strain as found in fcc metals, in bcc metals it is the *difference* between the flow stresses at the two temperatures which is independent of strain. Only the athermal component τ_G is proportional to the square root of the dislocation density, and the flow stress is given by

$$\tau = \tau^*(T, \varepsilon) + \alpha G b \rho^{1/2}$$

As the temperature dependence of the shear modulus is very small, the effect of temperature and strain rate on the yield and flow stresses of bcc metals is described primarily by τ^*. By subtracting the flow stress at a reference temperature T_0 (usually 300°K) from that measured at a lower

temperature T, the temperature-dependent term is obtained directly,

$$\tau_T - \tau_{T_0} = \tau^*(T) = \Delta\tau^*(T)$$

(if $\varepsilon = \text{const}$). We can now express $\Delta\tau^*$ as a function of T for either the yield stress or for the flow stress at a given strain. Figures 1.15 and 1.16 show two versions of the relationship between $\Delta\tau^*$ and T for iron single crystals and polycrystals.

The differences between the results shown in these two figures are of fundamental importance because this should be the critical experiment which decides between the two main theories of the mechanism responsible for the high strength of bcc metals at low temperatures. Fleischer[121] has recently summarized the present state of this field of research and the following paragraphs show the main lines of his treatise.

It is generally agreed that the process responsible for the very rapid rise in yield stress at low temperatures is thermally activated and that it rapidly becomes more difficult to operate as the available thermal energy decreases. The large sensitivity of the flow stress to changes in strain rate supports this conclusion. Furthermore, it is widely agreed that the mechanism concerned involves the frictional forces acting on moving dislocations rather than the release of dislocations from their pinning points. As the mechanism involved is thermally activated, the forces must act over short distances in order that the small thermal energies available may be significant. There are two possible basic mechanisms which can give rise to these forces, lattice-hardening and solution-hardening.

Lattice-hardening arises because of the periodic nature of the atomic binding forces in a crystal. If a straight length of dislocation lies in the potential valley between two rows of atoms, a force is needed to move this dislocation over the potential hill into the adjacent valley. These potential hills form a barrier to dislocation motion which must be overcome not once but continually if the dislocation is to move through the crystal. Dorn and Rajnak[122] and Arsenault[123] have carried out detailed calculations which show that the overcoming of the Peierls–Nabarro stress by the production of double kinks in straight dislocations can provide a suitable rate-controlling mechanism for the plastic deformation of bcc metals at low temperatures.

Solution-hardening. Substitutional impurities present in cubic lattices produce symmetrical distortions which only interact relatively weakly with dislocations. In contrast, interstitital defects can lead to large asymmetrical lattice distortions in bcc lattices which interact strongly with dislocations and can thus provide frictional forces which impede the motion of dislocations gliding on neighboring slip planes. The motion of dislocations past interstitial defects has been shown by Fleischer[124] to be a possible rate-controlling mechanism responsible for the plastic deformation of bcc metals at low temperatures.

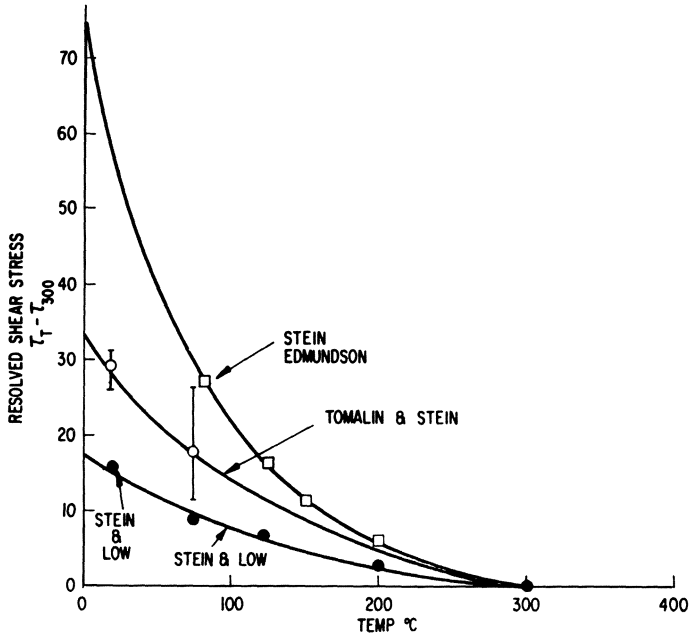

Fig. 1.15. Data which show how the thermal component of the flow stress of iron varies with specimen purity in apparent agreement with solution-hardening theories (after Stein[118]).

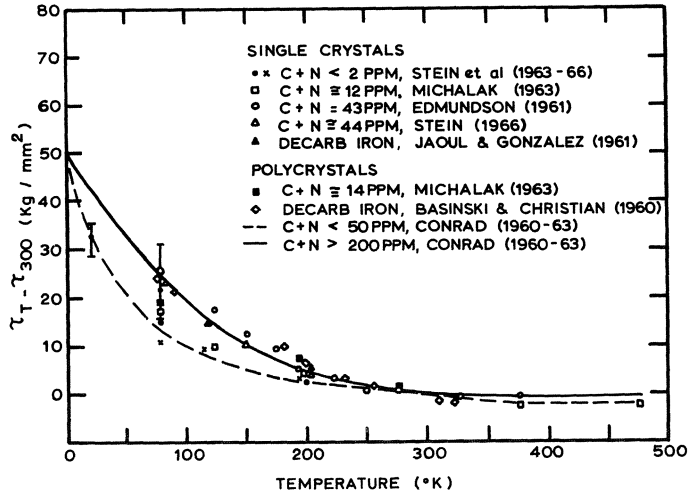

Fig. 1.16. Alternative data which show that the thermal component of the yield stress of iron is only weakly affected by specimen purity in apparent agreement with lattice hardening theories (Conrad[119]).

Both mechanisms predict a similar form of flow stress–temperature relationship, and more or less acceptable values for the parameters connected with the rate equation–activation energy, volume, and frequency factor. The really significant difference between them lies in their predictions of the effect of solute concentration. If the flow stress remains substantially unaltered by a variation in solute concentration, then impurity-hardening can be rejected. If, on the other hand, the low-temperature flow stress does vary significantly with solute concentration, then lattice-hardening can be ruled out as the dominant hardening mechanism. Hence, the criticality of the experimental results shown in Figs. 1.15 and 1.16.

Figure 1.15 shows[118,120] that a reduction of carbon content from the usual 200 atom ppm or greater, to a value less than 0.025 ppm causes the flow stress at all temperatures to be reduced to less than 40% of its original value. *If* this result is correct, it must follow that, for normal-purity iron, lattice-hardening is not the major source of strength.

In contrast, the results shown[119] in Fig. 1.16 indicate that the flow stresses of both superpure and normal-purity iron tend toward the same value at absolute zero. If *these* results are correct, then impurity-hardening can be ruled out as the ultimate source of strength.

High-purity metal from the same source was used to obtain both sets of results, so one possible source of the discrepancy has already been ruled out. A further possibility is that the temperature dependence of the yield stress may differ from that of the subsequent flow stress. It is, of course, also possible that the terms of reference of the "critical experiment" may be modified to resolve this dilemma, but at the time of writing an impasse appears to exist, with both sides[125–128] taking a firm stand on this fundamental issue. In an attempt to take some of the heat out of the argument, Kelly[129] has pointed out that even the very pure specimens used by Stein and Low[115] showed the type of sharp yield point associated with dislocation locking (see section 2.4). He therefore suggests that a halt be called in this controversy until theories are developed which incorporate dislocation locking into their explanation of the low-temperature behavior of bcc metals, or until even purer specimens are available which do not exhibit sharp yield points.

1.5.4. Engineering Parameters

As stated earlier, bcc metals of commercial purity are rarely used for low-temperature applications. They are to be particularly avoided in structural applications where their liability to brittle fracture could lead to catastrophic failure. Armco iron, because of its favorable magnetic properties, might occasionally be used at low temperatures, while recent design studies have considered the possibility of supondercucting power

cables with pure niobium conductors. Niobium is one of the more ductile group Va metals, but as yet it is not available commercially in its high-purity form, and the problems of handling and joining high-purity metals "in the field" should not be lightly dismissed.

1.6. THE EFFECT OF TEMPERATURE ON THE YIELD AND FLOW OF PURE HEXAGONAL-CLOSE-PACKED METALS

1.6.1. Single Crystals

Although some stress–strain curves for hcp single crystals show three distinct stages of strain-hardening, they occur for such limited combinations of orientation, temperature, and other testing variables that it would be a misrepresentation of the facts to imply that they were typical of the plastic deformation of hcp metals. The distinguishing characteristic of the metals is the predominance of stage I, or easy glide, which is associated with slip on the basal plane. Other, nonbasal slip systems as well as alternative deformation modes such as twinning also play an important part in determining the mechanical properties of hcp metals, and it has been found that the relative importance of the different deformation systems is strongly dependent on the axial (c/a) ratio of the metal. As the axial ratio decreases, (1) the principal slip system changes from basal to prismatic and back to basal and the total number of slip systems increases to a maximum and then decreases again; (2) the probability of cleavage on the basal plane first decreases and then increases again; (3) twinning on the $\{10\bar{1}2\}\ \langle 10\bar{1}\bar{1}\rangle$ system, which occurs under compression along the C axis in metals with c/a greater than $\sqrt{3}$, takes place under the influence of tensile stresses parallel to the C axis in metals with c/a less than $\sqrt{3}$. In titanium ($c/a = 1.587$), twinning also occurs in the $\{11\bar{2}1\}\ \langle 11\bar{2}\bar{6}\rangle$ and $\{11\bar{2}\bar{2}\}\ \langle 11\bar{2}\bar{3}\rangle$ systems and thus the number of possible twin systems is increased.

As a result of these factors, maximum ductility appears to be associated with c/a ratios of about 1.6, hence the strong current interest in zirconium ($c/a = 1.593$) and titanium ($c/a = 1.587$). These metals will be considered in more detail shortly. Most single-crystal studies have, however, concentrated on those metals that deform predominantly by basal slip, i.e., cadmium ($c/a = 1.886$), zinc ($c/a = 1.856$), and magnesium ($c/a = 1.624$), and more recently, beryllium ($c/a = 1.567$). The results[130] shown in Fig. 1.17 for cadmium single crystals of 99.999% purity are typical of the behavior of these metals.

Easy glide on the basal plane extends up to very large shear strains, of the order of hundreds of per cent at room temperature. The strain-

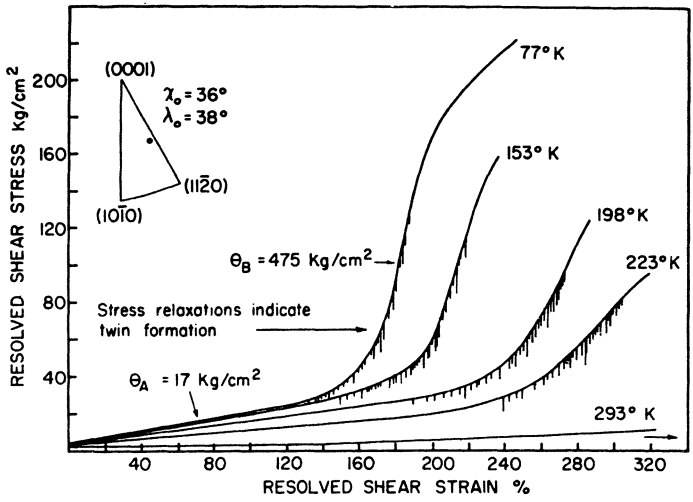

Fig. 1.17. Shear stress–strain curves for single crystals of cadmium tested at temperatures between 77 and 293°K (Risebrough and Teghtsoonian[130]).

hardening rate θ_I is low ($\sim 10^{-4}G$) and is similar to that observed during stage I deformation in fcc crystals. As the temperature is lowered, θ_I increases slightly and stage I decreases in extent, in contrast to fcc metals, in which θ_I remained almost constant and the extent of stage I increased.

Stage II is characterised by a higher, temperature-dependent strain-hardening rate θ_{II}, whose value is constant at $\sim 10^{-3}G$ below 150°K but falls off rapidly at higher temperatures. In the diagram, extensive twinning (indicated by the small load drops) is shown to occur during stage II, and under these conditions, strain-hardening must, to a large extent, be due to dislocation–twin boundary interactions. The relative importance of twinning and deformation on nonbasal slip systems is somewhat contentious and differs from metal to metal. The main effect of twinning probably lies in the fact that in grains initially oriented unfavorably for slip, twinning reorients the crystal into a more favorable position for subsequent slip. The small temperature dependence of θ_I implies that the critical resolved shear stress for slip on the basal plane in cadmium is only slightly temperature-dependent, similar behavior being shown by zinc, magnesium, and beryllium. In contrast, the crss for prismatic slip in these metals is much more temperature-dependent, e.g., it increases by two orders of magnitude in magnesium when the temperature is lowered from 600 to 77°K. In titanium, the position is reversed, basal slip being more temperature-dependent than prismatic.

There is also a third deformation stage visible in some of the curves of Fig. 1.17, but the fact that it is most prominent at 77°K and less evident

at higher temperatures makes it unlikely that it is due to cross-slip as in fcc metals.

1.6.2. Polycrystals

We saw earlier that at least five independent shear systems have to operate in polycrystals in order that they may deform homogeneously without change in volume. None of the three common systems listed in Table I for hcp metals (slip in the $\langle 11\bar{2}0\rangle$ directions on {0001}, $\{10\bar{1}0\}$, and $\{10\bar{1}1\}$ planes) can provide more than four independent shear mechanisms; thus, theoretically, gross ductility should not exist in polycrystalline hcp metals. The only simple slip system which can provide the required five independent deformation modes is the $\{11\bar{2}2\}$ $\langle 11\bar{2}3\rangle$, which is a second-order pyramidal type.[131] This mode is not often found in single crystals, but has been confirmed in many polycrystals, e.g., Cd,[130] Zn,[132] Ti,[133] Zr,[133,134] and Hf.[134]

The other possible mode of deformation which contributes to the gross ductility of hcp metals is twinning. It has been shown[135] that the strains associated with the complete conversion of a crystal into its twin orientation are low (~7% in magnesium), and thus twinning alone cannot account for the higher observed strains. It is more likely that its role is to activate other slip systems by reorientation of grains initially oriented unfavorably, by generating locally high stresses around twins, or by dislocation–twin interactions.

Thus, the occurrence of gross ductility in polycrystals depends on the action of nonbasal slip systems and/or deformation twinning. Its extent is limited by the onset of fracture which often occurs by cleavage on the basal plane. In the previous section, it was shown that the most favorable combination of factors influencing the ductility occurred for c/a ratios near 1.6, which means, in practice, titanium, zirconium, and magnesium. All three metals have the additional attraction of low or relatively low densities and they and their alloys are under evaluation for structural use at low temperatures. Particular attention is being paid to the possibilities of titanium, and in Fig. 1.18 a series of load/extension curves is shown for commercially pure titanium.[136]

The important features illustrated by these curves are the considerable rise in yield stress and significant increase in strain-hardening rate obtained by decreasing the temperature. (This is typical of hcp metals, and thus their behavior is intermediate between that of bcc metals, which showed a large increase in yield stress but no increase in strain-hardening rate, and the fcc metals, in which the yield stress was only slightly increased but whose strain-hardening rate became much higher as the temperature was lowered.) The uniform elongation improves as the temperature is decreased to 77°K, but at 4°K, the mechanism responsible for the serrations in the

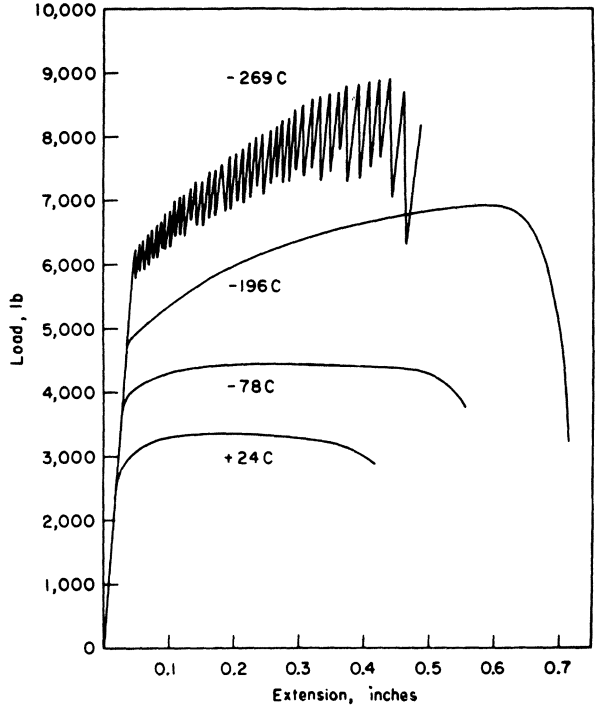

Fig. 1.18. Load-extension curves for commercially pure titanium (Kula and De Sisto[136]).

load–elongation curve causes a slight decrease in the ductility. Serrated stress–strain curves are considered in some detail in section 2.4.

1.6.3. Dislocation Structures

There is much less information available on the dislocation structures developed during the deformation of bulk hcp metals than there is for fcc and bcc metals. It would appear, however, that the structures are similar to those found in the bcc and fcc lattices with dislocations arranging themselves into cells. As in the bcc metals, the athermal component of the flow stress is probably given by $\tau_G = \alpha G b \rho^{1/2}$, but the detailed mechanism responsible for τ_G is not known. Whether or not the Cottrell–Stokes law is obeyed in hcp metals is not yet clear, as it does not appear to hold for titanium,[137] but is obeyed for cadmium[130] during the linear hardening region at temperatures below 150°K.

The magnitude of the thermal component of the yield stress τ^* varies from metal to metal, as does the relative importance of impurity concen-

trations. In Fig. 1.19,[43] the variation of τ^* with T is shown for Ti, Mg, and Zr with different impurity concentrations. It can be seen that magnesium is the least sensitive to interstitial impurities and titanium the most. Very-high-purity titanium has a τ^* which is virtually temperature-independent and in many ways resembles the behavior of fcc metals. Commercial-purity metal, on the other hand, has a highly temperature- and strain-rate-dependent τ^* which is virtually independent of strain and is thus similar to that found in bcc metals. The flow stress of commercial-purity titanium can therefore be written as

$$\tau = \tau^*(T, \varepsilon) + \alpha G b \rho^{1/2}$$

The effect of work-hardening rests almost entirely on the latter term and the yield stress depends mainly on the former.

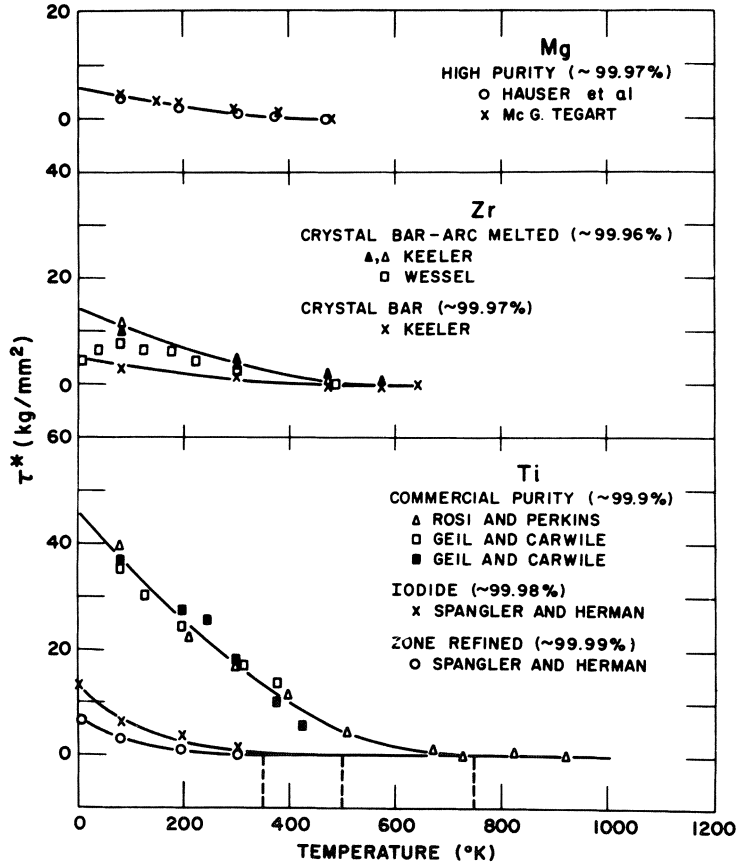

Fig. 1.19. Effect of temperature and purity on the thermal component of the yield stress of magnesium, zirconium, and titanium (Conrad[43]).

Furthermore, it has been found[138] that the value of the thermal component of the flow stress extrapolated to absolute zero, τ_0^*, is proportional to the square root of the concentration of interstitial impurities. This is consistent with Fleischer's model[139] for rapid solution-hardening caused by asymmetrical defects and there appears to be general agreement that solution-hardening is responsible for the high yield and flow stresses in titanium and possibly other hcp metals. Conrad[137] has suggested that the thermally activated overcoming of interstitial atoms by dislocations moving on first-order prism planes is the rate-controlling mechanism for the low-temperature deformation of titanium.

1.6.4. Engineering Parameters

Pure hexagonal-close-packed metals are rarely used at low temperature, mainly because of their limited ductility in the bulk form. Cadmium, which does remain ductile down to the lowest temperature, is very soft and liable to creep, while zinc is highly brittle. Of greater potential interest are titanium, zirconium, and beryllium. All three of these metals are, to a greater or lesser extent, sensitive to small concentrations of interstitial impurities, which considerably increase their yield strengths but seriously limit their ductility. The basic effect of interstitial impurities in these metals is to reduce the number of slip systems available for plastic deformation and to encourage the onset of cleavage fracture. Thus, to ensure good ductility, interstitial impurity concentrations have to be kept very low, but at the same time the yield stresses have to be increased if the metal is to be structurally useful. This can be done in two main ways. The most usual method is to alloy the pure metal with elements which strengthen either by forming substitutional solid solutions and/or by retaining a stronger high-temperature phase. These techniques will be considered further in sections 2.1 and 2.2. An alternative technique which will be discussed in the next section involves plastically deforming the pure metals at very low temperatures.

1.7. A COMPARISON OF THE MAIN CHARACTERISTICS OF FACE-CENTERED-CUBIC, BODY-CENTERED-CUBIC, AND HEXAGONAL-CLOSE-PACKED METALS

The effect of temperature on the yield stress of commercially pure metals of all three main crystal structures is shown[136] in Fig. 1.20. The abscissa is homologous temperature (ratio of temperature T to the melting point T_m), which allows a more convenient comparison of the data for the different metals. It can be seen that the yield stress of the fcc metals

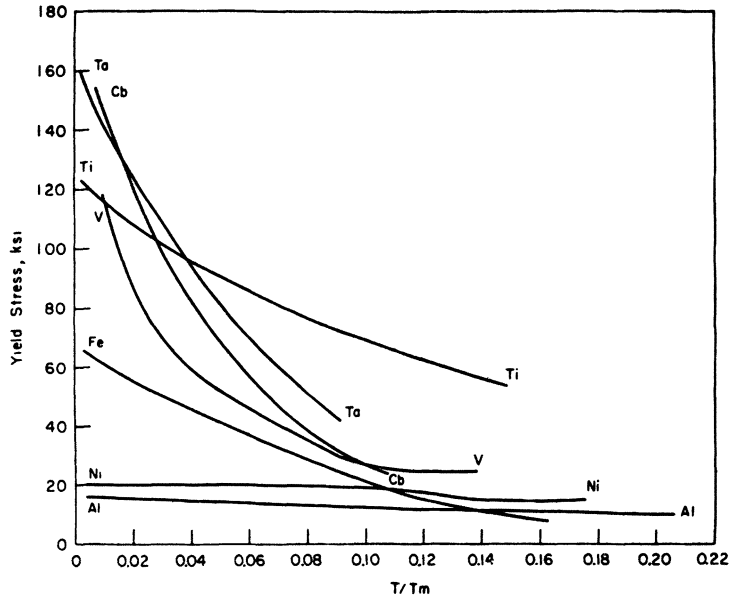

Fig. 1.20. Yield stress as a function of homologous temperature for various commercially pure metals of the three main crystal structures (Kula and De Sisto[136]).

changes little with temperature, in contrast to that of the bcc metals, in which it increases steeply at low temperatures, especially below $T = 0.1\,T_m$. The hcp titanium occupies an intermediate position between the other two structures.

The effect of temperature on the strain-hardening rate, flow stress, and ultimate tensile stress is not shown in the figure, but, summarizing the behavior described in sections 1.4–1.6, it is the opposite of that demonstrated by the yield stress. In fcc metals, the strain-hardening rate increases strongly as the temperature is lowered and the tensile stress rises accordingly. As the yield stress is almost temperature-independent, the ratio of tensile stress to yield stress increases as the temperature decreases, a characteristic which makes fcc metals highly suitable for cryogenic use. In bcc metals, the strain-hardening rate either remains the same or decreases as the temperature is lowered. In consequence, the curve of tensile strength versus temperature runs either approximately parallel to that for the yield stress or converges toward it as the temperature decreases. Thus, the ductility of bcc metals is reduced at low temperatures and many bcc metals show a transition from ductile to brittle behavior which severely limits their cryogenic use. The mechanical properties of hcp metals are critically

dependent on their c/a ratio and purity, but in general fall between those of fcc and bcc metals. In titanium, for example, both yield stress and strain-hardening rate increase as the temperature is lowered, so that the ratio of tensile stress to yield stress is maintained or even increased at low temperatures. This makes titanium an attractive proposition for cryogenic use.

We have seen in the preceding sections that, according to dislocation theory, the strength of a metal at a given temperature depends on the values of the shear modulus, Burgers vector, and stacking-fault energy. In Fig. 1.21, the values of tensile strength and modulus extrapolated to 0°K are plotted against each other for a number of commercially pure fcc and hcp metals. For comparison, the thermal component of the flow stress for bcc metals is also included. It can be seen that the ratio of shear strength to modulus near absolute zero ranges from ~ 0.5 to 1.1×10^{-2}, with fcc metals having the lowest value and hcp metals the highest. Conrad[43] has pointed out that this represents shear strengths of the order of one-quarter

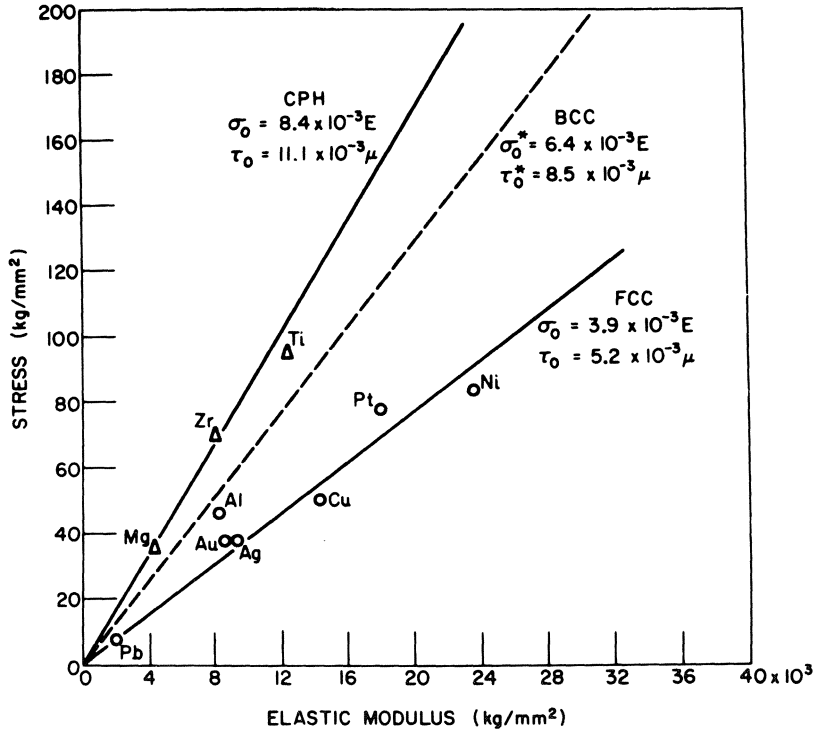

Fig. 1.21. Relationship between the tensile strength and elastic modulus at 0°K for fcc, bcc, and hcp metals (Conrad[43]).

to one-half the theoretical shear strength in metals ($\sim G/30$), which is as high as that currently achieved by the strongest known alloys. He goes on to suggest that by deforming a commercially pure metal at temperatures close to absolute zero (4°K could be close enough for practical purposes) very-high-strength metals could be obtained. Furthermore, in fcc and hcp metals, it is probable that most of this increase in strength would be maintained to temperatures as high as $\sim 0.5 T_m$ (which in most cases is above room temperature). The technique of cryogenic stretch-forming has already been used[140] to produce pressure vessels of type 301 stainless steel, but in this case, the strengthening is a result of a strain-induced austenite-to-martenite transformation rather than the inherent strain-hardening suggested for pure metals.

1.8. PLASTIC DEFORMATION AT CONSTANT STRESS: CREEP

When a stress in excess of the yield stress is applied to a metal, it produces a certain instantaneous extension. If, however, the applied stress remains constant, there is also a further time-dependent extension called creep, whose magnitude depends strongly on the temperature. At temperatures below $\sim 0.4 T_m$, no recovery is possible, the creep strain work-hardens the metal, and the creep rate drops off rapidly. The extension is proportional to log(time) and this is known as *primary* or *logarithmic* creep.

At higher temperatures, the creep strain rate does not drop off to zero but stabilizes at a constant value and the creep strain becomes a linear function of time. This is *secondary* or *steady-state* creep, which results from a balance between work-hardening and the thermal recovery processes occurring at these higher temperatures. It is of extreme importance in engineering applications where components are stressed at high temperatures, and special creep-resistant alloys have been developed for use under these conditions. Eventually, the creep rate starts to increase rapidly during *third stage* or *tertiary* creep and this soon terminates in creep rupture or fracture.

From a cryogenic point of view, creep is not a serious problem. Few metals have melting points low enough for $0.4 T_m$ to be at or below room temperature and so the secondary stage of creep is not reached. The strains involved in primary creep are small and could only become significant in high-precision components, where they might impair dimensional accuracy.

One of the few occasions where steady-state creep could occur and be troublesome at low temperatures is when pure indium wire is used to form a vacuum seal between two bolted flanges. If the joint is made at room temperature, the combination of creep and differential contraction on cool-

ing can lead to a bad seal at low temperatures. This problem, which has arisen in liquid-hydrogen bubble chambers, where the viewing windows have to be sealed onto the chamber body, has been overcome by increasing the pressure on the indium seal using an inflatable stainless steel bellows. In less critical cases, it is, of course, much simpler to replace the indium wire by one of aluminum or some other metal with a higher melting point.

Logarithmic creep is of interest from a fundamental point of view because it provides a method of studying the work-hardening processes occurring during the low-temperature deformation of metals. In section 1.4.3, we saw that the dislocation mechanisms responsible for plastic flow were thermally activated and that values for the various activation parameters, H, ν, and V, can be obtained from tensile and creep tests and compared with the values predicted by different theoretical models. The techniques involved in making these measurements, which usually involve changing the stress or temperature and observing the resultant change in creep rate, have recently been reviewed by Arsenault,[141] while the theoretical aspects are considered in some detail in the works by McLean[6] and Honeycombe.[7]

All theories of primary creep, whether of strain-hardening or exhaustion type, lead to a linear relationship between creep strain and temperature. Preliminary investigations by Glen[142] indicated that, whereas creep at 77°K was in agreement with these theories, that observed at 4.2°K was significantly larger than expected and, furthermore, that there was little change in reducing the temperature to 1.2°K. To account for these discrepancies, Mott[143] suggested that creep occurs by a temperature-independent quantum mechanical tunnel effect at very low temperature and this mechanism accounted for the major part of the observed creep at and below 4.2°K.

More recent work by Arko[144] on cadmium and mercury has, however, shown that creep is temperature-dependent down to 1.75°K and that it obeys the same logarithmic law as that found at higher temperatures. Measurements of activation energy and activation volume at 4.2°K gave values more consistent with thermal activation theories than with those of quantum mechanical tunneling and it was calculated that quantum mechanical tunneling was unlikely to be significant at temperatures above 0.04°K.

1.9. ANNEALING: RECOVERY AND RECRYSTALLIZATION

We have seen in the preceding sections that considerable changes in the strength and other mechanical properties of a metal can be brought about by cold-working at or below room temperature. The high density

of dislocations and point defects created during deformation not only alters the mechanical properties of the metal but also has a significant effect on some of its physical properties. If the temperature is raised, these imperfections can become mobile and rearrange themselves into more energetically favorable configurations or even annihilate each other. This general process of annealing is normally considered in two separate stages: recovery and recrystallization.

Recovery principally involves the movement of point defects (vacancies and interstitials), and, as these have their greatest effect on the physical properties of a metal, its progress is usually followed by measurements of the electrical resistivity or stored energy. These show that recovery can occur at temperatures as low as 4°K or less and that there are normally many different mechanisms involved, each with its own characteristic activation energy.

Dislocations are not very mobile at temperatures below $\sim \frac{1}{2} T_m$ and even at these temperatures there is no significant change in the dislocation density of a deformed metal. Dislocation rearrangements do, however, occur by climb and this results in the formation of an ordered dislocation cell structure, a process called polygonization.

There is little change in the mechanical properties of a metal during recovery, but if the annealing temperature is raised further, these properties alter sharply over a relatively small temperature range. This corresponds to the onset of recrystallization, a nucleation and growth mechanism in which new, equiaxial, strain-free grains grow within the old deformed ones. The density of both dislocations and point defects drops sharply during recrystallization and hence there is also a corresponding change in the physical properties.

The driving force which controls recrystallization (and recovery) is the reduction in strain energy achieved by the removal of excess point and line defects, and the three main factors which can influence this process are temperature, purity, and the amount of prestrain received by the metal.

(1) Recrystallization is a thermally activated mechanism which thus occurs more readily (i.e., more rapidly and after a shorter time) at higher temperatures.

(2) Other things being equal, a pure metal recrystallizes at a lower temperature than an impure one: impurities lower the mobility of dislocations and make it more difficult for recrystallization nuclei to form.

(3) For a metal of given purity, the greater the degree of cold-work, the more readily recrystallization occurs.

The combined effect of these three variables can be illustrated by the behavior of aluminum of two different purities.[145] After the same degree of cold-work at 77°K, zone-refined aluminum recrystallized at ~200°K, whereas 99.99% pure aluminum recrystallized at ~450°K.

In most practical cases, however, recrystallization only occurs at temperatures above ambient and it is thus not a serious cryogenic problem. Nevertheless, such temperatures are achieved in both the weld metal and heat-affected zone of a fusion weld, and thus this operation lowers the strength of the as-welded metal toward that of the annealed condition.

REFERENCES

Books and Other Reference Works

1. J. Wulff *et al.*, *The Structure and Properties of Materials*, Vol. 1 ("Structure") and Vol. 3 ("Mechanical Behavior"), John Wiley and Sons, New York (1965).
2. L. H. Van Vlack, *Elements of Materials Science*, Addison-Wesley, Reading, Mass. (1st ed. 1964, 2nd ed. 1970).
3. T. S. Serafini and J. L. Koenig, *Cryogenic Properties of Polymers*, Marcel Dekker, New York (1968).
4. H. F. Mark (Ed.), *Encyclopedia of Polymer Science and Technology*, Vol. 4, John Wiley and Sons, New York (1966), pp. 415–449.
5. L. J. Broutman and R. H. Krock, *Modern Composite Materials*, Addison-Wesley, Reading, Mass. (1967).
6. D. McLean, *Mechanical Properties of Metals*, John Wiley and Sons, New York (1962).
7. R. W. K. Honeycombe, *The Plastic Deformation of Metals*, Edward Arnold, London (1968).
8. F. A. McClintock and A. A. Argon, *Introduction to Mechanical Behavior of Materials*, Addison-Wesley, Reading, Mass. (1966).
9. A. H. Cottrell, *Dislocations and Plastic Flow in Crystals*, Oxford University Press, London (1963).
10. D. Hull, *Introduction to Dislocations*, Pergamon Press, Oxford (1965).
11. E. Schmid and W. Boas, *Kristallplastizitat*, Springer-Verlag, Berlin (1935). English Translation, F. A. Hughes, Chapman and Hall (1968).
12. B. L. Averbach *et al.* (Eds.), *Fracture*, M.I.T.-John Wiley and Sons, New York (1959).
13. A. S. Tetelman and A. J. McEvily, *Fracture of Structural Materials*, John Wiley and Sons, New York (1967).
14. American Society for Testing and Materials, "Metallic Materials for Low-Temperature Service," ASTM, Philadelphia, STP 302 (1961).
15. American Society for Testing and Materials, "Behavior of Materials at Cryogenic Temperatures," ASTM, Philadelphia, STP 387 (1966).
16. K. D. Timmerhaus (Ed.), *Advances in Cryogenic Engineering*, Plenum Press, New York, Vol. 16 (1971) and previous annual volumes.
17. R. B. Scott, *Cryogenic Engineering*, Van Nostrand, New York (1959).
18. G. G. Haselden, *Cryogenic Fundamentals*, Academic Press, London (to be published).
19. R. W. Vance and W. M. Duke, *Applied Cryogenic Engineering*, John Wiley and Sons, New York (1962).
20. R. Barron, *Cryogenic Systems*, McGraw-Hill, New York (1966).
21. R. H. Kropschot, B. W. Birmingham, and D. B. Mann, "Technology of Liquid Helium," N.B.S. Monograph 111 (1968). (All N.B.S. monographs sold by Superintendent of Documents, U.S. Govt. Printing Office, Washington 25, D.C.).
22. K. Mendelssohn, *Cryophysics*, Interscience, New York (1960).

23. H. M. Rosenberg, *Low-Temperature Solid-State Physics*, Clarendon Press, Oxford (1963).
24. F. E. Hoare, L. C. Jackson, and N. Kurti, *Experimental Cryophysics*, Butterworth, London (1961).
25. G. K. White, *Experimental Techniques in Low-Temperature Physics*, Clarendon Press, Oxford (1968), 2nd ed.
26. A. C. Rose-Innes, *Low-Temperature Techniques*, English Universities Press, London (1964).
27. G. T. Meaden, *Electrical Resistance of Metals*, Plenum Press, New York (1965).
28. E. S. Raja Gopal, *Specific Heats at Low Temperatures*, Plenum Press, New York (1966).
29. R. M. McClintock and H. P. Gibbons, "Mechanical Properties of Structural Materials at Low Temperatures," N.B.S. Monograph 13 (1960).
30. K. A. Warren and R. P. Reed, "Tensile and Impact Properties of Selected Materials from 20° to 300°K," N.B.S. Monograph 63 (1963).
31. R. P. Reed and R. P. Mikesell, "Low-temperature Mechanical Properties of Copper and Selected Copper Alloys," N.B.S. Monograph 101 (1967).
32. F. R. Schwartzberg, S. H. Osgood, R. D. Keys, and T. I. Kiefer. "Cryogenic Materials Data Handbook," Technical Document Report ML-TDR-280 (August 1964 and supplement March 1966).
33. "Cryogenic Data Book," University of California Radiation Laboratory, U.C.R.L. 3421.
34. "Low Temperature and Cryogenic Steels," United States Steel Materials Manual, 3rd ed., U.S. Steel Inc., New York (1968).
35. R. R. Conte, *Elements de Cryogenie*, Masson et Cie., Paris (1970).
36. R. B. Scott, W. H. Denton, and C. M. Nicholls, *Technology and Uses of Liquid Hydrogen*, Pergamon Press, Headington, Oxford (1964).
37. *Cryogenics*, Iliffe Press, Guildford, Surry, England.
38. *Journal of Low Temperature Physics*, Plenum Press, New York.
39. Ellen M. Codlin, *Cryogenics and Refrigeration; A Bibliographical Guide*, Plenum Press, New York (1968).

Reviews

40. A. Kelly, *Fibre Reinforcement of Metals*, H.M.S.O. London (1965).
41. T. E. Mitchell, "Dislocations and Plasticity in Single Crystals of Face-Centered-Cubic Metals and Alloys," in E. G. Stanford *et al.* (Eds.), *Progress in Applied Materials Research*, Vol. 6, Heywood and Co., London (1964), p. 119.
42. F. R. N. Nabarro, Z. S. Basinski, and D. B. Holt, "Plasticity of Pure Single Crystals," *Adv. Phys.* **13,** 50 (1964).
43. H. Conrad, "The Cryogenic Properties of Metals," in V. F. Zackay (Ed.), *High-Strength Materials*, John Wiley and Sons, New York (1964), p. 436.
44. P. G. Partridge, "The Crystallography and Deformation of Hexagonal-Close-Packed Metals," *Met. Revs.* **12,** 169 (1967).
45. H. M. Rosenberg, "Research on the Mechanical Properties of Metals at Liquid-Helium Temperatures," *Met. Revs.* **3,** 357 (1958).
46. "The Relation between the Structure and Mechanical Properties of Metals," National Physical Laboratory Symposium, H.M.S.O. (1963).
47. J. R. Low, "The Fracture of Metals," in *Progress in Materials Science*, Vol. 12, Pergamon Press, Oxford (1963), p. 1.
48. R. J. Corruccini, "Properties of Materials at Low Temperatures," *Chem. Eng. Prog.* **53**(6), 262; (7), 342; (8), 397 (1957).
49. E. G. Kendell, "Metals and Alloys for Cryogenic Applications," Technical Data Report, TDR-269 (4240-10)-6 (Jan. 1964).

50. R. R. McGee, J. E. Cambell, R. L. Carlson, and J. K. Manning, "The Mechanical Properties of Certain Aircraft Structural Metals at Very Low Temperatures," WADC TR 58-386 (November 1958).
51. R. J. Arsenault, "Low-Temperature Deformation Techniques," in H. Herman (Ed.), *Experimental Methods of Materials Research*, Vol. 1, Interscience, New York (1967).
52. J. F. Watson, "Materials at Cryogenic Temperatures," in *Materials for Missiles and Spacecraft*, McGraw-Hill, New York (1963).
53. J. F. Watson, J. L. Christian, and A. Hurlich, "Mechanical Properties of Metals," in *Physics of High Pressures and Condensed Phases*, John Wiley and Sons, New York (1965).
54. H. L. Martin and A. G. Imgram, "Effects of Low Temperature on Structural Metals," *J. Metals* **17,** 735 (1965).
55. R. M. McClintock and R. L. Hauser, "Current Trends and Prospects in Mechanical Properties," in K. D. Timmerhaus (Ed.), *Advances in Cryogenic Engineering*, Vol. 8, Plenum Press, New York (1963), p. 631.

Other References

60. H. B. Huntington, *Solid State Phys.* **7,** 213 (1958).
61. W. Köster, *Z. Metallk*, **39,** 145 (1948).
62. W. Köster and W. Rauscher, *Z. Metallk*, **39,** 111 (1948).
63. M. E. Fine and N. T. Kenny, *J. Metals* **4,** 151 (1952).
64. W. C. Overton and J. Gaffney, *Phys. Rev.* **98,** 969 (1955).
65. N. Dudzinski, *J. Inst. Metals* **81,** 49 (1952-3).
66. A. Kelly, A. Lassila and S. Sato, *Phil. Mag.* **4,** 1260 (1959).
67. W. Köster and H. Franz, *Met. Revs.* **6,** 1 (1961).
68. E. Orowan, *Z. Phys.* **89,** 605, 614, 634 (1934).
69. M. Polanyi, *Z. Phys.* **89,** 660 (1934).
70. G. I. Taylor, *Proc. Roy. Soc.* **A145,** 613 (1934).
71. F. C. Frank and W. T. Read, *Phys. Rev.* **79,** 722 (1950).
72. A. Seeger, "Mechanism of Glide and Work Hardening in Face-Centred Cubic and Hexagonal Close-Packed Metals," in *Dislocations and Mechanical Properties of Crystals*, J. Fisher *et al.* (Eds.), John Wiley and Sons, New York (1957).
73. W. M. Lomer, *Phil. Mag.* **42,** 1327 (1951).
74. A. H. Cottrell, *Phil. Mag.* **43,** 645 (1952).
75. E. O. Hall, *Proc. Phys. Soc.* **64B,** 747 (1951).
76. N. J. Petch, *J. Iron Steel Inst.* **173,** 25 (1953).
77. R. Von Mises, *Z. Angew. Math. Mech.* **8,** 161 (1928).
78. T. H. Blewitt, R. R. Coltman, and J. K. Redman, *J. Appl. Phys.* **28,** 651 (1957).
79. P. Hassen, *Phil. Mag.* **3,** 384 (1958).
80. A. H. Cottrell and R. J. Stokes, *Proc. Roy. Soc.* **A233,** 17 (1955).
81. R. P. Carrekar and W. R. Hibbard, *Acta Met.* **1,** 654 (1953).
82. H. Conrad, *J. Metals* **16,** 582 (1964).
83. Z. S. Basinski, *Phil. Mag.* **4,** 393 (1959).
84. G. Y. Chin, W. F. Hosford, and W. A. Backofen, *Trans. Met. Soc. AIME* **230,** 437 (1964).
85. B. A. Hands and H. M. Rosenberg, *Acta Met.* **17,** 455 (1969).
86. D. Hull and H. M. Rosenberg, *Phil. Mag.* **4,** 303 (1959).
87. I. A. Gindin, B. G. Lazerev, Ya. D. Starodubov, and M. B. Lazareva, *Phys. Metals Metallog.* **11**(1), 49 (1961).
88. I. A. Gindin, B. G. Lazerev, and Ya. D. Starodubov, *Phys. Metals Metallog.* **10**(3), 153 (1960).
89. D. Hull and H. M. Rosenberg, *Cryogenics* **1,** 27 (1960).
90. T. E. Mitchell, R. A. Foxall and P. B. Hirsch, *Phil. Mag.* **8,** 1895 (1963).

91. R. L. Smith and J. L. Rutherford, *Trans. AIME* **209,** 857 (1957).
92. J. W. Christian and T. L. Altshuler, *Acta Met.* **14,** 903 (1966).
93. E. Anderson, D. Law, W. King and J. Spreadborough, *Trans. Met. Soc. AIME* **242,** 115 (1968).
94. R. M. Codd and N. J. Petch, *Phil. Mag.* **5,** 30 (1960).
95. J. W. Christian and B. C. Masters, *Proc. Roy. Soc.* **A281,** 223, 240 (1964).
96. R. W. Thompson and O. N. Carlson, *J. Less Common Metals* **9,** 354 (1965).
97. E. A. Loria, *J. Less Common Metals* **10,** 296 (1966).
98. I. A. Gindin and Ya. D. Starodubov, *Phys. Met. Metallog.* **15**(5), 80 (1963).
99. C. N. Reid, A. Gilbert, and G. T. Hahn, *Acta Met.* **14,** 975 (1966).
100. D. K. Bowen, J. W. Christian, and G. Taylor, *Can. J. Phys.* **45,** 903 (1967).
101. S. S. Lau, S. Ranji, A. K. Mukherjee, G. Thomas, and J. E. Dorn, *Acta Met.* **15,** 237 (1967).
102. T. E. Mitchell and W. A. Spitzig, *Acta Met.* **13,** 1169 (1965).
103. J. H. Bechtold, *Acta Met.* **3,** 249 (1955).
104. R. J. Arsenault, *Acta Met.* **14,** 831 (1966).
105. T. E. Mitchell and P. L. Raffo, *Can. J. Phys.* **45,** 1047 (1967).
106. C. N. Reid, A. Gilbert and G. T. Hahn, *Trans. Met. Soc. AIME* **239,** 467 (1967).
107. A. Lawley and H. L. Gaigher, *Phil. Mag.* **10,** 15 (1964).
108. C. N. Reid, A. Gilbert, and G. T. Hahn, *Trans. Met. Soc. AIME* **236,** 1024 (1966).
109. D. F. Stein, *Can. J. Phys.* **45,** 1063 (1967).
110. P. Beardmore and D. Hull, *J. Less Common Metals* **9,** 168 (1965).
111. A. S. Argon and S. R. Maloof, *Acta Met.* **14,** 146 (1966).
112. J. C. Bilello, *Phil. Mag.* **19,** 583 (1969).
113. Z. S. Basinski and J. W. Christian, *Aust. J. Phys.* **13,** 299 (1960).
114. D. S. Tomalin and D. F. Stein, *Trans. Met. Soc. AIME* **233,** 2056 (1965).
115. D. F. Stein and J. R. Low, *Acta Met.* **14,** 1183 (1966).
116. T. L. Altshuler and J. W. Christian, *Phil. Trans. Roy. Soc.* **A261,** 235 (1967).
117. A. S. Keh and Y. Nakada, *Can. J. Phys.* **45,** 1101 (1967).
118. D. F. Stein, *Acta Met.* **14,** 99 (1966).
119. H. Conrad, *Acta Met.* **15,** 147 (1967).
120. D. F. Stein, *Acta Met.* **15,** 150 (1967).
121. R. L. Fleischer, *Acta Met.* **15,** 1513 (1967).
122. J. E. Dorn and S. Rajnak, *Trans. AIME* **230,** 1052 (1964).
123. R. J. Arsenault, *Acta Met.* **15,** 501 (1967).
124. R. L. Fleischer, *J. Appl. Phys.* **33,** 3504 (1962).
125. R. J. Arsenault, *Scripta Met.* **2,** 99, (1968).
126. R. L. Fleischer, *Scripta Met.* **2,** 113 (1968).
127. J. W. Christian, *Scripta Met.* **2,** 569 (1968).
128. R. L. Fleischer, *Scripta Met.* **2,** 573 (1968).
129. P. M. Kelly, *Scripta Met.* **3,** 149 (1969).
130. N. R. Risebrough and E. Teghtsoonian, *Can. J. Phys.* **45,** 591 (1967).
131. W. J. McG. Tegart, *Phil. Mag.* **9,** 339 (1964).
132. R. L. Bell and R. W. Cahn, *Proc. Roy. Soc.* **A239,** 494 (1957).
133. M. L. Picklesimer, *Electrochem. Technol.* **4,** 289 (1966).
134. D. H. Baldwin and R. E. Reed-Hill, *Trans. AIME* **233,** 248 (1965).
135. C. S. Barrett and T. B. Massalski, *Structure of Metals*, McGraw-Hill, London and New York (1966).
136. E. B. Kula and T. S. De Sisto, in "Behavior of Metals at Cryogenic Temperatures," Am. Soc. Testing Materials, STP 387 (1966).
137. H. Conrad, *Can. J. Phys.* **45,** 581 (1967).
138. H. Conrad, *Acta Met.* **14,** 1631 (1966).
139. Fleischer and W. R. Hibbard, in "The Relation between the Structure and Mechanical Properties of Metals," NPL Conference, H.M.S.O. London (1963), p. 261.
140. R. H. Alper, *Materials. Res. Standards* **4,** 525 (1964).

141. R. J. Arsenault, "Low-Temperature Deformation Techniques," in *Experimental Methods of Materials Research*, H. Herman (Ed.), Vol. 1, Interscience, New York (1967), p. 215.
142. J. W. Glen, *Phil. Mag.* **1**, 400 (1956).
143. N. F. Mott, *Phil. Mag.* **1**, 568 (1956).
144. A. Arko and J. Weertman, *J. Metals* **17**, 113 (1965).
145. O. Dimitrov, Conference on Properties of Very Pure Metals, C.N.R.S., Paris, (1960).

Chapter 2

Deformation Processes in Impure Metals and Alloys

Metals can be strengthened by work-hardening because the large numbers of sessile dislocations created during plastic deformation make it increasingly more difficult for mobile dislocations to move through the lattice. There is, however, a limit to the amount of strengthening which can be achieved by work-hardening and, as solute atoms also produce very efficient obstacles to dislocation motion, solution-hardening is usually a more effective method of increasing a metal's resistance to plastic deformation. In some alloy systems, solute atoms also extend the temperature range over which a certain crystal structure is stable, a particularly relevant example being the stabilization by nickel of the high-temperature fcc (γ) phase of iron to produce austenitic stainless steel.

In many alloys, solid solubility is limited in extent and this restricts the amount of solution-hardening possible. There are, however, a number of systems in which the solubility limit increases with temperature, thus allowing excess solute to be dissolved at high temperatures and then subsequently precipitated at a lower temperature. These hard precipitates, and the elastic distortion they produce in the lattice, are very effective barriers to dislocation movement, and very-high-strength alloys can be obtained by the technique of precipitation hardening.

The distinction between a precipitate and a second-phase particle is one of degree rather than substance, but we will consider an alloy which has a microstructure consisting of two or more resolvable phases to be the third basic type of alloy. In the following chapter, each of these three main types of alloy will be considered both from a fundamental point of view and also with regard to its use at cryogenic temperatures.

In most metals, yield and plastic deformation are continuous processes, but in some circumstances, yield can occur sharply. Serrated stress–strain curves are also found under certain testing conditions and these two phenomena are considered in the final section of this chapter.

2.1. YIELD AND FLOW IN SOLUTION-HARDENED SINGLE-PHASE ALLOYS

The addition of solutes to a metal has two main effects on its mechanical properties: it raises its yield stress and intensifies or prolongs the subsequent strain-hardening. The extent of these changes depends principally on the particular alloy system under consideration, the concentration of solute atoms, and the deformation temperature. Much basic information has been obtained from studies using single crystals with carefully controlled compositions, and it is possible to extrapolate many of the trends shown by these simple alloys to cover the more complex alloys commonly used in cryogenic applications.

2.1.1. Dislocation–Solute Interactions

An edge dislocation may be represented simply as an extra half-plane of lattice points inserted above the slip plane of a crystal. This extra half-plane distorts the lattice and produces an elastic strain field around the dislocation which is compressive above the slip plane and tensile beneath it. If a small substitutional impurity replaces one of the atoms in the compressive region, or a large substitutional impurity replaces an atom in the tensile region, the lattice distortion is reduced. This elastic interaction between a solute atom and an edge dislocation lowers the strain energy of the dislocation and makes it more stable. The dislocation is said to be "pinned" and it is then more difficult to move through the crystal.

Interstitial impurity atoms are also able to pin edge dislocations, their minimum energy configuration being in the tensile region near the dislocation core. In metals with a body-centered-cubic lattice structure, the common small impurity atoms, carbon, nitrogen, oxygen, and hydrogen, occupy interstitial sites at the face centers and edges of the unit cube. This leads to a tetragonal distortion of the lattice and the creation of both shear and hydrostatic stress systems. In this case, it is possible for both screw and edge dislocations to interact strongly with the interstitial impurity atoms and become pinned by them. In face-centered-cubic metals, both substitutional and interstitial atoms produce symmetrical distortions and hence can only interact with edge, not screw dislocations. Impurity pinning is thus relatively weak in these metals.

As we shall see in section 2.4, sharp yield points are found in metals and alloys which have strong dislocation–solute interactions. They are found in bcc metals with interstitial concentrations of a few tens of ppm but are absent in dilute fcc alloys, only becoming detectable when the solute concentration increases to many per cent, thus confirming that dislocations are more strongly pinned by impurities in bcc metals than in fcc metals.

2.1.2. The Effect of Solutes on the Yield Stress

It is well known that the addition of a solute raises the yield stress of a pure metal. In alloy systems showing complete solid solubility, the strengthening effect reaches a maximum at approximately equiatomic proportions, while for dilute alloys, the yield stress increases almost linearly with solute concentration. One of the prerequisites of extensive solid solubility in an alloy system is that the lattice distortion caused by the solute atom is small and thus the hardening rate, $\partial\sigma_y/\partial c$, is low. Solutes which have large size–valency differences relative to the solvent atoms distort the lattice much more and are soluble to a much smaller extent. The increased lattice distortion leads, however, to a much higher hardening rate, which can be one or two orders of magnitude larger than that shown by systems having extensive solubility.

A linear relationship between yield stress and concentration is obeyed for both single crystals and polycrystals and in Fig. 2.1 it is shown for copper polycrystals. Tin, with its large atomic size and high valency, gives a high hardening rate, but less than 1% is completely soluble in copper to form α-bronze. Up to 39 wt% zinc can go into solution in copper and form α-brass and its strengthening effect is correspondingly lower. The

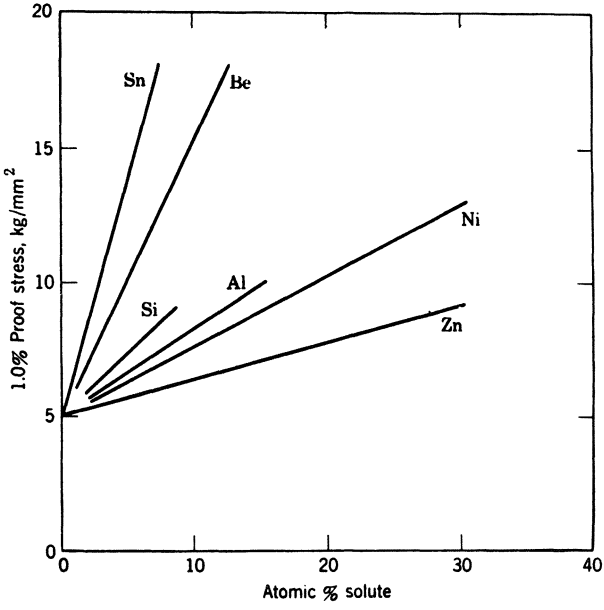

Fig. 2.1. Effect of solute concentration on the 1.0% proof stress of copper polycrystals at room temperature. Hardening is due to differences in size, valency, and crystal structure between solute and solvent atoms (after French and Hibbard[54]).

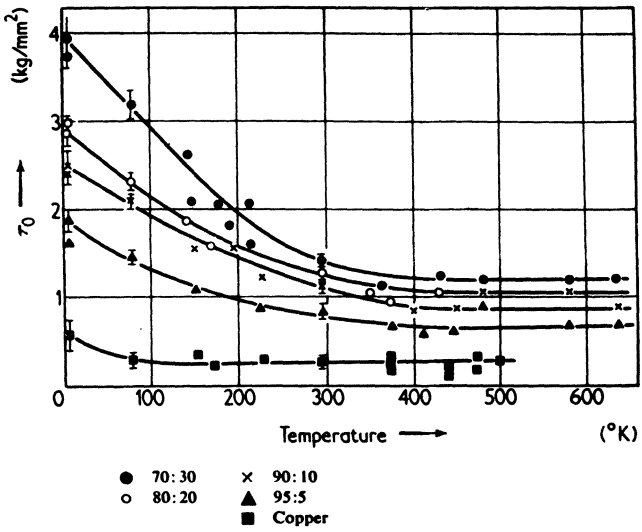

Fig. 2.2. Effect of solute concentration on the temperature dependence of the yield stress in a series of copper–zinc alloy crystals (after Mitchell[11]).

rate of change of yield strength with composition, $\partial\sigma_y/\partial c$, depends on three principal factors: the relative size of the solvent and solute atoms, the difference in their elastic moduli, and the electron/atom ratio of the alloy. Quantitative relationships between $\partial\sigma_y/\partial c$ and parameters describing each of these three factors have been shown to exist for a number of alloy systems, and in some alloys, size or modulus effects seem to be dominant, while in others, the electron/atom ratio is clearly more significant. In complex systems, all three effects contribute to the strength of the alloy.

The yield stresses of pure fcc metals are relatively unaffected by changes in termperature, but solutes, especially if present in high concentrations, increase the temperature dependence of the yield stress in fcc alloys. This is shown in Fig. 2.2 for single crystals of copper–zinc alloys,[11] similar results being obtained for polycrystals.

In section 1.4, the athermal component of the flow stress in pure fcc metals, τ_G, was shown to be greater than the thermal component τ^*. The enhanced temperature dependence of the critical resolved shear stress in the alloys shown in Fig. 2.2 suggests that the presence of solutes increases the relative importance of τ^*. As the thermal component of the flow stress is associated with the resistance to dislocation movement provided by small obstacles, which can be overcome with the aid of thermal fluctuations, it appears that, at higher solute concentration, thermal fluctuations are less able to play a significant part in helping dislocations overcome these barriers to their motion.

In section 1.5, we saw that bcc metals are characterized by a large thermal component of flow stress and that there is still no general agreement on whether this is due to an intrinsic property of the bcc lattice structure or to very small concentrations of interstitial impurities. The concentrations involved are very small indeed. Stein and Low[12] have observed "that at all temperatures the yield stress of iron crystals increases with increasing carbon content, as much or more, in the range from 5×10^{-3} to 0.9 ppm as in the range 0.9–40 ppm." Quantitatively, they find that the yield stress is proportional to the square root of the carbon concentration up to the normal solubility limit of a few hundred ppm.

Solution-hardening is not used as a practical method of strengthening bcc metals and, as was pointed out in section 1.5, they are little used at low temperatures because of their brittle behavior.

The yield stresses of pure hcp metals are in general more temperature-dependent than those of the fcc metals, and the addition of solutes further increases this tendency. Both magnesium and titanium can be hardened by elements whose atoms go into substitutional solid solution. Interstitial impurities in titanium behave, however, in many ways like those in bcc metals in that they increase the strength but also cause serious embrittlement. For this reason, titanium alloys used at low temperatures are specified as being in the extra low interstitial (ELI) condition.

2.1.3. The Effect of Solutes on Strain-Hardening

The effect of solutes on the various stages of strain-hardening is shown in Fig. 2.3(a) for a series of nickel–cobalt single crystals deformed at room temperature.[13] The critical resolved shear stress increases with concentration, as does the extent of stage I hardening, while the strain hardening rate θ_{I} is virtually unaltered, and thus the onset of stage II occurs at higher stresses.

A similar delay in the transition to stage II hardening was shown by the pure metal crystals of Fig. 1.9 and was caused by a decrease in testing temperature. The dislocation intersection model outlined in section 1.4 to explain this effect of testing temperature can also be used to describe the effect of alloying. It is assumed that easy glide ceases when the stress needed to move dislocations down the primary slip plane exceeds the critical resolved shear stress on a secondary slip system. In alloys, or in pure metals at low temperatures, greater stresses are required to initiate secondary slip. As neither alloying nor a decrease in temperature significantly alter the strain hardening rate θ_{I}, stage I must increase in extent in order that the flow stress can be raised to its critical value.

The correspondence between the effects of alloying and decreasing the temperature also holds for the second and third stages of deformation. Stage III starts when recovery mechanisms like cross-slip allow disloca-

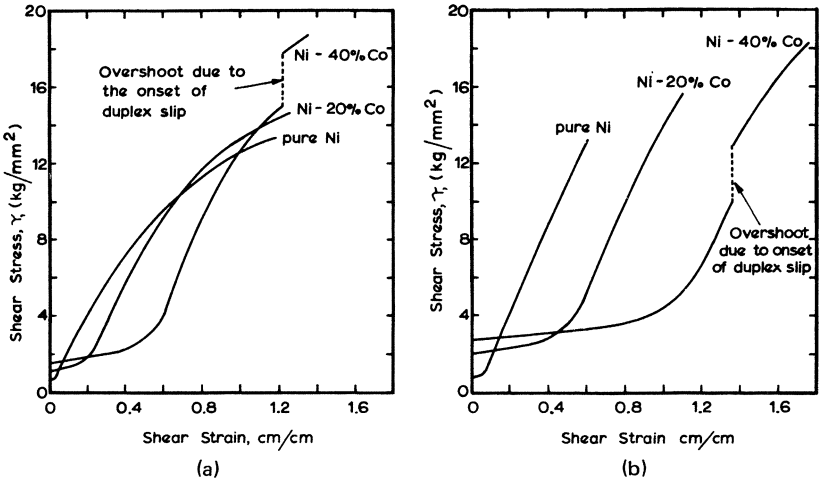

Fig. 2.3. Shear stress–strain curves for a series of nickel–cobalt alloy single crystals measured (a) at room temperature and (b) at 77°K (after Pfaff[13]).

tions to bypass the barriers to their motion responsible for the high strain-hardening rate of stage II. Both the presence of solute atoms and a decrease in temperature make it difficult for cross-slip to occur, and thus the onset of stage III is delayed to higher stresses. Furthermore, the strain-hardening rate θ_{III} is higher and falls off less rapidly at high strains.

The combination of decrease in temperature and alloying is shown in Fig. 2.3(b) for the same series of crystals tested at 77°K. To a first approximation, they are additive and the onset of stages II and III have been delayed to even higher stresses. A more detailed analysis shows, however, that a given decrease in temperature has a weaker effect in an alloy than in a pure metal. It would thus appear that, the more cross-slip is inhibited by the presence of solutes, the less scope is there for a further restriction by a decrease in temperature.

In section 1.3, equation (1.9), it was shown that the majority of the plastic deformation in polycrystals occurs under conditions which correspond to stage III in single crystals. We have just seen that solutes inhibit cross-slip and increase the strain hardening rate θ_{III} of alloyed single crystals. It thus follows that the strain-hardening rates of alloyed polycrystals should be higher than those of the pure metal and that, the more concentrated the alloy, the higher the strain-hardening rate at any given strain. Furthermore, these higher hardening rates are maintained until greater strains and there is a consequent increase in the uniform elongation. Finally, the combination of an intensified rate of strain-hardening with an increase in its extent results in a higher ultimate tensile stress.

2.1.4. Single-Phase, Solution-Hardened Alloys Used in Cryogenic Applications

Most solution-hardened alloys used at low temperature are based on one of the following metals: copper, nickel, aluminum, iron, and titanium. We will now consider briefly the mechanical properties of some of these alloys to illustrate the effects of solute concentration and temperature outlined in the previous paragraphs.

2.1.4.1. ***Copper-Based Alloys.*** The low-temperature mechanical properties of copper and many copper-based alloys have recently been compiled and reviewed by Reed and Mikesell.[2,14] These publications cover most available brasses, bronzes, and cupronickels, the only major alloy group omitted being the beryllium coppers, and data for these may be found in references 3 and 4.

Up to 39 wt% zinc can go into solution in copper at room temperature to form fcc α-brass. A duplex α–β structure is formed at compositions between 39 and 46.6%, while the bcc β-phase is stable for zinc concentrations between 46.6 and 50.6%: β-brass is considerably harder than α-brass but, unlike most alloys with a bcc crystal structure, it remains ductile down to the lowest temperatures because it is an electron compound type of solid solution.

Most brasses used at low temperatures are, however, α-phase. In Fig. 2.4, the stress-strain curves of two alloys, Cu–10Zn (commercial bronze) and Cu–28Zn 1Sn (admiralty brass) are compared with those of O.F.H.C. copper at room temperature and 20°K. (The 1% tin is added to the zinc in admiralty brass to improve its corrosion resistance and does not change

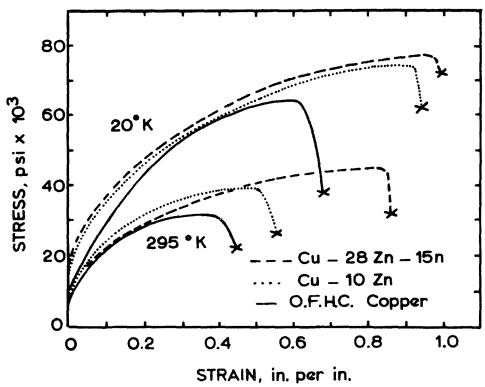

Fig. 2.4. Stress-strain curves for O.F.H.C. copper, commercial bronze, and admiralty brass measured at 20°K and room temperature (data from Reed and Mikesell[2]).

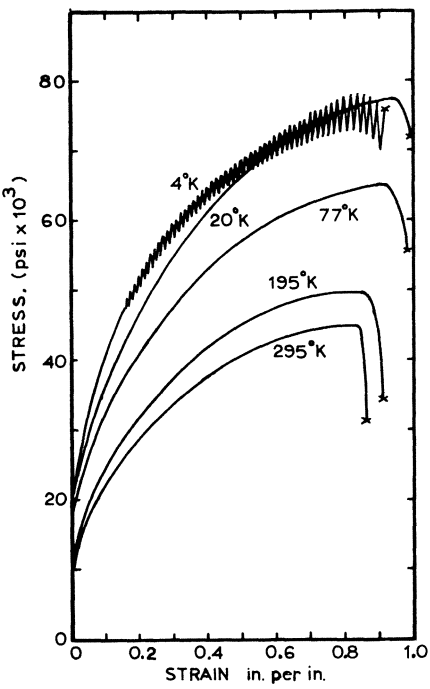

Fig. 2.5. Stress-strain curves for annealed admiraly brass, Cu-28Zn 1Sn, measured at temperatures down to 4°K (Reed and Mikesell[2]).

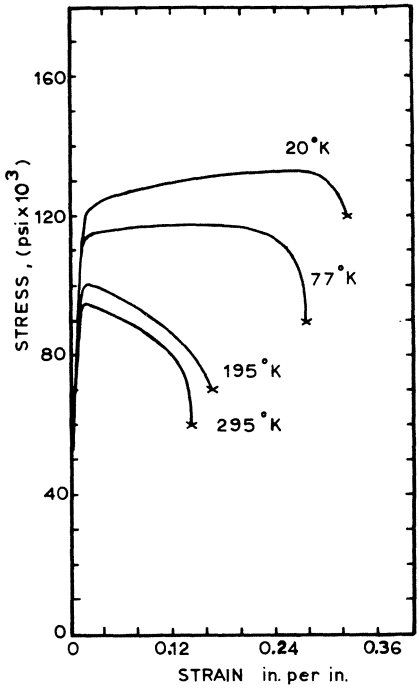

Fig. 2.6. Stress-strain curves for cold-drawn cartridge brass, Cu-30Zn, measured at temperatures down to 4°K (Reed and Mikesell[2]).

its mechanical properties significantly enough to affect the comparisons made in Fig. 2.4.)

The effect of solute concentration on the extent of strain-hardening is shown clearly by both the room-temperature and 20°K curves. In both cases, the uniform elongation and tensile stress are greatest for the most concentrated alloy. The influence of solute concentration on the rate of strain-hardening is not demonstrated quite so well, but the general trend is clearly visible. Apart from the initial parts of the room-temperature curve for the admiralty brass and the 20°K curve for O.F.H.C. copper, the strain rate at a given strain increases with solute concentration.

We saw in Fig. 2.2 that, for a series of copper–zinc single crystals, the temperature dependence of the yield stress increased with alloy concentration. An indication of this effect is just visible in the polycrystals of Fig. 2.4. Whereas it is impossible to detect the effect of concentration on the yield stress at room temperature, it can be seen that the alloys have higher yield stresses than the pure metal at 20°K.

The effect of temperature on the yield and plastic deformation of

admiralty brass is shown in Fig. 2.5. The yield stress rises slightly as the temperature decreases, but not nearly to the same extent as does the tensile stress. The alloy is extremely ductile at room temperature, becoming even more so at low temperatures. The 4°K curve shows a series of serrations at strains greater than about 15%; this phenomenon is discussed at some length in section 2.4. One effect of this discontinuous mode of plastic deformation is to cause slight reductions in the tensile stress and uniform elongation compared with the 20°K values.

Solution-hardening is only a moderately efficient method of increasing the strength of a metal, and it is quite common for additional strength to be obtained by cold-working. In Fig. 2.6, a series of stress–strain curves are shown for cartridge brass (Cu–30Zn) that has been cold-drawn to the "$\frac{3}{4}$-hard" condition. It can be seen that a considerable increase in yield strength has been obtained but that this has taken place at the expense of ductility. At room temperature, for instance, yield is followed immediately by the formation of a neck and plastic deformation takes place under a decreasing applied stress. Not until the temperature drops to 76°K is the material able to strain-harden sufficiently for significant amounts of uniform elongation to occur.

Alpha-brasses are widely used for cryogenic purposes, especially for the construction of laboratory cryostats and other small-scale equipment. They have moderate strengths and good ductility: they are easy to machine and can be soldered and brazed. Brass is relatively cheap and readily available in many forms, including a particularly useful series of hard-drawn, thin-walled telescopic tubes which are very convenient for cryostat construction.

Another important series of copper-based alloys are the cupronickels. Copper and nickel form a complete series of solid solutions whose strength increases with nickel content. They usually also contain 0.3–0.8% manganese as a deoxidant and up to 1% iron to improve corrosion resistance. Copper-rich alloys containing 5, 10, 20, 30, 40, and 45% Ni are available for a range of applications where their corrosion and wear-resistant properties are advantageous, such as in condenser tubes. These alloys may be hot-worked with ease and the 20 and 30% Ni alloys in particular are very malleable. It is possible to draw Cu–30% Ni cupronickel tubes down to wall thicknesses of 0.1mm, and as such they are frequently used in cryostat construction because of their low thermal conductivities (which drop rapidly with increase in nickel content). The electrical resistivity of a Cu–40% Ni alloy, known as Constantan, has the relatively high value of $\sim 45 \mu\Omega$-cm, which is almost independent of temperature. Its thermal conductivity is also low and it is widely used in wire form for heater windings and as a thermocouple element.

The nickel silvers are ternary alloys which contain 7–30% nickel, ~60–65% copper, and the remainder zinc. They are single-phase, have

quite good corrosion resistance, and are easily worked. They may be bent, deep-drawn, and spun, and one nickel–silver in particular, German silver (60–65% Cu, 20% Ni, 20–15% Zn), is widely used in cryogenic apparatus in the form of thin-walled tubes. It is, however, less reliable and more corrodable than the 70/30 cupronickel mentioned earlier and is becoming obsolete (in fact, thin-walled stainless steel tubing is usually preferred to both of these alloys). There is also another German silver alloy, the free-machining α–β type, which has a composition 47% Cu, 9% Ni, 41% Zn, and 2% Pb. As this two-phase alloy is prone to porosity troubles, it is not, however, likely to be used in thin-walled tubes for cryostat construction.

2.1.4.2. ***Nickel-Based Alloys.*** Monel (68% Ni, up to 3% Fe, 0.5–1.25% Mn, Bal Cu) is another important alloy in the copper–nickel series frequently used where low thermal conductivities are required. It is also very corrosion-resistant and, as this resistance is not affected by cold-working or heat treatment, it is widely used in the fabrication of chemical plants. However, care must be exercised during welding to avoid sulfur contamination, which can cause serious embrittlement and stress corrosion problems. It is also of particular use in rocket and other systems which use liquid fluorine. Cold-drawing raises the room-temperature proof stress of Monel 400 from ~45,000 psi to ~80,000 psi with a corresponding reduction of elongation from 40 to 20%. Still higher strengths can be obtained from the age-hardenable forms of the alloy as indicated in section 2.2.

Inconel (80–72% Ni, 14–17% Cr, 6–10% Fe) is another nickel-based alloy with a low thermal conductivity and good corrosion resistance. Its excellent oxidation resistance and good strength at temperatures up to ~750°C account for its widespread use in furnaces, exhaust manifolds, chemical plants, etc., while its single-phase fcc structure also makes it ideal for use down to the lowest temperatures. Cold-drawing increases the room-temperature proof stress of Inconel 600 from ~37,000 psi to ~150,000 psi and decreases its elongation from ~38% to 7%. Still higher strengths are obtained from the precipitation-hardened versions of this alloy.

2.1.4.3. ***Aluminum-Based Alloys.*** Aluminum and its alloys possess a number of characteristics which make them suitable for use in cryogenic applications, including low density, high toughness, good availability, and ease of fabrication. There are two main groups of aluminum alloys which receive their strength from solution-hardening: those having manganese (3000 series)* and magnesium (5000 series) as the principal alloying ele-

*See Appendix I for a brief summary of the standard temper designation system for aluminum alloys.

ments. The 3000 series alloys contain between 1.0 and 1.5% manganese and up to 0.7% silicon and iron. The 3003 alloy is most commonly used for low-temperature applications such as tube plate heat exchangers, as it contains little or no copper or magnesium and can thus be brazed in molten salt baths using an aluminum–silicon brazing alloy. It is also readily welded. In the annealed condition, its yield and tensile strengths are only about 20%–50% higher than those of the commercially pure 1100 series aluminum and it is widely used for tubes and other fabricated components. Additional strength may be achieved by cold-working, but subsequent welding lowers the strength of the heat-affected zone to that of the annealed state.

Considerably higher strengths can be obtained from the 5000 series alloys, whose major alloying addition is up to 5.5% Mg: minor alloying additions whose concentration varies from alloy to alloy include manganese, silicon, iron, and zinc. These alloys are weldable if the correct fillers and welding techniques are used and have the additional advantage of requiring no post-weld heat treatment. In general, weld strengths are high, reaching 42,000 psi for type 5456, which is widely used for the construction of large storage tanks, transporters, heat exchangers, and other items of cryogenic plant. Higher strengths are often attained by cold-working, but this is usually accompanied by a reduction in their ductility and toughness (see, for example, Fig. 2.15).

Aluminum alloys will be considered further in section 2.2, which covers precipitation-hardened types.

2.1.5. Alloy Stabilized High-Temperature Phases

In a number of important alloy systems, solute atoms not only strengthen the metal but also have a strong influence on the temperature range over which a particular crystal structure is stable. There are two main reasons for this effect: (a) the addition of solutes can raise or lower the temperature at which the relevant allotropic or eutectoid phase transformation takes place; and (b) large solute atoms diffuse so slowly through the solvent metal that the reaction rate is lowered and the transformation becomes very sluggish.

In some systems, the transformation temperature is lowered so much that, when it is reached, the transformation is unable to occur and the high-temperature phase is stabilized. There are two alloy systems of particular interest for cryogenic applications which belong in this category: the austenitic iron-based alloys and the stabilized titanium alloys.

2.1.5.1. ***Iron-Based Alloys.*** At 910°C, pure iron undergoes an allotropic transformation from the high-temperature fcc γ-phase (austenite)

to the low-temperature bcc α-phase (ferrite). The maximum solubility of carbon in the bcc ferrite is 0.02 wt%, whereas up to 2.06 wt% is soluble in the fcc austenite. An alloy containing carbon in concentrations between these limits undergoes a eutectoid phase transformation at about 723°C (eutectoid composition 0.8 wt% carbon), in which austenite transforms to a binary mixture of ferrite containing 0.02% carbon and the hard intermetallic compound Fe_3C, cementite.

Some alloying elements, including chromium, tungsten, vanadium, and silicon, stabilize the bcc ferrite by raising the transformation temperatures. More important from a cryogenic point of view is that other elements, in particular manganese, nickel, cobalt, and copper, lower the transformation temperatures and tend to stabilize the fcc austenite. As nickel is added to steel, the eutectoid temperature is lowered, with a large drop occurring at about 8% Ni, while more than ~29% Ni depresses the transformation to below room temperature. At these temperatures, diffusion rates are negligible but transformation can still take place via the diffusionless shear (martensite) mechanism, this being the dominant mechanism over the composition range 9–33% Ni. At higher nickel contents (>42%), the high-temperature γ-phase is completely stabilized.

A high-nickel alloy widely used at cryogenic temperatures contains 36% nickel, 0.2% carbon, and 0.5% manganese and is known as Nilo 36 or Invar. The expansion coefficient of this alloy is almost zero between 0 and 100°C, while its linear thermal contraction between 300 and 0°K is about one-sixth that of stainless steel. It is thus widely used for transfer lines and pipework where contraction stresses have to be kept to a minimum. It has a fully stabilized austenitic structure with moderately high strength and good ductility, both of which improve at low temperatures. Additional strength can be achieved by cold-work with little decrease in ductility. Some welding problems initially encountered with this alloy were found to be due to the formation in the weld and heat-affected zones of low-melting point eutectics containing sulfur and selenium. This trouble has now been overcome by using fillers containing 3% manganese and 1% titanium, which preferentially combine with these dissolved gases and contaminants to give sound, ductile weld deposits.[15]

One of the most important classes of alloy used at very low temperatures is the 300 series austenitic chromium–nickel stainless steels. These steels were originally developed for their excellent corrosion resistance and contain a range of minor alloying additions which increase their scaling resistance, or improve machinability or weldability, etc. All of the steels in this series are nominally austenitic at room temperature, but their stability at lower temperatures depends on their nickel content and other factors which vary from alloy to alloy.

Type 310 stainless contains 24–26% Cr, 19–22% Ni, 2% Mn, 1.5%

Si, and up to 0.25% C. Its nickel content is high enough to ensure complete stability of the austenite phase down to the lowest temperatures even during plastic deformation. A series of stress–strain curves for annealed type 310 stainless is shown[20] in Fig. 2.7 for the temperature range 300–4°K. At normal strain rates, the 300, 195, 76, and 20°K curves all show the usual sequence of a gradual yield followed by work-hardening up to the ultimate tensile stress and terminated by a more or less ductile failure. The serrations shown in the normal 4°K curve, and for the high strain rate at 20°K, are thought to be due to adiabatic heating and are discussed further in section 2.4.2.

The effects of temperature on the yield and tensile strengths and the percentage elongation of annealed type 310 are shown in Fig. 2.8. The yield stress increases considerably on cooling from 300 to 4°K, as would be expected for a solution-hardened fcc alloy. Similarly, the even greater increase in tensile stress follows the pattern set by pure fcc metals. The percentage elongation has a high value at room temperature and shows a slight decrease below ~80°K.

One possible disadvantage of this material is its relatively low yield

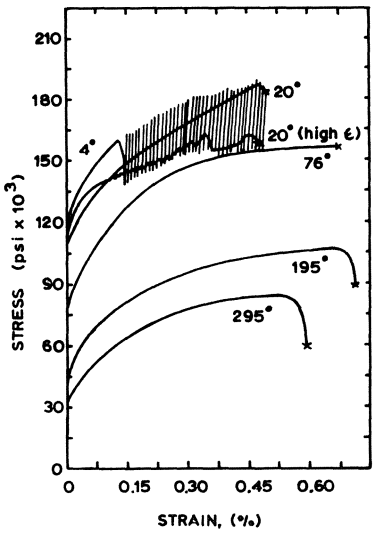

Fig. 2.7. Stress–strain curves for type 310 stainless steel measured at temperatures down to 4°K (Warren and Reed[3]).

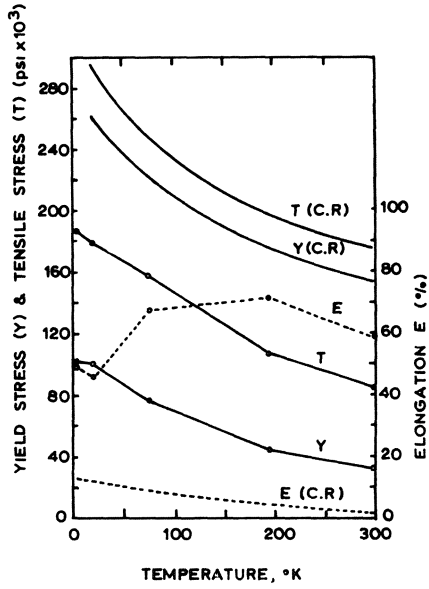

Fig. 2.8. Effect of temperature on the yield strength, tensile strength, and percentage elongation of type 310 stainless steel in the annealed and cold-rolled conditions (after Warren and Reed[3]).

stress in the annealed condition at room temperature. Accordingly, it is often cold-worked for additional strength and, as can be seen from Fig. 2.8, 75% cold-rolling increases the room-temperature yield stress from ~30,000 psi to ~80,000 psi. This increase is, as usual, obtained at the expense of the ductility, which is reduced to a few per cent at room temperature and to just over 10% at 20°K. A decrease in temperature causes a further rise in yield stress and an even greater increase in tensile stress.

The fully stabilized type 310 stainless steels are eminently suitable for use at very low temperatures because of their reliability, availability, ease of formation, and weldability. The liquid-hydrogen tanks of the Centaur missile were, for example, fabricated from 75% cold-rolled type 310 sheet. Fully stabilized austenitic stainless steels are also widely used in cryogenic equipment which has to operate in a magnetic field, e.g., superconducting magnet formers and bubble chamber bodies. Special high-nickel-content casting alloys such as Kromarc-55 and modified CK 20 have been developed recently for bubble chamber castings, but these alloys are not, as yet, readily available in the wrought form. If very high strengths are required the precipitation-hardenable A-286 alloy can also be used as it too is fully stabilized (see section 2.2).

The nickel contents of most other 300 series stainless steels are too low to ensure complete stability of the austenite, and transformation to martensite occurs under certain conditions. The final transformation product is the hard, relatively brittle, body-centered cubic α' phase which is ferromagnetic (the fcc austenite is paramagnetic) and this enables the degree of $\gamma \rightarrow \alpha'$ transformation to be obtained from direct or indirect measurements of the magnetic permeability. In Table II, the intrinsic permeabilities of a number of 300 series steels both after cold-work at room temperature and cycling to 77°K are correlated with their compositions. (The larger the intrinsic permeability, the higher the α' content).

Table II. The Stability of 300 Series Stainless Steels

Number	Intrinsic permeability at 300°K (μ=1) (H=200 G)		Composition, %			Tensile strength after CR, psi
	After CR at 300°K[17,19,55]	After cycling to 77°K[18,19,55]	Ni	Cr	Other major additions	
310	0.005 (64% CR)	0.005	20.7	24.3	—	192,600
316	0.01 (84% CR)	0.004–0.01	13.4	17.5	2.4 Mo	194,100
347	3.12 (90% CR)	0.004–0.01	10.7	18.4	0.95 Nb	216,500
321	8.4 (70% CR)	0.004–0.01	10.3	18.3	0.68 Ti	201,300
304	3.7 (84% CR)	1	10.7[a]	19.0	—	302,800
301	18.0 (55% CR)	(Large)	7.8	17.6	—	222,400

[a] The AISI composition limits for nickel in type 304 are 8–12%. This is a large range and most commercial alloys have nickel contents of between 8.5 and 10%. The value of 10.7% quoted is uncommonly high.

As we saw earlier, type 310 is stable under all conditions. Type 316 shows only minimal evidence of transformation during cold-working at room temperature or cycling to 77°K, but does transform during deformation at low temperatures. Types 347 and 321 show little spontaneous transformation on cycling to 77°K but appreciable amounts of martensite are formed during cold-working at room temperature and this is even more pronounced after deformation at low temperature.

The behavior of a number of 304 and 304L alloys have been studied in detail by Gunter and Reed[20,21,52] and it is worth considering these alloys in a little more detail. All alloys show considerable transformation after cold-working at room temperature; the lower the nickel content, the greater the amount of martensite formed by a given degree of cold-work. A much greater variation is, however, found in their stability with respect to cycling between 300 and 77°K and this can be correlated with small variations in the carbon and nitrogen contents. These elements tend to stabilize the austenitic phase and hence 304 alloys with high carbon and nitrogen contents are less likely to transform spontaneously to martensite than those with low carbon and nitrogen contents.

More detailed study of the martensite transformation of austenitic stainless steels has shown that there is an intermediate hexagonal-close-packed ε phase formed prior to the body-centered α' phase. Careful metallographic and X-ray analysis has enabled the amounts of ε and α' present to be correlated with the characteristic features of the stress–strain curves of these metals. In Figs. 2.9 and 2.10, the stress–strain curves of two different type 304 alloys are shown for temperatures at and below 300°K. Figure 2.9 is for an alloy with the relatively high carbon content of 0.055%, which shows little spontaneous transformation on cycling to 77°K. Figure 2.10 is for a 304L alloy containing 0.017% carbon, which does transform spontaneously on cycling to 77°K and which had been so treated as to contain 7.5% α' prior to testing at the various temperatures shown.

Examination of the 76°K curve of Fig. 2.9 shows that yield is followed by a region of low strain-hardening which lasts up to ~8% strain. During this deformation, there is considerable $\gamma \rightarrow \varepsilon$ transformation, with up to 36% ε having been found at a strain of 8%. At higher strains, the rate of work-hardening increases considerably and this corresponds to the onset of significant transformation to the harder α' phase. In contrast, the 76°K curve of Fig. 2.10 shows that yield is followed immediately by a high rate of work-hardening. This alloy already contained 7.5% spontaneous α' prior to the test and plastic deformation of 76°K rapidly increases the α' content.

The high work-hardening rates of these metastable stainless steels at and below 76°K are thus the result of a stress-induced martensitic transformation. Further confirmation of this hypothesis may be obtained from

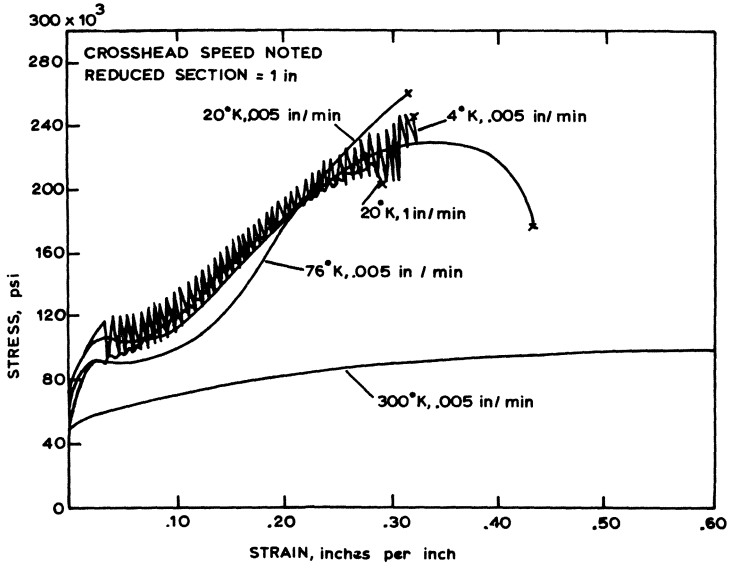

Fig. 2.9. Stress-strain curves for annealed type 304-3 stainless steel sheet tested at temperature down to 4°K. Little or no spontaneous transformation occurs on cooling this alloy (Gunter and Reed[52]).

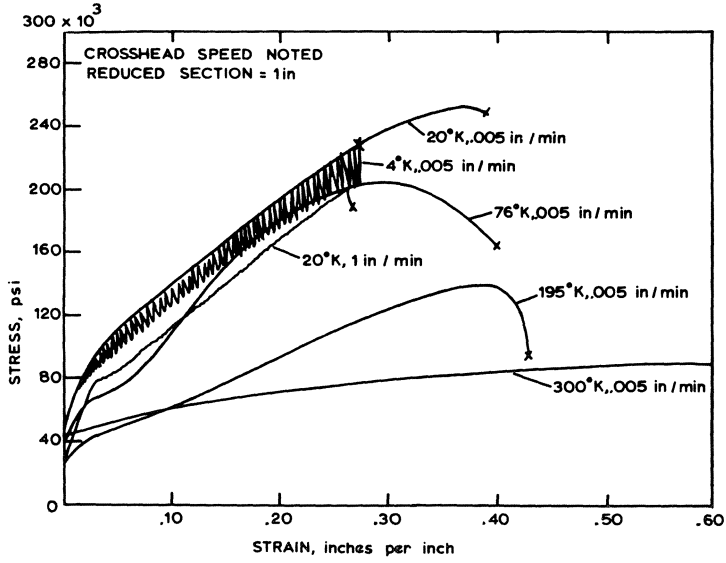

Fig. 2.10. Stress-strain curves for type 304-L stainless steel which had been cycled to produce 7.5% α' prior to tensile testing (Gunter and Reed[52]).

a comparison of the work-hardening rates at 76°K of the metastable type 304 alloys of Figs. 2.9 and 2.10 and the stable type 310 of Fig. 2.7. Comparing these rates at a convenient strain of 18% shows that the 304 alloys work-harden between three and seven times more rapidly than the type 310.

Type 301 stainless, with a composition of 16–18% chromium and 6–8% nickel, has the lowest nickel content of the 300 series steels and is the least stable. A large amount of $\gamma \rightarrow \alpha'$ transformation occurs during deformation at room temperature and a correspondingly high work-hardening rate is obtained.

The presence of large quantities of α' in the metastable 300 series steels can thus result in a considerable increase in their strength compared with that of the stable 310 alloy and this is obviously of interest in applications where high strength/weight ratios are required. Measurements of the notched-tensile strength of these alloys has, however, shown a serious decrease in this property below 76°K in those alloys that have a high percentage of the intermediate ε phase formed at low strains. It is probable that this is caused by the relative ease with which cracks can be nucleated in the hexagonal-close-packed ε phase. Alloys that have been extensively cold-worked prior to deformation and which therefore contain a large proportion of α' do not show this decrease in notched-tensile strength and neither do the stable 310 type alloys.

It may thus be concluded that the martensitic transformation in austenitic stainless steels has a considerable influence on their mechanical properties at low temperatures. Before using these materials, it is important to consider the possible effects of spontaneous or stress-induced martensitic transformation on the material in its proposed application. Not only are the strength and toughness liable to be affected but, as we saw earlier, the magnetic permeability will increase considerably if martensite is present, a factor of obvious importance in, for example, bubble chamber construction, where high magentic fields are present. Furthermore, the $\gamma \rightarrow \alpha'$ transformation results in dimensional changes which could adversely affect the performance of, for example, a low-temperature expansion turbine, which has a very small tolerance on its bearing clearances. In this case, a nontransforming steel should be used or, if this is not possible, the part should be cycled to, and held at, low temperatures long enough for transformation to occur prior to final machining.

We saw earlier that austenite stability was improved if the nitrogen content of type 304 stainless was increased. There is also a considerable increase in yield strength to be gained by relatively small additions of nitrogen to these austenitic stainless steels and this factor has been exploited in the recent development of the "Hi-proof" grades of 304, 316, and 347. These steels contain approximately 0.2% nitrogen and have proof and

tensile stresses about 15,000 psi higher than those of the normal grades: their ductilities are slightly lower than those of the untreated grades (~35% and ~46% elongation, respectively, at ambient temperature) but this is not considered a serious drawback.

The austenitic stainless steels are in general considered to be readily weldable by both manual arc welding and by semiautomatic and fully automatic gas shielded metal arc techniques. There are, however, two main types of defect associated with welds in stainless steel, "weld decay" and "hot cracking." Weld decay occurs in some types after they have been heated within the temperature range 400–800°C and is due to the precipitation of very thin intergranular films of chromium carbides (mainly Cr_4C), an effect known as "sensitization." The carbide films are formed when carbon combines with chromium from the matrix *and so depletes the layer of metal adjacent to the grain boundary that its corrosion resistance is seriously impaired.* The heat-affected zones are typically about $\frac{1}{16}$–$\frac{1}{8}$ in. away from the edge of the weld and intercrystalline corrosion cracks can be formed in these regions if the material is exposed to certain corrosive environments. From a cryogenic viewpoint, the sensitization of stainless steels such as type 304 is particularly undesirable because the embrittling effect of the carbide film also causes the impact strength to decrease rapidly below ~100°K.

Sensitization, and hence weld decay, can be avoided if the carbon content is reduced to 0.03% (as in type 304L), but this in turn increases the probability of low-temperature martensitic transformation. Alternatively, carbide-forming elements such as titanium (in types 316 and 321) and niobium (in types 318 and 347) can be added to the alloy to combine with the excess carbon and prevent chromium depletion. Niobium stabilization is in fact becoming the preferred method because titanium-stabilized steels occasionally suffer from a defect known as "titanium streaking." This arises if there is more titanium present than is necessary to combine with the excess carbon (six times the carbon content in excess of 0.02%) and this extra titanium forms stringers which can extend through the thickness of thin-walled tubes and create leak paths. A further reason for preferring niobium for stabilization, especially in filler rods, is the high rate at which titanium is oxidized during welding. The only drawback to niobium-stabilized steels is their liability to hot-cracking during welding of thick sections, but thicknesses less than ~$\frac{3}{4}$ in. are considered satisfactory.

Hot-cracking in austenitic stainless steels takes place when contractional stresses open up cracks along the planes of weakness which occur between the large columnar crystals formed in the throat of a weld. It is avoided by using filler rods containing 2–4% molybdenum, which refines the grain structure of the weld and forms small islands of free ferrite (~6% free ferrite is considered necessary to prevent hot-cracking). Care must be taken when welding the nitrogen-bearing steels discussed earlier,

as the nitrogen can diffuse out of the parent metal during welding and, as it is an austenite stabilizer, it may render the weld metal completely austenitic and thus liable to hot-cracking. This is best avoided by ensuring that there is adequate free ferrite present in the filler metal to compensate for this effect.

Finally, if high-chromium-content austenitic or ferritic steels are heated to between 600 and 950°C for long periods, an ordered, body-centered iron–chromium structure called sigma phase can be formed. This can cause severe embrittlement at room temperature and its formation should be avoided. Further discussion of this topic is, however, outside the scope of this text, but it has been reviewed recently.[53]

As stated earlier, manganese is also a strong austenite stabilizer and the only other cryogenically important group of stainless steels are the high-manganese, chromium–nickel 200 series, typified by type 202, which contains 18% chromium, 5% nickel, and 8% manganese. A more recently developed[22] alloy with improved cryogenic toughness contains 15% manganese and has tensile and yield strengths that are 25,000 psi greater than the corresponding strengths for type 304 at room temperature. Such low-nickel-content stainless steels may become more widely used if the current nickel shortage continues or intensifies.*

2.1.5.2. ***Titanium-Based Alloys.*** Pure titanium undergoes an allotropic phase change at 882°C from the hcp α-structure to the high-temperature bcc β-structure. Some alloying elements such as aluminum and tin have greater solubilities in the α-phase than in the β-phase and tend to stabilize the α-phase by raising the temperature of the $\alpha \rightarrow \beta$ transformation. Other elements, including molybdenum, niobium, vanadium, iron, chromium, and manganese, are more soluble in the β-structure and stabilize this high-temperature phase.

Titanium alloys may be divided into three main groups: single-phase α, single-phase β, and duplex $\alpha + \beta$ types. All were initially developed for use at temperatures up to about 500°C in aerospace applications, where their combination of good resistance to corrosion and oxidation and high strength/weight ratios could justify their greater cost. The β-phase alloys are more easily worked than the α-alloys, but are generally weaker and less stable at high temperatures. For cryogenic applications, they have the additional serious drawback of undergoing a ductile/brittle transition at about 200°K and are thus rarely if ever used below room temperature.

The aluminum-stabilized α-phase alloys are relatively difficult to fabricate but are strong, stable, and oxidation resistant at high temperatures. They do not undergo a ductility transformation at low temperatures but show a very useful increase in yield strength as the temperature decreases.

* See note on page 88.

In sections 1.6 and 1.7, it was shown that hcp metals such as α-titanium are in this respect intermediate between fcc and bcc metals and are, in principle, potentially useful for low-temperature applications. As already mentioned, the main obstacle to their successful exploitation has been the difficulty in reducing the concentration of interstitials, especially oxygen, to an acceptably low value. Special extra low interstitial (E.L.I.) grades of the α-stabilized Ti–5Al–2.5Sn and the (α + β)-phase Ti–6Al–4V, which guarantee a maximum oxygen content of 0.12 wt%, are now available for cryogenic use. It has been shown[23] that oxygen concentrations above this value lead to excessive notch brittleness below 77°K, especially for severely notched specimens.

It is believed that the deleterious effect of oxygen in titanium can be attributed to the formation of an interstitial solid solution and the interactions between interstitial impurities and dislocations of both edge and screw character. In this respect, the metal is similar to typical bcc metals. Substitutional impurities, on the other hand, interact only with edge dislocations as in an fcc metal, and do not lead to embrittlement.

There is one further factor to be considered, and that is the effect of the residual iron present in the titanium sponge after reduction. Although this is usually only 0.1–0.2%, iron is a very strong β-stabilizer in titanium and so will tend to counteract the α-stabilizing effect of the aluminum and tin. As long as the iron content does not exceed 0.2%, the effects are acceptable, but higher concentrations lead to a reduction in the notched-tensile strength.

Titanium alloys are outstandingly attractive for those cryogenic applications in which the strength/weight ratio is critical. In Fig. 2.11, the yield strength/density ratio is shown as a function of temperature for a titanium alloy, a stainless steel, and an aluminum alloy. The differences between these metals are barely significant at room temperature, but the superiority of titanium is unquestionable at or below 77°K. High strength/weight ratios are required for the pressure vessels used to contain liquid or pressurized helium in rockets and space capsules, and the Ti–5Al–2.5Sn α-alloy is generally chosen for use at or below 20°K, while the Ti–6Al–4V (α + β)-alloy is considered acceptable down to 77°K.

Despite the undoubted strength of titanium alloys at low temperatures, their moderate room-temperature strengths can sometimes be a drawback, especially if the design of a component has to be based on its room-temperature strength. Attempts at improving the strength of Ti–5Al–2.5Sn alloys by cold-rolling have met with little success, there being little improvement in their room-temperature strengths while notched-tensile strengths at 20°K are seriously reduced.

Some improvement in the toughness of the single-phase alloys can

be achieved[24] by processing and fabricating in the β-field. This type of treatment is, however, much more common for the duplex ($\alpha + \beta$)-alloys, where fine-grained structures can be obtained by forging the material in the temperature range in which the α separates from the β.

2.2. YIELD AND FLOW IN PRECIPITATION-HARDENED ALLOYS

There are a large number of alloy systems in which precipitation-hardening is possible and the details of the heat treatment and the resultant structures vary from alloy to alloy. In general, however, fine coherent precipitates or zones form first, further aging transforms them into larger, less coherent intermediate precipitates, while overaging results in a coarse distribution of precipitates of the equilibrium phase. The mechanical properties of these alloys, and the way in which they vary with temperature, depend on the type, shape, size, and distribution of the precipitates. It is, however, possible to make a few general comments on their yield and plastic deformation, as these processes depend basically on the nature of the interactions between precipitates and dislocations.

Under the influence of an applied stress, dislocations move along their slip planes until they become obstructed. If the obstacle is a precipitate, there are two main ways in which the dislocation may overcome this barrier to its motion: It may cut through the precipitate, or bypass it. In lightly aged alloys with fine coherent precipitates or zones, it is usually possible for the dislocations to cut through the zone once the stress reaches a high enough value. This is reflected in the sharpness of the yield in this type of alloy. Work still has to be done to force subsequent dislocations through the precipitates, but in general this does not lead to a significant increase in the flow stress and the strain-hardening rate is low.

In more heavily aged alloys, where the precipitates are coarser and often incoherent, it is much more difficult to force dislocations through the particles and they start to bend around them. A residual dislocation loop is left around a precipitate by each dislocation that bypasses it and this has the effect of reducing the interparticle spacing. Every important theory of precipitation-hardening leads to an inverse relationship between the particle separation and the stress necessary to force dislocations between them, $\tau \propto 1/d$, and each dislocation that passes between two precipitates effectively reduces the space between them. This increases the stress necessary to force the next dislocation through the gap and gives a relatively high rate of strain-hardening.

2.2.1. Simple Binary Alloys

One of the most investigated and best understood alloy systems that can be heat-treated to produce precipitates is that of aluminum containing a few per cent copper: it is also the basis for the 2000 series alloys, which are widely used down to cryogenic temperatures. Thus, it is not only a relevant alloy system, but also one which is simple enough for changes in particle size and distribution to be correlated with their effect on the gross mechanical properties of the alloy.

Shear stress–strain curves are shown[25] in Fig. 2.12 for a number of single crystals of an Al–4.5 wt% Cu alloy which have been heat-treated to produce a number of different precipitate configurations. The tensile tests were carried out at 77°K to avoid the possibility of strain-induced precipitation, which can lead to complications at higher testing temperatures. Curve 1 is for the as-quenched condition with all the copper retained in solid solution and it shows a considerable increase in yield stress compared with that of the pure metal ($\sim$100 g/mm^2). The actual value of the yield stress is quite sensitive to crystal orientation, as is the rate of strain-hardening during easy glide. The large extent of the easy glide region is consistent with the theories of solution-hardening outlined in section 1.8. Curve 2 is for a crystal aged at 130°C for two days to produce fine, coherent, disk-shaped G.P.1 zones. The yield stress is much higher and the sharp yield is usually followed by a period of yield elongation. The strain-hardening rate is only slightly higher than that of the solution-

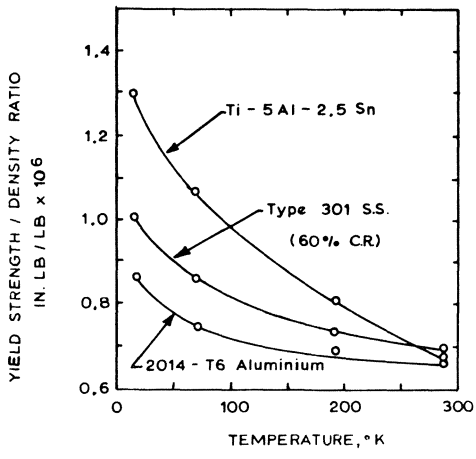

Fig. 2.11. Yield strength/density ratio as a function of temperature for aluminum and titanium alloys and stainless steel (after Kendell[16]).

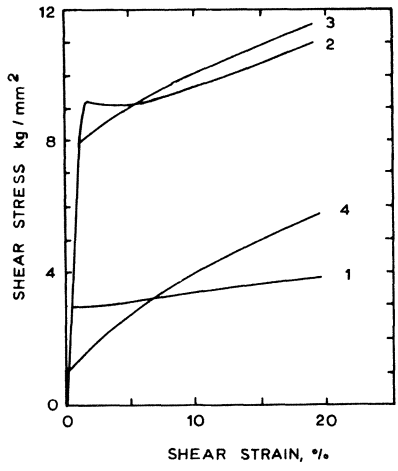

Fig. 2.12. Shear stress–strain curves for a series of Al–4.5% Cu alloy crystals heat-treated to produce different precipitate structures (after Greetham and Honeycombe[25]).

hardened alloy and it is thought that dislocations are able to cut through the G.P.1 zones once the yield stress is exceeded.

In the third crystal, an aging treatment of 27½ hr at 190°C has produced larger, slightly less coherent, G.P. 2 zones (also called θ'' precipitates) and θ' precipitates. This represents the optimum aged condition, despite the slightly lower yield stress shown in curve 3. Of much greater significance is the much higher initial strain-hardening rate, which implies that dislocations are no longer able to cut through the precipitates but have to move around them. Finally, curve 4 is for an overaged crystal which contains coarse particles of the equilibrium θ ($CuAl_2$) phase. The yield stress is low because the precipitates are too widely spaced to exert much direct influence on the moving dislocations. Their main effect is to encourage secondary slip in the earliest stages of deformation and to bring about a high rate of strain-hardening. The parabolic nature of curves 3 and 4 suggest that some cross-slip or other relief mechanism can operate during the latter stages of deformation.

The general pattern shown by this alloy system, i.e., low strain-hardening rates associated with fine, coherent precipitates and higher rates with coarser, less coherent particles, is confirmed by further work on the aluminum–copper,[26,28] aluminum–silver,[28] copper–beryllium,[27] and copper–cobalt[27] systems. Furthermore, the inverse relationship between yield stress and particle spacing has been experimentally verified for these and many other precipitation- or dispersion-hardened systems, in particular for copper containing SiO_2, BeO, and Al_2O_3 particles.[29]

The temperature dependence of the yield and flow stresses in heat-treated alloys is also determined basically by the size and shape of the particles they contain. We have just seen that dislocations are able to cut through thin, coherent precipitates such as G.P. 1 zones. Liebfried[30] has shown that thermal fluctuations are able to reduce the stress necessary to force dislocations through the zones, and hence the yielding process is thermally activated. At very low temperatures, there is less thermal energy available and larger applied stresses are necessary before the zones can be cut. This is reflected by the increase in yield and flow stresses below about 150°C shown[31] for single crystals of Al–2 wt% Cu containing G.P. 1 zones.

In contrast, the yield and flow stresses of single crystals of Al–20 wt% Ag are virtually temperature-independent.[32] The incoherent precipitates present in this alloy are spheres about 50 Å in diameter, and in this case, thermal fluctuations are unable to reduce the stress needed to cut through the precipitates.

This effect of particle size and shape on the temperature dependence of the yield stress in heat-treated alloys is shown[26] clearly in Fig. 2.13 for a series of Al–1.7 wt% Cu crystals aged to produce different precipitate configurations. The critical resolved shear stress τ_0 of crystals containing

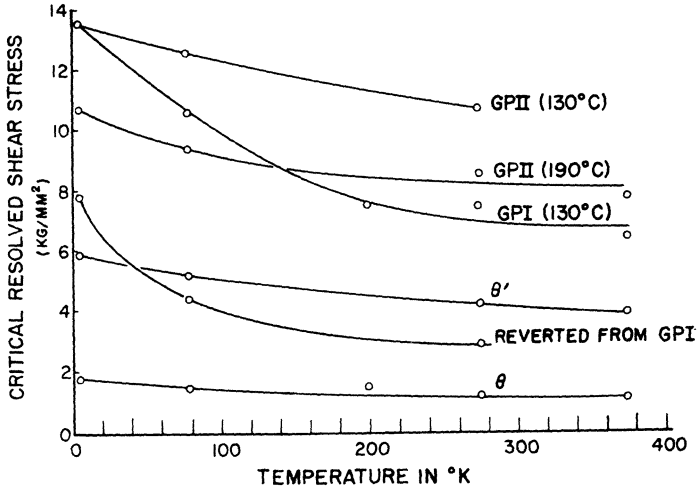

Fig. 2.13. Effect of precipitate structure on the temperature dependence of the yield stress of Al–1.7% Cu alloy crystals (after Byrne *et al.*[26]).

thin G.P. 1 zones increases more at low temperatures than either of the crystals containing the larger G.P. 2 zones. As these zones develop into θ' precipitates, the temperature dependence of τ_0 decreases further and finally almost disappears for the coarse, incoherent particles of $CuAl_2$ which constitute the θ-phase.

So far, we have only considered the deformation of these alloys in single-crystal form, but polycrystals behave in a similar manner, especially when the alloy has been aged to peak hardness. This is reasonable, as the barriers to dislocation movement set up by the precipitates are far more numerous than those which result from the grain boundaries in polycrystals.

2.2.2. Precipitation-Hardened Alloys Used in Cryogenic Applications

2.2.2.1. ***Aluminum-Based Alloys.*** Most commercially available, heat-treatable alloys are far more complex than the simple, binary alloys we have just considered. For example, the specification for a 7075 alloy shows it contains 5.1–6.1% Zn, 2.1–2.9% Mg, 1.2–2.0% Cu, 0.7% Fe, 0.5% Si, and more than 0.1% Cr, Mn, and Ti. There are, consequently, precipitates of many different shapes and sizes as well as solute atoms present in the alloy in its hardened state. Nevertheless, it is instructive to see how closely the results obtained from the simple, binary alloys are reflected by their more practical counterparts.

There are a large number of aluminum alloys currently in use and extensive compilations of data are available on their mechanical properties.

In this section, we will examine the properties of two typical precipitation-hardened alloys, types 2014 and 7075, and compare them with those of a solution-hardened alloy, type 5052, and commercially pure aluminum, type 1100. The commercially pure aluminum is given first, Fig. 2.14(a) to establish the effect of temperature on its yield and tensile strengths so

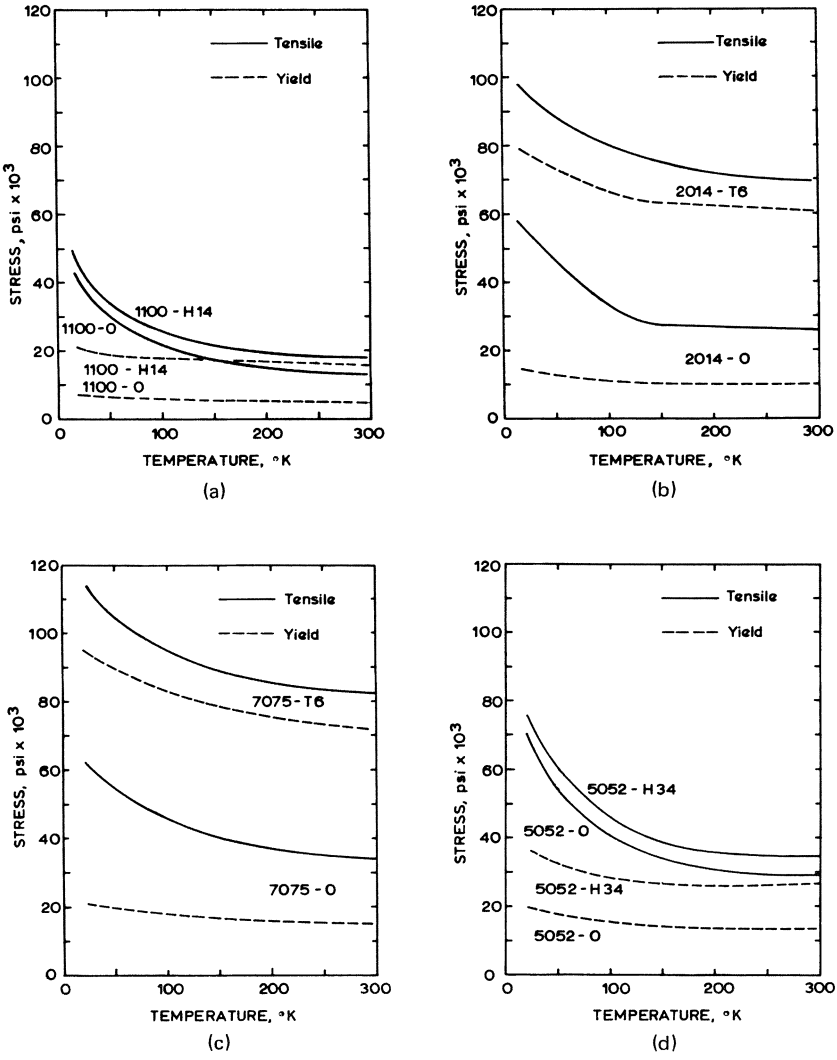

Fig. 2.14. Variation with temperature of the yield and tensile strengths of; (a) type 1100 aluminum in the O and H14 conditions, (b) type 2014 alloy in the O and T6 conditions, (c) type 7075 alloy in the O and T6 conditions, and (d) type 5052 alloy in the O and H34 conditions (data from McClintock and Gibbons[8]).

that it may be used as a standard of comparison for the alloys which follow. The 2014 alloy of Fig. 2.14(b) contains between 3.9 and 5.0% Cu as its main alloying addition, 1.0% Fe, 0.4–1.2% Mn, 0.5–1.2% Si, and small amounts of Cr, Zn, and Ti. It is a typical member of the well-established 2000 series of alloys which can be aged to give moderately high yield and tensile strengths. The 7075 alloy of Fig. 2.14(c), whose composition was given earlier, is a typical member of the 7000 series alloys, which can be heat-treated to give strengths higher than those obtainable from the 2000 series alloys. Finally, Fig. 2.14(d) shows the behavior of a solution-hardened 5052 alloy whose major alloying addition is 2.2–2.8% Mg, but which also contains 0.45% Si and Fe, 0.15–0.35% Cr, and small amounts of Cu, Mn, and Zn. In many applications, the alloy is also cold-worked to give it additional strength.

The effect of temperature on the yield and tensile strengths of commercially pure aluminum shown in Fig. 2.14(a) is similar to that illustrated in Fig. 1.12 for O.F.H.C. copper. In the annealed and recrystallized O condition,* the yield stress is virtually temperature-independent, while the tensile stress increases strongly as the temperature falls. Cold-working to the half-hard H14 condition raises the yield stress at 300°K from 5000 to 16,000 psi and increases its temperature dependence very slightly. The tensile stress at 300°K is raised from 13,000 to 18,000 psi by this treatment and this additional 5,000 psi persists down to the lowest temperatures.

The 2014 alloy of Fig. 2.14(b) is shown for two tempers, the O and T6 conditions. In the annealed and recrystallized "O" condition, the alloy has been grossly overaged and the large precipitates of the equilibrium $CuAl_2$ phase are very widely separated ($\sim$10 μm apart). This is too large a separation for them to exert much influence on the yield process, and the temperature dependence of the yield stress increases strongly, especially below $\sim$160°K, a reflection of the strong temperature dependence of the flow stress† of the pure metal. The main influence of the precipitates is to encourage multiple slip and a high rate of strain-hardening.

In the T6 condition, the alloy is artifically aged and contains G.P. 2 zones and θ' precipitates. Although thicker than G.P. 1 zones, these zones are still thin enough for thermal activation to influence the yield process

---

* A brief summary of the standard temper designation system for aluminum alloys is given in Appendix I.

† The temperature dependence of the tensile stress cannot be related directly to that of the flow stress because, whereas the flow stress can be quoted for a given value of strain, the strain or elongation at which the engineering stress becomes a maximum is itself a function of temperature. However, a *crude* indication of the effect of temperature on the flow stress can be obtained from the variation of the yield and tensile stresses with temperature. If the curves are parallel, the temperature dependence of the flow stress is the same as that of the yield stress. If the curves diverge, the flow stress increases more rapidly with decreases in temperature than does the yield stress. If they converge, then the flow stress is less temperature-dependent than the yield stress.

and the yield stress increases quite steeply below ~ 150°K. This is analogous to the behavior shown in Fig. 2.13 for the Al–1.7 wt% Cu alloy containing G.P. 2 zones. The temperature dependence of the tensile strength is virtually the same as that of the yield strength, indicating that in the fully hardened condition both yield and subsequent plastic flow are controlled by the interaction of dislocations with the thin zones present.

The 7075 alloy of Fig. 2.14(c) contains more alloying elements than the 2014 and develops higher yield and tensile strengths. Even in the annealed and recrystallized condition with large, well-separated precipitates of the equilibrium phase, the yield and tensile strengths of the 7075 alloy are about 5000 psi higher than those of the 2014 alloy at 300°K. This can probably be attributed to solid solution-hardening by some of the minor alloying elements: the slightly higher temperature dependence of the yield and tensile stresses lends support to this conclusion. In the fully hardened condition, both yield and tensile strengths have a temperature dependence similar to that of the 2014 alloy.

Finally, Fig. 2.14(d) shows the behavior of a 5052 alloy in both the O condition and after cold-working and stabilization to the half-hard H34 condition. The yield stresses, especially below 150°K, are more temperature-dependent than those of either of the precipitation-hardened alloys or those of the pure metal, this being analogous to the effect shown in Fig. 2.2 for single crystals of copper–zinc alloys. The tensile stress of both the O and H34 conditions increases rapidly as the temperature falls below ~200°K in a very similar manner to that shown by the pure metal. It would thus appear that solution-hardening has little or no effect on the temperature dependence of the flow stress in aluminum alloys, its main

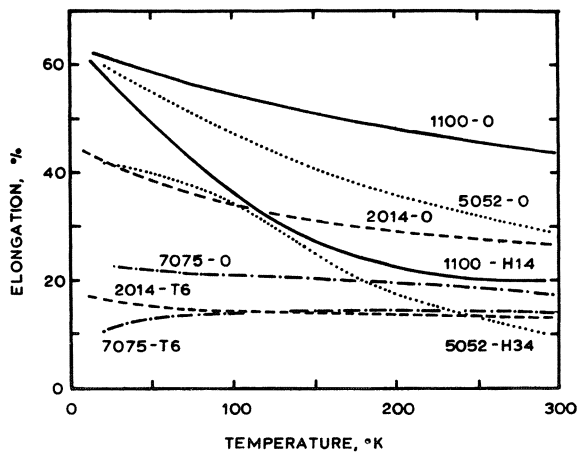

Fig. 2.15. Variation with temperature of the ductility of types 1100, 2014, 7075, and 5052 aluminum alloy in the annealed and cold-drawn or heat-treated conditions (data from McClintock and Gibbons[8]).

effect being seen in the increased temperature sensitivity of the yield stress.

The effect of temperature on the ductility of these alloys is also highly relevant to a consideration of their suitability for use at low temperatures. Figure 2.15 shows how the elongation of each of the four alloys varies with temperature. As might be expected, the pure metal is the most ductile, becoming even more so as the temperature falls. Cold-rolling halves the elongation at room temperature, but has less effect on its value at lower temperatures. The solution-hardened 5052 alloy is quite ductile at room temperature when in the annealed and recrystallized state and its elongation increases as the temperature is lowered to approach that of the pure metal at 20°K. Cold-working, however, causes a drastic decrease in the elongation at 300°K, although this is partially offset by its very rapid rise at lower temperatures. Of the two precipitation-hardened alloys, type 2014 is the more ductile, both in the O and T6 tempers. Furthermore, its ductility improves as the temperature falls. In contrast, the elongation of type 7075 in the hardened condition decreases at low temperatures, especially below ~100°K. As this loss of ductility is accompanied by a decrease in notch toughness and impact strength, the alloy is not recommended for use at low temperatures.

The characteristic mechanical properties of aluminum and its alloys are summarized in Table III and Fig. 2.16. These give data and stress–strain curves at 300, 78, and 4.2°K for pure aluminum and for a B.95 alloy[33] (very similar to a 7075) in both the as-quenched and fully hardened conditions. In the as-quenched condition, the alloying elements are in solid solution and the curves are typical of a solution-hardened alloy, showing relatively moderate yield stresses, high strain-hardening rates, and reasonable ductilities. In the fully hardened condition, the alloy has a very limited capacity for strain-hardening and the high tensile stress is reached after a short period of uniform elongation.

Further insight into this behavior can be obtained by comparing the measured with the true tensile and fracture stresses given in Table III. For both the pure metal and the unheat-treated alloy, the uniform reduction in area prior to necking increases as the temperature falls, and the true tensile strength is considerably higher than its measured value at 4°K. Furthermore, in the pure metal, and to a lesser extent in the unhardened alloy, there is at all temperatures a further large reduction in area prior to fracture, and the true fracture stresses are, in consequence, much higher than the measured values. In the hardened condition, however, the uniform reduction in area decreases as the temperature falls and a neck develops after a small amount of plastic deformation. There is little further deformation in the neck prior to fracture and the true fracture stress is not much above the measured value. At 4.2°K, the true fracture stress of the hardened alloy is, in fact, slightly lower than that of the pure metal and, as we saw in section 1.7, it has been suggested that this high potential

Table III. Data on Aluminum and Its Alloys[a]

Metal	Temperature T, °K	Tensile strength σ_B, kg/mm²	Uniform reduction in area ψ_B, (%)	True tensile strength S_B, kg/mm²	Stress at fracture σ_z, kg/mm²	Reduction in area at fracture ψ_k, %	True fracture stress S_k, kg/mm²	Uniform elongation ε_k, %
Pure aluminum	4.2	32	30	45	30	57	115/70	47
	78	16	26	21	8	89	70/58	42
	300	8	18	9	5	95	54/20	29
B. 95 (Unhardened)	4.2	55	8	60	55	19	70/66	14
	78	45	7	49	45	22	58/57	12
	300	34	6	36	33	22	45/41	10
B. 95 (Hardened)	4.2	83	1	84	83	11	97/89	2
	78	75	3	78	75	13	88/85	5
	300	65	7	69	63	19	80/75	8

[a] The true tensile stress S_B is obtained by dividing the measured tensile stress σ_B by the effective cross-sectional area $(1-\psi_B)$. Due to the difficulty of obtaining accurate values of fracture stress σ_z and final reduction in area ψ_k, maximum and minimum values are given for the true fracture stress S_k.

strength might be exploited by the plastic deformation of pure metals at temperatures near absolute zero.

The general pattern shown by these three metals, that is, for an increase in strength to be almost invariably accompanied by a decrease in ductility, is typical of many alloy systems. It illustrates one of the basic

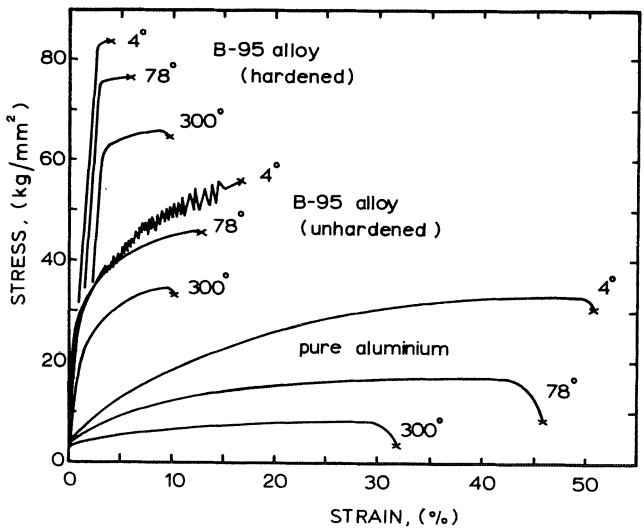

Fig. 2.16. Stress–strain curves for pure aluminum and for a B.95 alloy both in the as-quenched and fully hardened conditions (after Klajvin and Stepanov[33]).

dilemmas which confront the materials technologist, how best to combine high strength with adequate ductility and toughness. This problem will be discussed further in chapter 3 once the basic aspects of fracture have been considered.

2.2.2.2. ***Other Alloy Systems.*** We have considered at some length the properties of aluminum alloys because they are probably the best understood of the heat-treatable alloy systems as well as being in very widespread cryogenic use. There are also a number of other precipitation-hardenable alloys used at low temperature, but lack of space prevents more than a brief examination of some of the most important of them. As we have seen, metals with an fcc structure are the most suitable for use at very low temperatures, and most fcc alloys obtain their strength from solution-hardening. A few, however, can be heat-treated to give higher strengths, and these include the nickel-based alloys Inconel and Monel, beryllium copper, and various stainless and other types of steel.

The composition of normal Inconel is approximately 78% Ni, 15% Cu, and 7% Fe. The addition of ~2.5% Ti and 1% Al produces Inconel X, which is hardened by the precipitation of the intermetallic compounds Ni_3Al and Ni_3Ti. This alloy has a high strength/weight ratio, good corrosion resistance, weldability, and formability as well as excellent high- and low-temperature strengths. For these reasons, it has been widely used for bolts, fasteners, and other components of missiles which are liable to experience both very high and very low temperatures.

Monel varies somewhat in composition, but is basically ~63% Ni, ~30% Cu, ~2% Fe plus small amounts of Mn, Si, etc. The addition of 2–4% Al and 0.25–1% Ti gives K Monel, and this is heat-treatable to produce precipitates of $Ni_x(Al, Ti)_y$ which strengthen the alloy. K Monel is most commonly used where complicated shapes have to be formed from soft sheet material, as fabrication and welding can be done in the solution-treated condition prior to age-hardening.

There are a number of other heat-treatable, high-strength nickel- or cobalt-based alloys originally developed for their high-temperature strength and corrosion resistance which have since been found suitable for use at low temperatures. These include Inconel 718, S Monel, Hastelloy, Rene 41, Haynes 25, Elgiloy, etc.

One of the few copper-based alloys that can be heat-treated is beryllium copper. It contains ~1.8% beryllium and can be aged to give yield strengths of ~100,000 psi at room temperature compared with the ~10,000 psi typical of the pure metal. Both yield and tensile strengths increase at low temperatures, while the ductility remains adequate. However, the presence of the precipitates considerably decreases the thermal and electrical conductivities and, since as in most applications pure copper is used *because*

of its high conductivity, this factor weighs heavily against the use of the precipitation-hardened alloy.

Finally, some steels are precipitation-hardenable, e.g., an A-286 alloy containing ~25% Ni and ~15% Cr retains the fcc austenite phase down to the lowest temperatures. The presence of ~2% Ti among the minor alloying constituents allows particles of the intermetallic compound Ni_3Ti to be precipitated during aging. Ductility is not impaired by this treatment and moderately high strengths ($\sigma_y \approx 120{,}000$ psi) are achieved at room temperature and below. The material is frequently used for low-temperature fasteners, although its strength is lower than that of Inconel X.

The 17–7 PH and related steels do not have a high enough nickel content (17% Cr, 7% Ni, 1.2% Al) to stabilize the austenite phase and are martensitic in structure. They can be heat-treated to give yield strengths of over 200,000 psi, but below ~100°K, their ductility drops to zero and they are rarely used at very low temperatures.

The more recently developed Maraging steels have yield strengths of ~250,000 psi at room temperature, rising to almost 400,000 psi at 20°K. There are a range of compositions possible; one of the most common contains 18% Ni, 8% Co, and 5% Mo, as well as some Ti and Al. Due to their low carbon content (~0.03%), the martensite formed is soft and ductile in the unhardened state and machining is easy. Aging results in the precipitation of an intermetallic nickel compound (+Mo_3Ti, etc.) which is responsible for the high strengths. Elongations of about 4% are typical of the hardened alloy and the ductility does not decrease at low temperatures. The material thus has potential for cryogenic applications in situations where its low ductility is not a drawback, e.g., as the grips or anvils of testing machines.

In conclusion, the technique of precipitation-hardening allows the production of many of the highest-strength alloys in use today. These high strengths are usually achieved at the expense of ductility and toughness and it is important that great care is taken in their specification if serious failures are to be avoided.

2.2.2.3. ***Welding Precipitation-Hardened Alloys.*** Most small components which can be fabricated while in the unhardened condition require no further attention after heat treatment. Larger objects, however, often have to be assembled from smaller components because suitably large facilities are not available for heat treating the finished article. Welding is one of the most widely used assembly techniques, but its use with heat-treated alloys requires some care. Apart from specific problems such as joint efficiency and weldability of the particular alloy concerned, there are also more general issues involved. Age-hardened alloys derive their strength from a carefully controlled sequence of heat treatments which are designed

to produce the optimum distribution of zones or precipitates in the metal. The heating and cooling cycles induced in the weld and heat-affected zone almost invariably destroy this aged structure and lower the strength of the affected regions. Some alloys are able to age-harden naturally and partially regain their former strength, while in others the weld metal strain hardens so rapidly that it reaches the strength of the parent metal after a small amount of deformation. In general, however, there are only two ways of overcoming this loss of strength: carry out a full post-weld heat treatment or, if this is not possible, redesign the joint to operate at a lower stress level compatible with the strength of the weld metal.

2.3. YIELD AND FLOW IN TWO-PHASE ALLOYS

We have now covered two of the most important groups of alloys, those that are strengthened by solutes and those by precipitates; the other main group of alloys are those in which its microstructure contains two or more distinct phases. There is no hard and fast distinction between precipitates and second phases, but it is often convenient to limit the use of the term second phase to particles that can be resolved by conventional optical microscopy.

There are many different types of two-phase (duplex) microstructure, but in general they may be grouped as follows. Those in which: (1) the second phase is ductile and is softer than the matrix, e.g., lead in free-cutting brass; (2) the second phase is ductile but is harder than the matrix, e.g., (α–β)-brass, (α–β)-titanium, etc.; (3) the second phase is brittle but is softer than the matrix, e.g., graphite in cast iron; (4) the second phase is brittle and harder than the matrix, e.g., cementite in steel.

In each case, the properties of the alloy depend not only on the volume fraction of the second phase but also on its size, shape, and distribution. In general, it has its most beneficial effect when finely divided and distributed uniformly throughout the material. In contrast, the preferential deposition of a hard and brittle second phase as a continuous film along the grain boundaries can seriously weaken the alloy. This occurs, for example, when small amounts of bismuth, antimony, or lead are added to copper, or when stainless steel is sensitized (cf. section 2.1.5.1).

A further important factor is the shape of the second-phase particles. In many alloy systems, the second phase forms on cooling through a solid-state transformation and its shape depends on the rate of cooling through this transformation range. Acicular (needlelike) microstructures are generally formed by rapid cooling, whereas slow cooling produces a more equiaxed structure. Additional control over the grain structure can be achieved by cold-working, which tends to produce an oriented texture, or

by suitable annealing treatment, which can spherodize previously acicular structures. Although the detailed effect of these treatments vary from alloy to alloy, equiaxed or spherodized microstructures tend to produce tougher materials.

2.3.1. Soft, Ductile Second Phases

From a practical point of view, the most important example of this type of alloy is that of leaded, or free-cutting brass. The addition of up to ~4% Pb greatly improves the machinability of brass by causing the turnings to break up into small pieces. Lead is insoluble in both the liquid and solid states and forms globules at the grain boundaries. In certain cases, this can lead to porosity, and therefore free-cutting brasses should not be used for making thin-walled components. Similarly, hard soldering tends to volatilize the lead and accentuate the porosity of the material.

2.3.2. Hard, Ductile Second Phases

There are a number of important alloy systems which fall into this category, the most familiar of which is probably (α–β)-brass. The bcc β-phase is harder than the fcc α-phase and the resulting duplex alloy is stronger but less ductile than the single-phase α-alloy. Muntz metal (60% Cu, 40% Zn) is the most common commercial alloy of this type.

The relative properties of the α- and β-phases can be varied by altering the alloy composition, and much basic work on the deformation of duplex alloys has been done on this system. It has been found that for volume fractions of β less than ~30%, the relative deformations are given by

$$\varepsilon_{\text{duplex}} = \varepsilon_\alpha V_\alpha + \varepsilon_\beta V_\beta$$

(ε_α and V_α being the strain and volume fraction of α-phase, etc.). At higher volume fractions, the strains in the two phases are equalized, i.e., $\varepsilon_{\text{duplex}} = \varepsilon_\alpha = \varepsilon_\beta$, and under these conditions, the stresses are given by

$$\sigma_{\text{duplex}} = \sigma_\alpha V_\alpha + \sigma_\beta V_\beta$$

and thus the stress is increasingly carried by the stronger phase. This is the basic result which permits the construction of usable composites from high-strength fibers, a topic which will be considered further in section 4.3.

It is difficult to generalize on the properties of this type of duplex alloy, as the second phase may be formed by a wide range of phase reactions, including nucleation and growth from a liquid, eutectic and peritectic transformations, solid-state allotropic or eutectoid transformations, etc. In each case, the cooling rate has a strong influence on the resultant microstructure, which in turn strongly influences the mechanical properties of the material. Some degree of consistency may, however, be obtained

by using materials covered by one of the relevant ASM, ASTM, BS, etc. specifications.

2.3.3. Soft, Brittle Second Phases

Ordinary cast irons are basically impure iron–carbon–silicon alloys containing between 2 and 4 wt% carbon and 0.4–3.5 wt% silicon. If the alloy is cooled slowly, its microstructure consists of free graphite flakes in a matrix of ferrite and/or pearlite and it is known as grey cast iron. The graphite is soft and brittle, it contributes nothing to the tensile strength of the alloy, and it may, in many respects, be considered as a void in the metal. Furthermore, when the graphite is present in the form of flakes which have very sharp edges, the alloy effectively contains a large number of acute internal notches. These render it very brittle in tension, but have a far less adverse effect on its compressive properties.

The addition of small amounts of magnesium and/or cerium to cast iron causes the free graphite to form as spheroids and produce spheroidal graphite (S.G.) cast iron. Although the graphite spheroids still have negligible strength, they no longer act as internal notches, because of their smooth, regular shape. The S.G. iron thus produced is a much tougher material than ordinary cast iron and it combines an increased strength (50–130,000 psi compared with 20–50,000 psi for ordinary cast iron) with plastic elongations of up to ~30% at room temperature.

In most cast irons, the matrix is in the ferritic (bcc) form, and hence they undergo a ductile/brittle transformation at some temperature which can be above ambient for ordinary cast irons containing graphite flakes, but which is usually below ambient for S.G. cast irons.[34] Ferritic cast irons are thus rarely used at low temperature, but they have occasionally been utilized in circumstances where their high rigidity, wear resistance, and damping capacity are valuable and where they are not liable to receive impact loads. In these cases, the components are designed to withstand stresses much in excess of anything liable to be met in practice.

Recently, a series of austenitic ductile cast irons have been developed[35] which are suitable for producing castings for cryogenic valves, pumps, compressors, etc. These alloys contain a minimum of 21% nickel and 3.75% manganese and this ensures that the austenite is stable down to the lowest temperatures. The graphite is present in the spheroidal form and the alloy composition is adjusted to prevent the occurrence of primary iron carbide, which would lower the impact strength of the material.

2.3.4. Hard, Brittle Second Phases

When a 0.8% plain carbon steel cools through its eutectoid transformation at ~723°C, it forms a microstructure called pearlite, which consists of a lamellar mixture of soft ferrite and the hard, brittle, intermetallic

compound Fe_3C. If the cooling rate is slow, the transformation takes place just below the eutectoid temperature, the pearlite is coarse, and the carbide lamellae are separated by relatively large regions of ferrite. If, however, the majority of the transformation takes place at a lower temperature, the pearlite is finer and the carbide lamellae are more closely spaced. The strength and hardness of the material are found to be directly related to the spacing of the carbide lamellae; the closer the spacing, the harder the material (to be exact, hardness is inversely proportional to the log of the mean ferrite path).

This is a general result for the deformation of duplex structures in which a soft matrix is reinforced by a hard, brittle second phase. The majority of the deformation takes place in the matrix and, for a given concentration of the hard second phase, the maximum degree of strengthening is obtained when the second-phase particles are most finely divided and closely spaced. A similar result is, of course, also obtained for strengthening by precipitates.

One further fundamental point may be illustrated by reconsidering the 0.8% carbon steel. The lamellar pearlitic structures produce a hard but relatively brittle steel, whereas a softer and tougher material is often required. This can be obtained by suitable heat treatments which cause the carbide particles to form spheroids instead of lamellae (spheroidization). There is again a direct relationship between spheroid separation and strength, with the highest strengths obtained for the most closely spaced particles. Furthermore, it is possible to produce both lamellar and spheroidal microstructures having the same mean ferrite path and it is found that, whereas the lamellae give a harder material, the spheroidal steel is tougher. This is again a general result applicable to many other duplex microstructures.

Most steels, especially those used for cryogenic purposes, have a much lower carbon content than 0.8%. In this case, the microstructure would usually consist of grains of ferrite as well as pearlite, with the majority of the deformation taking place in the ferrite grains. In some respects, this may be considered as a duplex structure, with the harder pearlite colonies reinforcing the softer ferrite grains. As these steels are ferritic, they undergo a ductile/brittle transition at some temperature and, as we shall see in the next chapter, the size of the pearlite grains and the separation of the carbide particles within these grains have a strong effect on the temperature at which this transformation takes place.

2.4. YIELD DROPS AND SERRATED STRESS-STRAIN CURVES

For many metals, the transition from elastic to plastic deformation takes place gradually; plastic deformation is a continuous process and the

stress–strain curve is smooth and unbroken. There are, however, occasions when deformation takes place discontinuously and the stress–strain curve shows one or more load drops or serrations. These phenomena can be split into two basic groups: those associated with a sharp initial yield point and those that take place during subsequent plastic deformation, especially at very low temperatures.

2.4.1. Yield Drops

The most well-known occurrence of sudden yielding accompanied by a load drop is in mild steel tested at or near room temperature (see Fig. 1.4). Such yield drops are also found in a wide range of materials, but are especially common in bcc metals containing small concentrations of impurities in interstitial solid solution, e.g., carbon, nitrogen, and oxygen in iron, molybdenum, niobium, and tantalum.

Sharp yield points have also been found in hcp metals containing interstitial impurities, e.g., N_2 in Cd and Zn. Dilute alloys of fcc metals, in which the impurities are in substitutional solid solution, do not normally exhibit sharp yield phenomena, but they are quite common in more concentrated solid solutions, e.g., 70/30 brass, Al–Mg alloys, and a number of Cu alloys, including Cu–Zn, Cu–Sn, Cu–Sb, Cu–In, etc. Yield drops are thus observed in all three main crystal structures and are generally believed to be caused by the pinning of dislocations by strong interactions with impurity atoms.

The original explanation of the yield point in iron given by Cottrell and Bilby[36] assumed that the dislocations were locked by an atmosphere of carbon impurities. Sharp yielding occurred when the stress reached a value high enough to unlock these dislocations (the upper yield stress), while their subsequent movement required a lower stress (the lower yield stress).

Later work by Johnson and Gilman[37] on lithium fluoride has shown that the rapid generation of new dislocations during yielding can result in a load drop in a specimen deformed at constant strain rate. According to simple dislocation theory, the strain rate can be expressed as $\dot{\varepsilon} = Nvb$, where N is the number of mobile dislocations per unit area, v their average velocity, and b the Burgers vector.

Hence, a given strain rate could be maintained by N dislocations moving with velocity v or $2N$ with velocity $v/2$. If there is a direct relationship between the applied stress and dislocation velocity, it follows that a rapid increase in N leads to a decrease in v and a corresponding drop in the stress necessary to continue deformation.

Hahn[38] has shown that the yield points shown by bcc metals can also be explained on this basis, as they have the required strong dependence of

dislocation velocity on applied stress. Some form of impurity–dislocation interaction is apparently still necessary for the occurrence of sharp yield points, as they are not found in zone-purified metals. The most probable role played by impurities is to lock pre-existing dislocations until the applied stress is large enough to operate prolific sources of new dislocations. The other phenomena normally associated with sharp yielding, such as the delay time and Lüders strain, can be explained by this model, as can the temperature, strain-rate, and grain-size dependence of the yield and flow stress in bcc metals.

As the temperature is lowered, the dislocation velocity becomes more stress-dependent and yield becomes sharper, as shown in Fig. 2.17 for molybdenum. The pre-yield strain initially increases as the temperature falls, but as the metal undergoes its ductile/brittle transition, it rapidly falls to zero. Below the transition temperature, brittle fracture usually occurs immediately after yielding. The Lüders extension, which is common in bcc metals and concentrated solid solutions but not in dilute alloys, also initially increases in extent as the temperature is lowered but falls to zero below the ductile/brittle transition.

Finally, there are a few other circumstances under which yield points are obtained. The first is a high-temperature effect which is found between~ 100 and 300°C in iron and at various temperatures in brass and other concentrated alloys of copper and aluminum. Called the Portevin–Le Chatelier

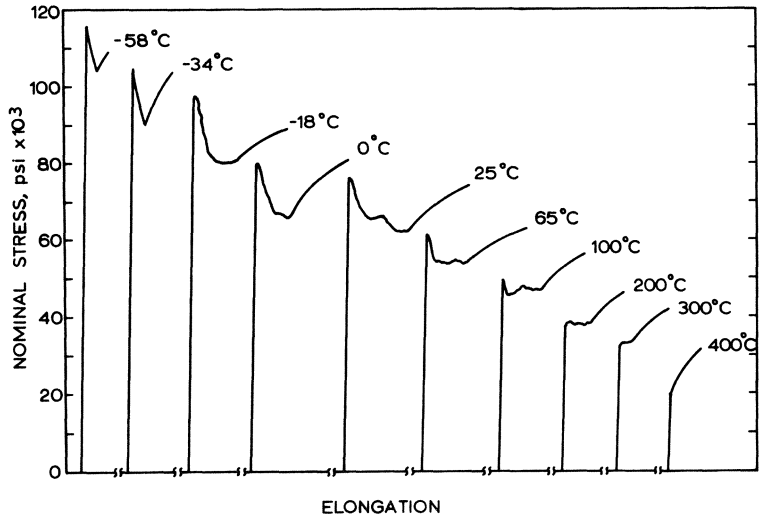

Fig. 2.17. Series of stress–strain curves for molybdenum, showing the sharpening of the yield point with decrease in temperature (after Hahn[38]).

effect, it appears as a series of small yield points. They are caused by the repeated unlocking and repinning of dislocations by solute atoms which diffuse easily at these temperatures, a process known as strain-aging.

The second circumstance, work-softening, is found, for example, in pure aluminum[39] when a specimen is strained at a high temperature after previous deformation at low temperature. There is a small yield drop followed by a Lüders extension before strain-hardening recommences. This is thought to be due to the rearrangement of the dislocation structure produced during straining at low temperature into a different configuration which is more stable at the higher temperature.

A different yield-point mechanism has been found in pure aluminum,[40] nickel,[40] and copper[41] when single crystals are strained, unloaded, and then restrained at the same temperature. It is thought that some irreversible process, such as the formation of Lomer–Cottrell sessiles, occurs during unloading, which prevents large-scale reverse plasticity.

2.4.2. Serrated Stress Strain Curves

As we have just seen, initial yield drops can occur over quite a wide range of temperatures. Serrated stress–strain curves, on the other hand, are characteristically a low-temperature phenomenon, the only other conditions under which they are observed being during high-temperature testing of metals which undergo strain-aging. The nature of the serrations depends on the metal concerned and on the conditions of the test, especially the stiffness of the testing machine. Sometimes, there are just a few large serrations, on other occasions, very many small ones; in some cases, they start immediately the metal yields, in other cases, there is considerable continuous plastic deformation before they commence. In general, they are caused by the operation of deformation modes which act very rapidly and cause the applied load to drop within about 10^{-4} sec.

Many possible mechanisms have been proposed to explain the appearance of these serrations, including deformation twinning,[43] strain-induced martensite formation, [44,45] and "burst" dislocation formation.[42] There are, however, many metals which neither twin nor undergo martensitic transformations yet exhibit highly serrated stress–strain curves at low temperature, and hence a more general explanation of the phenomenon is required. Basinski[46,47] has shown that the most probable mechanism is that of "adiabatic deformation."

At very low temperatures, the specific heat of a metal is proportional to the third power of the temperature and thus a constant-energy input will produce a local rise in temperature which rapidly becomes larger as the general temperature falls. The magnitude of the temperature rise depends on the thermal conductivity of the metal and it has been shown that in an

aluminum alloy of rather poor conductivity totally immersed in liquid helium, the temperature at the center of the specimen can rise as much as 60°K.

If the flow stress decreases rapidly with increase in temperature, as it does with most of the metals that exhibit serrations, it is possible for the decrease in flow stress caused by local heating to exceed the increase in flow stress caused by strain-hardening. This is an unstable condition and the heated region of the specimen will flow catastrophically under a decreasing applied stress until the load relaxes to a lower value. Flow then ceases, the material cools down, and the load increases elastically to its former value before plastic deformation can be resumed.

As long as the ultimate tensile stress has not been reached, each successive serration commences at a slightly higher load than the previous one, as shown in the inset of Fig. 2.18. Under these conditions, each deformation occurs in a different region of the specimen. Once the ultimate tensile stress (shown in Fig. 2.18 by the maximum in the upper envelope containing the serrations) is exceeded, catastrophic flow becomes localized in the necked region of the specimen and the magnitude of the load drops increases until fracture occurs.

Good agreement is found between observed and calculated values of the length of flowing region necessary for plastic deformation to take place under adiabatic conditions and of the magnitudes of the resultant load drops and increases in temperature. It is, however, still necessary to postulate a "nucleating deformation" for the process, as the increases in temperature and plastic flow which cause the load drop only occur after the load has started to fall. One possibility is that enough energy is liberated during ordinary slip at very low temperatures to nucleate catastrophic flow.

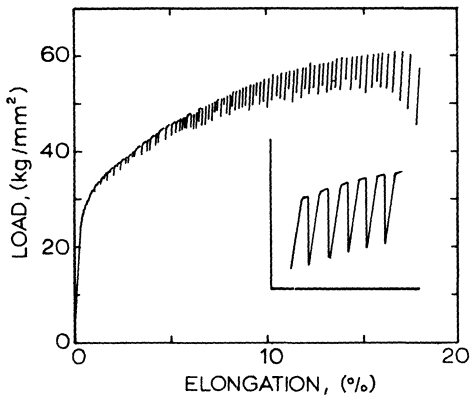

Fig. 2.18. Typical serrated load-elongation curve for an aluminum alloy. Inset: Detail of serrations, showing each commencing at a slightly higher load than the previous one (after Basinski[46,47]).

The surface condition has also been found[48] to play an important part in determining the strain at the first serration and the number of subsequent events; the rougher the surface, the easier it is to nucleate a serration. Furthermore, the amount of nucleating deformation necessary increases as the deformation temperature is raised, due to the rapid rise in specific heat of the metal. In the aluminum alloy, it was found that under normal conditions serrations were not observed above 12°K, but that they could be nucleated up to 15°K if the cryostat were tapped or vibrated, as extra energy is made available by these means.

In those metals that twin or transform to martensite, these deformation mechanisms may aid nucleation and enable adiabatic deformation to occur at higher temperatures. This is possibly one of the reasons why serrations are observed at temperatures up to 78°K in iron,[49] which cannot be entirely accounted for by the twins present. The strong temperature dependence of the flow stress in bcc metals is a further contributory factor which encourages adiabatic flow in iron and steel at higher temperatures than in fcc metals.

One very important class of metals which exhibit serrated stress–strain curves are the AISI 300 series stainless steels. These, as we saw earlier, are basically austenitic, but some members of this series transform to martensite at low temperatures either spontaneously or during plastic deformation. Type 304 L stainless steel undergoes both spontaneous and strain-induced transformations, and, as may be seen from Fig. 2.10, exhibits a highly serrated stress–strain curve on deformation at 4°K. A few per cent of both transformation products, ε and α', were already present prior to the first serration and so their initiation cannot be correlated with the onset of a burst-type martensitic transformation.[50] This is confirmed by the presence of serrations in the 4° and 20°K stress–strain curves of type 310 stainless steel (Fig. 2.7), which does not transform to martensite even during straining at the lowest temperatures.[52]

A further point illustrated in Fig. 2.7 is the effect of strain rate on the occurrence of discontinuous flow. At the normal strain rate of 0.005 in./min, deformation at 20°K was continuous right up to fracture. A 200-fold increase in strain rate not only increased the yield stress (as would be expected from the strain-rate dependence of τ^*), but led to the appearance of small-amplitude serrations. This is consistent with the thermal instability mechanism of adiabatic flow, as nucleation will be made easier by the increase in flow stress caused by the higher strain rate. The smaller amplitude of the serrations at 20°K compared to those at 4°K reflects the much larger specific heat at the higher temperature.

The only group of metals having stress–strain curves showing serrations which cannot satisfactorily be attributed to adiabatic flow are the fcc metals of small stacking-fault energy, copper, silver, and gold. The flow

stresses of these metals are much less temperature-dependent than that of aluminum near absolute zero (Fig. 1.10) and thus one of the prerequisites of the Basinski theory is not applicable to these metals.

Suitably oriented single crystals of copper, silver, and gold have been shown[43] to twin during deformation at 4° and 78°K, as illustrated in Fig. 2.19 for copper at 4°K. Normal slip operates up to a strain of about 50%, further deformation then taking place by discontinuous slip characterized by a large number of small-amplitude serrations in the stress–strain curve. Metallographic and X-ray examinations showed that there had been no twinning during this discontinuous slip, which only occurred at 4°K, not at 78°K. Blewitt and co-workers[43] attribute discontinuous slip to an avalanche of slip lines, but the possibility of adiabatic flow cannot entirely be ruled out.

After about 70% strain, the curve shows a large load drop followed by a period of discontinuous deformation at more or less constant stress. This was unequivocably correlated with the propagation of a twin through the length of the specimen. Once the sample had twinned completely, strain-hardening by discontinuous slip recommenced and continued until fracture. Examination of the specimen showed that twinning occurred on the (111) plane in the [112] direction with a shear of ~0.71, as required theoretically.

Recent studies[14] on a number of copper-based engineering alloys have shown that many of these materials have serrated stress–strain curves when tested at 4°K (as shown in Fig. 2.5 for admiralty brass). Furthermore, the yield and flow stresses of many of these materials are lower at 4°K than at

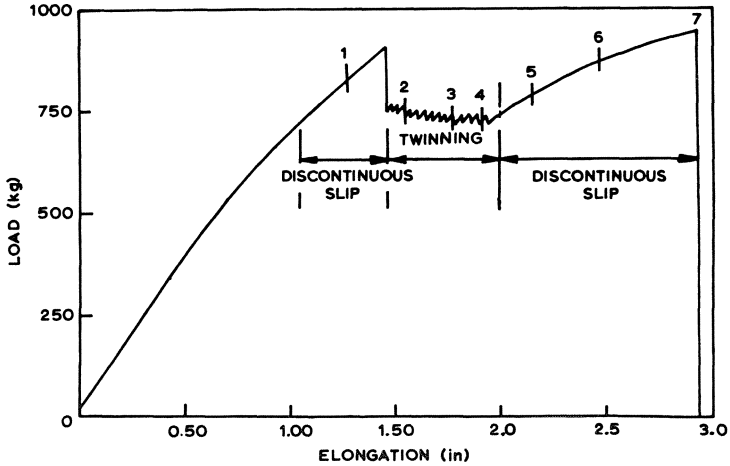

Fig. 2.19. Load–elongation curve for a single crystal of pure copper tested at 4.2°K and showing regions of discontinuous slip and twinning (Blewitt *et al.*[43]).

20°K, in contrast to the normal temperature dependence of these parameters. In order to explain this anomaly, it is proposed that the stress needed to nucleate twins decreases with decreasing temperature and that deformation at 4°K occurs primarily by deformation-twinning. Further work would appear to be necessary before the deformation mechanism operating in copper and its alloys at very low temperatures can be definitely identified.

Finally, Basinski has drawn attention to the significance of the widespread occurrence of thermal instability during the plastic deformation of metals at low temperatures. Where such serrations occur, it is unrealistic to assume that deformation actually takes place under isothermal conditions or at constant strain rates even if these conditions are nominally imposed. Furthermore, the fact that serrations are only detected if a hard testing machine is used must cast doubt on some of the smooth curves obtained at very low temperatures by investigators using soft testing machines.

NOTE ADDED IN PROOF

Recent work by Larbalestier and King[57,58] has produced further information on the problems of martensite stability and the magnetic behavior of 300 series stainless steels at low temperatures. Considering first the question of martensite stability, they find that the temperature, M_s, at which α' martensite starts to form spontaneously on cooling in specimens which were in the fully softened condition ($\frac{1}{2}$ hour anneal at 1025–1075°C followed by a water quench) correlated well with that predicted by the Eichelman–Hull[59] equation:

$$M_s(°K) = 1580 - 1667(C + N) - 61.1(Ni) - 41.7(Cr) - 33.3(Mn) - 27.8(Si)$$

where (Ni) ≡ wt% nickel, etc.

A number of the commonly available 18/8 steels were evaluated, and in Table IIA the calculated M_s temperatures are shown for a hypothetical series of specimens which were assumed to have compositions which were exactly in the middle of their allowable ranges.

Table IIA. Calculated M_s Temperatures for Hypothetical "Median-Composition" Stainless Steels

Grade	304L	304	304Hi	305	316L	316	316Hi	321	347	310
M_s	+50	−17	−250	−65	+12	−55	−234	+79	+15	∼−2000

A number of points arise from these data. First, they show the very beneficial effect produced by the extra nitrogen in the "Hi-proof" grades

of types 304L and 316L. The presence of 0.2 wt% N lowers the M_s temperature by about 300°K compared with the equivalent normal grade, and this is sufficient to depress M_s below 0°K even for the "leanest" specimens. As these steels also have significantly better mechanical properties than the normal grades, their use for cryogenic applications should increase significantly as they become more widely available. Second, the ranking order for stability given by the calculated values of M_s corresponds quite well with that found experimentally, i.e., 321, 347, and the low-carbon versions of 304 and 316 are less stable than normal 304, 305, and 316. However, as one can get a possible variation of almost 500°K between the "richest" and "leanest" materials allowed within a grade, it is not possible to read too much significance into changes in M_s of a few tens of degrees between grades. Furthermore, the formula does not take any account of the effect of O, P, S, Cu, Mo, Nb, and the other elements normally found in these stainless steels which must also influence their stability.

As noted earlier, cold work also plays a highly significant role in determining the stability with respect to martensite transformation. Cold work at room temperature or above can either enhance or inhibit transformation on subsequent cooling,[60,61] but plastic deformation at low temperatures can break down all of the 18/8 grades, although here again the high-nitrogen versions show the greatest stability. Welding also reduces the stability of stainless steels due to the precipitation of austenite stabilizing elements from solution, this, as noted earlier, being particularly important in the case of the high-nitrogen-content grades. Furthermore, the weld zone is usually ferromagnetic because of the 5–10% free ferrite incorporated to prevent hot tearing.

Turning to the magnetic behavior of austenitic stainless steels, they find that there are two separate causes for ferromagnetic behavior at low temperatures: the familiar irreversible ferromagnetism caused by martensitic transformation to α' which can be measured at both low and ambient temperatures, and a change from low-temperature antiferromagnetism to ferromagnetism in high-nickel-content alloys which is measurable only at low temperatures. All the 18/8 stainless steels have been shown[62,63] to be antiferromagnetic at 4.2°K and to have Néel temperatures in the region of 40°K. Larbalestier and King have shown that the Néel temperature falls with increasing alloy content, type 309 (23% Cr, 14% Ni) having a T_N of 12°K while in type 310 (25% Cr, 20% Ni) the Neél temperature is below 0°K. This alloy is in fact in a superparamagnetic/ferromagnetic state at 4.2°K, showing no signs of saturation even in fields of 120 kOe, and it has the characteristics of a steel very close to the borderline between ferro- and antiferromagnetic behavior. Fully developed ferromagnetism is, in fact, observed in higher alloy steels of the Incoloy 800 type which contain 20% Cr and 32% Ni.

Table IIB. The Effect of Temperature on the Susceptibility, $\chi = M/H$, and Permeability, $\mu = B/H$, of Three Stainless Steels

Type of steel	Temperature of measurement		
	298°K	77°K	4.2°K
304L	$\chi = 2 \times 10^{-4}$	$\chi = 5 \times 10^{-4}$	$\chi = 7 \times 10^{-4}$
309	$\chi = 1.5 \times 10^{-4}$	$\chi = 5 \times 10^{-4}$	$\chi = 19 \times 10^{-4}$
310	$\chi = 2 \times 10^{-4}$	$\chi = 6 \times 10^{-4}$	$\mu_{100\ \mathrm{Oe}} = 1.3$ $\mu_{1\ \mathrm{kOe}} = 1.15$ $\mu_{80\ \mathrm{kOe}} = 1.02$

Note: $B = H + 4\pi M = H(1 + 4\pi\chi)$; $\mu = 1 + 4\pi\chi$.

In Table IIB the susceptibilities (or, where appropriate, permeabilities) of types 304L, 309, and 310 are given for temperatures of 298, 77, and 4.2°K. It can be seen that even for the nonferromagnetic samples of 304L and 309 the volume susceptibility increases sharply at low temperatures, thus giving rise to strong tractive forces in regions where the magnetic field gradient is high. Although type 309 does not transform spontaneously on cooling, partial transformation to α' can be produced by plastic deformation at low temperatures; 310, on the other hand, has been shown[52] to be completely stable even after extensive deformation at 4.2°K. It would therefore appear that thermodynamic stability and "nonmagnetic" behavior are mutually incompatible at very low temperatures: the stable high alloy grades such as type 310 are intrinsically superparamagnetic/ferromagnetic at 4.2°K, while the intrinsically antiferromagnetic 18/8 types are liable to transform partially either spontaneously or after cold work to the ferromagnetic α' martensite. On balance use of the "Hi-proof," nitrogen-containing grades of 304L or 316L would appear to offer the best compromise, especially if deformation at low temperatures is unlikely.

REFERENCES

Textbooks and Reference Work

1. D. McLean, *Mechanical Properties of Metals*, John Wiley and Sons, New York (1962).
2. R. P. Reed and R. P. Mikesell, "Low-Temperature Mechanical Properties of Copper and Selected Alloys," N.B.S. Monograph 101 (1967).
3. K. A. Warren and R. P. Reed, "Tensile and Impact Properties of Selected Materials from 20°K to 300°K", N.B.S. Monograph 63 (1963).
4. F. R. Schwartzberg, S. H. Osgood, R. D. Keys, and T. I. Keifer, "Cryogenic Materials Data Handbook," ML-TDR-280 (August 1964) and supplement (March 1966).
5. K. D. Timmerhaus (Ed.), *Advances in Cryogenic Engineering*, Plenum Press, New York.
6. R. W. K. Honeycombe, *The Plastic Deformation of Metals*, Arnold, London (1968).

7. American Society for Metals Handbook, 8th ed., Am. Soc. Metals, Cleveland, Ohio (1961).
8. R. M. McClintock and H. P. Gibbons, "Mechanical Properties of Structural Materials at Low Temperatures," N.B.S. Monograph 13 (1960).

Other References

11. T. E. Mitchell, "Dislocations and Plasticity in Single Crystals of Face-Centered Cubic Metals and Alloys", in E. G. Stanford *et al.* (Eds.)., *Progress in Applied Materials Research*, Vol. 6, Heywood and Co., London (1964), p. 119.
12. D. F. Stein and J. R. Low, *Acta. Met.* **14**, 1183 (1966).
13. F. Pfaff, *Z. Metallk.* **53**, 411, 466 (1962).
14. R. P. Reed and R. P. Mikesell, *J. Materials* **2**, 370 (1967).
15. International Nickel Co. Data Sheet, "Low-Expansion 36% Ni-Fe Alloys for Cryogenic Service."
16. E. G. Kendell, "Metals and Alloys for Cryogenic Applications," Technical Data Report, TDR-269 (4240-10)-6 (January 1964).
17. C. B. Post and W. S. Eberly, *Trans. ASM* **39**, 868 (1947).
18. B. W. Birmingham, D. B. Chelton, D. B. Mann, and H. P. Hernandez, *ASTM Bull.* **240**, 34 (1959).
19. International Nickel Co. Data Sheet, "Mechanical and Physical Properties of Austenitic Chrome-Nickel Stainless Steels at Room Temperature, Also Further Sheet on Low Temperature Properties.
20. C. S. Gunter and R. P. Reed, in Ref. 5, Vol. 6 (1960), p. 565.
21. R. P. Reed, *Acta. Met.* **10**, 865 (1962).
22. C. E. Spaeder, J. C. Magelich, and K. G. Bricknev, *Metal Progress* **1969** (July), p. 57.
23. J. L. Christian, "Effects of Chemistry and Processing on the Mechanical Properties of Engineering Alloys at Cryogenic Temperatures", Proc. 1964, Golden Gate Metals Conf., San Francisco, California (February 1964).
24. R. G. Broadwell and R. A. Wood, *Materials Res. Standards* **1964** (October), 549.
25. G. Greetham and R. W. K. Honeycombe, *J. Inst. Metals* **93**, 432 (1964-65).
26. J. G. Byrne, M. E. Fine, and A. Kelly, *Phil. Mag.* **6**, 1119 (1961).
27. A. Kelly and R. B. Nicholson, "Precipitation Hardening," in "Progress in Materials Science," Pergamon, Oxford (1963).
28. D. Dew-Hughes and W. D. Robertson, *Acta. Met.* **8**, 612 (1960).
29. M. F. Ashby, *Z. Metallk.* **55**, 5 (1964).
30. G. Liebfried, in J. Fisher *et al.* (Eds.) "Dislocations and Mechanical Properties of Crystals," John Wiley and Sons, New York (1957), p. 495.
31. A. Kelly and C. Chiou, *Acta. Met.* 6 565 (1958).
32. A. Kelly, A. Lassila, and S. Sato, *Phil. Mag.* **4**, 1260 (1959).
33. O. V. Klajvin and A. V. Stepanov, *Soviet Phys.—Solid State* **1** (6), 955 (1959).
34. P. J. Rickards, *British Cast Iron Res. Assn. J.* **16** (5), 438 (1968).
35. W. K. Abbott, in Ref. 5, Vol. 8 (1963), p. 654.
36. A. H. Cottrell and B. A. Bilby, *Proc. Phys. Soc.* **A62**, 490 (1951).
37. W. G. Johnson and J. J. Gilman, *J. Appl. Phys.* **30**, 129 (1959); **33**, 2050 (1962); **33**, 2716 (1962).
38. G. T. Hahn, *Acta. Met.* **10**, 727 (1962).
39. A. H. Cottrell and R. J. Stokes, *Proc. Roy. Soc.* **A233**, 17 (1955).
40. P. Haasen and A. Kelly, *Acta. Met.* **5**, 192 (1967).
41. M. J. Makin, *Phil. Mag.* **3**, 287 (1958).
42. E. T. Wessel, *Trans. ASM* **49**, 149 (1957).
43. T. H. Blewitt, R. R. Coltman, and J. K. Redman, *J. Appl. Phys.* **28**, 651 (1957).
44. G. V. Uzhik. *Izv. Akad. Nauk SSSR, Otd. Tekhn. Nauk* **1**, 57 (1955).

45. S. C. Collins, F. D. Ezekial, D. W. Sepp, and J. W. Rizika *Proc. ASTM* **56**, 687 (1956).
46. Z. S. Basinski, *Proc. Roy. Soc.* **A240**, 229 (1957).
47. Z. S. Basinski, *Aust. J. Phys.* **13**, 354 (1960).
48. O. V. Klajvin and A. V. Stepanov, *Phys. Met. Metallog.* **17** (4), 106 (1964).
49. R. L. Smith and J. L. Rutherford, *Trans. AIME* **209**, 857 (1957).
50. J. F. Watson and J. L. Christian, *J. Iron Steel Inst.* **195**, 229 (1957).
51. R. P. Reed and J. F. Breedis, ASTM STP 387, Am. Soc. Testing Mat., Philadelphia (1966), p. 60.
52. C. S. Gunter and R. P. Reed, *Trans. ASM* **55**, 399 (1962).
53. E. O. Hall and S. H. Algie, *Metallurgical Reviews* **11**, 104 (1966).
54. R. S. French and W. R. Hibbard, *Trans. AIME* **188**, 53 (1950).
55. R. P. Reed and R. P. Mikesell, in Ref. 5, Vol. 4 (1960), p. 84.
56. Handbook of the American Aluminum Association, 420 Lexington Avenue, New York, N. Y. 10017.
57. D. C. Larbalestier, Ph. D. Thesis, Imperial College, London, 1970.
58. D. C. Larbalestier and H. W. King, Rutherford High Energy Laboratory Report RHEL/R133, 1971; *Cryogenics* (to be published).
59. G. H. Eichelman and F. C. Hull, *Trans. ASM* **45**, 77, (1953).
60. R. Lagneborg, *Acta Met.* **12**, 823, (1964).
61. H. C. Fiedler, B. L. Averbach, and M. Cohen, *Trans. ASM* **47**, 267, (1955).
62. E. I. Kondorsky and V. L. Sedov, *J. Appl. Phys.* **31**, 331S (1960).
63. W. H. Meiklejohn, *J. Appl. Phys.* **32**, 274S (1961).

Chapter 3

Fracture

The elastic and plastic deformation of materials subjected to an applied stress is terminated by an inhomogeneous form of deformation termed fracture. Just as the macroscopic characteristics of elastic and plastic deformation in crystalline materials are determined by the basic atomic and microscopic processes such as slip, so the large-scale characteristics of fracture can be shown to be a result of the basic micromechanisms which cause atomic bonds to be broken and new crack surfaces to be created. There are a variety of modes of fracture, ranging from the completely brittle failure of perfectly elastic materials to the fully shear failure of amorphous materials such as clay. However, in most materials, particularly metals, fracture is neither fully brittle nor completely ductile and the actual modes of failure are determined by a number of factors, which include the crystal structure of the material, its purity, and its thermal and mechanical history, and by the environmental and other conditions under which it is loaded. In the first section of this chapter, the basic mechanisms responsible for ductile and brittle failure in metals are examined both with respect to their role in the initiation of microcracks or voids and in the initial stages of crack growth. It is shown, for example, that shear and cleavage failure are alternative modes of fracture in body-centered and hexagonal-close-packed metals, while in face-centered-cubic metals, only shear failure is possible because of the ease with which slip takes place in this lattice structure.

Failure on a macroscopic scale demands that cracks or flaws, which either pre-exist in the material or which are created during the initial stages of deformation, grow under the influence of an applied tensile stress to cause complete separation of the body into two or more parts. The growth of such cracks can take place in a brittle, low-energy-absorbing mode or in a tough, high-energy-absorbing mode and the toughness of a material is a measure of its ability to resist the propagation of cracks in a low-energy mode. In fully brittle materials, the fracture strength of a body is completely determined by the size of the largest flaw it contains: the toughness of metals is determined by a number of factors which include their strength,

the number, size, and distribution of second-phase particles or flaws they contain, their environment, and the type of applied stress system they experience. In high-strength materials, these factors may combine to give a low toughness, and failure can occur in a low-energy mode. The concepts of fracture mechanics have been used to explain these effects and to give a rational basis for the design of structures which may contain flaws, stress concentrators, or other potential crack initiators, and these topics are considered in considerable detail in section 3.2.

The ductile–brittle transition which takes place in such important ferrous alloys as plain and low-alloy steels is a particularly relevant aspect of the failure of materials at low temperatures, and in section 3.3, this phenomenon is considered both from a basic point of view and also in terms of the type of test which can be used to determine the transition temperature of a given material. The relationships between the results obtained from full-scale tests and those given by simpler, less expensive methods such as the Charpy V notch impact test are also examined to see how far the simpler tests may be used for the purposes of materials selection and quality control.

Finally, in section 3.4, failure by fatigue, corrosion, hydrogen embrittlement, and other time-dependent processes is considered briefly to show their relevance to the fracture of materials at low temperatures.

3.1. BASIC MECHANISMS OF DUCTILE AND BRITTLE FAILURE

On an atomic scale, fracture occurs when atomic bonds are broken and a fresh crack surface is created. Failure is by *cleavage* if the *tensile* forces concentrated at a crack tip exceed the cohesive stress of the material and rupture bonds perpendicular to the fracture plane. *Shear* failure is caused by the rupture of these same bonds by forces applied *parallel* to the fracture plane. In crystalline materials, both cleavage and shear deformation (slip) take place preferentially on certain crystallographic planes, the cleavage and slip planes respectively, and the relative ease with which these two processes operate depends principally on the crystal structure of the material. Other relevant factors include the testing temperature, strain rate, applied stress system, and the physical and chemical purities of the material.

We have already seen that slip in crystalline solids takes place at stresses far below the theoretical shear stress of the crystal because dislocations can move at these lower stresses. If the material is always able to deform plastically and relieve potential stress concentrations, the cleavage strength of the crystal can never be exceeded and cleavage failure is not possible. Slip occurs readily in fcc metals at all temperatures, their shear

strengths are always lower than their cleavage strengths, and they always fail in a ductile manner. In contrast, dislocations can be pinned and slip inhibited in bcc and hcp metals, large tensile stresses can concentrate at the tips of microcracks, and cleavage failure is possible. Cleavage and shear are thus alternate modes of failure in these metals.

If slip is completely inhibited, as, for example, in bcc metals at low temperatures, cleavage failure occurs before general yield. However, the shear strength is often initially lower than the cleavage strength and the metal then yields and deforms plastically until the shear strength is increased by strain-hardening to a value higher than the cleavage strength.

In most metals, fracture is *transgranular* whether by shear or cleavage, but under certain circumstances the boundary between adjacent grains is weaker than the grains themselves and fracture takes place *intergranularly*. Intergranular cleavage is usually associated with the presence of impurity atoms segregated at the grain boundaries and is the only type of brittle fracture possible in fcc metals. Intergranular shear failure is not important at low temperatures, but in the related form of grain boundary sliding it can be a problem at high temperatures.

In polycrystalline metals, the grains have a range of orientations with respect to the tensile axis and some grains are more favorably oriented for slip or cleavage than others. On a microscopic scale, a cleavage crack follows the cleavage planes of individual grains where possible, on a larger scale, it propagates perpendicular to the applied tensile stress to give a characteristic flat crystalline fracture surface. As the path of an advancing shear crack is determined both by the applied stress system and by any internal stress raisers such as voids and inclusions, ductile fracture can occur by one or more different characteristic modes. On a microscopic scale, however, the crack advances by shear failure on alternate planes of maximum resolved shear stress inclined at approximately 45° to the tensile axis. The surface of a ductile fracture has a characteristic dull, fibrous appearance indicative of the extensive plastic deformation which takes place during failure.

Few materials fail exclusively by one particular mode of fracture: in most cases, more than one mode is operative and the fracture is described as mixed. For example, fracture of a mild steel Charpy V notch specimen tested at room temperature is usually initiated by plastic deformation at the notch root, but once initiated, it spreads by cleavage across much of the specimen until it reverts to a shear mechanism to form the characteristic shear lips at the edges and at the side furthest from the notch (see, for example, the photograph of the fracture halves of Charpy specimens in Fig. 3.27b). The operative mode at any instant is that which requires the smallest strain at the tip of the advancing crack and this is determined by a number of factors, predominant among which is the effective state of

stress. The stress system plays an important role in determining the mode of fracture and this topic will be reconsidered once the basic fracture modes have been described.

3.1.1. Ductile Fracture

Ductile failure can propagate by a number of different modes, each of which produces certain characteristic features on part or all of the fracture surface. Some of the most important types of fracture produced by the action of these basic failure modes are shown schematically in Fig. 3.1.

Pure shear failures have fracture surfaces like that shown in Fig. 3.1 (a), which is known variously as "chisel-edged," "slant," or "sliding off." Such fractures are common in single crystals of hcp metals, where extensive basal slip takes place on a few widely spaced slip bands, final separation occurring by glide plane decohesion. Pure shear failures are also possible in polycrystalline and amorphous materials if large shear strains are concentrated on one of the planes of maximum resolved shear stress lying at 45° to the tensile axis.

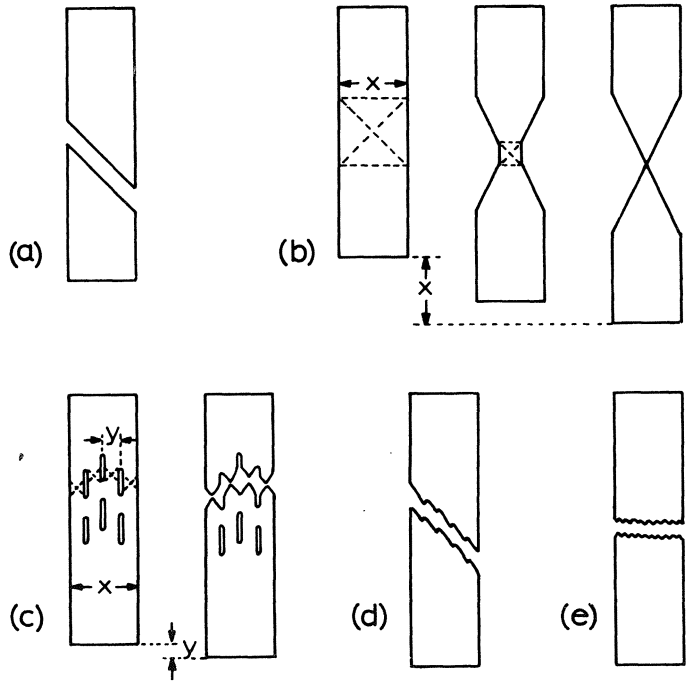

Fig. 3.1. Schematic representations of the principal modes of ductile failure. (a) pure shear, (b) knife-edge, (c) fibrous rupture, (d) shear rupture, (e) normal rupture.

A particularly relevant case is that of *adiabatic shear rupture*, which is, for example, found in pure and precipitation-hardened aluminum fractured at or below ~40°K.[11] We saw in section 2.4.2 that unstable plastic flow can take place if local thermal softening is able to overcome the normal strain-hardening. If the load can relax rapidly enough, the deformation is stabilized, if not, it continues until terminated by adiabatic shear rupture. As adiabatic flow is only possible at temperatures where the specific heat is low, a transition to another mode of ductile fracture occurs at higher temperatures.

Pure and adiabatic shear failures only occur if strain-hardening is negligibly small and deformation is restricted to one shear plane. It is more common, however, for shear to take place simultaneously along two planes of maximum resolved shear stress leading to "necking" and "knife-edge" or "chisel-point" fracture as shown in Fig. 3.1(b). Such fractures are found, for example, in single crystals of fcc metals such as silver and copper, which neck down to a knife edge, slip having taken place on two intersecting slip systems. Extensive necking can also occur in pure polycrystalline materials, some of which (e.g., gold, lead, aluminum) neck down to a point, thus giving a 100% reduction in area prior to failure. In this case, plastic deformation takes place in a thick zone of initial length equal to the width of the specimen (x in Fig. 3.1b), and for a fully ductile material, the tensile elongation is equal to the width x.

Most metals and alloys contain second-phase particles as precipitates which have a strong or even controlling influence on the mode of fracture. In many cases, decohesion occurs between the second-phase particles and the matrix and this leads to the creation of internal cavities or voids. Such a situation is illustrated in an exaggerated form in Fig. 3.1(c), where y is the average spacing between voids. If the matrix material between the voids fails by internal necking as indicated, the failure elongation will now only be equal to y, not x as was the case of the void-free material. Furthermore, if y is much smaller than x, the material may appear macroscopically brittle even though failure on a microscopic scale is ductile: The final appearance of the fracture surface will depend on the coarseness and distribution of the second-phase particles. *Fibrous* rupture as indicated in Fig. 3.1(c) is found in many ductile alloys, such as brass, in which fairly coarse inclusion are possible. If there is a strong shear component present "sliding off" or "*shear rupture*" can occur. In this case, the cavities are distorted by the shear stress and, although failure occurs by necking on a microscopic scale, the macroscopic appearance is that of a 45° shear failure (Fig. 3.1d). In low-strength materials, the shear surface is rough enough to be identified by the naked eye or with a low-power microscope, while in high-strength materials, the shear surface can be so smooth that electron microscopy is necessary to identify the inclusions and distinguish it from

the pure shear failure of Fig. 3.1(a). Thin sheets of metals can fail exclusively by shear rupture and such failures are also commonly found as one component of a mixed fracture, occurring usually at the extremities of thick sections where plane stress loading conditions exist.

Finally, it is possible for ductile failure to occur by *normal rupture* as in Fig. 3.1(e). Fracture on a microscopic scale is by internal necking or shear on alternate planes inclined at $\sim 45^\circ$ to the tensile axis, but there is little or no macroscopic shear. Complete normal rupture of a tensile specimen is relatively rare, but it is very common to find areas of normal rupture at the center of thick bars or plates where triaxial stresses are greatest and fracture takes place under plain strain loading.

The most familiar type of ductile failure found in engineering materials is probably the "*cup and cone*" fracture, whose formation is illustrated in Fig. 3.2.[11] Most structural alloys contain second-phase particles such as oxide inclusions which are either introduced accidentally during fabrication or added purposely to strengthen the alloy. During the plastic deformation which follows yielding, it is common for decohesion to occur at the interfaces between the particles and the matrix, leading to the formation of voids which subsequently become elongated as deformation proceeds (Fig. 3.2a). Once the ultimate tensile stress is exceeded, deformation becomes localized to the necked region of the specimen and the material

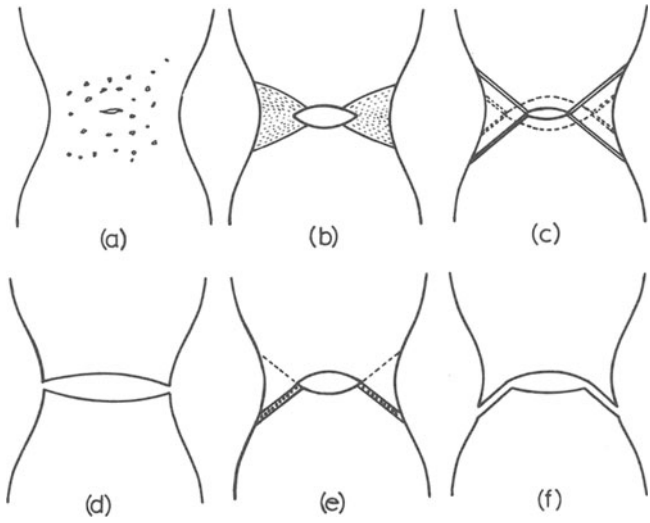

Fig. 3.2. Probable sequence of events during formation of double-cup and cup-and-cone fractures in ductile metals. (a) Initial void formation, (b) growth of central crack, (c) crack growth by localized shear, leading to (d) double-cup fracture, (e) realignment of voids along weakened shear hand, leading to (f) cup-and-cone fracture (after Chin *et al.*[11]).

within this region is no longer subject to a purely uniaxial tensile stress. Instead, a complicated system of triaxial tensile and shear stresses is set up in which the maximum stresses occur at the center of the specimen.[12] Cavities in this central region grow and eventually join together, by the process of internal necking discussed earlier, to form a small central crack (Figs. 3.2b and 3.3a). As the true stress in the necked region increases, this central crack spreads outward in a zigzag fashion by shear on alternate 45° planes of maximum resolved shear stress. The macroscopic result is, however, the formation of a central region of normal rupture and a crack shaped like a thin lens.

The subsequent mode of propagation of this crack depends largely on the purity of the metal. In moderately pure polycrystalline aluminum,[11] for example, a double-cup fracture is obtained at room temperature and down to ~40°K. As indicated in Fig. 3.2(c), crack growth occurs by localized shear in the 45° bands ahead of the crack tip, and as the crack tip propagates, new shear bands are formed in the manner shown by the dashed lines, a continuation of this process leading to the double-cup fracture of Fig. 3.2(d). In less pure materials, such as tough pitch copper and mild steel, crack growth does not occur by the continual formation of new shear bands. Instead, new cavities are nucleated in, and existing voids are realigned along, one of the shear bands as shown in Fig. 3.2(e). Further deformation is now concentrated in this weakened shear band and final fracture takes place by sliding off rupture (cf. Fig. 3.1d) to give the cup-and-cone fracture of Figs. 3.2(f) and 3.3(c). (It should be pointed out that perfect cup-and-cone fractures do not always occur during tensile tests. Very often, "slipped cup and cone" fractures are obtained in which parts of both cup and cone are found on the same fracture half. This is usually due to imperfect alignment of the specimen axis with the tensile stress.)

Evidence for the realignment of cavities along a narrow shear band is given in Fig. 3.3(b),[14] which shows a section through the "cone" part of a fractured copper tensile specimen. Although fracture occurred along the shear band *AB*, a complementary narrow shear zone is clearly visible along *AC* in which void reorientation may be seen.

The extent to which a ductile metal reduces its area prior to failure in a tensile specimen is determined by a number of factors, the most important of which is the volume fraction of second-phase particles. The true failure strain of copper is shown[15] in Fig. 3.4 to rise very rapidly as the volume fraction of hard, second-phase particles is decreased. The shape of the included particles has been found to have some effect on the ductility, lenticular inclusions being more embrittling than equiaxial ones especially if their major axes were perpendicular to the tensile stress: in contrast, the particle size has little or no effect on the true failure strain.

(a)

(b)

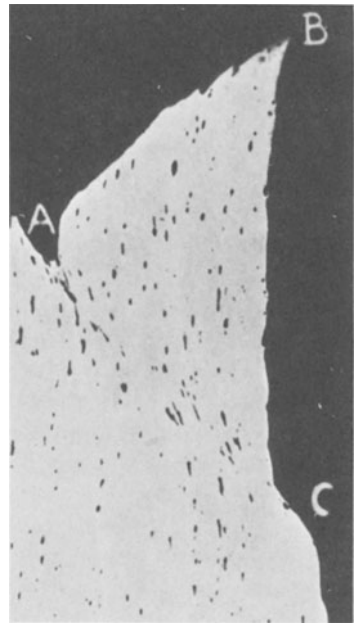

(c)

Fig. 3.3. (a) Central crack and voids in a longitudinal section through the neck of a tensile specimen of tough-pitch copper (Puttick[13]). (b) Cup-and-cone fracture in mild steel. (c) Section through the "cone" part of a tensile specimen of tough-pitch copper showing void reorientation and grain flow (Puttick[14]).

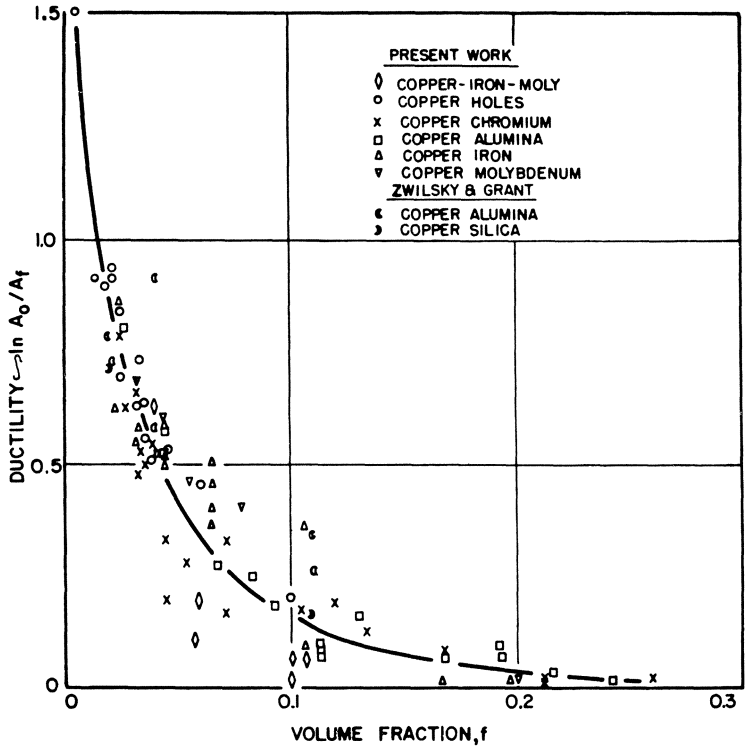

Fig. 3.4. Influence of the volume fraction of voids and inclusions on the ductility of copper (after Edelson and Baldwin[15]).

In many systems, voids nucleate when the local stress exceeds the strength of the inclusion–matrix interface, and decohesion occurs; in other systems, nucleation occurs when the stress becomes large enough to crack the inclusion itself. The rate of strain-hardening also influences the nucleation of voids—the lower the strain-hardening rate, the larger the strain needed to increase the stress to a value high enough for decohesion to occur. Commercially pure aluminum exhibits a larger reduction in area at room temperature than does copper of a similar purity and this difference can be explained by a combination of these two factors, aluminum having both a higher matrix–inclusion interface strength and a lower strain-hardening rate than copper.

As the strain-hardening rate of most fcc metals increases when the temperature is lowered, it might be concluded from the previous argument that their reduction in area would decrease at low temperatures (assuming that the strength of the matrix–inclusion interface is independent of temperature). There is, however, a second factor to be taken into consideration. Once the voids have nucleated, they grow and coalesce by

internal necking, as discussed earlier, but the higher rate of strain-hardening operative at low temperatures will make their growth more difficult. Thus, the slight decrease in reduction in area shown by most commercially pure fcc metals at low temperature reflects a balance between these two effects. From a design point of view, this small decrease is of no consequence, as it is more than compensated by the increase in the uniform elongation characteristic of fcc metals at low temperatures.

Of all the events occurring during the development of ductile fracture—void nucleation, growth, and coalescence; crack formation and propagation and final rupture—it is the initiation of voids which is the most critical. Void nucleation can be inhibited almost completely if large hydrostatic pressures are applied during the tensile deformation of inclusion-containing metals, and the large increases in ductility which can be achieved by this technique are exploited during wire-drawing and hydrostatic extrusion.

Void growth and coalescence take place during the formation of the neck in a tensile specimen, and a detectable crack does not form until just before final rupture. In low- and medium-strength materials, this crack grows in a stable manner under an increasing true stress even though the applied load is decreasing, the rate of crack propagation being determined largely by the spring constant of the testing machine or loading system. In very-high-strength materials, however, an unstable type of low-energy tear fracture can occur under certain loading conditions, but further consideration of this topic is best deferred until the basic concepts of fracture toughness have been examined in section 3.2.

3.1.2. Brittle Fracture

As we shall see in section 3.2, preinduced flaws in ideally brittle solids can propagate directly as cleavage cracks when the elastic stress concentrated at the flaw tip reaches the theoretical cohesive stress of the material. In semibrittle materials such as high-strength metals, plastic relaxation at the tip of a *static* flaw prevents the build up of large elastic stress concentrations, and their direct propagation as a cleavage crack is not possible. Nevertheless, it has been found that inhomogeneous plastic deformation can provide the stress concentrations necessary for the nucleation of microcracks and their initial growth until they are large enough to become self-propagating. There is now a considerable amount of evidence to show that plastic yielding is intimately associated with cleavage fracture in brittle metals and that in *flaw-free* metals the fracture stress σ_F is never less than the yield stress σ_y. For example, in Fig. 3.5, the *fracture* stresses of a series of polycrystalline iron specimens fractured in tension at 77°K show exactly the same dependence on grain size as the *yield* stresses of specimens

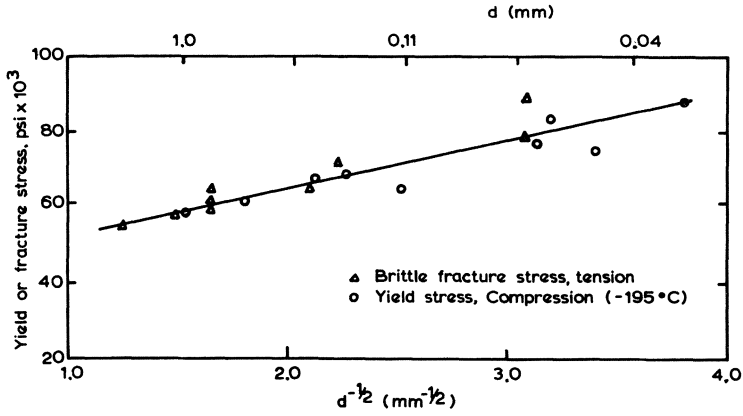

Fig. 3.5. Brittle fracture stress of tensile specimens showing the same grain-size dependence as the yield stress of compression specimens of polycrystalline iron tested at 77°K (after Low[16]).

of the same material measured in compression.[16] The inference to be drawn from this and other, more direct experiments is that a certain, albeit small, amount of plastic deformation is a prerequisite of cleavage fracture.

It is possible to identify three distinct phases in the cleavage fracture of a polycrystalline metal: the nucleation of a microcrack, its initial growth through the grain in which it was nucleated, and its subsequent propagation into and across adjacent grains. The observed fracture stress then corresponds to the stress necessary to carry out the most difficult of these three phases. For example, nucleation and the initial stages of crack growth are, in general, the most difficult phases of fracture in relatively pure metals and, once initiated, the cleavage crack spreads easily into the neighboring grains to cause failure. In contrast, crack nucleation and the initial stages of growth are relatively easy in less pure metals containing inclusions, but these microcracks are readily stopped by the stronger grain boundaries. Many microcracks can then be formed before unstable fracture propagates from one or more suitable cracks, and microcracks stopped by grain boundaries or inclusions can be seen in micrographs of specimens strained almost to fracture, such as that in Fig. 3.7.

We have already seen that the yield stress of a metal is determined both by intrinsic factors, such as its grain size and purity, and extrinsic factors, which include the temperature and rate at which deformation takes place. These variables also influence the fracture stress of the metal and hence determine whether it yields or fails by cleavage. Considering a change in just one of these factors, if it is such as to increase the yield stress from a value less than the fracture stress to an equal value, it will induce a change from shear deformation to cleavage failure and the metal

will undergo a ductile–brittle transition. Such transitions can be obtained by changing one or more of the above variables and, before considering the macroscopic aspects of ductile–brittle transitions in section 3.3, we will examine briefly some of its microscopic aspects.

One of the first mechanisms proposed to explain the nucleation of cleavage cracks by inhomogeneous plastic deformation was that due to Zener[17] shown schematically in Fig. 3.6(a). Edge dislocations from a source

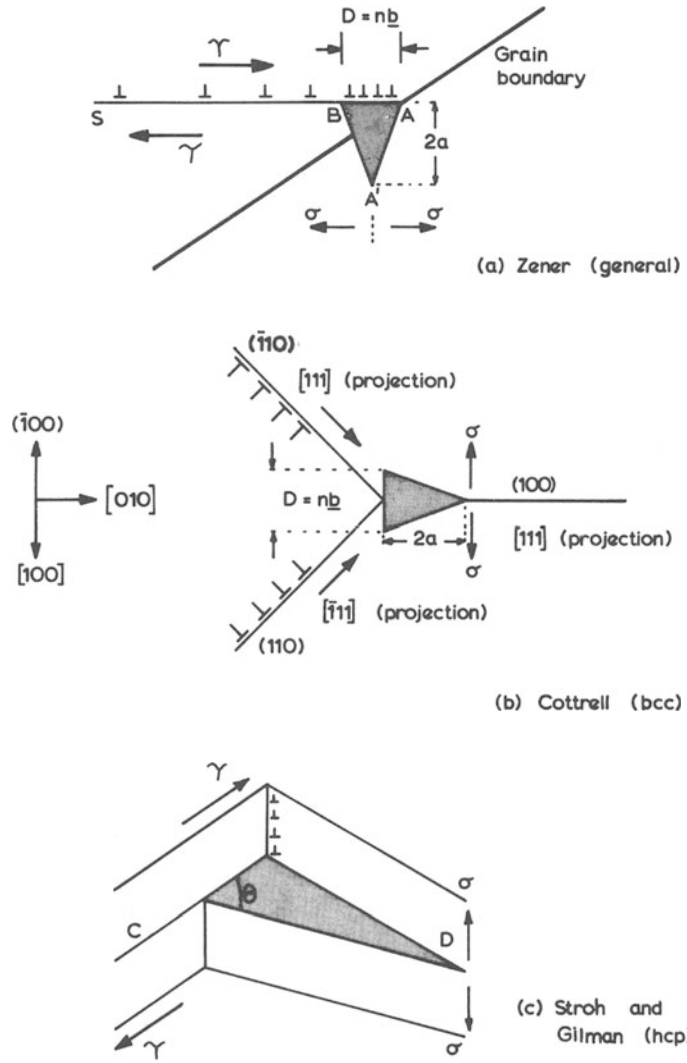

Fig. 3.6. Mechanisms for the nucleation of cleavage cracks by inhomogeneous plastic deformation, proposed by (a) Zener[17], (b) Cottrell,[18] and (c) Gilman[20] and Stroh[21].

S move down their slip plane until they become blocked by a grain boundary A; they pile up against it and large shear stresses are concentrated at the tip of this glide band. However, as edge dislocations are equivalent to extra half-planes of atoms lying perpendicular to the slip plane, a group of r dislocations of Burgers vector b produces a wedge of height rb between A and B which induces large tensile stresses in the cleavage plane AA'. A cleavage crack then nucleates when these tensile stresses are large enough to exceed the cohesive stress of the material. It should be noted that the crack has been nucleated by the shear stress τ acting along the plane SA and that such cracks can in fact be nucleated by applied *compressive* stresses. They will not, however, propagate until a sufficiently large tensile stress is applied perpendicular to the plane AA'.

Obstacles strong enough for this mechanism to operate are provided by grain boundaries in polycrystals and by hard second-phase particles in dirty metals. If such phases are segregated at the grain boundaries, crack nucleation can be facilitated because the brittle second-phase particles crack readily. If the cleavage planes of the matrix are well-aligned with those of the particle, the crack spreads easily into the matrix. If, however, they are badly misoriented, it is more difficult for the crack to cross the particle–matrix interface and propagation is hindered. Furthermore, grain boundary segregation of impurities can, in some systems, be so severe as to produce intergranular fracture if the boundary is weaker than the matrix.

As grain boundaries and second-phase particles do not exist in pure single crystals, it is necessary to postulate further mechanisms by which cleavage fracture can be nucleated in these materials. It is believed that the deformation processes can themselves produce barriers which are strong enough to block dislocations and generate the required stress concentrations. The actual mechanisms proposed depend on the crystal structure of the material concerned and that shown in Fig. 3.6(b), due to Cottrell,[18] is for bcc metals. Dislocations gliding on two intersecting $\{110\}\ \langle 111\rangle$ systems interact to form a dislocation whose Burgers vector lies on the (001) cleavage plane, and succeeding dislocations combine in the same way to nucleate a microcrack. As before, a tensile stress applied perpendicular to the (001) plane is necessary before the crack can propagate. Cleavage cracks formed by this mechanism have been observed in silicon iron single crystals strained at 77°K.[19]

In hexagonal metals, both slip and cleavage take place on the basal plane and the mechanism[20,21] illustrated in Fig. 3.6(c) can generate cleavage cracks under these conditions. A low-angle tilt boundary lies normal to the basal plane and slip occurring in plane C causes a crack to form along plane D.

In Fig. 3.6(b), the cleavage crack was produced by intersecting dis-

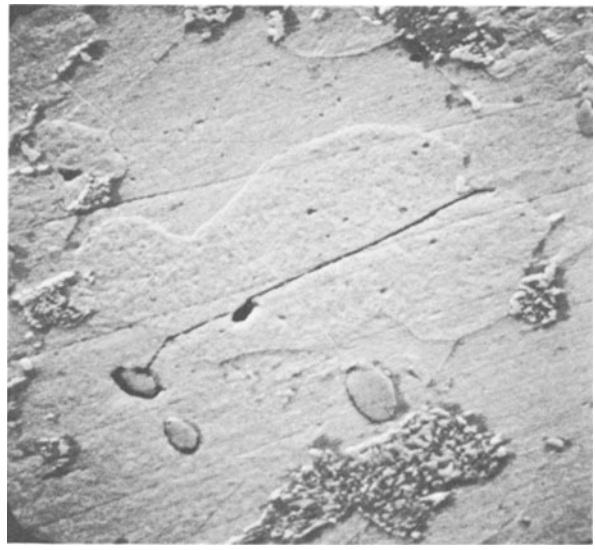

Fig. 3.7. Microcrack stopped at the grain boundaries of a mild steel specimen fractured in the ductile/brittle transition region.

locations; a similar mechanism involving the successive interaction of deformation twins can also form microcracks as shown in Fig. 3.8.[22] Twinning is a favorable mode of deformation in bcc metals both at low temperatures and high strain rates and it is a possible mechanism for the nucleation of cleavage cracks under these loading conditions. It is thought to occur in single crystals of bcc metals, such as iron, where the fracture behavior at low temperatures is determined largely by the orientation of the cleavage plane with regard to the tensile axis. Both cleavage and twinning are favored when there is a large tensile stress normal to the cleavage plane: at temperatures above the ductile–brittle transition, they deform by twinning, at low temperatures, they fail by cleavage. If, however, twinning is prevented by prestraining at room temperature and the crystals are subsequently strained at low temperature, cleavage failure does not occur, the crystals deform by slip, and failure is by shear in a chisel-point mode.[23] This is, however, only circumstantial evidence for, not definite proof of, the hypothesis that twin–twin interactions are the active crack-nucleating mechanism. The relationship between mechanical twinning and brittle fracture in bcc metals has been reviewed recently by Reid,[24] who concludes that there is not, as yet, a proven one-to-one correlation between twinning and cleavage crack nucleation and that until the origin of fracture can be located unambiguously at such a site, the hypothesis cannot be considered proven.

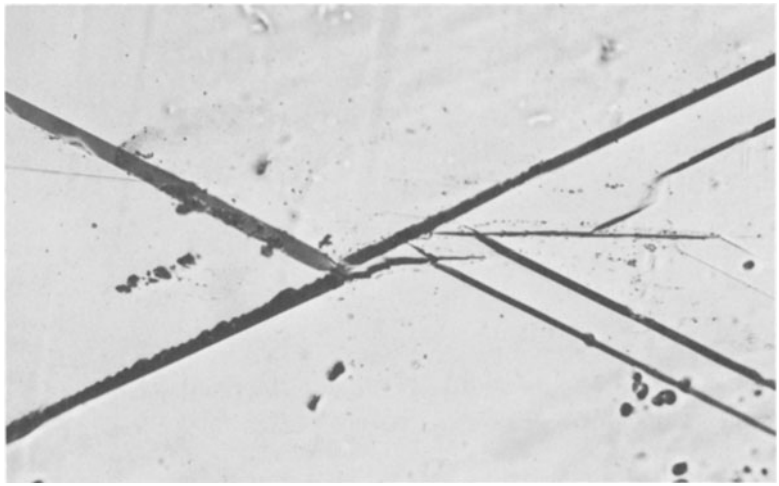

Fig. 3.8. Nucleation of a transgranular cleavage crack in silicon–iron by the intersection of deformation twins (Hull[22]).

As stated earlier, there are three basic stages in the cleavage failure of a polycrystalline metal: nucleation, initial growth, and passage through the first major barrier encountered by the crack. It was assumed by Stroh[25] that crack nucleation was the most difficult of these three stages and that, once nucleated, the first crack formed spread to cause complete cleavage failure. This is possibly true for cleavage fracture in some single crystals, but the fracture criteria derived from this assumption were unable to explain a number of the observed details of cleavage failure in polycrystalline metals, in particular the occurrence of stopped microcracks and the fact that cleavage failure can occur after a period of plastic deformation and strain-hardening. Even more damning was its inability to explain the transition from brittle to ductile behavior brought about by a reduction in grain size of the metal.

In contrast, Cottrell[18] and Petch[26] assume that the initial stages of crack growth are the most difficult. In Fig. 3.6(b), a pile up of a dislocation was shown to produce a plastic displacement nb at the base of a wedge-shaped crack. The effective shear stress on the plane SA necessary to produce this displacement is $\tau - \tau_i$ (the applied shear stress minus the friction stress), which is equal to nbG/L (b is the Burgers vector, G the shear modulus, L the slip band length). The work done is the applied stress multiplied by the plastic displacement, $\sigma \times nb$, and *it is assumed that this must be greater than, or equal to, the effective surface energy of fracture,* $2\gamma'$, *in order that the cleavage crack may propagate without being blunted by plastic relaxation at its tip,* i.e.,

$$2\gamma' \leqslant \sigma nb \leqslant \sigma[(\tau - \tau_i)/G]L \leqslant \sigma[(\tau - \tau_i)/G]d \qquad (3.1)$$

where the slip band length is assumed to be half the grain size, $2d$. Once yield has occurred in one or two grains, the applied shear stress is equal to the yield stress, i.e., $\tau = \tau_y$. But the Hall–Petch equation (1.8) showed that the yield stress σ_y is related to the friction stress σ_i and the grain size by the equation $\sigma_y = \sigma_i + k_y d^{-1/2}$, or $\sigma_y - \sigma_i = k_y d^{-1/2}$.

As $\sigma \simeq 2\tau$,

$$\tau_y - \tau_i \simeq \tfrac{1}{2} k_y d^{-1/2}$$

Substituting in equation (3.1) for $\tau_y - \tau_i$ and rearranging, we get

$$\sigma_{\text{growth}} \simeq (4G\gamma'/k_y)d^{-1/2} \qquad (3.2)$$

for the stress necessary to produce initial crack growth. If initial growth is the most difficult of the three stages of fracture, the growth stress equals the fracture stress, i.e.,

$$\sigma_f \simeq (4G\gamma'/k_y)d^{-1/2} \qquad (3.3)$$

In Fig. 3.9, both yield and fracture stresses are shown as a function of grain size for a series of mild steel specimens fractured at 77°K. In fine-grained specimens, the yield stress is lower than the fracture stress and strain-hardening is necessary to increase the stress by $\Delta\sigma$ to the fracture stress σ_f. As the grain size is increased ($d^{-1/2}$ decreased), less strain-harden-

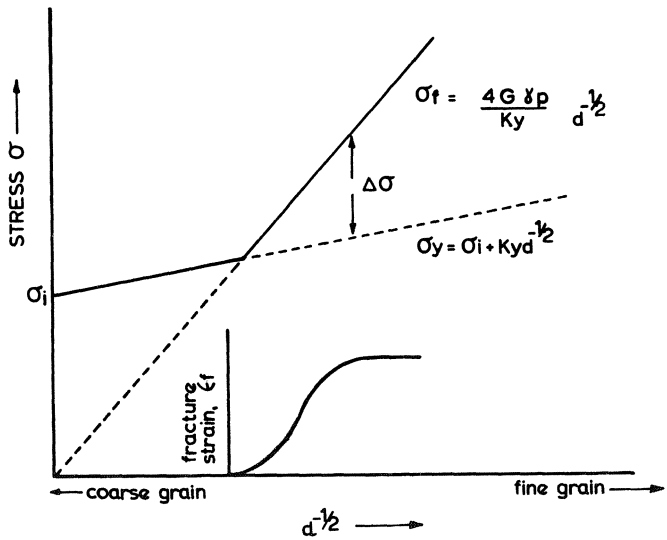

Fig. 3.9. Grain-size dependence of the yield and fracture stresses of a series of mild-steel specimens tested in tension at 77°K showing occurrence of ductile brittle transition. Ductility falls to zero as the grain size is increased to the critical value.

ing is needed to reach the fracture stress and hence the percentage elongation decreases to become zero at $\sigma_y = \sigma_f$. When the grain size is larger than this critical size, the effective fracture stress departs from the line $\sigma_f = 4G\gamma' d^{-1/2}/k_y$ to follow the yield stress line because crack nucleation cannot take place until yield has occurred in at least one grain.

None of the terms in the right-hand side of equation (3.3) are strongly dependent on temperature and, to a first approximation, the fracture stress may be considered almost temperature-independent. In contrast, we have seen in sections 1.5 and 1.6 that the friction stress σ_i of bcc metals (and hence the yield stress, as $\sigma_y = \sigma_i + k_y d^{-1/2}$) increases strongly as the temperature falls. This situation is illustrated in Fig. 3.10, where σ_{y1} and σ_{f1} are the yield and fracture stresses, respectively, of a bcc metal having a certain composition, grain size, etc. The curves cross at temperature T_1, which is the transition temperature for this material. As before, the fracture stress follows the yield stress curve below T_1 because the yield stress must be exceeded before nucleation is possible. If the grain size of this material is refined, both yield stress and fracture stress will be increased to σ_{y2} and σ_{f2}, respectively, where the increase $\Delta\sigma_f$ will be greater than the increase $\Delta\sigma_y$. (This follows from the relative slopes of the lines for σ_f and σ_y as a function of $d^{-1/2}$ in Fig. 3.9). Thus, the transition temperature will drop to T_2 for this fine-grained specimen. In contrast, other metal-

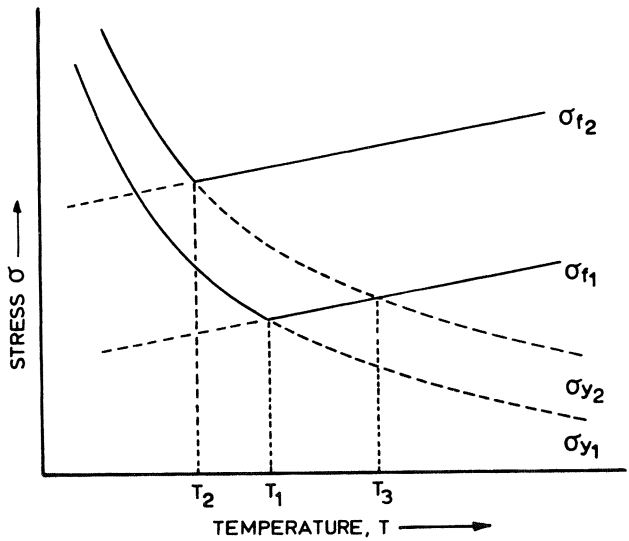

Fig. 3.10. Temperature dependence of the yield stresses (σ_{y1} and σ_{y2}) and fracture stresses (σ_{f1} and σ_{f2}) of coarse-grained (1) and fine-grained (2) specimens of a bcc metal having ductile–brittle transition temperatures at T_1 and T_2, respectively. The transition at T_3 is for a coarse-grained specimen whose yield stress has been increased to σ_{y2} by cold-work.

lurgical treatments, such as cold-working or solution-hardening, which raise the yield stress but not the fracture stress must produce a rise in transition temperature. In the diagram, such a treatment is assumed for convenience to raise the yield stress to σ_{y2} thus causing the transition temperature to rise to T_3. It is difficult to make such generalizations on the effect of precipitates, as they can influence both nucleation and initial growth. Coarse, segregated particles with poor inclusion–matrix interfaces are likely to aid nucleation and lower the fracture stress; fine, well-dispersed precipitates can reduce the active slip lengths and increase the fracture stress. For example, quenched and tempered plain carbon steels have lower transition temperatures than annealed steels because this treatment produces a very small grain size and finely dispersed carbide particles.

Expressions of the form $\sigma_f = (4G\gamma'/k_y)d^{-1/2}$ can be derived for most crack nucleation mechanisms, as they all make use of the Petch relationship between yield stress and grain diameter. It is possible to explain the effect of most intrinsic and extrinsic variables on the fracture stress σ_f by considering their effect on the parameters γ' and k_y, or the ratio γ'/k_y: for example, k_y for twinning is greater than that for slip and hence the fracture stress is increased when twinning is inhibited. The effective surface energy γ' plays an important role in determining σ_f and hence the probability of cleavage fracture. In ideally brittle materials, $\gamma' \equiv \gamma_t$, the surface energy, and as γ_s is small, σ_f is small and cleavage is easy. In metals, plastic deformation takes place at the tip of a moving crack and some of the stored energy is dissipated during plastic work. The effective surface energy is then given by γ_p, the work of plastic deformation, which is usually much larger than γ_s.

There are a number of mechanisms by which energy can be absorbed during plastic deformation; in single crystals, one of the most important is the formation of cleavage steps which are created by the interaction of the moving crack with defects in the crystal and which appear as river lines. The other important dissipative process is the generation of mobile dislocations at or near the crack tip. This process leads to plastic relaxation and blunting of the crack tip, and the greater the amount of plastic relaxation, the more difficult it becomes for the crack to propagate. Furthermore, it can be shown that a finite time is required for a dislocation to be nucleated and move down its glide plane away from the crack tip: thus, if the velocity of a cleavage crack is low, many dislocations can be formed as it passes through any given region and considerable plastic relaxation can occur. If the crack velocity is high, few dislocations are generated during its passage and little energy is dissipated. Friedel[27] uses this concept to differentiate between ductile and brittle fracture, brittle fracture occurring when cracks are able to propagate rapidly without significant plastic relaxation at the tip of the moving crack. Factors which inhibit dislocation motion and thus minimize plastic relaxation include: (1) a

high Peierls force for dislocation movement (section 1.5.3), (2) a large increase in this force at low temperatures (section 1.5.1), (3) the strong pinning of dislocations by impurity atoms (section 1.5.3), and (4) a highly strain-rate-sensitive yield stress (section 1.5.3).

All these factors can be found in bcc metals and, to a lesser extent, in hcp metals, and thus brittle fracture is favored in these metals; they are absent in fcc metals and hence failure in these metals is always ductile, as rapid crack propagation is not possible.

In polycrystalline metals, the grain boundaries provide an additional powerful mechanism for absorbing energy from a moving crack. If the angle of mismatch between adjacent grains is small, the crack is able to cross the boundary quite easily and the effective boundary strength σ_B is small. In contrast, for large misorientations, the boundary strength is high (the effective boundary surface energy $\gamma_B \simeq \gamma'/\cos^4 \phi$, where ϕ is the angle of misorientation) and moving cracks can be slowed down or even halted. In semibrittle metals, it is probable that cleavage propagates discontinuously, with new microcracks being nucleated ahead of the main crack front, probably on a plane distinct from that of the main crack; these cracks then join together by tearing in the grains between them. Such behavior is found in many bcc metals at temperatures just above or just below their ductile–brittle transition, but at very low temperatures, cleavage crack propagation can be continuous.

Once a moving cleavage crack has successfully overcome the first strong barrier that it encounters, it is usually large enough to grow solely by the release of elastic energy supplied by the tensile component of the applied stress. The conditions for the propagation of such a crack were first considered by Griffith[28] for completely brittle materials such as glass, but such an analysis also provides a convenient starting point for an examination of the fracture of nonideally brittle solids such as metals.

3.2. CRACK PROPAGATION: FRACTURE TOUGHNESS

3.2.1. The Energy Balance Approach

Any notch, crack, or void in a material acts as a stress raiser and the degree of elastic stress concentration which it causes depends largely on its form and sharpness. Inglis[29] has shown that the maximum stress σ_m developed at the tip of an elliptical crack of length $2a$ and root radius ρ is given approximately by

$$\sigma_m = 2\sigma(a/\rho)^{1/2} \tag{3.4}$$

where σ is the applied stress.

In ideally brittle solids, even relatively small applied stresses can be

magnified sufficiently for the stress at the tip of an atomically sharp crack to exceed the theoretical cohesive strength of the material: atomic bonds are then broken and the crack starts to propagate. Elastic strain energy is released during this process, but work must also be done in order to create new crack surfaces. Considering the system shown in Fig. 3.11 in which a tensile stress σ is applied to a thin plate of unit width which contains either an elliptical center crack of length $2a$ or a semielliptical edge crack length a, the elastic strain energy released by the extension of such a crack is given by

$$U_E = -\pi a^2 \sigma^2 / E \tag{3.5}$$

The surface energy gained by the creation of these two new crack surfaces is

$$U_S = 4a\gamma_s \tag{3.6}$$

where γ_s is the true surface energy per unit area. Griffith[28] postulated that such a crack will propagate in an unstable manner when an incremental increase in its length no longer changes the net energy of the system, i.e., when

$$\partial U/\partial a = \partial(U_E + U_S)/\partial a = (-2\pi a \sigma_F^2/E) + 4\gamma_s = 0$$

or

$$\sigma_F = (2E\gamma_s/\pi a)^{1/2} \tag{3.7}$$

Once a crack of the critical length $2a$ has formed, its further extension can take place at a lower applied stress, due to the inverse relationship between crack length and stress, and the crack accelerates rapidly to a limiting velocity slightly less than that of sound in the material concerned.

In extremely brittle materials such as glass, the critical crack sizes

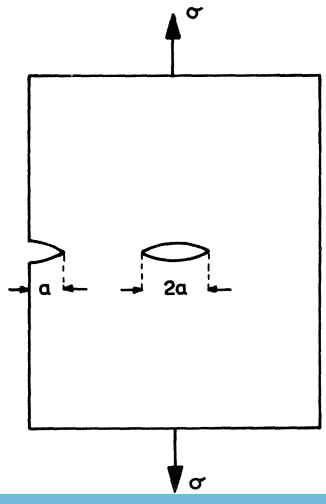

Fig. 3.11. Schematic representation of a material containing a Griffith crack.

predicted by the Griffith criterion are of the order of a few microns in length and are similar to those found experimentally. Further proof of the dominant role played by these microcracks was provided by the fact that carefully prepared, freshly drawn fibers which contained no such cracks were found to have strengths which approached the theoretical value for glass.

In the above analysis, the Griffith criterion was developed for a thin sheet subjected to plane stress loading. Other workers have extended the analysis to oblate spheroidal cracks in thicker material and have shown that a small correction due to Poisson's ratio must be added for the plane strain stress system. Furthermore, it can also be extended to cover biaxial stress systems and compressive stresses. It then predicts that the stress required to cause unstable fracture under a uniaxially applied compressive load is eight times higher than the uniaxial tensile failure stress. Such results have been experimentally verified and are exploited in commercial glass production, where compressive stresses are induced into the surfaces of glass plates in order to improve their strength.

The application of the Griffith criterion to the failure of apparently brittle metals did not, however, meet with much success. As we saw in section 3.1.2, a certain amount of plastic deformation is needed for the initiation of cleavage cracks in metals. Furthermore, plastic deformation which takes place during crack growth tends to blunt the crack tip and thus increase the energy needed for its propagation. Plastic deformation therefore plays an important role in the fracture of brittle metals and Orowan[30] has shown that, when plastic deformation is concentrated in a region ahead of the crack tip which is small in comparison to the length of the crack, the Griffith equation may be modified to

$$\sigma_F = [2E(\gamma_s + \gamma_p)/\pi a]^{1/2} \tag{3.8}$$

where γ_p is the work of plastic deformation at the tip of a growing crack. As for most metals $\gamma_p \simeq 10^3 \gamma_s$, the modified Griffith criterion can often be simplified to

$$\sigma_F \simeq (2E\gamma_p/\pi a)^{1/2} \tag{3.9}$$

Hence, for metals, the energy balance is between the *elastic* energy released by crack growth and the *plastic* work done during such growth. Furthermore, as $\gamma_p \simeq 10^3 \gamma_s$, critical crack lengths in brittle metals are of the order of a few millimeters instead of a few microns as found for more truly brittle solids such as glass.

The work of plastic deformation γ_p depends on the magnitude of the stresses and strains developed in the material during fracture, and, in order for a material to be tough and to absorb a considerable amount of energy during fracture, both stresses and strains must be high. As many of the

metallurgical factors which increase the strength of a metal simultaneously cause a large decrease in the strains developed during failure, it is sometimes found that high-strength alloys have such unacceptably low toughnesses that they are unsuitable for general use. This important relationship between strength and toughness will be considered further in section 3.2.4.

3.2.2. The Fracture Mechanics Approach

An alternative approach to the problem of unstable crack propagation is due to Irwin,[31] who developed a *stress intensity criterion* for fracture as opposed to the *energy criterion* developed by Griffith. He showed that the local elastic stresses developed near the root of a crack could be described in terms of a *stress intensity factor* K which, for a thin, infinitely wide plate containing an infinitely sharp elastic crack of length $2a$ and subjected to a nominal tensile stress σ is given, for plane stress loading, by the relationship

$$K = \sigma(\pi a)^{1/2} \tag{3.10}$$

Unstable fracture is assumed to occur at stress σ_F when K is equal to the *critical stress intensity factor* K_c, which is also known as the *fracture toughness* and which is a characteristic of the material concerned, i.e.,

$$K_c = \sigma_F(\pi a)^{1/2} \tag{3.11}$$

Irwin also defined a parameter G called the *crack extension force* which, for plane stress loading, is given by the relationship

$$G = K^2/E \tag{3.12}$$

and at fracture this has the critical value G_c, which is the *crack resistance force* or *toughness* of the material. Hence

$$G_c = K_c^2/E \tag{3.13}$$

As at fracture $K_c = \sigma_F(\pi a)^{1/2}$, where σ_F is the nominal fracture stress, we have, on substitution,

$$G_c = \sigma_F^2 \pi a/E$$

i.e.,

$$\sigma_F = (EG_c/\pi a)^{1/2} \tag{3.14}$$

On comparison, it can be seen that equations (3.7) and (3.14) have the same form and that

$$G_c \equiv 2\gamma_s \tag{3.15}$$

Hence, both the Griffith and Irwin approaches lead to similar results, although the concepts involved are different in the two cases.

Similar calculations have been performed for a variety of simple crack

shapes and for a number of different stress distributions, but all tend to a relationship similar to that given in equation (3.14), modified if need be by a term involving Poisson's ratio ν and a shape correction factor Q.

The above relationships were developed on the basis of linear elastic fracture mechanics and they apply rigorously only to completely brittle solids, as does the unmodified Griffith equation. We have seen, however, that the propagation of cracks in metals is governed by the plastic deformation which both precedes and accompanies crack growth and this fact must therefore be recognized and allowed for if the Irwin analysis is to be applied to metals. Such an extension is, in fact, only possible if the volume of metal subjected to plastic deformation is small in comparison to that stressed elastically. This in turn implies that the plastic zone size is small in comparison to both the crack length and the net remaining cross section of material. Current procedure,[33] which is based on suggestions made originally by Irwin,[32] is to allow for plastic deformation in the small zone ahead of the crack tip by adding an extra increment r_y to the original crack length a, i.e.,

$$a_{\text{mod}} = a + r_y = a[1 + (r_y/a)] \tag{3.16}$$

where the plastic zone correction factor r_y is defined by the relationship

$$r_y = (1/2\pi)(K/\sigma_y)^2 \tag{3.17}$$

σ_y being the yield strength of the material. But, from equation (3.11), at fracture, $K_c = \sigma_F(\pi a)^{1/2}$; hence, on substitution and rearrangement,

$$r_y/a = \tfrac{1}{2}(\sigma_F/\sigma_y)^2 \tag{3.18}$$

Now, the lower the ratio r_y/a, the smaller the correction necessary for the plastic zone size and thus the smaller will be the errors which arise from the application of linear elastic fracture mechanics to the failure of non-ideally brittle solids such as metals. It follows from equation (3.18) that this situation is most nearly realized for high-strength alloys in which the gross fracture stress σ_F is small compared with the yield strength σ_y. The errors increase as σ_F approaches σ_y, and when measuring K_c, it is common practice to limit σ_F to $\leqslant 0.8\sigma_y$ in order to ensure that excessive plastic deformation does not precede fracture. When $\sigma_F \geqslant \sigma_y$, fracture occurs after general yield, and linear elastic fracture mechanics cannot be applied to this type of failure. The analysis of such failures has, however, been attempted by Wells and his collaborators by use of the crack opening displacement approach, and this topic will be reconsidered in section 3.3.3.1.

Returning now to the application of fracture mechanics to the failure of metals, we saw that, for ideally brittle solids, G_c, the crack resistance force, was given by equation (3.14), $G_c = \pi a\sigma_F^2/E$. If we now replace a

by the corrected crack length $a[1 + (r_y/a)]$ and substitute from equation (3.18) for $r_y/a = \frac{1}{2}(\sigma_F/\sigma_y)^2$, we obtain

$$G_c = (\pi a \sigma_F^2/E)[1 + \tfrac{1}{2}(\sigma_F/\sigma_y)^2] \tag{3.19}$$

for the crack resistance force corrected for plastic zone size.

A similarly modified expression can also be obtained for the fracture toughness K_c of nonideally brittle metals. For a perfectly elastic solid, we had, from (3.11), $K_c = \sigma_F(\pi a)^{1/2}$ or $K_c^2 = \sigma_F^2 \pi a$. To allow for the effect of plastic deformation, we substitute a_{mod} for a, where $a_{\text{mod}} = a + r_y$. Now by definition, $r_y = (1/2\pi)(K_c/\sigma_y)^2$ at fracture. Hence, on substitution in (3.11),

$$K_c^2 = \sigma_F^2 \pi a[1 + (1/2\pi a)(K_c/\sigma_y)^2] \tag{3.20}$$

This can be rearranged to give the more common form

$$\sigma_F = K_c/[\pi a + \tfrac{1}{2}(K_c/\sigma_y)^2]^{1/2} \tag{3.21}$$

We saw in equation (3.18) that the errors introduced by the use of the term r_y to correct for plastic deformation are determined by the ratio of fracture strength to yield strength, and it should be noted that the strain-hardening characteristics of the material also influence the validity of this correction. A further important factor which must be considered is the type of stress system operative at failure, and this in turn is determined by the specimen thickness and other geometric effects. A schematic diagram of the crack surface, crack front, and the plastic zone is shown in Fig. 3.12.

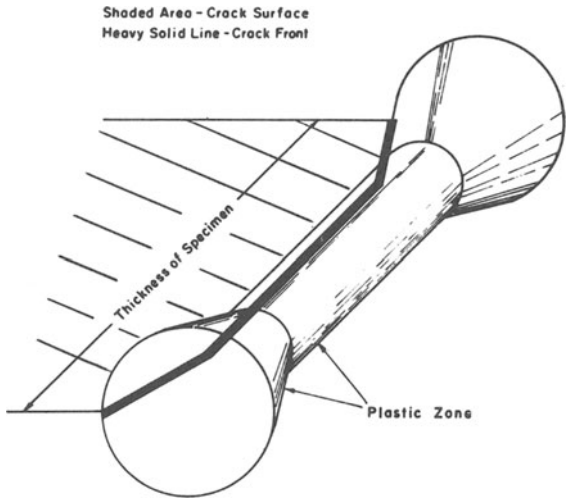

Fig. 3.12. Schematic diagram of the crack surface, crack front, and plastic zone in a specimen showing both slant and square failure (Weiss and Yukawa[70]).

The constraint to plastic deformation provided by the surrounding elastically stressed material is greatest at the center of the specimen, the radius of the plastic zone is small, the material is at its most brittle, and the crack is effectively under plane strain loading. At the edges of the specimen, however, the constraint to plastic deformation is less and the radius of the plastic zone is larger. The material is here subjected to plane stress loading and failure is usually by a shear mechanism which absorbs a larger amount of energy. The fracture toughness is thus determined by the relative amounts of slant (high-energy shear) and square (low-energy shear or cleavage) failure and this is itself a function of the specimen thickness B. In Fig. 3.13, the fracture toughness of a 7075 aluminum alloy is shown as a function of specimen thickness, B, and also as correlated with the percentage of square fracture appearing on the failure surfaces. It can be seen that, for very thick specimens, the fracture toughness decreases asymptotically toward a limiting value denoted as K_{1c}, the *plane strain fracture toughness* (the subscript 1 denotes the opening mode of crack extension as defined by Irwin, in which the applied tensile stress is normal to the faces of the crack). For such thick specimens, the constraint to plastic deformation is at its greatest and fracture is entirely square. As the thickness B is reduced, shear lips appear at the edges of the specimen and K_c rises as the ratio of square/slant fracture decreases. Eventually, a maximum fracture toughness is obtained for thin specimens when failure is either fully slant or "vee-slant" (i.e., plane stress loading). The reduction in toughness which takes place for even thinner sheets is associated with a reduction in the total volume of material which undergoes plastic deformation. For most metals, however, this decrease in toughness occurs at thicknesses be-

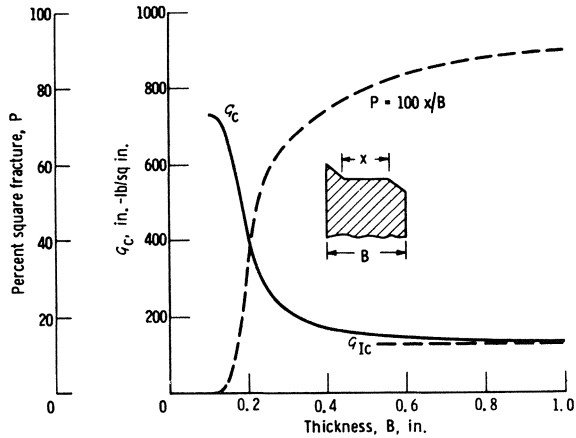

Fig. 3.13. Variation of fracture toughness G_c and the percentage of square fracture with specimen thickness in a 7075-T6 aluminum alloy (Srawley and Brown[34]).

low those of practical interest. (The low toughness characteristic of very thin sheets may be illustrated by the ease with which aluminum cooking foil may be torn!)

As the sheet thickness B has such a strong influence on the degree of plastic constraint and hence on the transition from plane stress to plane strain failure, a parameter β_c is defined by the relationship

$$\beta_c = K_c^2/B\sigma_y^2 \tag{3.22}$$

to give an indication of the degree of constraint due to specimen thickness. If $\beta_c = 2\pi$, $B = r_y$ and failure is completely shear; when $\beta_c > 4$, shear lips usually occupy more than half the fracture surface; and when $\beta_c < 1$, the shear lips are small.

When the surfaces of fractured sheet specimens are examined, it is found that only in the case of fully slant failures does the crack front propagate linearly across the thickness of the sheet, as illustrated in Fig. 3.14(a). For most mixed fractures, the "square" part of the crack advances ahead of the shear lip as illustrated schematically in Fig. 3.14(b) and the shape of the crack front is approximately parabolic. The characteristic chevron markings also indicated are formed perpendicular to the advanc-

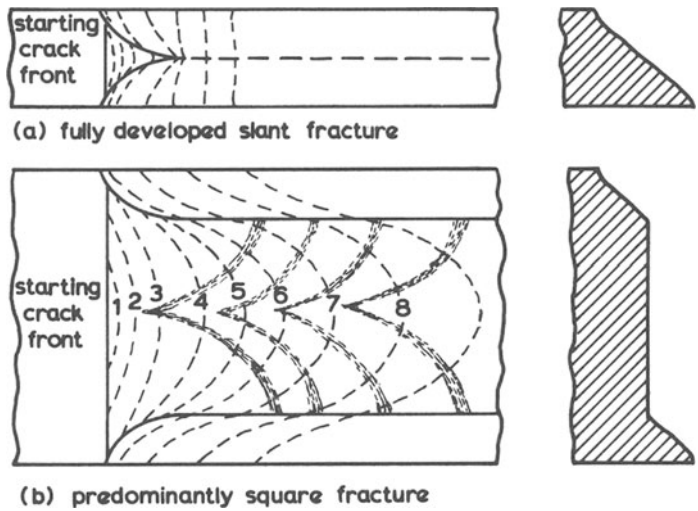

Fig. 3.14. Schematic representations of the advancement of the crack front in (a) a thin specimen which shows a slant fracture and (b) a thicker specimen which shows both slant and square fracture. In the latter case, the square portion advances fastest and leads to the formation of the characteristic chevron markings, which are also illustrated (after Srawley and Brown[34]).

ing crack front and point back toward the origin of the failure, thus facilitating the identification of the initiation site. These chevrons or radial markings form because the advancing crack front branches and propagates on a number of different levels, the radial markings denoting the boundaries between adjacent noncoplanar fracture surfaces. When the crack approaches the free surface, the radial markings bend outward to become normal to the surface as they cross the shear lip.

It must be emphasized that the relationship between fracture toughness and specimen thickness described above is an intrinsic effect found for homogeneous materials and is not a result of the various metallurgical processes which may have been used to form the material. Such inhomogeneities are, for example, produced by the differences in cooling rates between the center and edges of thick sections and they must of course be allowed for when using such materials. As K_c varies with specimen thickness even for homogeneous materials, it cannot be considered a true material constant, as such a property should be independent of testing conditions. In contrast, the plane strain fracture toughness K_{1c} is not dependent on B and thus it may be considered as a material constant if care is taken to ensure that it is measured in a meaningful manner. Much experimental effort has been expended in determining K_{1c} for a large number of materials in a variety of shapes and tested under a range of environments, temperatures, etc. This emphasis on K_{1c} values does not, however, mean that measurements of K_c are any less valuable. They can provide valid engineering design data which are characteristic of the thickness of material tested, and under circumstances where thin-sheet materials are to be used for structural application, such data are in fact more valuable than those obtained for thicker material which may have had a different metallurgical history and, hence, mechanical properties.

3.2.3. Measurement of Fracture Toughness

Although a detailed consideration of fracture toughness testing techniques is outside the scope of this text, a brief indication of some basic points is considered necessary to illustrate some of the precautions which have to be taken to obtain valid results. In essence, artificial cracks of known size, sharpness, and form are introduced into specimens of suitable geometry and dimensions. These are loaded slowly while both crack extension and applied load are measured and K_c or K_{1c} values are derived from the stresses and crack sizes at which significant rapid crack growth takes place or at which instability is reached. Almost any specimen shape and notch geometry could theoretically be used for such tests as long as they were amenable to suitable stress analysis. In practice, however, there

are five main types of specimen which have become accepted as standards and whose characteristics are discussed in detail by Srawley and Brown.[34,35] They are as follows.

3.2.3.1. ***The Center-Cracked or Symmetrically Edge-Cracked Specimens.*** These specimens were the first to be recommended by the ASTM Special Committee[33] and they have since been widely used. A plate of width W containing a central crack of half-length a, or two collinear edge notches each of length a, is loaded in tension to a stress σ. The stress intensity factor K is given by

$$K = \sigma[\tan(\pi a/W)]^{1/2} \tag{3.23}$$

and both K_c and K_{1c} can be measured by this technique.

3.2.3.2. ***The Single Edge-Notched Plate.*** Such a plate, again loaded in tension, gives values of K_{1c} only, as do all the remaining tests. Less material and lower test loads are required for these specimens compared to the previous types, but the formulas used for deriving K values are more complex.

3.2.3.3. ***Notched Bend Specimens.*** Both three- and four-point loading can be used for these specimens, but the latter is considered more reliable. Formulas for K_{1c} are again complex and, although a convenient test, it tends to give less accurate results than the previous two methods.

3.2.3.4. ***Surface-Flawed Plate Specimens.*** This type of specimen, which contains a semielliptical surface crack, is especially relevant, as it simulates the effects of cracks commonly found to have caused failure in pressure vessels and which are particularly dangerous, as their presence is not revealed by fluid leakage. However, such specimens have the disadvantage of needing testing machines of high loading capacity to cope with the plate thicknesses used for this type of application.

3.2.3.5. ***Circumferentially Notched Round Bars.*** Such bars loaded in tension have been widely used for revealing the notch sensitivity of brittle materials. Approximate K_{1c} values can also be obtained from these tests if suitable cracks are produced and if loading is sufficiently axial.

Returning to the center- or edge-cracked plates of 3.2.3.1, it has been found that the values of K_c given by such tests can be low if either the width of the plate is too small or if the critical crack length is too short. The first of these effects is illustrated in Fig. 3.15, where K_c is shown as a function of plate width W; also indicated on the same diagram is the ratio of the net section stress σ_N to the yield stress σ_y. It can be seen that K_c becomes independent of W when $\sigma_N/\sigma_y \leqslant 0.8$; the same criterion has also

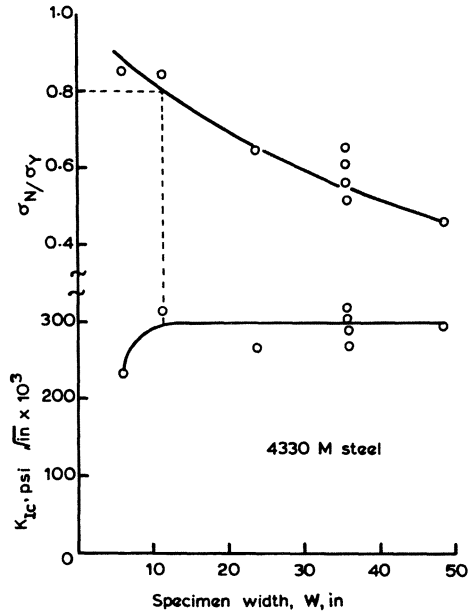

Fig. 3.15. Measured K_c values and the ratio of net section stress to yield stress, σ_N/σ_y, plotted as a function of specimen width to show that K_c values are invalid if σ_N/σ_y increases above 0.8 (data from Ref. 71).

been found to hold for the length of a critical crack in a plate of constant width. Thus, the ASTM committee recommend that σ_N at instability must not be greater than $0.8\sigma_y$; while initial crack lengths of up to 1/3 of the specimen width are commonly used to ensure reliable values of K_c.

A further point of importance concerns the required sharpness of the preinduced notch. As testing experience was built up, it became apparent that the sharpest possible cracks were needed to give reproducible results and it is now common practice for a machined notch to be sharpened by the initiation of a natural crack at its root. This is usually achieved by fatigue, although hydrogen embrittlement, partial cleavage, and electrical discharge machining are also occasionally employed. A variety of techniques are used to measure the length of the crack during its subcritical growth: these include displacement gauges, electric potential probes, cinematography, acoustical sensors, etc. Further details of these techniques can be found elsewhere.[34,35] It is worth noting that the largest source of error in the measurement of G_c or K_c lies in the uncertainty with which the critical crack length can be obtained at the point of instability.

In the previous section, we saw that the plane strain fracture toughness K_{1c} determines the critical flaw size and fracture stress in very thick materials; K_{1c} may thus be obtained directly by measurement of these quantities at instability in thick specimens. It is, however, also possible to obtain K_{1c} values from thinner sheet specimens by use of the "pop-in"

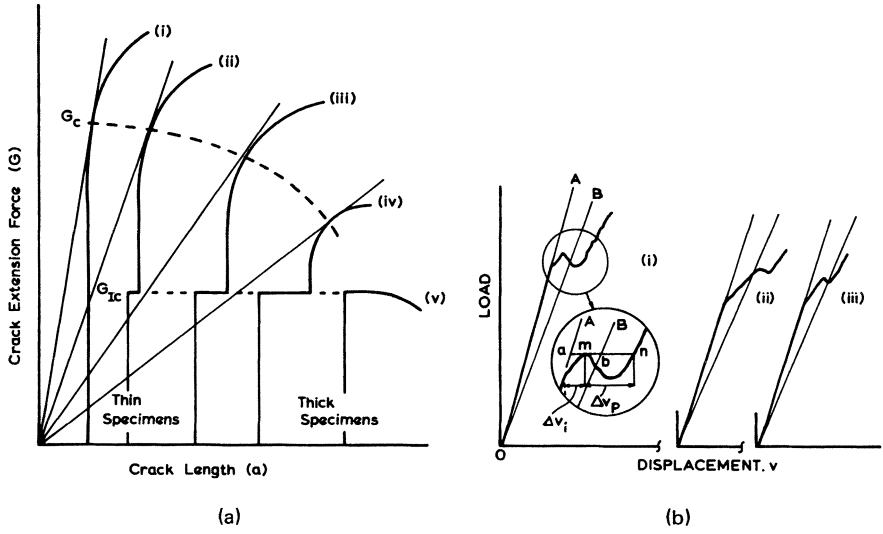

Fig. 3.16. (a) Crack extension force as a function of crack length for specimens of varying thickness showing "pop-in" occurring at G_{1c} for the thicker specimens (after Srawley and Brown[34]). (b) Determination of G_{1c} by the secant offset technique (after Brown and Srawley[10]).

technique first described by Krafft *et al.*[36] They noticed that, in sheet specimens thick enough to exhibit both slant and square fracture, the initiation of crack growth from a preinduced flaw occurred as a distinct burst or "pop-in" which appeared as a discontinuous jump on the strain-recording device and usually also as an audible click. Furthermore, "pop-in" was found to occur at a value of G (or K) approximately equal to the G_{1c} (or K_{1c}) value of the material, thus giving a convenient method of measuring these parameters. This behavior is illustrated in Fig. 3.16(a), where the crack extension force G is shown as a function of crack length for a series of specimens of varying thicknesses. For the thinnest specimen (i), failure is entirely by shear and instability occurs at $G = G_c$. For the thicker specimens (ii), the crack begins to grow rapidly under plane strain conditions at the center of the specimen, when $G = G_{1c}$ (for example, it might advance from position 1 to position 5 in Fig. 3.14) and this is indicated by a discontinuous jump in crack length. The crack does not, however, grow to the critical size before it is arrested by the plastic work done in breaking through at the free surfaces of the sheet to form shear lips. Further slow crack propagation then occurs until instability is reached at $G = G_c$. For the thicker specimens (iii) and (iv), G_c is lower and "pop-in" more pronounced, while for the thickest sheet (v), unstable crack growth develops at a value of $G = G_{1c}$.

In practice, however, load–displacement curves do not always give such a clear indication of pop-in as inferred from Fig. 3.16(a) and it has been found necessary to develop suitable criteria and methods of analysis to determine whether or not the derived K_{1c} values are valid. In particular, difficulties arise with curves which show either excessive deviation from linearity preceding pop-in, or pop-in of insufficient magnitude. Brown and Srawley[10] have proposed that a secant offset criterion be used to determine the acceptability of any questionable events, and the basis of their method is illustrated in Fig. 3.16(b). A pop-in indication is defined as a temporary maximum in the load–displacement curve followed by an increase in displacement which occurs without the load rising above this maximum value. Such an event is shown by curve (i). Line OA is a linear extension of the initial portion of the load–displacement curve, while OB is a secant whose slope is determined by a set of rules detailed by Brown and Srawley. With reference to the enlarged portion of these curves shown in the inset, deviation from linearity Δv_i is deemed to be acceptable if the maximum m falls between the lines OA and OB, i.e., $\Delta v_i = am < ab$, while pop-in is of sufficient magnitude if the pop-in displacement Δv_p is at least equal to the maximum permitted deviation from linearity ab, i.e., $mn \geqslant ab$. Thus, the event occurring in curve (i) would be acceptable, while that of curve (ii) fails because of excessive deviation from linearity, and that of curve (iii) fails as the pop-in is of insufficient magnitude.

The curves shown in Fig. 3.16(a) are often known as "R curves," where the parameter R is the resistance to crack growth. During the slow crack growth which precedes instability, the crack resistance is equal to the rate at which energy is absorbed during crack growth, while at instability, R equals G_c, the critical crack extension force. This condition is achieved when the tangent from zero touches the R curve and such tangents are also shown in Fig. 3.16(a) for the five specimens. As before, it can be seen that G_c decreases with increase in specimen width, and for the very thick sample, the tangent touches the R curve at $G = G_{1c}$. Srawley and Brown[34] have suggested that the parameter R is, in fact, more basic than G_c, which is just a limiting value of R for a long crack in a wide plate. Furthermore, it has also been suggested[37] that the concept of R curves may be used to explain slow crack growth during fatigue and also crack arrest phenomena such as those shown in the Robertson test.

So far, we have discussed fracture toughness testing on the assumption that reliable values of K_c or G_c are required for use in rigorous analyses based on the principles of fracture mechanics. While this is undoubtedly true in a large number of cases, there are also occasions when the basic principles of fracture mechanics can be applied less rigorously to indicate whether a given material is likely to be notch-brittle in service or, more frequently, to show which of a range of available materials is likely to

prove the least notch-sensitive. Such tests, for example, are frequently used during alloy development and in the evaluation of different types of material for use in a particular application. Much of the work performed on the toughness of materials at cryogenic temperatures comes into these categories and Schwartzberg[38] has reviewed the work carried out up to 1967 and discussed some of its limitations. In particular he has shown that some of the earlier work involved the use of undersized specimens, with the result that ranking orders derived from these tests were erroneous. This is illustrated in Fig. 3.17, where K_c is shown as a function of specimen width W for two materials I and II. These curves have the same form as that in Fig. 3.15, where it was shown that the low K_c values obtained with narrow plates were due to ratios of net section stress/gross yield stress in excess of 0.8. Thus, although material I actually has a higher fracture toughness than material II, the narrow plate specimens used for the cryogenic tests inverted this ranking due to excessive plastic deformation in the specimen of material I. It should, however, be noted that the results obtained from the narrow specimen *underestimated* the real fracture toughness and thus gave overconservative design criteria.

The need for a simple, cheap screening test for materials selection was recognized by the ASTM special committee on fracture toughness and they recommended the use of fixed-width, sharp edge-notch or center-notch specimens, with the preferred measure of merit being the notch-strength ratio at the minimum possible service temperature. (The notch-strength ratio, otherwise known as the notch sensitivity ratio or the notch-tensile ratio, is defined as the net stress in the notched specimens at maximum load divided by the ultimate tensile stress in an unnotched specimen.) It was recognized that this test had its limitations and it was therefore sug-

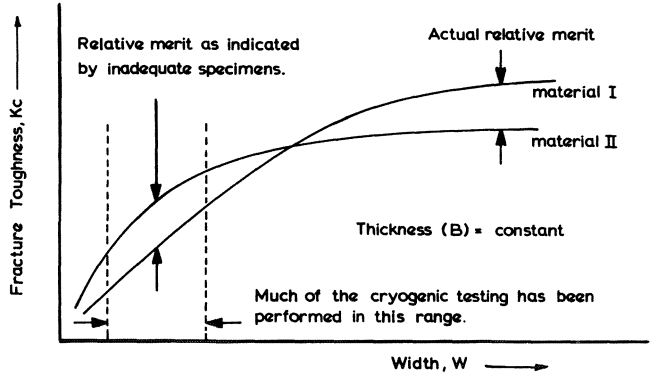

Fig. 3.17. Variation of fracture toughness with specimen width for two different materials, showing how incorrect ranking orders can be obtained by the use of undersized specimens (after Schwartzberg[38]).

gested that the appearance of the fracture surface, and in particular the ratio of slant to square fracture, should also be taken into consideration. As experience built up on the use of the notch–strength ratio criterion for screening tests, it became apparent that the geometry of the notch chosen, and in particular the value of the stress concentration (or notch acuity) factor K_t, had a strong influence on the value of the notch–strength ratio. Low stress concentration factors, e.g., $K_t \approx 2$, were found to be too insensitive to distinguish between notch-tough and notch-brittle materials, while K_t values in excess of $\sim$12 made even tough materials appear brittle. Most workers therefore settled for a compromise and K_t values of about 6 were usually selected, e.g., 6.0 by Brisbane[39] and 6.3 by Christian[40] and his co-workers. With these values of K_t, it has been found[41] that, if the notch–strength ratio is less than about 0.70, there is a strong probability of an unstable fracture developing in service. Watson *et al.*[42] have taken this process a step further by correlating the results of notch–strength tests with those obtained from high-stress axial fatigue tests of welded stainless steel specimens, to show that fatigue resistance is high when the notch–strength ratio exceeds unity and low when the ratio drops much below unity.

Finally, it should also be noted that Kaufman and Johnson[43] have shown that a much more consistent rating of a range of aluminum alloys was obtained when the notch–yield ratio (the ratio of the tensile strength of a notched specimen to the yield strength of an unnotched specimen)

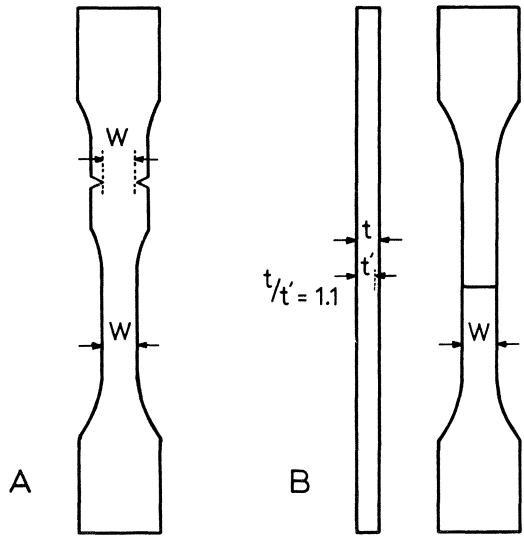

Fig. 3.18. Schematic illustration of the significance of the notch–yield ratio. (A) Series arrangement of smooth and notched tensile specimens. (B) More realistic situation in which the specimen has a scratch on its surface (after Kaufman and Johnson[43]).

was used instead of the notch-strength ratio. Furthermore, the rating achieved was almost independent of notch geometry and sharpness, in contrast to the variability noted earlier for the notch-strength ratio. In view of the importance of plastic deformation in determining the notch toughness of metals, it is also argued[44] that the notch-yield ratio is a more meaningful parameter, its significance being illustrated in Fig. 3.18. If the material from which specimen *A* is made has a notch-yield ratio of less than unity, it will fracture at the notch before it yields in the straight portion of the specimen. The larger the notch-yield ratio, the greater the amount of plastic deformation which precedes fracture and the tougher the specimen. A more realistic example is that shown in case *B*, which represents a smooth tensile specimen with a scratch across its surface. If the depth of the scratch is 10% of the sheet thickness, then a design criterion based on a notch-yield ratio in excess of 1.1 would afford some protection against failure in service due to the accidental development of such a scratch.

3.2.4. The Relationship between Strength and Toughness in Metals

Before proceeding to discuss the application of fracture mechanics to the design of load-bearing components made from materials with low fracture toughness, it is appropriate to note briefly some of the main classes of material which come into this category and also to consider some of the metallurgical factors responsible for their low toughness. We have already seen that, for many metals and alloys, an increase in strength is accompanied by a decrease in both tensile ductility and toughness. Although this relationship is not completely rigid, it does provide a convenient starting point for examining the fracture toughness of metals. Following Tetelman and McEvily,[1] it is convenient to define high-strength materials as those which have yield strengths at room temperature in excess of 1/150 of their elastic modulus E, medium-strength materials such that $E/150 > \sigma_y > E/300$, and low-strength materials as those for which $E/300 > \sigma_y$. If these criteria are applied to steels, aluminum alloys, and titanium alloys, the classification shown in Table IV is obtained.

Table IV[a]

	Approximate relations	Steels	Aluminum alloys	Titanium alloys
High strength	$\sigma_y > E/150$	$\sigma_y > 180$	$\sigma_y > 60$	$\sigma_y > 110$
Medium strength	$E/150 > \sigma_y > E/300$	$180 > \sigma_y > 90$	$60 > \sigma_y > 30$	$110 > \sigma_y > 55$
Low strength	$\sigma_y < E/300$	$\sigma_y < 90$	$\sigma_y < 30$	$\sigma_y < 55$

[a] All stresses are in ksi ($\equiv 10^3$ psi). E is the elastic modulus.

3.2.4.1. ***High-Strength Materials.*** For these materials, the amount of energy absorbed during normal or shear rupture is low and in consequence they have low fracture toughnesses. Now we saw earlier that the energy absorbed during fracture in a metal was determined largely by the work of plastic deformation at the crack tip, γ_p, and that this, in turn, depended on both the stresses and strains developed in the material during failure. It can, in fact, be shown that, for most metals,

$$G_{1c} = 2\gamma_p \simeq 2\sigma_y \rho \varepsilon_{f'} \tag{3.24}$$

where σ_y is the yield stress, ρ is the radius of the crack tip, and $\varepsilon_{f'}$ is the ductility of the specimen at the crack tip. The low values of G_c in high-strength materials are due to the low values of ρ and/or $\varepsilon_{f'}$ that characterize failure in these metals. For example, fracture in many high-strength materials occurs by the formation and subsequent coalescence of voids in the plastic zone ahead of the crack tip. These voids form when second-phase particles or inclusions are cracked by the stresses induced in the plastic zone, and the higher the yield stress, the larger the number of particles cracked. This effectively decreases the spacing between voids and, as we saw in Fig. 3.1(c), it lowers the ductility $\varepsilon_{f'}$ by reducing the amount of internal necking which takes place during void coalescence. This decrease in $\varepsilon_{f'}$ outweighs the influence of the increase in σ_y in equation (3.24) and the net result is a lowering of G_{1c}. In other cases, e.g., cleavage fracture, the low toughness can be ascribed more to a decrease in crack root radius ρ, but as $\varepsilon_{f'}$ and ρ are highly interrelated, it is not really possible to separate these two factors.

It should be noted that virtually all metallurgical processes which are used to produce high-strength materials—precipitation-hardening or second-phase hardening, cold-work, etc.—also lower their notch toughnesses by encouraging low-energy tear or cleavage failure. Thus, high strength and good notch toughness are virtually incompatible in such materials unless some way can be found to reduce the plastic stress concentrations which are produced by the presence of cracks and other flaws. One solution to this problem is to provide weak interfaces along planes perpendicular to that on which the crack propagates. If these interfaces have low shear strengths, they will be split by the triaxial stresses set up ahead of the advancing crack and when the crack reaches such a boundary it will be blunted and/or deflected. The crack can then only advance once the stress has built up sufficiently for it to be reinitiated, and large amounts of energy can be absorbed if this splitting process can be made to occur frequently. In Ausformed steel, the required weak interfaces are produced parallel to the working direction and very high strength and toughness are obtainable for this material. It is, in fact, widely known that the notch toughnesses of many metals can be highly anisotropic due to the structures

developed during metallurgical working processes such as rolling and extrusion. It is therefore important that the relevant G_c value is known for the most critically stressed orientation of the material. Finally, it should also be noted that the principle of "toughness by weak perpendicular interfaces" is exploited by nature in the form of bone, bamboo, and many other naturally occurring fibrous materials. Furthermore, man is now following this example by the development of composite materials in which high-strength fibers are embedded in low-strength metal or plastic matrices to produce strong, yet tough engineering materials. This topic will be reconsidered in more detail in chapter 4.

3.2.4.2. ***Medium-Strength Materials.*** The criterion used to divide materials into high-, medium-, and low-strength types was based on their yield strengths at room temperature. However, as we saw in chapters 1 and 2, the yield strength of a number of important alloys can increase quite considerably below room temperature, and if σ_y exceeds the value of $E/150$, the material behaves at low temperature as if it had a high strength at ambient temperature. Its failure mode changes from a high-energy-absorbing shear mode to a low-energy-absorbing type which can be either cleavage or low-energy tear. The material thus undergoes a tough–brittle transition at low temperatures, G_c has a low value, and safe design procedures for low-temperature operation should therefore be based on the principles of fracture mechanics. The effect of temperature on the toughness of medium-strength materials will be considered in more detail in section 3.2.6.

3.2.4.3. ***Low-Strength Materials.*** The toughness of low-strength materials is determined fundamentally by their liability to failure by cleavage. If the material cannot fail by cleavage, fracture is always by a high-energy-absorbing tear mechanism and it is tough under all operating conditions unless there are very large and easily identifiable flaws present. This is the situation which holds for all low-strength metals with a face-centered-cubic structure. If, on the other hand, the material is able to fail by cleavage, it undergoes a ductile–brittle transition at some temperature which is determined by the mechanical properties of the material and the conditions under which it is stressed. At high temperatures, where failure is by ductile rupture, it has a high G_c value: at low temperatures, where cleavage failure occurs, G_c is low and unstable fracture is possible. As cleavage failure can take place in the body-centered-cubic form of iron and steel, these materials undergo a ductile–brittle transition at some temperature and they may be used safely only above this transition. The exact determination of safe operating temperatures for such important materials as low alloy steels is, however, a complex subject and this is discussed further in section 3.3.

3.2.5. Applied Fracture Mechanics

Fracture in a low-energy mode is thus a potential hazard in high-strength materials at ambient temperature and in some medium- and low-strength materials at low temperatures; under such circumstances, the only successful basis for safe design is one which prevents the initiation of such failures. This in turn requires that the operating stress is at all times maintained below the fracture stress σ_F, as determined by the fracture toughness of the material and the size and shape of the largest flaw present. Historically, the initial impetus for the application of fracture mechanics to this problem came from the analysis of a large number of failures in pressure vessels and other highly stressed components in which fracture was found to have originated at a small crack or flaw. By determining the size and shape of the critical flaw, calculating the stresses likely to have been present at failure, and measuring K_c for specimens cut from the failed component or similar material, it was possible to show that the observed values of a_{crit} agreed well with those predicted by the basic fracture mechanics equation $\sigma_F = (EG_c/\pi a_{\text{crit}})^{1/2}$ and $K_c = \sigma_F(\pi a_{\text{crit}})^{1/2}$, providing that they were expressed in a form suitable for the material and crack geometry concerned.

Some failures were found to be due to incorrect design and/or materials selection, where the toughness was so low and the applied stress so high that the critical flaw size was too small to be detected; in other cases, residual stresses were responsible for causing the local stress to exceed σ_F even though the general level of applied stress was much lower. The other main cause of failure was due to the material used having a lower toughness than that specified, and this usually arose through one of two mechanisms. It was frequently found that failure was initiated at a processing defect such as a bad weld, a large inclusion, a slag particle, or a blow hole in a casting and that this flaw was either large enough to initiate failure directly or that it acted as a nucleus from which slow crack growth occurred until the flaw reached its critical size. Alternatively, if the material was free from defects yet had a toughness lower than that specified, it was usually possible to trace this to an incorrect heat-treatment which had altered its structure, or to some environmental effect, such as stress corrosion or hydrogen embrittlement, which lowered the toughness and/or caused a subcritical flaw to grow.

Once enough experience had been built up in the application of fracture mechanics to such failures and it had been proven that the values of K_c and G_c obtained from specimen testing could be correlated with those obtained from the destructive testing of full-scale pressure vessels and other types of hardware, it became possible to extend the use of fracture mechanics

to the safe design of highly stressed components. Of the three main types of flaw commonly encountered—the through-the-thickness flaw, the surface flaw, and the embedded flaw—only the first normally gives advance warning of its presence, by causing fluid leakage or a loss of pressure. Although surface and embedded flaws can, in some cases, grow to form through-the-thickness cracks prior to instability, it is frequently found that their critical crack sizes are smaller than the wall thickness of the vessel and such flaws are thus particularly dangerous. Much effort has therefore been directed at this aspect of the problem. Stress analysis is most easily carried out for elliptical or semielliptical flaws and fortunately it has been found that the majority of observed cracks are of this type. Various factors have been used to quantify such flaws, such as their area, $a/2c$ ratio etc., but Tiffany and Masters[45] claim that the best correlations are obtained by the use of the a/Q ratio, where Q, the flaw shape parameter, is defined by the relationship

$$Q = \phi^2 - (0.212)(\sigma/\sigma_y)^2 \tag{3.25}$$

and ϕ is the complete elliptical integral of the second kind. Furthermore, the presence of the ratio of gross stress to yield stress, σ/σ_y, gives an automatic correction for the plastic zone size r_y, and hence it is not necessary to use the modified form of the basic fracture mechanics relationships as derived in equations (3.19) and (3.21). For example, the relevant equation for a semielliptical surface flaw is

$$(a/Q)_{\text{crit}} = (1/1.21\pi)(K_{1c}/\sigma)^2 \tag{3.26}$$

while for an embedded elliptical flaw, it becomes

$$(a/Q)_{\text{crit}} = (1/\pi)(K_{1c}/\sigma)^2 \tag{3.27}$$

This relationship between applied stress and a/Q ratio is shown graphically in Fig. 3.19 for a range of values of K_{1c}, the dotted curve at the high-stress end of the curve for the lowest K_{1c} value indicating that the applied stress could never in practice exceed the ultimate tensile stress of the material. In Fig. 3.20, the relationship between flaw shape parameter Q and $a/2c$ is shown for various ratios of σ/σ_y together with sketches which define a and $2c$ for surface and embedded flaws.

Thus, in theory, it is possible to predict the maximum allowable design stress of a vessel if suitable values of a, Q, and K_c are known. In practice, the major difficulties arise in deciding what are the most suitable values for these parameters.

We have already seen that the fracture toughness K_c is influenced by a number of factors, of which the operative stress system is one of the most important. This, in turn, is determined by the width and thickness of the

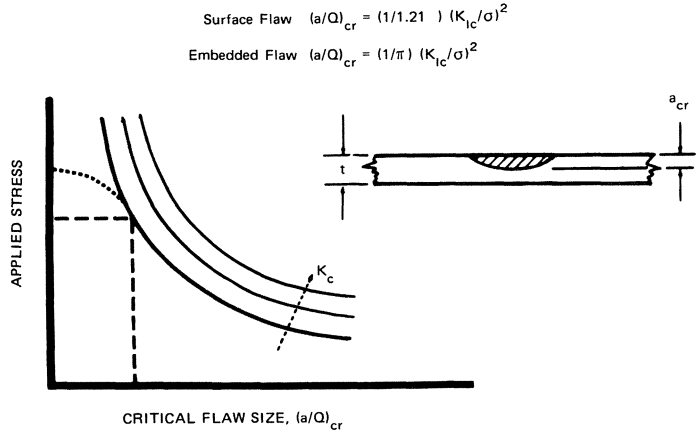

Fig. 3.19. Relationship between applied stress and critical flaw size $(a/Q)_{crit}$ for materials with different values of K_c.

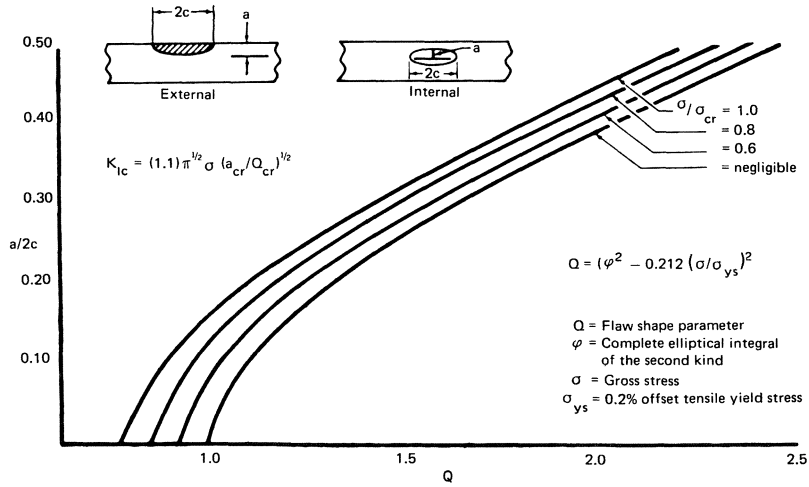

Fig. 3.20. Relationship between flaw shape parameter Q and $a/2c$ for various values of σ/σ_{ys}. Inset: Definition of a and $2c$ for internal and external flaws (Tiffany and Masters[45]).

material concerned and by its prior mechanical and thermal history, as these factors are largely responsible for its strength and toughness. Furthermore, most materials, especially those which have been rolled or forged, are anisotropic and thus their toughness varies throughout the structure. If it has been welded, it is probable that the toughness of both the weld metal and the heat-affected zone will have been reduced compared with that of the parent metal; while, if the structure has to operate in a corrosive environment or at a temperature other than ambient, it is important

to use the value of K_c appropriate to these conditions. Thus, in order to ensure that a safe design is achieved, it is essential to specify the value of K_c relevant to the worst possible conditions that the material is likely to meet in service.

The stress analyses necessary for solution of the fracture mechanics equation can also be complicated, especially if the vessel concerned is of a complex shape or if it contains welds or other stress raisers which can give high local stresses. Furthermore, as both the applied stress and the toughness of the material differ from point to point within the structure, the critical flaw size will also vary and the potentially fatal flaw will be that which has the most unfavorable combination of applied stress and material toughness. Such combinations are often to be found in or near weldments, and, in pressure vessels, joints in the short transverse direction are particularly prone to brittleness.

Estimation of the size of flaws likely to be present in the structure also presents a problem and it is usual to use as a starting point the size of the largest flaw which can remain undetected by the nondestructive testing technique employed. Furthermore, if loading is such that this flaw could grow during subsequent service by, for example, fatigue or stress corrosion, it is necessary to make allowances for such growth and this is usually done by measuring the rate of crack growth on a range of samples exposed to such conditions.

Despite these acknowledged difficulties in choosing suitable values for the parameters involved, it is worth considering an example of the application of fracture mechanics to a realistic cryogenic problem. Spheres made from forged Ti–5Al–2.5Sn alloy have been used to store helium gas at liquid-hydrogen temperature. The yield stress of Ti–5Al–2.5Sn at 20°K is ~210 ksi and K_{1c} for wrought, fine-grained sheet or plate has a value of about 55 ksi $\sqrt{\text{in}}$. If the design stress is chosen, rather conservatively, as 110 ksi and if we assume for the purpose of this analysis that a typical surface flaw might have a depth/length ratio ($a/2c$) of 0.2, then, from Fig. 3.20, we find that the flaw shape parameter Q has a value of ~1.3 for this flaw in a metal with $\sigma/\sigma_y = 110/210 = 0.52$. Inserting these values into equation (3.26) for a surface flaw, we have $(a/Q)_{\text{crit}} = (1/1.21\pi)(K_{1c}/\sigma)^2$ i.e., $a_{\text{crit}} = (1.3/1.21\pi)(55/110)^2 = 0.085$ in. Thus, the critical crack has a depth of 0.085 in. and a length of 0.42 in. If the thickness of the vessel were ~0.400 in., it would be reasonable to expect that such a crack would be detected by a moderately sensitive radiographic technique.

If, however, a less favorable K_{1c} value of 35 ksi $\sqrt{\text{in.}}$ is taken to be more typical of the toughness of wrought titanium alloy, then a similar analysis gives a critical crack of depth 0.035 in. and length 0.165 in. Such a crack size would be close to the resolution limit of most radiographs and thus could possibly pass undetected. If the vessel had to be accepted or

rejected at this stage, it is highly probable that it would be rejected as unsafe and thus the possibilities for weight saving offered by its high strength/weight ratio would go unexploited.

There is, however, a further way in which the concepts of fracture mechanics can be applied to this problem. Before they are accepted for service, virtually all pressure vessels undergo a proof test in which they are subjected to a proof stress σ_p which is higher than the proposed operating stress σ_{op} by a factor α known as the proof-test factor, i.e., $\sigma_p = \alpha\sigma_{op}$. If the vessel passes this test successfully, it can be inferred from the upper curve in Fig. 3.21, which shows the relationship between the applied stress and the flaw size parameter, a/Q, that the test has also established that no flaw of size greater than $(a/Q)_i$ can exist in the vessel, i.e., for an embedded flaw, the proof test demonstrates that

$$(a/Q)_i \leqslant (1/\pi)(K_{ic}/\sigma_y)^2 \leqslant (1/\pi)(K_{ic}^2/\alpha\sigma_{op})^2$$

But, at the operating stress,

$$(a/Q)_{crit} = (1/\pi)(K_{ic}/\sigma_{op})^2$$

Hence, on elimination of $(1/\pi)(K_{ic}/\sigma_{op})^2$ between these two equations, we find

$$(a/Q)_{crit} \geqslant \alpha^2(a/Q)_i \tag{3.28}$$

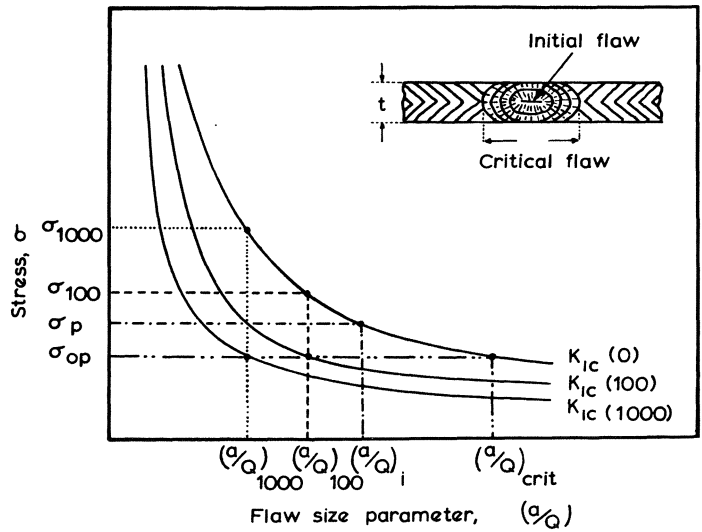

Fig. 3.21. Relationship between applied stress and flaw size parameter, illustrating the establishment of various flaw size safety factors by proof testing at different stress levels. The upper curve represents K_{1c} values for static loading and the lower curves are for cyclic lives of 100 and 1000 cycles, respectively (after Tiffany and Masters[45]).

Thus, the proof test has also established a flaw size safety factor for the vessel.

The analysis can also be taken a stage further by considering the length of time in a corrosive environment or the number of fatigue cycles that it would take before a subcritical flaw could grow to reach the critical flaw size $(a/Q)_{crit}$. Considering, for example, the case of slow crack growth by fatigue, it can be shown[45] that the number of cycles to failure is a function of the ratio of the initial stress intensity K_{Ii} to the critical stress intensity K_{Ic}, and that this relationship can be determined experimentally by fatigue testing a range of notched specimens at different levels of stress intensity. The results of these experiments can be plotted to give cyclic life curves as shown, for example, in Fig. 3.21 for 100 and 1000 cycles. Thus, 100 cycles at the operating stress σ_{op} would be needed to enlarge a flaw of initial size $(a/Q)_{100}$ to the critical size $(a/Q)_{crit}$ and a proof test carried out at a stress σ_{100}, would establish whether or not a flaw of this initial size were present in the uncycled vessel. If, on the other hand, the vessel were required to undergo 1000 cycles at the operating stress, a proof test at the higher stress of σ_{1000} would be needed to ensure the absence of a flaw of initial size $(a/Q)_{1000}$ which could grow to the critical size in 1000 cycles.

Finally, it was noted earlier that a stable through-the-thickness crack in a pressure vessel would probably indicate its presence by causing a loss of pressure or a leakage of fluid before it grew to the critical size. This phenomenon can, in fact, be used as a basis for safe design by deliberately choosing the wall thickness t to be such that the vessel leaks before it breaks catastrophically. As illustrated in the inset of Fig. 3.21, this implies that $t \leqslant 2a$ for an embedded flaw, although if such a leak-before-break criterion were used as a basis for design, it would be necessary to include a further safety factor to ensure that the through crack remained stable for a long enough time to allow its presence to be observed. In cryogenic pressure vessels, the existence of such cracks is usually signalled by the establishment of an easily recognizable "cold spot" or by a sudden loss of vacuum or insulation efficiency, which leads in turn to a rapid increase in the boil-off rate from the vessel.

3.2.6. The Effect of Temperature on Fracture Toughness

As we saw in section 3.2.4, there are two main classes of materials whose toughness decreases as the temperature is lowered—the low-strength ferrous alloys, where low toughness is associated with cleavage failure, and the medium-strength alloys whose yield strengths increase at low temperatures until they behave in the same way as high-strength materials at

room temperature. The ferrous alloys are such important construction materials that they will be considered in detail in section 3.3; the basic characteristics of the second group will be discussed here.

It is important to distinguish from the outset two distinct facets of the effect of temperature on the toughness of materials. We saw earlier that the fracture toughness K_c could not be considered a true materials constant because it varied with plate thickness, plate width, and other geometric effects peculiar to the specimens used. The plane strain fracture toughness K_{1c} was, however, independent of specimen configuration and its variation with temperature gives a meaningful insight into the effect of temperature on fracture toughness. Such changes are illustrated in Fig. 3.22 for a number of aluminum and titanium alloys, and it can be seen that, for titanium, K_{Ic} decreases steadily as the temperature falls, similar behavior being also found for a number of high-strength steels.[47] In contrast, K_{Ic} remains unaltered or increases at low temperatures for most aluminum alloys, the increase being most marked for types 2014–T651 and 6061, which are considered to be potentially the most useful for cryogenic applications.

The effect of temperature on K_c is, however, more complex. We saw earlier that the measured fracture toughness of a material was dependent

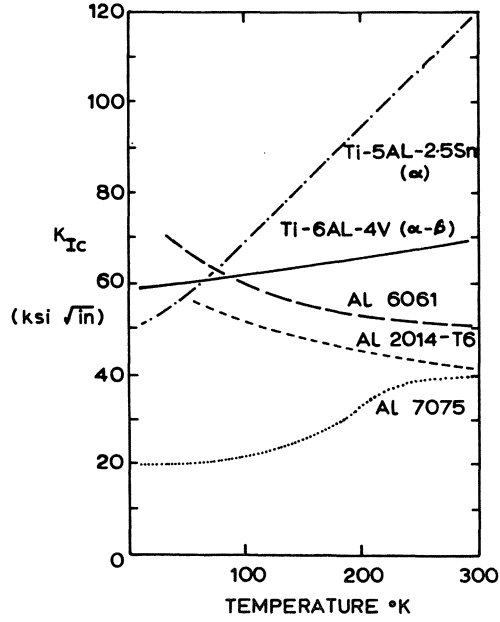

Fig. 3.22. Temperature dependence of K_{1c} for a number of aluminum and titanium alloys.

on its thickness B through the factor $\beta = K_c^2/B\sigma_{y2}$ and that, at a given temperature, maximum toughness occurred when $\beta \geqslant 2\pi$, i.e., in thin sheets which failed completely by oblique shear or slant fracture. As the thickness B increased, the degree of plastic constraint intensified, β fell, and more of the fracture area failed in the low-energy flat rupture mode. This in turn caused K_c to fall until it reached the constant value of K_{1c} when shear failure was entirely absent. (See, for example, Fig. 3.13.)

Reconsidering the problem for a material of constant thickness B whose yield stress increases as the temperature falls, at a high enough temperature, σ_y will be low enough for β to exceed 2π and failure will be 100% slant, as in specimen (a) of Fig. 3.23. If, however, the temperature is lowered, σ_y will increase and β will fall, thus increasing the degree of plastic constraint and allowing the central portion of the specimen to fail in the low-energy flat fracture mode. The larger the increase in yield stress, the

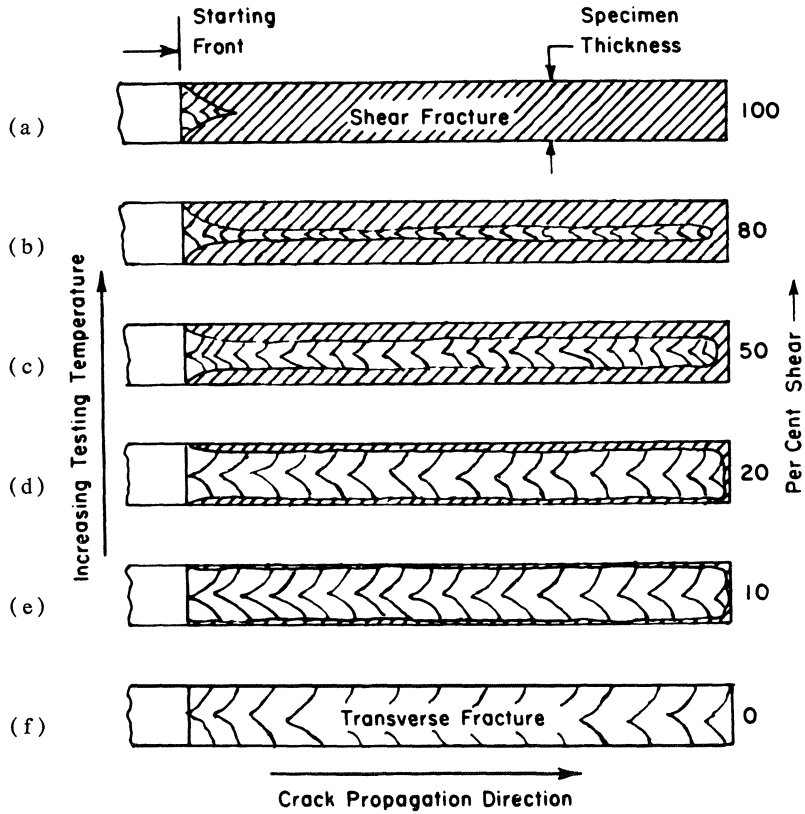

Fig. 3.23. Change in appearance of fracture surface, particularly the percentage of shear failure, caused by a change in testing temperature (ASTM committee report[33]).

greater will be the plastic constraint and the smaller the percentage of shear failure [specimens (b)–(f)]. Thus, as the temperature decreases, so does the measured fracture toughness. This thickness effect will be superimposed on any intrinsic change in fracture toughness with temperature and, for many materials, it will be the stronger effect. If, therefore, K_c is to be measured over a range of temperatures to obtain meaningful values for use in a fracture mechanics analysis, it is important that the thickness of the specimens tested should be the same as the sheet intended for use in the critically stressed areas of the structure concerned.

To illustrate this effect, the apparent plane stress fracture toughness of cold-rolled type 301 stainless steel is shown in Fig. 3.24 as a function of testing temperature.[48] The specimens used were 0.025 in. thick, 4 in. wide, and contained through-thickness machined center notches of initial length 1.2 in. Also shown as a function of temperature is the ratio of net fracture stress to yield stress, because, as we saw earlier, excessive plastic deforma-

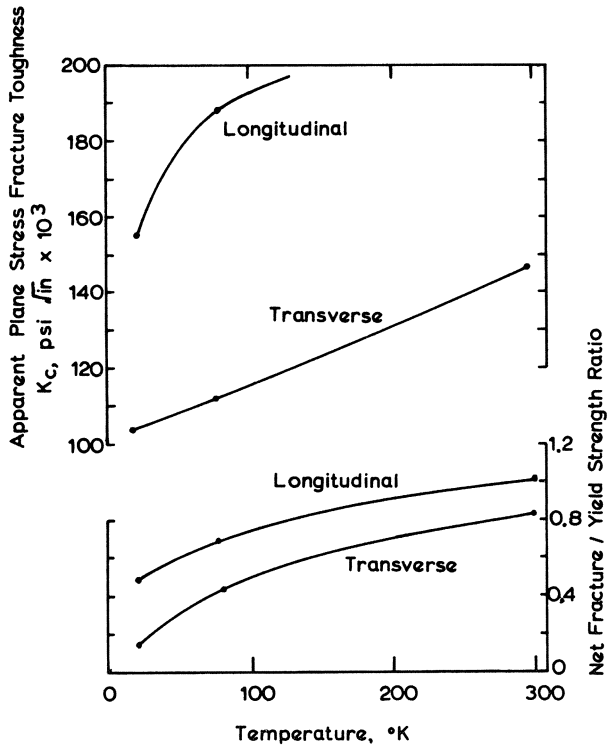

Fig. 3.24. Variations with testing temperature of the apparent plane stress fracture toughness of cold-rolled type 301 stainless steel (after Christian[48]).

tion occurs when this ratio exceeds 0.8. For the transverse specimen, only the room-temperature test fell outside this range and hence the apparent K_c values are meaningful. For the longitudinal specimen, only the tests at 20 and 77°K had a σ_F/σ_y ratio less than 0.8 and thus the apparent K_c is only shown for these temperatures, not for room temperature, where excessive plastic deformation preceded failure. The term "apparent fracture toughness" has been used in describing these results because subsequent investigations on the relationship between K_c and specimen width showed that the 4-in. specimens were too narrow and underestimated the K_c values, 18-in. specimens being found necessary for reliable results for such thin-gauge metals.

3.3. THE DUCTILE–BRITTLE TRANSITION IN FERROUS METALS

3.3.1. The Basic Problem

In section 1.5, we saw that the most marked effect on the mechanical properties of pure iron caused by a decrease in testing temperature was a rapid increase in its yield stress. Similar behavior is shown by plain carbon and low-alloy steels, as illustrated in Fig. 3.25 for a 0.2% plain carbon steel normalized at 880°C and tested at 77, 195, and 295°K. The stress–strain curves of Fig. 3.25(a) show the same features as those for Armco iron in Fig. 1.14, namely a strong increase in yield stress and a reduced ability to strain-harden at low temperatures. In Fig. 3.25(b), the yield strength, tensile strength, and elongation derived from these stress–strain curves are shown as a function of testing temperature and it can be seen that, below about 200°K, the yield strength increases more rapidly than the tensile strength and that the two curves coalesce at ~50°K. The elongation falls to zero between ~100 and 50°K, and below this temperature, the steel is, for practical purposes, completely brittle.

The loading conditions imposed during the uniaxial tensile testing of smooth tensile specimens are, however, less severe than those liable to be found in service, and impact tests on notched specimens are frequently used to simulate these more extreme conditions. In Fig. 3.26, the amount of energy absorbed by a standard Charpy V notched bar fractured by an impact blow from a pendulum hammer is shown as a function of testing temperature for the same plain carbon steel as that used for the tensile tests of Fig. 3.25. The elongation measured in these tensile tests is also shown for comparison and it can be seen immediately that the toughness transition defined by the impact test occurs at a much higher temperature than the ductility transition given by the tensile test. It can be inferred

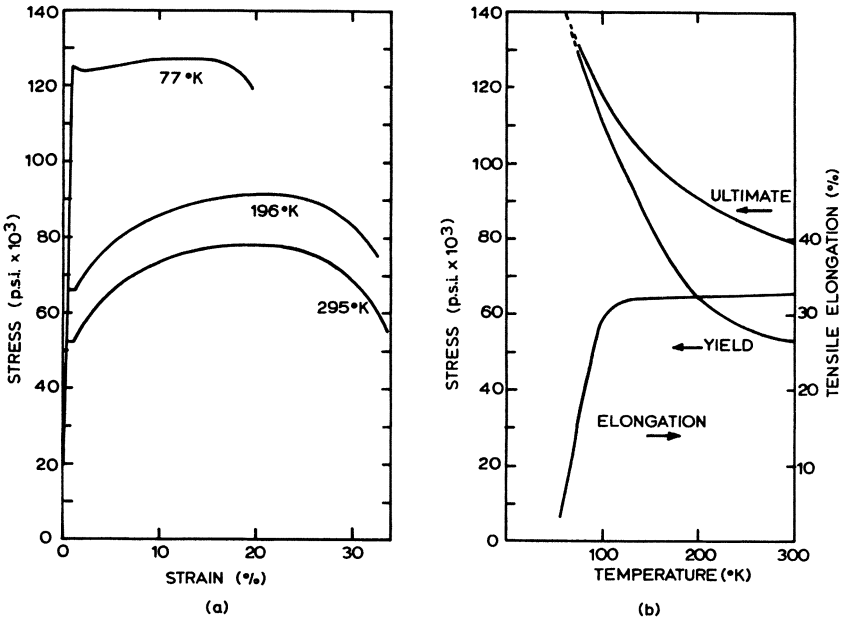

Fig. 3.25. (a) Stress-strain curves for a 0.2% plain carbon steel tested at 295, 196, and 77°K. (b) Temperature dependence of the yield strength, tensile strength, and elongation for the same steel.

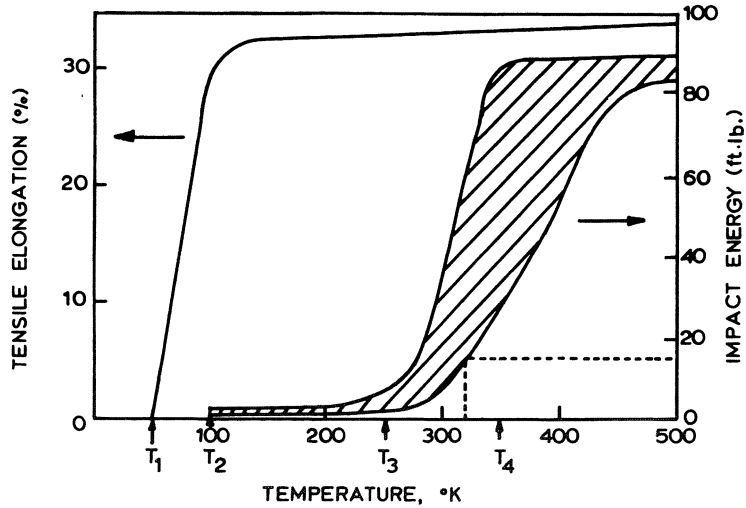

Fig. 3.26. Temperature dependence of the tensile elongation and impact energy of a 0.2% plain carbon steel.

from these results that, at temperatures above T_4, the metal will be tough and ductile under all conditions normally encountered in service; below T_1, it is unquestionably brittle. Between T_2 and T_3, it will fail in a ductile manner if it is deformed at low strain rates and under uniaxial loading conditions, but it will be brittle if subjected to triaxial stresses at high loading rates.

The change in appearance of the fracture halves of both the smooth tensile specimens and the Charpy bars is shown in Fig. 3.27 as they go through their ductile–brittle and tough–brittle transitions, respectively. For the tensile specimens, the shear lip becomes less and less pronounced as the temperature falls, and it is completely absent in the fully brittle specimen. Figure 3.27 also illustrates the crystalline nature of the fracture surface. The Charpy specimens are particularly illustrative, as they show that, at 390°K, failure occurs entirely by a high-energy-absoring shear mechanism but that, as the temperature decreases, more and more of the fracture surface shows crystalline, or cleavage, failure. At and below 260°K, failure is 100% crystalline.

Now, in terms of the criteria used in section 3.2.4 to classify materials into high-, medium-, and low-strength categories, plain carbon steel

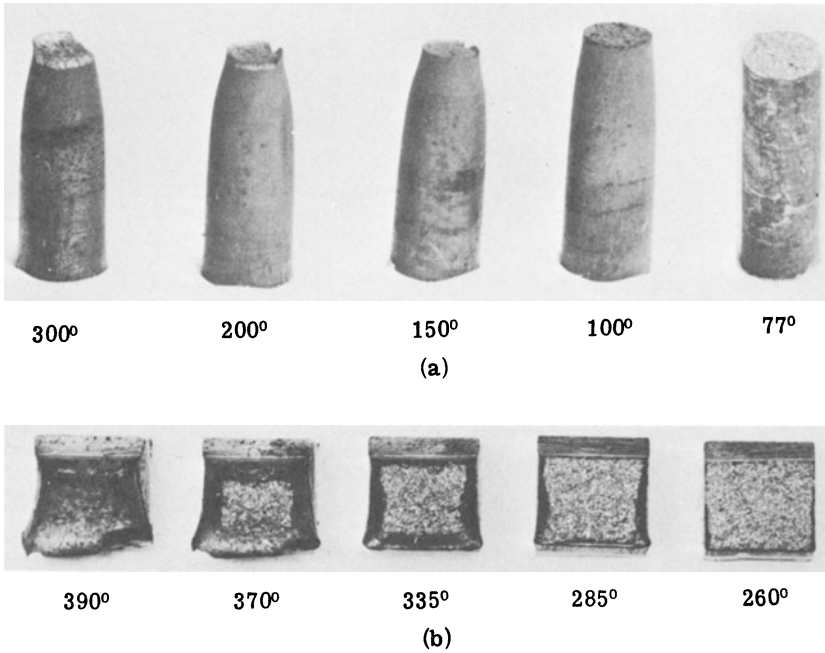

Fig. 3.27. (a) Change in appearance of the fracture surfaces of a series of mild-steel tensile specimens as they go through the ductile–brittle transition. (b) Corresponding change in appearance for a series of Charpy V-notch specimens.

with a room-temperature yield strength of about 50,000 psi is a low-strength material. Its brittleness transition occurs because at high temperatures it has a high fracture toughness and fails in a high-energy-absorbing shear mode, while at low temperatures it has a low fracture toughness because it fails by cleavage and absorbs much less energy. As, for this material, shear failures are tough while cleavage failures are brittle, its overall toughness depends essentially on the relative amounts of failure which occur by shear and cleavage. It is possible to define a transition temperature T_{trans} above which there is a sufficiently high proportion of shear failure to ensure adequate toughness, but the exact definition of such transition temperatures is a little more complex and this topic will be reconsidered in section 3.3.2. Regardless of the actual definition used to fix T_{trans}, it is found that there are at least five readily identifiable, if not completely separable, factors which determine the transition temperature for steels. They are the strain rate, the degree of plastic constraint, the size of the material, its metallurgical structure, and its composition. Although some of these factors have already been mentioned in sections 3.1, it is worth reconsidering them briefly here.

3.3.1.1. ***Strain Rate.*** As we saw in section 1.5, the yield stress of body-centered-cubic metals is highly dependent on the applied strain rate, high strain rates giving high yield strengths. Furthermore, as shown in section 3.1.2, the shear to cleavage transition takes place when the yield stress σ_y equals the fracture stress σ_F (which is only weakly influenced by a change in strain rate). Thus, a transition from shear to cleavage failure can be brought about by an increase in strain rate from a low value, for which $\sigma_y < \sigma_F$ to a high value, where $\sigma_F = \sigma_F$. The change in strain rate from about 10^{-3} per minute typical of many tensile testing machines to approximately 10^3 per minute, which is similar to that applied during a Charpy impact test, has been found[49] to increase the transition temperature of mild steel by about 90°K. Reference to the curves of Fig. 3.26 shows, however, that the difference between the two transition temperatures is more nearly 200–250°K, the additional increase in transition temperature being due to the plastic constraint produced by the notch in the Charpy specimen.

3.3.1.2. ***Degree of Plastic Constraint.*** The factors which determine the degree of plastic constraint in the region ahead of a flaw have been considered in detail in section 3.2 on fracture toughness. A simple explanation of notch brittleness in steels was, however, put forward by Ludwik, Davidenkow, and Orowan before the concepts of fracture mechanics were developed to their present level of sophistication. It can be shown that if a deep, symmetrical notch is placed in a tensile specimen subject to an applied load, the material beneath the root of the notch will be in a state of triaxial tension and plastic deformation will be constrained

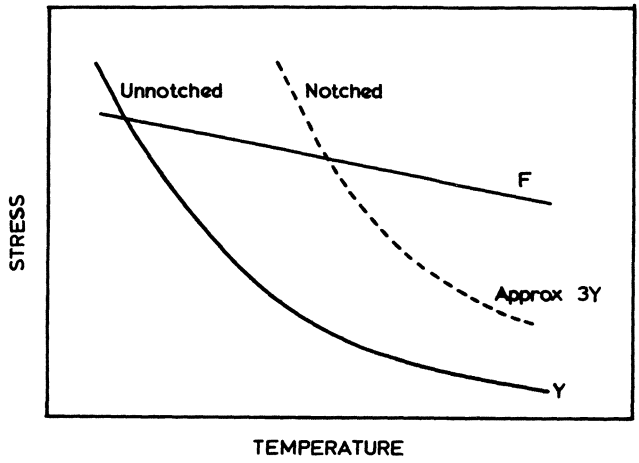

Fig. 3.28. The Ludwik–Davidenkow–Orowan criterion for notch-brittleness.

by the unyielded material above and below the notch. The degree of plastic constraint produced is theoretically 2.57 if the Tresca criterion is used or 2.82 if the von Mises criterion is applied, but for simplicity it is frequently taken as 3. It then follows that the *nominal yield stress* for the notched specimen (i. e., the tensile yield load/notched section area) is approximately three times greater than the stress Y at which yield would occur in an unnotched specimen subjected to a uniaxial tensile stress. The way in which this constraint to plastic deformation encourages the transition from ductile to brittle fracture is illustrated in Fig. 3.28. Plastic flow and brittle fracture are assumed to be independent processes each with its own characteristic tensile stresses Y and F respectively. The flow stress Y increases rapidly as the temperature decreases, but the fracture stress F is assumed to be relatively insensitive to such a change. Two yield curves are shown ; that marked Y is for the unnotched material, while that marked $3Y$ is for the notched specimen with a plastic constraint factor of 3. At high temperatures, where $F > 3Y$, the material is ductile : at low temperatures, where $F < Y$, it is brittle. At intermediate temperatures, where $Y < F < 3Y$, the material is notch-brittle, i.e., ductile under simple uniaxial loading conditions but brittle when subjected to triaxial stresses by the presence of a notch or other stress raisers. In practice, plastic constraint factors are often considerably less than 3, but the above example serves to illustrate the principles involved.

In this example, the plastic constraint produced by the notch gave a multiplying factor which increased the severity of an applied load. It should also be noted that there are occasions where a pre-existent stress, which may or may not vary with temperature, is effectively added to any

applied load to increase the nominal yield stress to the cleavage fracture stress of the material. Such additional stresses are, for example, almost invariably set up in the region of a weld during cooling and, if severe, these thermal stresses can lead to hot-cracking and other obvious defects. Less severe thermal stresses can, in some respects, be more insidious, as they only lead to failure when the structure is loaded. Post-weld heat-treatment is therefore almost always carried out to reduce these stresses unless, as in the case of 9% nickel steel, such treatment causes other metallurgical changes which have an even more deleterious effect on the toughness of the material.

3.3.1.3. ***Material Size.*** There are basically two ways in which the size, and in particular the thickness, of a material influences its ductile brittle transition temperature. Firstly, as we saw in section 3.2, the fracture toughness of a homogeneous material is low for thick sections because of the large degree of plastic constraint set up in these circumstances. Second, the inhomogeneities created during most metallurgical processes used to form ferrous materials are more pronounced in thick sections. For example, the different cooling rates experienced by the center and outsides of a bar or sheet can lead to a variation in grain size or structure across the section and these factors almost invariably increase the transition temperature for thicker materials. Such effects are, however, less severe in steels alloyed with elements which have an intense grain-refining action.

3.3.1.4. ***Metallurgical Structure.*** We have already seen in section 3.12 how a decrease in grain size reduces the transition temperature of ferrous metals. The factors affecting this parameter in alloy steels will be examined shortly, but it should be noted that in plain carbon steels the grain size can be altered by varying the rate at which the metal cools: the more rapid the cooling, the finer the microstructure. In practice, this generalization has to be qualified by the observation that a whole range of pearlitic, bainitic, and martensitic structures can be produced by varying the cooling or quenching rates. The ferritic-pearlitic steels are the most widely used for low-temperature applications, as in general the higher strength martensitic types are too brittle for use in the as-quenched state. It is, however, possible to improve the toughness of such steels by tempering them after quenching. This lowers their strength slightly but increases their toughness by reducing the residual strains and by producing a microstructure which is more equiaxial and less acicular than that of the quenched state. Prolonged tempering causes the cementite particles to spheroidize and produce a tough microstructure. The details of these processes are, however, outside the scope of this work, but they are well described by Tetelman and McEvily[1] and in a number of other metallurgical texts.

Finally, we saw in section 3.12 that the fracture strength of polycrystalline materials was strongly influenced by the strength of the boundary between adjacent grains. This factor is of particular importance in steels, as grain-boundary embrittlement can be caused by a number of different mechanisms, including the preferential segregation of cementite films and other carbides at the grain boundaries.

3.3.1.5. ***Composition.*** In section 3.12, it was shown that plastic deformation is an essential prerequisite for cleavage fracture, and, thus, alloying additions which alter the yield stress of steel have a direct bearing on its cleavage fracture. Furthermore, in the earlier sections of this chapter, we saw that the toughness of most materials decreases as their yield strength increases. This relationship also holds for steels and it has been shown that, as in most cases the fracture strength is virtually temperature-independent, a 1000-psi increase in yield strength causes the ductile–brittle transition temperature of steel to increase by about 2°C. Now, the Hall–Petch relationship introduced in equation (1.8) shows that the yield stress is given by $\sigma_y = \sigma_i + k_y d^{1/2}$, and two of the effects of alloying additions are to increase the friction stress σ_i by dislocation pinning and to reduce the grain size d. The mechanisms by which the grain size is decreased are normally either by lowering the temperature of the eutectoid transformation and thus causing the nucleation of more, smaller grains, or by forming precipitates and third-phase particles which hinder grain growth.

The other main factor which can influence the cleavage fracture of steels was shown in section 3.12 to be the strength of the grain boundary which a growing microcrack has to overcome before it can propagate and become a Griffith crack. If alloying additions or impurities lower the strength of this boundary, microcrack growth is made easier. In extreme cases, such as those created by high oxygen concentrations, the grain boundaries can become so embrittled that the mode of fracture changes from transgranular to intergranular.

Most commercial steels contain such a wide range of alloying elements and impurities that it is difficult to isolate completely the effect of specific elements on the ductile–brittle transition. However, the main effects are as follows.

Carbon content. The maximum amount of carbon soluble in the body-centered-cubic ferrite is 0.02% at the eutectoid temperature of ~723°C and this is also the lower limit of carbon contained by most commercial steels. As the concentration is raised above ~0.015%, increasing amounts of cementite form at the ferrite grain boundaries, thus weakening them and causing an increase in the transition temperature. For carbon concentrations in excess of about 0.05%, the main effect is to increase the proportion of pearlite in the microstructure and, as pointed out in section 2.34, this increases the yield strength of the material by second-phase hardening: the smaller the size of the pearlite colonies and the lower the

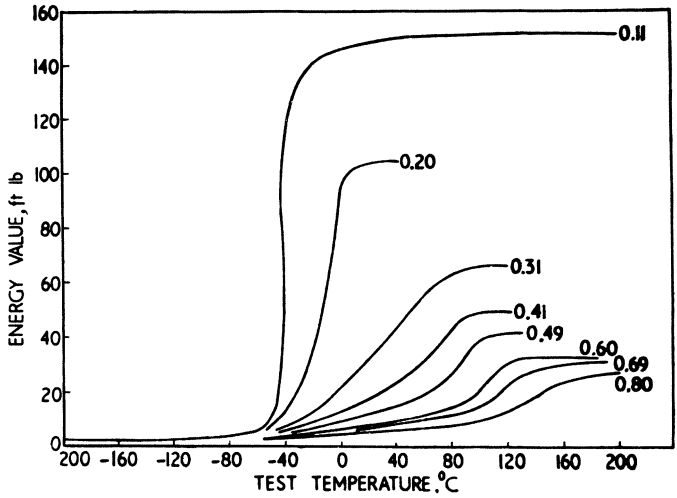

Fig. 3.29. Effect of carbon content on the transition temperature and Charpy impact energy of a series of normalized plain carbon steels (Burns and Pickering[69]).

separation of the carbide particles within these colonies, the larger the yield stress and hence the higher the ductile–brittle transition temperature. This effect is shown in Fig. 3.29 for a series of normalized plain carbon steels and it can also be seen that the maximum energy absorbed in a Charpy V test decreases as the carbon content rises.

Nitrogen content. Both nitrogen and carbon cause the yield stress of plain carbon steels to increase by about 8000 psi per 0.01% added up to their solubility limit of 0.02%. This is mainly a result of the strong dislocation pinning caused by these small interstitial impurities, a characteristic which also leads to the phenomenon of strain-aging and embrittlement. The strength is also increased by the formation of iron nitride particles which dispersion-harden the ferrite and so increase its transition temperature. These effects can, however, be controlled by the gettering action of elements, such as manganese and aluminum, which preferentially combine with the nitrogen to form less harmful nitrides.

Phosphorus, sulfur, and oxygen. Each of these elements can increase the yield stress of ferrite when in solution, but their most harmful effects are due to the grain-boundary embrittlement they produce. Large increases in transition temperature result from this embrittlement and virtually all steels contain alloying additions which preferentially combine with one or more of these impurities to reduce their effect.

Manganese is the most common such alloying addition and most steels contain at least 0.5% manganese to act as a deoxidizer and, more importantly, to combine with free sulfur and form manganese sulfide. It also

has two further beneficial effects: it discourages the formation of grain boundary cementite films in low carbon steels, and it has a very strong grain-refining action which produces a fine pearlite structure. These factors cause a large decrease in the transition temperature. For example, 0.5, 1 and 2% manganese added to a 0.05% carbon steel lower its transition temperature from 120°C to 60, 20, and −40°C, respectively. Furthermore, it is not simply the manganese content which decreases the transition temperature so much as the manganese/carbon ratio. Thus, the low-temperature toughness may be improved either by increasing the manganese content or by decreasing the carbon content. There are in fact three main classes of low-alloy steel used for the construction of equipment working below room temperature: plain carbon steels, where the Mn/C ratio is ~2.5, for use down to about −30°C; carbon–manganese steels with Mn/C ⩾ 4.5, which can be used down to −60°C; and fine-grained carbon-manganese steels which have been treated with aluminum, niobium, vanadium, etc., for extra grain refinement and which can be used down to about −90°C. It should, however, be noted that these temperatures are approximate, the actual minimum operating conditions depending on plate thickness, degree of stress relief, etc.

Silicon and aluminum. These are added to steels to deoxidize or "kill" them. Depending on the amount of deoxidant added, the steels are either "fully killed" or "semikilled" and a steel fully killed with silicon and aluminum has a lower transition temperature than a semikilled steel of equivalent tensile strength. Silicon dissolves in ferrite and increases its strength and thus tends to increase the transition temperature; aluminum, on the other hand, combines with some of the nitrogen already in solution and decreases the ferrite strength, thus lowering the transition temperature. Furthermore, the particles of aluminum nitride so created inhibit ferrite grain growth and this grain refinement further reduces the transition temperature. In most steels containing both silicon and aluminum, the effect of the latter is dominant and the transition temperature is lowered.

As noted earlier, *niobium*, *molybdenum*, *vanadium*, and *copper* are added to some steels to produce a very fine-grained structure. Their main action is to produce carbides which inhibit the growth of the ferrite grains and reduce the pearlite content and hence the strength of the steel. This in turn lowers the transition temperature of these alloys.

It is, however, the *nickel* content which exercises the strongest influence over the transition temperature of steels, and in Fig. 3.30, the Charpy K impact energy is shown as a function of temperature for a range of low-carbon steels containing 0, 2, $3\frac{1}{2}$, $8\frac{1}{2}$, and 13% nickel. As we saw in section 2.1.5.1, nickel is a powerful austenite stabilizer and its presence lowers the eutectoid transformation temperature, thus encouraging a much smaller grain size in the transformed ferrite. This grain refinement, together

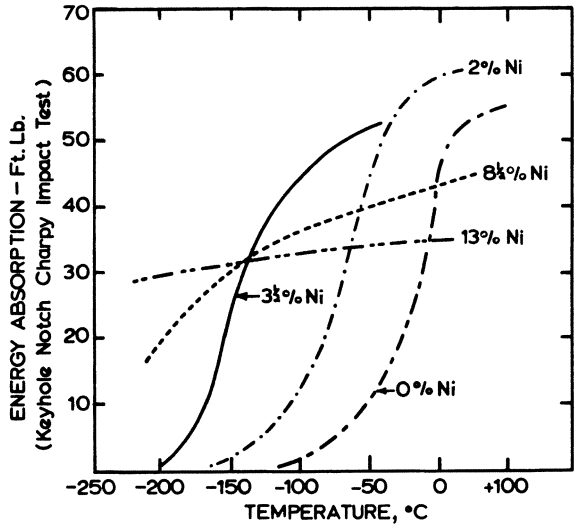

Fig. 3.30. Effect of nickel content on the transition temperature of steel (International Nickel Company data[68]).

with a reduction in the free nitrogen content, is one of the factors responsible for the large decrease in transformation temperature shown by the nickel-containing alloys.

In practice, only $2\frac{1}{4}\%$, $3\frac{1}{2}\%$, and 9% nickel steels are available commercially, as it has been found that these three grades are sufficient for most common low-temperature applications.[68] The $2\frac{1}{4}$ and $3\frac{1}{2}\%$ nickel steels may be used at temperatures down to 213°K (−60°C) and 173°K (−100°C), respectively, but many designers prefer $3\frac{1}{2}\%$ nickel steel for use at the higher temperatures because of the additional safety margins conferred by its lower transition temperature. Furthermore, it is readily welded with electrodes of the same composition and it may be used without postweld heat treatment.

The present widespread use of 9% nickel steel in the construction of cryogenic plant and large vessels for the storage of liquid nitrogen and natural gas stems from the acceptance by the ASME of code case 1308 (1962). This permitted the use of 9% nickel steel at temperatures down to −200°C without postweld heat-treatment for thicknesses up to and including 2 in.: the first time that a ferritic steel was accepted for use at such low temperatures. Nine per cent nickel steel is available in two main forms, (1) quenched and tempered and (2) double normalized and tempered. Both forms are covered by code case 1308, the quenched and tempered variety having a slightly higher yield stress and a marginally lower ductility at room temperature. Postweld heat-treatments actually reduce

the toughness of this alloy and hence they are not recommended. As we shall see in chapter 6, the high yield strength of 9% nickel steel makes its use particularly attractive where a yield-point design code is employed, but the high cost of the complex electrodes needed to weld the alloy can go a considerable way toward offsetting the favorable economics offered by the parent metal.

3.3.2. Transition Temperatures in Ferrous Alloys

We have as yet not given a rigorous definition of the term "transition temperature" and there are in fact a number of such temperatures which describe the relative ease with which fracture may initiate or propagate in a low-energy mode in ferrous materials. Although alloy steels are most likely to be used for the construction of low-temperature equipment, much of the original work on the brittle fracture of load-bearing structures was carried out on mild steel in an attempt to discover the reason for the large number of service failures which occurred in the all-welded Liberty Ships produced between 1939 and 1945. From this work came a basic understanding of the factors involved in brittle fracture and in particular the effect of temperature on the initiation and propagation of cleavage cracks in large load-bearing structures.

As we have seen in the earlier sections of this chapter, a small amount of plastic deformation is necessary for the initiation of cleavage cracks in a flaw-free material, and thus the fracture stress is never less than the yield stress in such circumstances. However, although some localized plastic deformation may be necessary before a pre-existing crack can start to propagate in an unstable mode, it is possible, as we saw in section 3.2, for unstable fracture in a flawed material to occur at an applied stress which is lower than that necessary to cause yielding *across the whole of the section concerned:* the larger the flaw, the lower the fracture stress in relation to the gross yield stress. Thus, at a given temperature, the stress at which cleavage failure occurs is governed by the size of the largest crack contained by the material, while, as we saw in section 3.3.1, the cleavage–shear transition is itself a function of temperature. In order to show how these factors are interrelated for mild steel, Pellini and Puzak[51] introduced the fracture analysis diagram illustrated in Fig. 3.31.

For the flaw-free structure at high temperatures, failure is entirely by shear and the fracture stress is equal to the ultimate tensile stress (UTS). As the temperature falls, the yield stress increases faster than the fracture stress and the ratio σ_F/σ_Y falls until, at T_D, cleavage failure occurs at the yield stress. Thus, T_D is the transition temperature for initially flaw-free materials. Now let us consider a flawed structure, such as a wide plate which contains a small crack (usually defined as $\leqslant 0.25$ in.) whose pre-

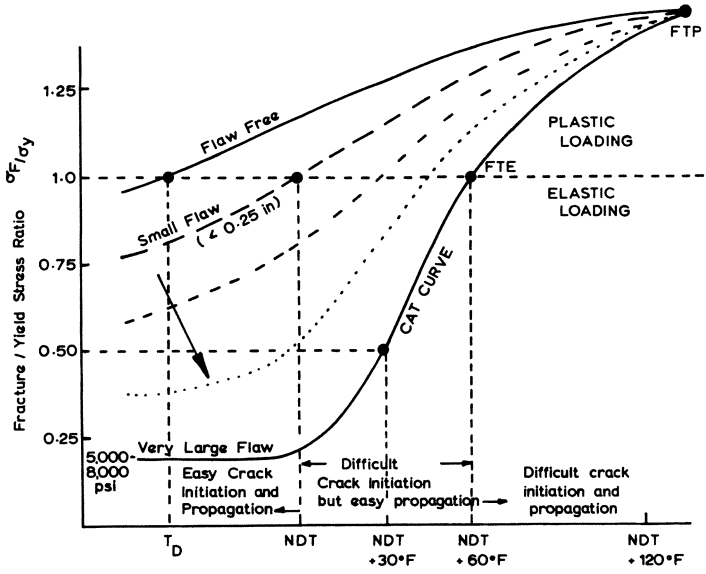

Fig. 3.31. Fracture analysis diagram for mild steel (after Pellini and Puzak[51]).

sence does not affect the gross yield stress of the plate. Below T_D, failure is entirely by cleavage as in the flaw-free material. At temperatures above T_D, a small amount of localized plastic deformation must occur in the immediate vicinity of the flaw before a cleavage crack can be initiated, but, once initiated, it spreads by cleavage at a stress σ_F which is below the gross yield stress σ_Y. Under these circumstances, the fracture stress σ_F is determined by the length of the crack, the toughness G_c of the material, and the degree of plastic constraint existing at the crack tip, i.e., it is governed by the criteria described in section 3.2 on fracture toughness. As the temperature is increased further, the toughness G_c increases rapidly until, at the *nil-ductility temperature* (NDT), the fracture stress σ_F is equal to the gross yield stress σ_Y. Fracture mechanics are now inapplicable, as gross plastic deformation precedes fracture, and cleavage failure only occurs after some shear deformation. Above the NDT, the ratio of shear/cleavage failure increases with temperature until, at a high enough temperature, it is entirely shear.

If the size of the flaw is increased, the ratio σ_F/σ_Y decreases until, for a very large flaw, it reaches the *crack arrest temperature* (CAT) curve, which defines the highest temperature at which unstable cleavage fracture can occur at a given level of applied stress, such failures being impossible for all combinations of stress and temperature which lie on the high-temperature side of the CAT curve. It has been found that, even for an in-

finitely long crack, the CAT curves of most types of steel level out below the NDT at an applied stress of between 5000 and 8000 psi, and thus unstable cleavage is impossible if the applied stress is maintained below this level. At higher temperatures, the increase in toughness with temperature causes the CAT curve to rise steeply until, at the *fracture transition elastic* (FTE), unstable fracture cannot take place at stresses below the gross yield stress σ_Y. Above the FTE, gross plastic deformation precedes cleavage failure, while at the *fracture transition plastic* (FTP), the fracture stress is equal to the ultimate tensile stress, failure is completely shear, and the material behaves as if it were flaw-free.

Thus, in summary, at temperatures below the NDT, it is easy for a cleavage crack to initiate at a small pre-existing flaw and then propagate in a low-energy mode. Unless the applied load is maintained below about 5000 psi, unstable fracture can only be prevented by ensuring that the material is flaw-free. Above the NDT, the initiation of cleavage cracks becomes more difficult, but, once initiated, such cracks propagate easily in a cleavage mode, while at temperatures higher than the FTE, both initiation and propagation are difficult and failure is by shear except in the plastically loaded regions, where cleavage failure occurs. Above the FTP, failure is entirely by shear deformation.

Design criteria for mild-steel structures can also be derived from this diagram for various ratios of applied stress/gross yield stress. If, for example, the applied stress will never exceed the yield stress, then the FTE defines the lowest temperature at which the structure will be safe from brittle fracture, while for smaller applied stresses, a lower operating temperature may be used. For most mild steels, it has been found that the FTE is about 30°C (60°F) higher than the NDT, while the FTP is about 60°C (120°F) above the NDT. As the NDT may be measured directly, these design criteria are often quoted in terms of the NDT + x°C, e.g., for applied stresses which do not exceed the gross yield stress, the minimum operating temperature would be 30°C above the NDT. It should, however, be emphasized that the exact relationships between the NDT, FTE, and FTP temperatures have only been obtained for mild steel and that they are not directly applicable to other materials. In such cases, the full CAT curve has to be derived before suitable design criteria can be formulated.

3.3.3. Testing for Resistance to Brittle Failure

There are a large number of tests which have been developed to measure the susceptibility of a material to brittle failure and they can be grouped into two main classifications: the *specific* type of test, which yields information which may be applied directly to structural design calculations, and

the *comparative* types, which indicate the manner in which a given material is liable to fail under a particular set of loading conditions. In general, the specific types of test use large specimens which simulate as closely as possible the conditions likely to be met in service and they are carried out to establish design data such as the safe working stress for a given plate thickness and operating temperature, or the safe operating temperature of a structure subjected to a certain applied stress. They are also employed to establish the probable causes of service failures.

Having used these tests to develop suitable design criteria or codes of practice, it is then necessary to have a much simpler, easily reproducible, and less expensive method of selecting or ranking available materials and verifying that they are in the same condition, and have the same properties, as the material used in the more elaborate specific tests. Furthermore, it is vitally important that the results of these two types of test are correlated correctly if the comparative tests are to provide a meaningful guide to the service behavior of full-sized plates or other load-bearing structures. It is also important to ensure that these correlations are valid for the material concerned, as the criteria developed for one type of material are not necessarily valid for another.

3.3.3.1. ***Specific Tests.*** The *Robertson test*[52] provides a direct measurement of the crack-arrest temperature curve which was introduced in the fracture analysis diagram of Fig. 3.31. The experimental arrangement is shown schematically in Fig. 3.32. A uniform tensile stress is applied across a full thickness plate which also has a temperature gradient super-

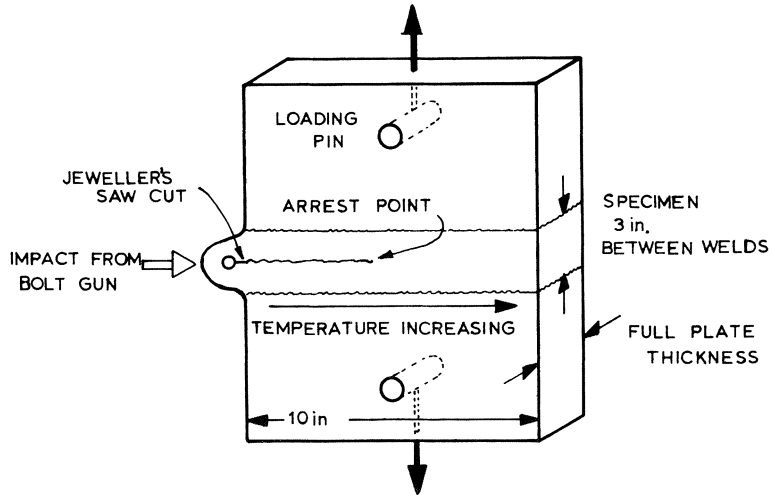

Fig. 3.32. Schematic representation of the experimental arrangements for a Robertson test (after Robertson[52]).

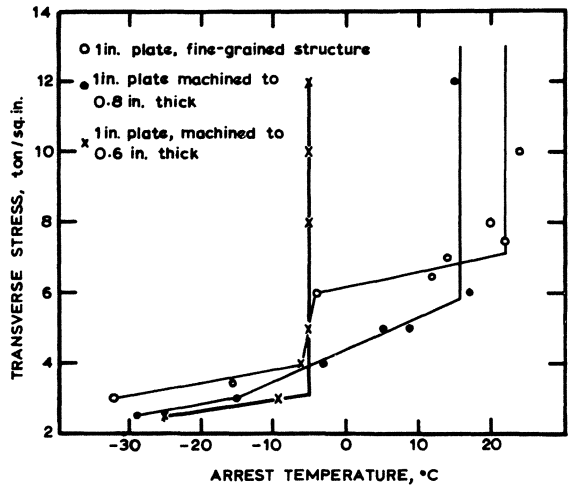

Fig. 3.33. Effect of specimen thickness on the crack-arrest temperature curves for mild steel as determined by the Robertson test (after Robertson[52]).

imposed in a direction perpendicular to the applied stress. At the cold edge of the plate, there is a projection which contains a jeweller's saw cut and when the projection is struck by an impact blow from a boltgun, a cleavage crack is nucleated from the root of the saw cut. This crack spreads toward the hotter side of the plate until it is arrested at some point where the temperature corresponds to the CAT for the applied stress and plate thickness. The crack is arrested because it runs out of the cold region, where the toughness is low, into a hotter region, which has a high resistance to dynamic crack propagation; the crack is then able to spread further only if the applied stress is raised above the yield stress. By carrying out a series of such tests for a given material, the full CAT curve is established, while the effect of plate thickness may be found by repeating the tests with materials of different thickness. Typical results are shown in Fig. 3.33.

The Robertson test is both expensive and laborious and there have been numerous attempts to establish a simple and inexpensive alternative which can yield fundamental data and also be correlated with the experience obtained from analysis of service failures. The most widely used such test is the *Pellini drop weight*,[53] which is illustrated in Fig. 3.34. A brittle weld bead is attached to one face of the specimen, which is typically 14 in. long by $3\frac{1}{2}$ in. wide by 1 in. thick, and a small notch, about $\frac{1}{4}$ in. in length, is cut into the weld bead. Once the specimen has reached the desired testing temperature, it is supported at its ends, so that the weld bead is on the lower face, and then impacted by allowing a standard weight

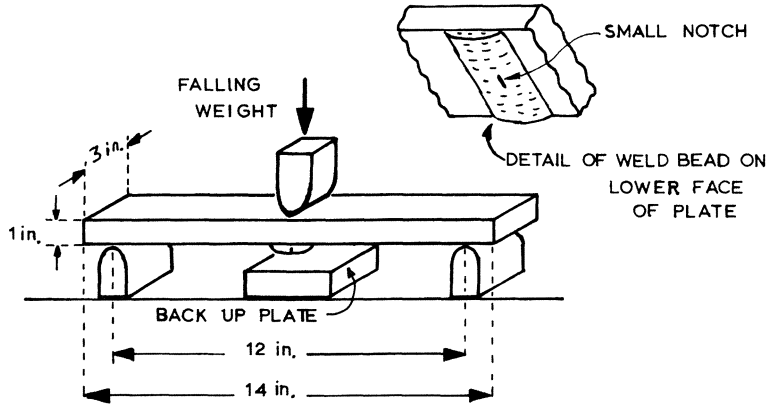

Fig. 3.34. Schematic representation of the experimental arrangements for a Pellini drop weight test (after Puzak *et al.*[53]).

to fall onto it from a fixed height. A backup plate is placed beneath the specimen to reduce the maximum deflection of the plate to a value such that the stress along its tension face cannot exceed the yield stress of the material. At low temperatures, the crack initiated at the notch root is able to propagate completely across the specimen, but as the testing temperature is increased, a stage is reached where the crack only just manages to propagate. This, by definition, is the nil-ductility temperature of the material because it is the highest temperature at which a small flaw can initiate fracture at its yield stress. This test thus gives a direct measurement of the NDT of the material, and once this is known, it is possible to use the NDT + $x°$ design criteria discussed in the previous section.

The philosophy underlying the use of both the Robertson and Pellini tests is based on the concept that steels possess a crack-arrest transition temperature above which unstable fracture cannot take place. For low-strength steels, the change in toughness associated with a transition from cleavage to shear failure is sufficient to ensure that this concept is valid even in the case of structures such as pressure vessels or pipelines in which the load is maintained during crack propagation. For these materials, it is therefore safe to adopt a design philosophy which is based on the selection of materials to prevent unstable crack *propagation*, i.e., one which accepts that cracks may be initiated in locally embrittled regions but which prevents their propagation beyond these regions by specifying a material tough enough to arrest such cracks. This is achieved by selecting a material whose crack-arrest temperature is below the minimum service temperature for the given design stress. Such an approach is especially suitable for the lower-strength steels whose yield and fracture strengths are particularly sensitive to both temperature and strain rate. As the conditions

which apply during crack propagation are those of high-strain-rate loading, a crack once initiated can propagate easily below the crack-arrest transition temperature because of the reduction in toughness associated with the higher yield stresses produced by the high strain rates (cf. section 3.3.1).

Although such a philosophy yields inherently safe design criteria for low-strength steels, it suffers from the disadvantage that it requires the use of the more expensive grades of steel, which have low nil-ductility temperatures. It is also, in some respects, overconservative, as it sets out to prevent the propagation of cracks which may never initiate. Furthermore, there is evidence[54] to suggest that the concept of a crack-arrest temperature is invalid for medium-strength steels, as unstable fractures could be made to propagate at temperatures up to $\sim$300°C as long as there was sufficient energy stored in the loading system, e.g., in gas-loaded pressure vessels or pipelines. This is, of course, consistent with the fracture mechanics approach described in section 3.2, and under such circumstances, it is preferable to use an alternative design philosophy, one which accepts that defects will occur in real structures and which then selects materials to prevent *fracture initiation* rather than its propagation.

Most structures are welded during their construction and it has been found that the most common location of defects is in the weld metal itself or in the adjacent heat-affected zones. Furthermore, welding can also cause strain-aging effects and residual stresses and these can lower the fracture toughness of the material in, or adjacent to, the weld zone. Thus, when selecting materials for their resistance to brittle fracture, it is not sufficient to test the base metal alone; the tests must take account of the effects produced by welding as well as the other relevant variables such as material thickness, testing temperature, strain rate, etc. The only large-scale laboratory test which satisfies these requirements is the *British Welding Research Association* (BWRA) notched and welded *wide-plate test*, which is shown schematically in Fig. 3.35. A full-thickness plate is cut in half parallel to the direction in which the stress is to be applied, jewellers' saw cuts are made at the center of each half-plate, and the central butt weld is completed in such a way as to leave the sawcut notches unwelded. In this way, the material at the notch tips is subjected to both the strain-aging effects and the residual stress fields set up during welding. The plate is then tested in tension at the required temperature and strain rate and the stress–strain behavior is recorded. By carrying out such tests over a range of temperatures, it has been shown that the as-welded test pieces fail at stresses below the yield point when tested below a certain temperature. Above this temperature, it is necessary to cause yielding and a certain amount of plastic strain before fracture initiates and propagates in a brittle manner. The criterion used[55] to interpret these results is based on the temperature

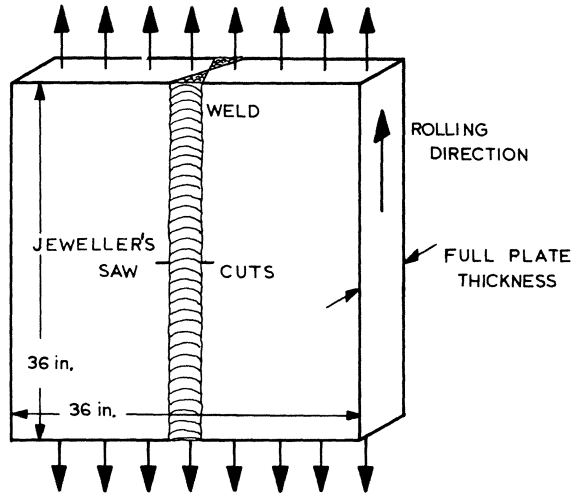

Fig. 3.35. Schematic representation of the experimental arrangements for a British Welding Research Association notched and welded wide-plate test (after Woodley *et al.*[55]).

at which the prefracture plastic strain is at least four times larger than the yield strain before fracture initiates (this criterion is sometimes expressed in terms of a critical strain of 0.5%). It has been found to give a good correlation with measurements made on material taken from service failures, which show that the strain close to the fracture path is several times greater than the yield strain (measured on a 5 in. gauge length).

By carrying out a large number of wide-plate tests on material of different thickness, composition, heat-treatment, etc., it is possible to see how these variables influence the fracture initiation temperature as defined by the wide-plate test. Furthermore, by comparing the behavior of samples with and without a postweld heat-treatment, it was found that failure in the stress-relieved samples normally occurred after yielding, whereas at the same temperature, the unheat-treated samples failed below the yield stress. An alternative way of expressing this point is to note that the initiation transition temperature of the stress-relieved material is lower than that of the untreated material, and this fact is recognized by most design codes by allowing lower operating temperatures for materials which have been stress-relieved. (See, for example, Figs. 3.38 a, b).

The BWRA wide-plate test is, however, expensive and time-consuming, and, just as the Pellini drop weight test was developed as an inexpensive alternative to the Robertson test, so the *crack opening displacement* (*COD*) *test* has been used to complement the wide-plate test. As shown in Fig. 3.36, the COD specimen is a square bar containing a notch which ex-

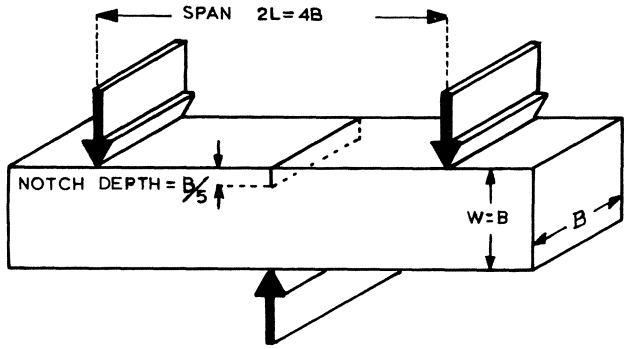

Fig. 3.36. Specimen configuration and loading geometry for a crack opening displacement notched bend test (Burdekin[56]).

tends to a depth one-fifth of that of the specimen; it is loaded slowly in three-point bending to enable the measurement of δ, the crack opening displacement which precedes fracture. By carrying out a number of such tests at different temperatures, it is possible to develop a COD transition curve as illustrated in Fig. 3.37 and, as long as the tests are carried out on full-thickness specimens, the results correlate well with those of the wide-plate test. Furthermore, it is possible to measure the COD transitions of various parts of a welded material by cutting the notch in the required region of the weld. In Fig. 3.37, such transitions are shown for the parent metal, the fine- and coarse-grained regions of the heat-affected zone, and the weld metal itself, and it can be seen that for this carbon–manganese steel the weld metal has the highest transition temperature and is therefore the most embrittled region.

Although the COD test has been introduced here as an auxiliary to the wide plate test, Burdekin and Wells[57] have shown that it has a more fundamental significance. In section 3.2, we saw that it is impossible to apply linear elastic fracture mechanics to situations where more than a small amount of plastic deformation occurs at the crack tip. Although such criteria are satisfied for high-strength steels, fracture in the lower-strength mild steels normally initiates after considerable plastic deformation at the crack tip. Under such circumstances, it is claimed that COD techniques can be used to give a measure of a material's resistance to fracture initiation and that δ, the critical COD to fracture, is closely related to the fracture toughness parameters G_c and K_c derived from the elastic analysis. At low stresses, where the two approaches overlap, $G_c = \sigma_y \delta$, i.e., the crack resistance force is equal to the yield stress multiplied by the critical crack opening displacement. Furthermore, although G_c cannot be measured for specimens which yield before fracture, crack opening displacements

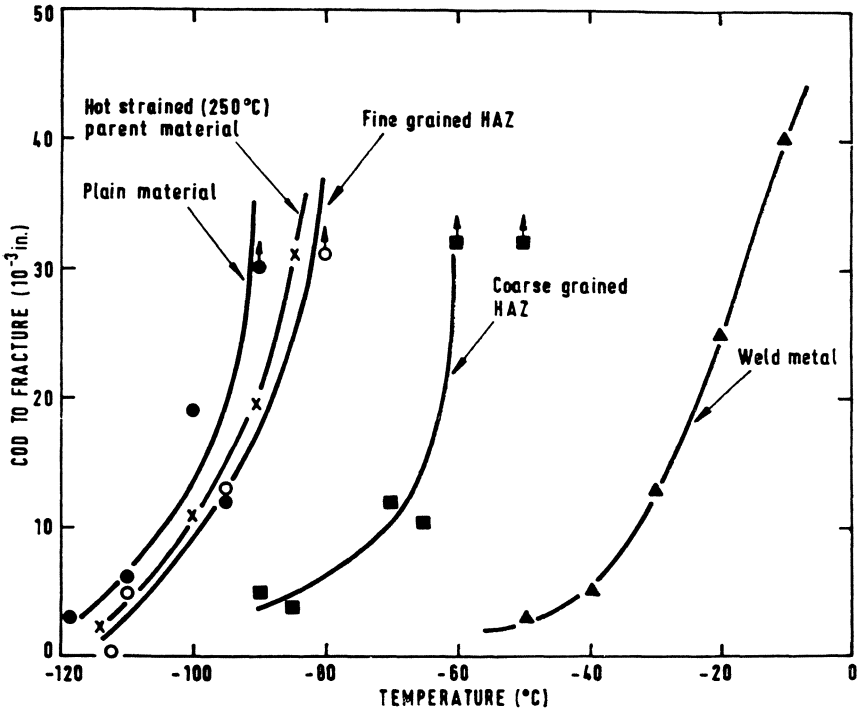

Fig. 3.37. COD transition curves for various regions of a weld in a carbon–manganese steel (Burdekin[56]).

can, and it is thought that by this means the concepts of fracture mechanics can be extended to cover those materials which yield before they fracture in an unstable mode.

As stated earlier, one of the main uses of specific tests such as the Robertson CAT and the BWRA wide-plate tests is in the establishment of design codes for materials intended for service at low temperatures. A recent revision of such a code proposed by an OCMA* working party[58] has been based on the results obtained from BWRA wide-plate tests using a prefracture plastic strain of 0.5% as the transition criterion. The recommended working temperatures for various grades of steel are given as a function of material thickness for the as-welded condition in Fig. 3.38(a) and for the postweld heat-treated condition in Fig. 3.38(b). These temperatures include safety factors derived from a conservative assessment of service experience and they assume that the nominal design stress is 2/3 of the

* OCMA: Oil Companies Materials Association (London).

(a)

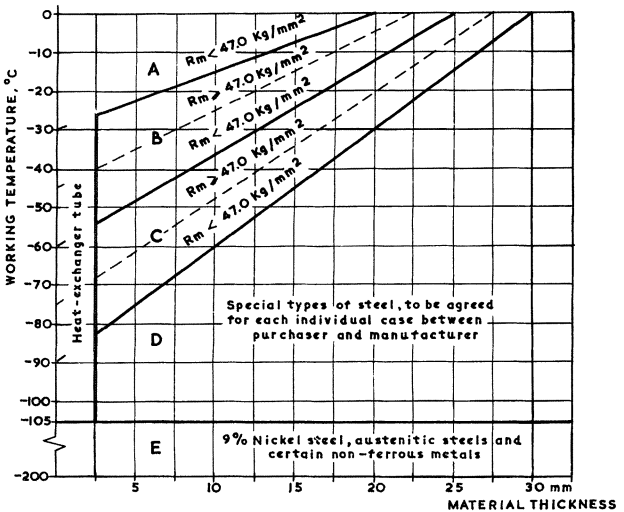

(b)

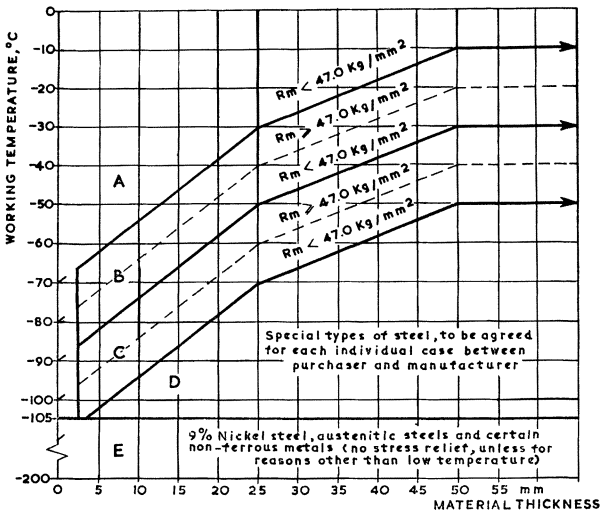

(c)

Material Group	Type of Steel
A	C steel, Mn/C ⩾ 2.5 Si killed (and semi-killed)*
B	C-Mn steel, Mn/C ⩾ 4.5 Si killed (and semi-killed),* (with or without grain refinement)
C	C-Mn steel, Mn/C ⩾ 4.5 Si killed, with addition of Al, Nb, V etc. for grain refinement
D	Special types of low-temperature steels, to be approved by the principal for each individual case
E	9% Nickel steel,** austenitic steels, and certain non-ferrous metals

* Use of semi-killed steel restricted to 0 °C. Lower temperatures are permitted provided this has been agreed between purchaser and manufacturer.

** Note that 9% Nickel steel, like other high-tensile-strength steels, is particularly prone to hydrogen embrittlement caused by corrosive environment.

Fig. 3.38. Recommended working temperatures for various grades of steel, (a) in the as-welded and (b) in the postweld heat-treated conditions (Derungs[58]). Part (c) is a key to (a) and (b).

yield stress at room temperature, loading is static, and that normal attention has been paid to design and weld quality. The lower limits of groups, *A*, *B*, and *C* apply to materials whose tensile strength is below 47.0 kg/mm² (67,000 psi), while the dashed lines indicate the lower limit of applicability for steels with tensile strengths above this value. One of the most striking features shown by a comparison of Figs. 3.38(a) and 3.38(b) is the much lower operating temperatures allowed for materials in the postweld heat-treated condition. Both diagrams also show clearly the rise in allowable working temperature with increase in material thickness, a factor discussed in detail in sections 3.3.1 and 3.2.

3.3.3.2. ***Comparative Tests.*** As stated earlier, simple, reproducible, and inexpensive tests are required for the initial selection or comparative assessment of materials and for quality control to ensure that the chosen material meets its specification. One of the oldest and most widely used of these is the *Charpy impact* test, in which a notched square section bar of standard dimensions is broken in three-point bend by an impact blow from a pendulum hammer (Fig. 3.39). The shape of the notch employed depends on the purpose of the test. For quality control at room temperature, a relatively blunt U-notch or keyhole-shaped notch is frequently employed, but for assessing the sensitivity of a steel to brittle fracture when in service at low temperatures, the sharp V-notch is preferred. For metals, the standard Charpy bar of dimensions 55–60 mm by 10 mm by 10 mm is given a 2-mm-deep V-notch with an included angle of 45° and a root radius of 0.25 mm. As the toughness of most steels varies with respect to the final rolling direction, it is important to specify the regions from which the specimens are cut. As illustrated in Fig. 3.40, a much higher toughness is obtained from a specimen cut parallel to the rolling direction and notched in the rolled surface, as in this case crack blunting is most probable (cf. section 3.2.4.1). Most specifications thus require that, for

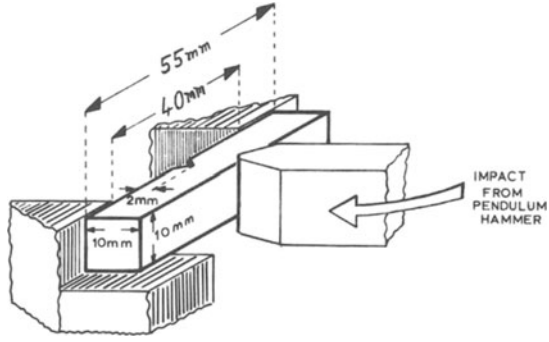

Fig. 3.39. Experimental arrangements for a Charpy V-notch impact test.

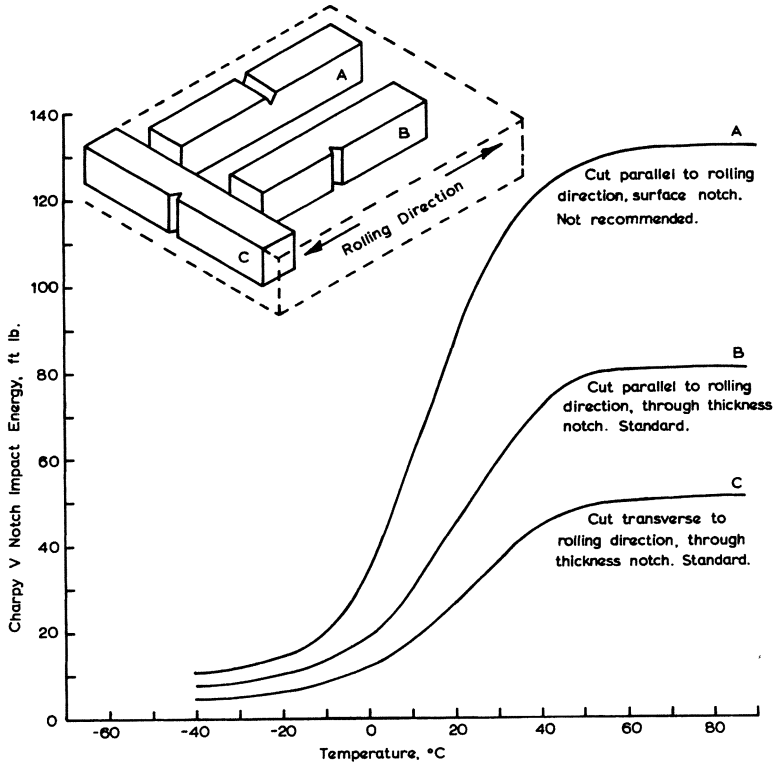

Fig. 3.40. Effect of specimen orientation on the Charpy impact energy of mild steel.

both transverse and longitudinal specimens, the notch is cut in the through-thickness direction.

The energy absorbed by the specimen during fracture has no direct application, i.e., it cannot be put into an equation to give the fracture stress of the material. The *change* in impact energy over a range of testing temperatures from a high to a low value does, however, indicate the decrease in toughness which accompanies a change in the fracture mode from high-energy shear to either of the low-energy modes, cleavage or low-energy tear. The test is especially suitable for use with the low-strength mild steels which fail by cleavage at low temperatures, because there is a large difference in the energies absorbed during cleavage and shear fracture, and a large amount of effort has been applied in an attempt to correlate results from Charpy tests with those obtained from full-scale tests and service failures in these steels. The starting point for correlation lies in relating the nil-ductility temperature of a material to the amount

of energy it will absorb in a Charpy test and it is now clear that the relationship between these two quantities is *not constant* for all grades of steel. For example, in low-strength carbon steels, the NDT is equivalent to 8 ft lb energy absorbed in a V-notch test, while in semikilled steels and high-strength quenched and tempered steels, the values are approximately 25 and 50 ft lb, respectively. This is due to the large amount of energy needed to initiate fracture in these tougher steels. Thus, it is necessary to find the Charpy energy which corresponds to the NDT for each grade of steel before it is possible to use the NDT + x°C type of design criterion discussed earlier. If, for example, the NDT does correspond to 8 ft lb absorbed energy for the steel used to obtain the results shown in Fig. 3.41, then the NDT is at ~ -6°C. If we wished to use a NDT + 30°F (+17°C) design criterion for this material, it would give a minimum operating temperature of +11°C, which, from Fig. 3.41, corresponds to an impact energy of $\sim$ 15 ft lb.

The other feature shown in Fig. 3.41 is the change with testing temperature of the percentage of the fracture surface which showed crystalline failure (see, for example, the photographs of such fracture surfaces in Fig. 3.27b). The appearance of the fracture surface is, in many respects, a more reliable guide to a material's susceptibility to cleavage failure than is the energy absorbed in the impact test, and criteria based on the percentage crystallinity usually give the most reliable correlation with service failures. For example, it has been found that, if the surface of a Charpy bar is less than 70% crystalline when fractured at a certain temperature, there is a high probability that cleavage fracture will not occur in service at this temperature if the applied stresses do not exceed half the yield stress. For some mild steels (such as that used in Fig. 3.41), an impact energy of 15 ft lb corresponds to 70% crystallinity and this, at one time, gave rise to the erroneous belief that any material which could absorb 15 ft lb of energy in a Charpy test would not fail in a brittle manner. Such generalizations are, however, not justified, as, in other steels, the 70% crystallinity temperature corresponds to impact energies as high as 50 ft lb and, as a general rule, criteria based on fracture appearance are usually to be preferred to those based on impact energy. Furthermore, although there is no rigorous correlation between the percentage crystallinity shown by a Charpy bar and the three principal transition temperatures, it is often found that the NDT is approximately equivalent to the 85% crystallinity temperature, the FTE to 55% crystallinity, and the FTP to the 0% crystallinity temperature. Finally, there are at least two other variables which can be measured from the fracture halves of Charpy bars which have been tested through the brittleness transition temperature range. The first is the notch root contraction, which is zero for 100% cleavage failure and which increases at higher temperatures.

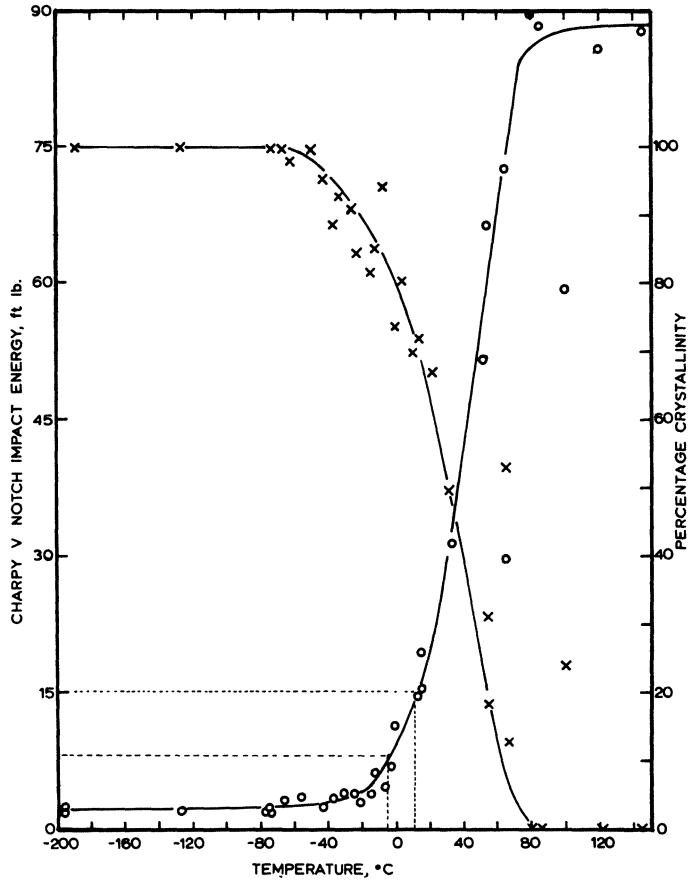

Fig. 3.41. Correlation between the transitions determined by the energy absorbed in a Charpy impact test and the amount of shear failure appearing on the fracture surface.

The second is the appearance of the fracture surface immediately below the root of the notch, and it has been suggested[58] that the temperature at which there is no evidence of shear failure at the notch root correlates well with the fracture initiation temperature discussed earlier in relation to the BWRA tests.

There are a number of limitations to the usefulness of the Charpy test. There is usually a large scatter on the impact energies, especially those determined in the transition range where the toughness is changing rapidly. To a large extent, this is due to inhomogeneities in the composition, structure, or degree of residual stress in the specimens, but the small size of the specimens compared to those used in full scale tests probably exaggerates this scatter. It is usually overcome by testing a large number

of samples from the same material, to avoid such variations and to overcome the statistical errors in the results. A more fundamental disadvantage is its inability to show clearly the toughness transition in materials which fail by low-energy tear instead of cleavage and, as this includes all the medium- and high-strength fcc metals suitable for cryogenic use, this is a severe limitation on its use. Nevertheless, there are a number of design codes which still require Charpy tests to be carried out on aluminum alloys and stainless steels intended for cryogenic applications, particularly where these materials have been welded. Where possible, it is preferable to use the more sensitive *drop weight tear test* (DWTT), which also breaks specimens with an impact blow from a pendulum hammer. Its specimens are, however, much larger—plates 18 in. by 5 in. by 1 in., which contain a deep embrittled weld as a crack initiator—and they require much more energy to fracture them. This enables a clearer distinction to be made between the high-energy and the low-energy modes of shear failure.

Yet another disadvantage of the Charpy test is its inability to accept specimens which are less than 5 mm thick (one-half standard size specimens) ; as noted earlier, notch embrittlement in thin sheet materials is best evaluated by use of the notched tensile tests described in section 3.2. Other types of test using notched specimens have been employed for comparative tests, one example being the *Tipper* test, which is a notched tensile test carried out on a full-plate-thickness specimen containing double V-notches in its sides. There are also a variety of slow bend tests, e.g., the *Van der Veen* test, which again uses a full-thickness specimen, but which contains a simple 45° V-notch in the tension side of a plate tested in three-point bend.

The topic of brittle fracture in steel structures has been reviewed recently by Boyd.[72] In this very useful work he covers not only the basic metallurgical factors involved but also the design considerations which affect the choice of steels for structural applications. Furthermore, he gives a valuable guide to recommended selection procedures and ends by enumerating a set of "golden rules" which, if obeyed, should minimize the possibility of brittle failure in this important class of engineering materials.

3.4 TIME-DEPENDENT FAILURE

In the earlier sections of this chapter, we saw that the fracture stress of a material is strongly influenced by the presence of cracks and flaws and there are three principal mechanisms by which such cracks may form or intensify during service. These are fatigue, corrosion (especially stress corrosion and corrosion fatigue) and hydrogen embrittlement. None of these are specifically low-temperature phenomena ; indeed, the fatigue lives

of many metals increase at low temperatures, while the rate at which most corrosion reactions occur drops very rapidly as the temperature is lowered. Rather, they increase the probability of unstable failure under service conditions which would normally be considered satisfactory. Their effect is due basically to one or more of the following effects : they lower the toughness of the material, they provide a mechanism by which a crack may sharpen and thus increase the degree of stress concentration it produces, or they allow a subcritical crack to grow at stresses below the gross yield stress until it reaches the critical length required for unstable propagation.

3.4.1. Fatigue

Fatigue failure occurs in a material subjected to cyclic or fluctuating stresses which may or may not be superimposed on a static applied stress. Failure under such loading conditions can take place at stresses which are considerably below the ultimate tensile stress or gross yield stress, even in materials which are normally considered to be tough and ductile. Fatigue must therefore be considered as a possible mode of failure in any piece of cryogenic equipment subjected to cyclic loading or vibration, e.g., pumps and turbines, or to periodic changes in pressure, such as storage vessels and process plant. To indicate the severity of this problem, it is worth noting that it has been estimated that fatigue is responsible for about 50% of the failures encountered in general engineering practice.

There are three main stages in the fatigue fracture of a component : initiation, slow crack growth until the critical size is reached, and the final rapid failure of the remaining section either by cleavage or ductile rupture. Plastic deformation is involved in at least the first two of these stages. In pure metals, the initiation of a fatigue crack usually occurs at the surface of the material as a result of inhomogeneous shear deformation, while in alloys and less pure metals, the crack frequently nucleates at the interface of a second-phase particle or at a flaw which may or may not lie in the surface of the material. Another very common cause of initiation stems from the introduction of local stress concentrators such as keyways, badly radiused corners, imperfect welds, and other fabrication defects. The surface finish of a component also plays an important role in the initiation of fatigue cracks, smooth surfaces being more resistant than rough ones, while the surface hardness is known to have a strong influence on the fatigue life of materials. Materials with surfaces which are softer than their interiors (such as aluminum alloy plates coated with pure aluminum to improve their corrosion resistance) have an enhanced probability of fatigue failure. Hence, one way of improving the fatigue life of a component is to harden its surface and this is often achieved in ferrous metals by carburizing or nitriding treatments. Another method which has

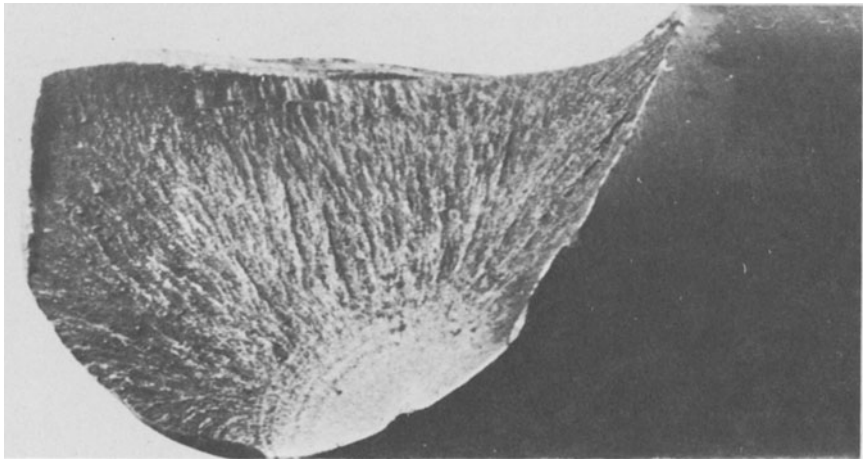

Fig. 3.42. Classical torsional fatigue failure in a case-hardened steel.

a wider applicability is to work-harden the surface by treatments such as shot-peening and this has the added benefit of introducing compressive stresses which also inhibit fatigue crack initiation.

Once initiated, a fatigue crack extends a small amount during each stress cycle, the direction of propagation depending on the type of applied stress. For example, the crack grows in a direction normal to the applied stress for tensile loads, but on a 45° plane for torsional stresses. Such a failure is illustrated in Fig. 3.42, which shows clearly that fracture initiated at a corrosion pit in the case-hardened surface of the steel. It then grew slowly to produce the "thumbnail-shaped" region, in which can be seen "clamshell" markings which indicate successive stages in the slow crack propagation. Final failure was by torsional shear rupture, as indicated by the radial markings which extend from the edge of the smooth thumbnail-shaped region to the extremities of the rod.

Fatigue failures thus occur after a rather complex series of events, not all of which can be quantified. Prediction of the fatigue lives of materials is therefore subject to a rather large margin of error, but it is possible to draw a number of conclusions from the results obtained by testing a large number of specimens over a range of applied stress or strain amplitudes. These results are usually plotted in terms of the stress (or strain) (S) to cause failure after a certain number (N) of cycles (S–N curves), and some representative curves are shown schematically in Figs. 3.43 (a, b). In Fig. 3.43 (a), S–N curves are illustrated for both smooth and notched specimens of mild steel, and two points clearly emerge. First, the curves level off at about 10^6 cycles to give a *fatigue limit*. This is typical of ferritic

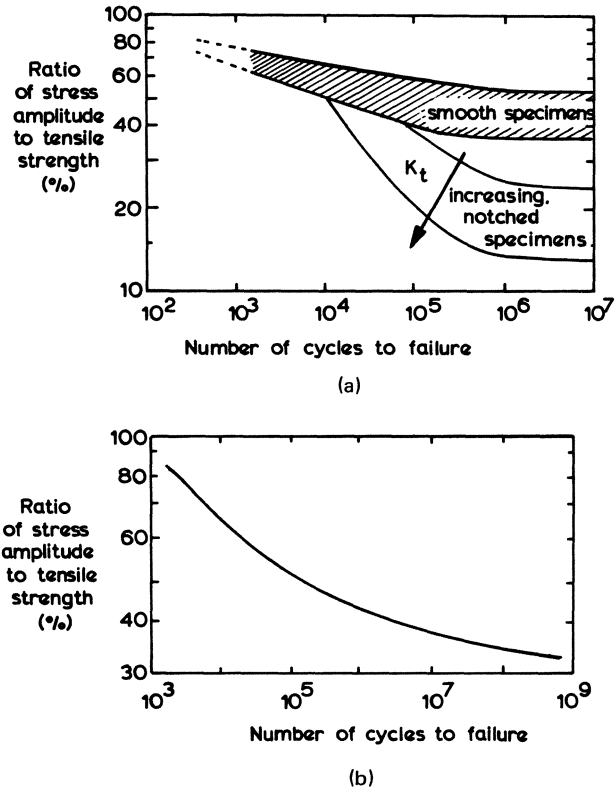

Fig. 3.43. (a) Typical S–N curves for smooth and notched specimens of mild steel. (b) Typical S–N curve for smooth specimens of most nonferrous alloys.

steels below~200°C and also of the aluminum–magnesium alloys at room temperature. The cause of the fatigue limit in these alloys is not yet completely understood, but it is thought to be due to strain-aging. The second point is the lower fatigue lives and fatigue limit shown by the notched specimens ; the more severe the notch, the lower the values of these quantities. This notch-sensitivity adds to the difficulty of predicting the fatigue lives of components which may contain unknown flaws which act in the same way as the notches machined into the experimental specimens. It is, however, generally assumed that, for smooth specimens, the fatigue limit of ferrous alloys corresponds to a stress of about half the ultimate tensile stress.

The S–N curves of Fig. 3.43 (b) are typical of most nonferrous alloys and also of the austenitic stainless steels in that they show no fatigue limit even after more than 10^9 stress cycles. Under these circumstances, the stress

which produces failure after, say, n cycles is known as the *endurance limit* at n cycles, and for many alloys, the endurance limit at 10^9 cycles is approximately 1/3 of their UTS. For most metals, the UTS increases as the temperature is lowered and it is thus reasonable to expect that their endurance limits will also be increased at low temperatures. That this is so is shown by the curves given for pure aluminum in Fig. 3.44. Ordinary tensile tests carried out on similar material showed that the ratio of the UTS to the stress necessary to cause fatigue failure after 10^5 cycles was virtually independent of testing temperature. Two main conclusions were drawn from these results.[60] First, that crack initiation is due to some mechanism which involves the interaction of dislocations or slip planes, as initiation mechanisms which rely on chemical corrosion or atomic diffusion are unlikely to operate at 4.2°K. Second, the consistency of the tensile stress/endurance limit ratio over the large range of testing temperatures suggests that the same mechanism is operative in both cases. We saw in chapter 1 that the increase in UTS with decrease in temperature was a direct result of the higher rates of strain-hardening at low temperatures and it would thus appear that strain-hardening also plays an important role in the initiation and/or propagation of fatigue cracks.

The low-temperature fatigue properties of engineering alloys have also been investigated with the by-now familiar emphasis on those alloys likely to be of use in aerospace applications. The results of Nachtigall *et al.*[61] on materials for rocket engines are representative of such studies, the four

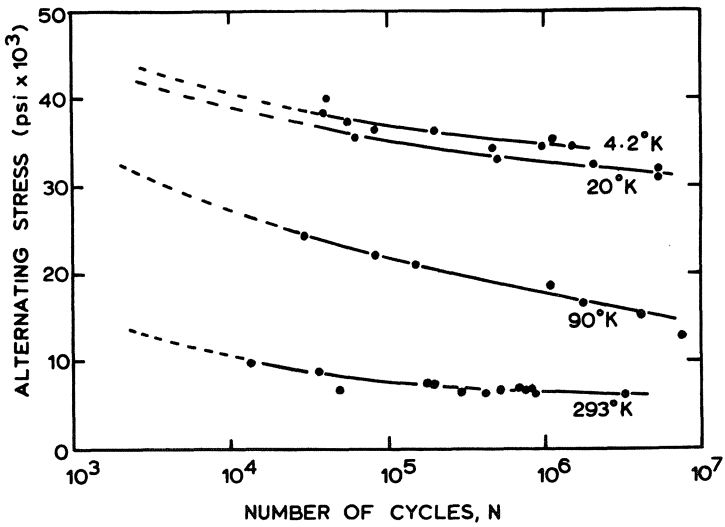

Fig. 3.44. Series of S–N curves for pure aluminum specimens tested at 293, 90 20, and 4°K (after McCammon and Rosenberg[60]).

alloys under evaluation being type 2014-T6 aluminum, Inconel 718, 5Al–2.5Sn alpha-stabilized titanium, and type 301 stainless steel. Data were obtained for both smooth and sharp-notched ($K_t > 17$) sheet specimens; tests were tensile and carried out at room temperature, in liquid nitrogen, and in liquid helium with a minimum to maximum stress ratio $R = 0.14$. Ordinary tensile tests were also carried out on smooth and notched specimens to allow comparison with the fatigue tests. In Fig. 3.45, the results for Inconel 817 are given, as they illustrate clearly the trends shown by most materials. It can be seen that at all temperatures the fatigue lives of the notched specimens are considerably lower than those of the unnotched specimens; while for both types of specimen the fatigue lives at a given stress increase steadily as the temperature decreases. For low lifetimes, the curves are horizontal, indicating that there is a constant maximum stress for fatigue failure after a small number of cycles. This region corresponds in fact to the low-cycle, high-strain type of fatigue, which will be discussed shortly.

The results obtained for the 2014-T6 alloy show the same trends as just described for Inconel. Other work by Schwartzberg *et al.*[62] confirms these results on type 2014-T6 for both parent metal and weldment samples, similar satisfactory behavior being found for both 2219-T87 and 5456-H343. In contrast, types 2020-T6 and 7075-T6 show poorer fatigue properties.

In the 5Al–2.5Sn titanium alloy, the work of Nachtigall *et al.* shows that for smooth specimens the fatigue lives at a given stress increase as the temperature falls, but for notched specimens the trend reverses below 77°K, and the 4°K curve lies below that at 77°K and only just above the room-temperature curve. This behavior correlates well with the decrease in tensile strength shown by notched tensile specimens below 77°K. The be-

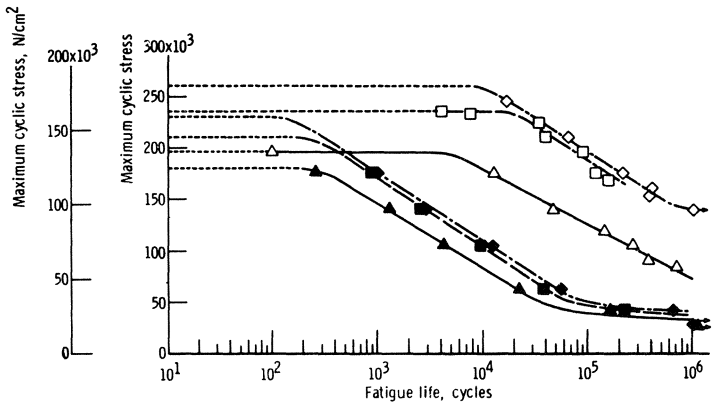

Fig. 3.45. *S–N* curves for smooth and notched specimens of Inconel 713 tested at 4°K, 77°K, and room temperature (Nachtigall *et al.*[61]). (Open symbols, smooth; closed symbols, notched specimens. ◇ ≡ 4°K, □ ≡ 77°K, △ ≡ room temperature.)

havior of type 301 stainless steel is even more anomalous in that, even for smooth specimens, the 4°K S–N curve lies below the 77°K curve and only just above that for room temperature, while for notched specimens the 77°K and room-temperature curves are virtually coincident and the 4°K curve falls even lower. Such behavior can, however, be explained in terms of the stress-induced martensitic transformations which are known to occur in type 301 stainless steel (cf. section 2.1.5.1). Furthermore, the lower fatigue lives correlate well with the results of the tensile tests on type 301, which show that the tensile strengths of the smooth specimens do not increase below 77°K while the UTS of notched specimens fall steadily as the temperature is decreased below ambient.

The fatigue properties of the fully stabilized grades of stainless steel follow the normal trends shown by the Inconel and aluminum alloys, namely, increased fatigue lives at low temperatures.

As noted earlier, the maximum stress necessary for fatigue failure in smooth specimens is constant up to about 10^3–10^4 cycles. Under these conditions, failure is due to accumulated persistent plastic deformation and it has been found that for many metals the number of cycles to failure N is related to the amplitude of the reversed plastic strain range ε_p by the Manson–Coffin law, $N^{1/2}\varepsilon_p = C$, a constant. Furthermore, as a rough rule of thumb, $\pm 1\%$ strain causes failure in 1000 cycles. As the Manson–Coffin law is obeyed for a wide range of materials with widely different strengths and ductilities, it would seem that the mechanism responsible for low-cycle fatigue is not strongly influenced by these factors. By counting the number of ripples appearing in the thumbnail part of the fracture surface and correlating this with their fatigue lives, it has been shown[63] that at least 75% of the fatigue life of smooth specimens which failed after a small number of cycles was spent during slow crack growth. In contrast, most of the lifetime of similar specimens which failed at 10^5–10^6 cycles was spent in the initiation stage. The importance of crack initiation in high-cycle fatigue is confirmed by experiments which show that large increases in fatigue life can be obtained by removing the damaged surface layer from specimens which have already undergone $\sim 10^4$ fatigue cycles.

A further difference between these two types of fatigue has been observed by Williams and Bily,[64] who found that the S–N curve of mild steel exhibits a discontinuity at about 10^3–10^4 cycles which corresponds to a transition from conventional to low-cycle, high-strain fatigue. There is also an associated change in fracture characteristics from eccentric fatigue crack propagation below the discontinuity to cup-and-cone failure above it. Furthermore, a comparison of the plastic extension attained prior to necking during monotonic loading (19.4%), with the total plastic deformation which occurred incrementally under cyclic loading (20.5%), revealed a very good correspondence. Thus, it appears that failure during

low-cycle fatigue occurred after exhaustion of the material's incremental strain-hardening capacity, whereas a stabilized strain-hardened condition was attained prior to the development of the eccentric failures typical of longer fatigue lives. These results further emphasize the importance of accumulated plastic deformation in low-cycle, high-strain fatigue.

A particularly relevant type of fatigue is *thermal fatigue*, in which the stresses and strains are produced by thermal cycling. High stresses can be built up if temperature gradients are nonlinear or if free expansion or contraction is restricted by external constraints, and such failures have been known to occur in regenerators after a large number of temperature reversals and in heat exchangers and other cryogenic plant after a relatively small number of warming and cooling cycles caused by plant shutdown.

So far, we have only considered fatigue due to simple alternating stresses, but in practice, loading cycles can be extremely complex and hence extrapolation from the results of simple laboratory experiments is of limited value. There are a number of empirical rules which attempt to improve the correlation with experience gained from service failures, one of which is *Miner's rule* for cumulative damage. This enables the number of cycles spent at different stress levels to be reduced to an equivalent number of cycles at a single stress. If the material undergoes n_1 cycles at a stress amplitude S_1 which has a predicted life of N_1 cycles, and n_2 cycles at stress S_2 for which the lifetime is N_2, etc., then Miner's rule says that failure will occur when $\sum n_i/N_i = 1$, although for additional safety the constant is usually taken as 0.6. Furthermore, in many applications it is found that the alternating stresses are superimposed on a mean tensile or compressive stress, and it is necessary to be able to predict the life of components under the effect of these combined stress systems. One way of doing this is to use the *Goodman diagram* illustrated schematically in Fig. 3.46. For most metals, it is found that the fatigue lives of smooth specimens subjected to these combined stresses lie quite close to the straight line which joins the appropriate endurance limit to the ultimate tensile stress. For notch-sensitive materials, however, both tensile strengths and endurance limits are lowered by amounts which depend on the material concerned and the severity of the notch. In this case, the lower line in Fig. 3.46 defines the upper limit of the allowable combined stresses.

Finally, *corrosion fatigue* is a mechanism by which the endurance limits of many metals may be severely reduced even though the amount of metal actually removed by corrosion is negligible. It is not necessary for the environment to be particularly corrosive for stress corrosion to occur; for example, the oxygen and water vapor present in normal air are sufficient to cause a considerable reduction in the fatigue lives of a number of aluminum alloys, while salt spray from the sea is particularly harmful.

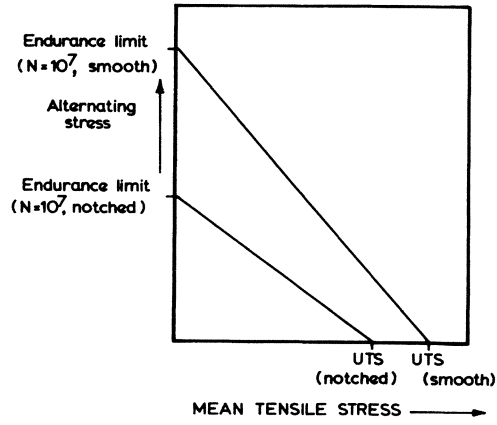

Fig. 3.46. Goodman diagram for fatigue under the action of combined static and alternating stresses for both smooth and notched specimens.

Similarly, the endurance limit at 10^7 cycles of plain carbon steel is lowered by about 50% for freshwater and by about 75% for saltwater environments. Corrosion fatigue failures have been known to cause failure in cryogenic equipment, especially air separation plants located by the sea or near chemical plants, and under such conditions it is necessary either to apply a protective coating to the metal or to specify an alloy such as stainless steel which is less susceptible to these effects. Even with stainless steel it is, however, important to take care to avoid other types of corrosion failure such as "shrouding" and crevice corrosion in brazed joints.

3.4.2. Corrosion and Embrittlement

These two processes can both cause delayed fracture in material subjected to a static stress, failure being liable to occur without prior warning after periods which can range from hours to years after the initial application of the load. It is not proposed to deal in this section with failures due to the bulk removal of metal by the various types of corrosion or oxidation; rather, the intention is to consider briefly a few mechanisms whose adverse effects do not depend on the quantity of material removed. Corrosion fatigue, discussed in the previous section, is one such mechanism; *stress corrosion* is another. Stress corrosion cracking occurs when materials are subjected to a static or slowly increasing load while in a corrosive environment. The stress may be externally applied or it may be an internal stress which was induced in the material by plastic deformation during fabrication or by the contractional strains produced by incorrect welding procedures. A large number of metals and alloys are susceptible to stress

corrosion cracking, including brass, aluminum, magnesium, steel, and titanium. The phenomenon is also found in nonmetals in the form of static fatigue in glass and stress-cracking in certain polymers. It is not specifically a low-temperature effect; indeed, most corrosion mechanisms are slowed down or inhibited at low temperatures, but it is a possible cause of failure in equipment intended for use at low temperatures.

The particular environment responsible for stress corrosion cracking depends on the material concerned, although water or its vapor is often one of the constituents. For example, "season cracking" occurs in internally stressed wrought brass components when they are exposed to moist air which contains traces of ammonia vapor or salt. In brass, cracking is intergranular and residual tensile stresses can cause complete separation of the fracture halves along the grain boundaries; in other systems, however, the cracks may propagate across the grains. Stress corrosion occurs occasionally in austenitic stainless steels, although for practical purposes the phenomenon of weld decay discussed in section 2.1.5.1 is a much more serious problem. It is also found in some types of aluminum and magnesium alloy after welding.

In most cases, the problem of stress corrosion can be overcome or minimized by annealing the affected component at a temperature which is high enough to relieve the initial stresses without causing appreciable softening of the cold-worked material.

Although delayed failure is probably the most spectacular manifestation of *hydrogen embrittlement*, it is only one aspect of a much larger problem which was initially encountered in high-strength steels but has since also been found in a large number of other alloys, including copper and aluminum, titanium and zirconium, and most of the bcc refractory metals. The characteristic effect of hydrogen on the mechanical properties of these metals is to cause a reduction in their ductility and sometimes their strength, and these factors can frequently also lead to failure. The basic cause of the problem is the ease with which the small hydrogen atoms are able to diffuse through the lattices of most metals at room temperature and above. Furthermore, hydrogen concentrations as low as a few parts per million are sufficient to cause serious embrittlement in many metals. The hydrogen usually comes in contact with the metal during its production or subsequent fabrication in such processes as pickling, plating, and welding, the latter in particular being a particularly serious source of hydrogen pickup due to the high temperatures involved. In many metals, such as aluminum, copper, chromium, nickel, and, in particular, iron, the equilibrium solubility of hydrogen increases with temperature, and thus larger amounts may be dissolved at high temperatures. For example, its solubility limit in iron increases by a factor of about 15,000 between room temperature and the melting point of iron, although in this metal the situa-

tion is further complicated by the fact that more hydrogen is soluble in the fcc austenite structure than in the bcc ferrite. The essence of the hydrogen embrittlement problem lies in the fact that, on cooling, the hydrogen picked up at high temperatures exceeds the solubility limit at lower temperatures and the excess hydrogen either has to diffuse out of the metal or be accommodated within it. As diffusion becomes less rapid at low temperatures, much of the excess hydrogen remains in the metal and tends to collect in pores or cracks, where it transforms from atomic to molecular hydrogen. As the temperature decreases further, the hydrogen pressure increases and can reach values high enough to cause the formation of blisters near the surface of ductile metals and cleavage cracks within bcc or hcp metals. The situation is particularly serious in most bcc and some hcp metals due to the very low solubility limits in these metals at room temperature. The formation of blisters and cracks is an example of irreversible embrittlement, the other main type of irreversible embrittlement being hydride formation, which is most serious in metals such as titanium which can dissolve large quantities of hydrogen in an exothermic reaction. The hydrides thus produced form low-strength, brittle particles within the metal which crack easily under an applied stress to nucleate microcracks. Wickstrom and Etheridge[66] have shown that hydrides can also form on the surface of titanium components subjected to thermal and pressure cycling in the presence of hydrogen gas. The hydride is brittle and spalls off during cycling to leave fresh titanium exposed to further corrosion. The affected components were part of a liquid-hydrogen storage system but it is improbable that the hydride formation occurred in the presence of the liquid, as the necessary diffusion and corrosion reactions are unlikely to take place at such low temperatures. In view of the strong affinity of titanium for hydrogen, it is best to keep the two apart wherever possible.

There is also a reversible type of hydrogen embrittlement which occurs as a result of the interaction of hydrogen atoms with dislocation; it is widespread in ferrous alloys and to a lesser extent is found in titanium alloys. One particular characteristic of this type of embrittlement is that it is most serious at low strain rates, which allow time for the hydrogen atoms to diffuse and repin the moving dislocations, and it reaches its ultimate limit in the delayed failures mentioned earlier, which can occur months or years after the hydrogen was absorbed by the metal. As suggested by the term reversible, failure due to this type of embrittlement can be prevented by removal of the hydrogen, and this is normally achieved by prolonged baking at $\sim$350°C. This treatment is, however, time-consuming and not very efficient for metals like titanium, and wherever possible it is better to prevent the initial pickup of the hydrogen. Thus, for example, acid cleaning or pickling processes in which nascent hydrogen is evolved at the surface of the metal are best avoided for these metals.

Electroplating processes have also been responsible for a large number of failures caused by hydrogen embrittlement. Not only are large amounts of hydrogen released at the cathode, but the layer of electrodeposited metal hinders diffusion and makes it more difficult for the trapped hydrogen to be removed during a subsequent baking treatment.

Finally, arc-welding is one of the most common causes of hydrogen pickup and although atmospheric moisture can produce the hydrogen, its most common source is in the electrode coatings, with both organic and inorganic types being suspect. This is a particularly troublesome cause of hydrogen embrittlement in high-tensile-strength steels and, as 9% nickel steel comes into this category, care must be taken during its welding if such embrittlement is to be avoided. The problem is particularly serious where sulfide contamination is also present, as the sulfide ion acts as a surface poison which promotes absorption of hydrogen by the metal but retards the evolution of the dissolved gas.

Hydrogen embrittlement in metals has recently been reviewed by Rogers[65] and is considered in detail in the work by Tetelman and McEvily.[1]

REFERENCES

Textbooks and Reference Works

1. A. S. Tetelman and A. J. McEvily, Jr., *Fracture of Structural Materials*, John Wiley and Sons, New York (1967).
2. B. L. Averbach *et al.* (Eds.), *Conference on Fracture*, M.I.T. Press and John Wiley and Sons, New York (1959).
3. D. C. Drucker and J. J. Gilman (Eds.), *Conference on Fracture of Solids*, Interscience, New York (1963).
4. J. R. Low, Jr., "Fracture of Metals," *Progress in Materials Science*, Vol. 12 Pergamon Press, Oxford (1963).
5. "Fracture Toughness Testing," ASTM STP 381, Am. Soc. Testing. Mat., Philadelphia (1965).
6. K. D. Timmerhaus (Ed.), *Advances in Cryogenic Engineering*, Plenum Press, New York.
7. "Proc. Int. Conf. on Fracture," Sendai, Japan (1965).
8. "Fracture of Engineering Materials," Am. Soc. Metals, Cleveland (1964).
9. "Fracture 1969," Proc. Second Int. Conf. on Fracture, Brighton, April 1969, Chapman and Hall (1969).
10. W.F. Brown, Jr., and J.E. Srawley, "Plane Strain Crack Toughness Testing of High Strength Metallic Materials," ASTM STP 410, Am. Soc. Testing Mat., Philadelphia (1966).

Other References

11. G. Y. Chin, W. F. Hosford, Jr., and W. A. Backofen, *Trans. Met. Soc. AIME* **230**, 437 (1964).
12. E. R. Parker, H. R. Davis, and A. E. Flanigan, *Proc. ASTM* **46**, 1159 (1946).

13. K. Puttick, *Phil. Mag.* **4**, 964 (1959).
14. K. Puttick, *Phil. Mag.* **5**, 759 (1960).
15. B. I. Edelson and W. M. Baldwin, *Trans. ASM* **55**, 230 (1962).
16. J. R. Low, in "Relation of Properties to Microstructure," Am. Soc. Metals, Cleveland (1953), p. 163.
17. C. Zener, *Trans. ASM* **A40**, 3 (1948).
18. A. H. Cottrell, *Trans. AIME* **212**, 192 (1958).
19. R. Honda, *Acta Met.* **9**, 969 (1961).
20. J. J. Gilman, *Trans. AIME* **200**, 621 (1954).
21. A. N. Stroh, *Phil. Mag.* **3**, 597 (1958).
22. D. Hull, *Acta Met.* **8**, 11 (1960).
23. W. D. Biggs and P. L. Pratt, *Acta Met.* **6**, 694 (1958).
24. C. N. Reid, *J. Less Common Metals* **9**, 105 (1965).
25. A. N. Stroh, *Adv. Phys.* **6**, 418 (1957).
26. N. J. Petch, in Ref. 2, p. 54.
27. J. Friedel, in Ref. 2, p. 498.
28. A. A. Griffith, *Phil. Trans. Roy. Soc.* (*London*) **A221**, 163 (1920).
29. C. E. Inglis, *Trans. Inst. Naval. Arch.* **55**, 219 (1913).
30. E. Orowan, *Trans. Inst. Engrs. Shipbuild., Scotland* **1945**, 165; *Rept. Prog. Phys.* **12** (1948–49).
31. G. R. Irwin, in "Encyclopedia of Physics," Vol. VI, Springer–Verlag Heidelberg (1958), p. 551.
32. G. R. Irwin, "Plastic Zone near a Crack and Fracture Toughness," in "Proc. 7th Sagamore Ordnance Mat. & Res. Conf." (August 1960).
33. "Fracture Testing of High Strength Sheet Materials," 1st Rept. of Special ASTM committee, *ASTM Bull.* No. 243 (January 1960), pp. 29–40 and *ASTM Bull.* 244 (February 1960), pp. 18–28.
34. J.E. Srawley and W.F. Brown, in Ref. 5, pp. 133–198; also, in "Fracture Toughness Testing," NASA Rept. TND-2599 (January 1965).
35. J. E. Srawley and W. F. Brown, NASA Tech. Man. X-52030 (1964).
36. J. M. Krafft, A. M. Sullivan, and R. W. Boyle, "Effect of Dimensions on Fast Fracture Instability in Notched Steels," in "Proc. Crack Propagation Symposium," Cranfield, (1961), pp. 8–28.
37. P. Kenny and J. D. Cambell, in *Progress in Materials Science*, Vol. 13, Pergamon Press, Oxford (1968), p. 135.
38. F. R. Schwartzberg, in Ref. 6, Vol. 12 (1967), p. 458.
39. A. W. Brisbane, in Ref. 6, Vol. 8 (1963), p. 641.
40. J. L. Christian, in Ref. 6, Vol. 10 (1965), p. 86.
41. F. A. McClintock, *Weld. J. Res. Suppl.* **26**, 202s (1961).
42. J. F. Watson, J. L. Christian, T. T. Tanalski, and A. Hurlich. in "Proc. ASTM Meeting," Atlantic City, New Jersey (June 1961).
43. J. G. Kaufman and E. W. Johnson, in Ref. 6, Vol. 8 (1963), p. 678.
44. R. M. McClintock and R. L. Hauser, in Ref. 6, Vol. 8 (1963), p. 631.
45. C. F. Tiffany and J. N. Masters, in Ref. 5, p. 249.
46. E. T. Wessel, "Some Basic and Engineering Considerations Regarding the Fracture of Metals at Cryogenic Temperatures" in "Behavior of Metals at Cryogenic Temperatures," ASTM STP 387, Am. Soc. Testing Mat., Philadelphia (1966), p. 32.
47. G. R. Irwin and A. A. Wells, *Metallurgical Review*, **10**, 223, (1965).
48. J. L. Christian. General Dynamics/Astronautics Rept. ASD-TDR-62-258, part II, New York, April 1963, quoted in ref. 38.
49. T. R. Wilshaw and P. L. Pratt in Ref. 7, B III, p. 3.
50. N. P. Allen, W. P. Rees, B. E. Hopkins, and H. R. Tipler, *J. Iron Steel Inst.* **174**, 108 (1953).
51. W. Pellini and P. Puzak, N.R.L. Report 5920 (March 1963).
52. T. S. Robertson, "Propagation of Brittle Fracture in Steel," *J. Iron Steel Inst.* **175**, 361 (1953).

53. P. Puzak, M. E. Schuster, and W. S. Pellini, *Weld. J.* **1954** (October), 481s–495s; also ASTM Standards E. 208 (1966), Part 30, pp. 606–624.
54. R. W. Nichols, "Prevention of Catastrophic Failure in Steel Pressure Circuit Components," *Nuclear Eng.* **11** (120), 369–373 (1966).
55. C. C. Woodley, F. M. Burdekin, and A. A. Wells, "Mild Steel for Pressure Equipment at Subzero Temperatures," *Brit. Weld. J.* **11** (3), 123–136 (1964).
56. F. M. Burdekin, *Weld. J. Res. Suppl.* **1968** (March), 129s–139s.
57. F. M. Burdekin, and A. A. Wells, Ref. 5, pp. 399–405.
58. W. A. Derungs, "Criteria for the Selection of Steels for Low Temperature Service," Rept. of Working Party II, IVth Congress, European Coal and Steel Community (1968).
59. P. P. Puzak, E. W. Eschbacher, and W. S. Pellini, *Weld. J. Res. Suppl.* **31**, 561s (1952).
60. R. D. McCammon and H. M. Rosenberg, *Proc. Roy. Soc.* **A242**, 203 (1957).
61. A. J. Nachtigall, S. J. Klima, and J. C. Freche, *J. Materials, JMLSA*, **3** (2) 425–443 (June 1968).
62. F. R. Schwartzberg, T. F. Kiefer, and R. D. Keys, in Ref. 6, Vol. 10 (1965), p. 1.
63. R. C. Boellner, C. Laird, and A. J. McEvily, *Trans. AIME* **233**, 379 (1965).
64. T. R. G. Williams and M. Bily, *Rheolog. Acta* **9** (1), 120–124 (1970).
65. H. C. Rogers, *Science* **159**, 1057–1064 (8 March 1968).
66. W. A. Wickstrom and B. R. Etheridge, in Ref. 6, Vol. 13 (1968), p. 334.
67. "Progress in Measuring Fracture Toughness and Using Fracture Mechanics," 5th Rept. of ASTM Special Committee, *Mat. Res. Standards* **4**, 107–109 (1964).
68. International Nickel Company Data Sheets on Nickel Steels for Low-Temperature Applications.
69. K. W. Burns and F. B. Pickering, *J. Iron Steel Inst.* **202**, 899 (1964).
70. V. Weiss and S. Yukawa, in Ref. 5, pp. 1–22.
71. "Progress in Measuring Fracture Toughness and Using Fracture Mechanics," *Mat. Res. Standards* **4**, 107–119 (1964).
72. G. M. Boyd, *Brittle Fracture in Steel Structures*, Butterworths, London (1970).

Chapter 4

The Properties of Nonmetals

4.1. POLYMERS

The mechanical properties of polymers differ fundamentally in many respects from those of metals and much of this difference can be ascribed to the characteristic structures of these two classes of material. Most polymers consist of long molecular chains which are built up from a large number of single molecular units called *mers*. These molecular chains vary in length and hence the material has a range of molecular weights whose average can vary from a few hundred for a simple polymer up to about a million for those with very long chains. The chains are rarely straight, being typically coiled or tangled randomly; they may have side branches, and they can be built up from two or more basic mers to form copolymer chains. Polymers can be divided into two basic groups, the thermoplastics and the thermosetting resins, and their dissimilar mechanical properties are a reflection of their different structures.

Thermoplastics have mechanical properties which are critically dependent on the *temperature* and *rate* at which they are deformed. The strains which they develop can be very large and they are often fully recovered when the applied stress is removed or when the material is heated. The constituent atoms that make up the molecular chains are held together by strong primary chemical bonds, but in uncrosslinked polymers there are no primary bonds between adjacent molecular chains, which are held together by weaker secondary bonds. At low enough temperatures, these bonds can be quite strong and the material is rigid, brittle, and behaves in most respects like an organic glass; at high temperatures, there is enough thermal energy for the bonds to be broken, the chains slide easily over each other, and the material is a viscous fluid. If polymers with suitable structures are cooled slowly enough, their chains can align themselves to form crystalline regions which prevent the chains flowing easily past each other. This makes crystalline polymers much more rigid and it is not until the melting point of the crystals is exceeded that viscous flow sets in.

Chain flow can also be restricted by crosslinking in amorphous polymers, and *elastomers* and *rubbers* are basically lightly crosslinked polymers which are able to undergo large amounts (~800%) of reversible elastic deformation at room temperatures (other polymers can also show elastomeric properties at temperatures above or below room temperature). The more the chains are crosslinked, the more restricted is the elastic strain and the greater the rigidity of the material. As the crosslinks are usually formed during a thermal curing process, it might be argued that rubbers are not strictly thermoplastics, and some authors consider them as a third basic type of polymer.

When a large number of crosslinks are formed during processing, the material is said to be thermosetting. Two or more constituents, which may be relatively simple mers or partially polymerized material, are mixed together and, as the mixture cures, a rigid three-dimensional network is formed with crosslinks between the molecules. Once formed, the mechanical properties of thermosets are virtually unaffected by changes of temperature below that at which the material degrades or decomposes; similarly, its properties are far less time- or strain-rate-dependent than those of thermoplastics. Typical thermosets of cryogenic interest are the casting resins, which are often used with particulate or fiber fillers to make them less brittle, and adhesives, especially those now used for bonding together large metal or composite structures.

In section 4.1.1, the basic outlines of the relationship between the structure and mechanical properties of polymers are discussed briefly in order to provide a suitable foundation for section 4.1.2, which covers those properties and materials that are of particular relevance for cryogenic applications. There are a large number of textbooks and works of reference which cover the properties of polymers, paramount among which is the *Encyclopedia of Polymer Science and Technology*,[1] which covers virtually every aspect of the subject and includes a section on cryogenic properties. There are many other volumes on their structure,[6,7,12] physical[3,4,11] and mechanical properties,[5,9] fracture,[2,20] and their use as engineering materials,[8,10] while a number of general texts[13–15] on materials have chapters on their properties. The more practical aspects of their use are discussed in the Society for the Plastics Industry Handbook[16] and other similar volumes,[17] while standards for their testing and use are published by the ASTM[18] and the BSI.[19] References to their cryogenic properties will be given in section 4.1.2.

4.1.1. The Relationship between the Structure and Mechanical Properties of Polymers

One important consequence of the extreme sensitivity of the mechani-

cal properties of thermoplastics to the temperature and rate at which they are deformed is that their transition temperatures are not fixed. Instead, they depend on the criteria used to define these changes of state; for example, the glass transition occurs at a temperature at which the strain produced by a given stress acting for a fixed time changes from a low value characteristic of the glassy state to a predetermined higher value. If the same stress were applied for a longer time, the required strain would be developed at a lower temperature. Thus, testing time and temperature are interrelated. Furthermore, the elastic moduli are also similarly affected: deformation produced at a high strain rate requires more force than that achieved at lower strain rates, and hence the elastic modulus (slope of stress–strain curve) increases with the strain rate. Therefore, when values are quoted for transition temperatures and mechanical properties of polymers, the experimental conditions used to obtain these quantities should be stated if they are to be completely unambiguous. Such precision is, however, rarely found in practice.

4.1.1.1. ***The Glass Transition.*** The relationship between specific volume and temperature is illustrated schematically in Fig. 4.1 for both amorphous and crystalline polymers. Considering first the amorphous material at high temperatures, the polymer is liquid and, as the temperature falls, its viscosity increases gradually and it contracts at a rate typical of that of a liquid (about $4\text{–}8 \times 10^{-4}$ cm^3/°C). The transition from liquid to the amor-

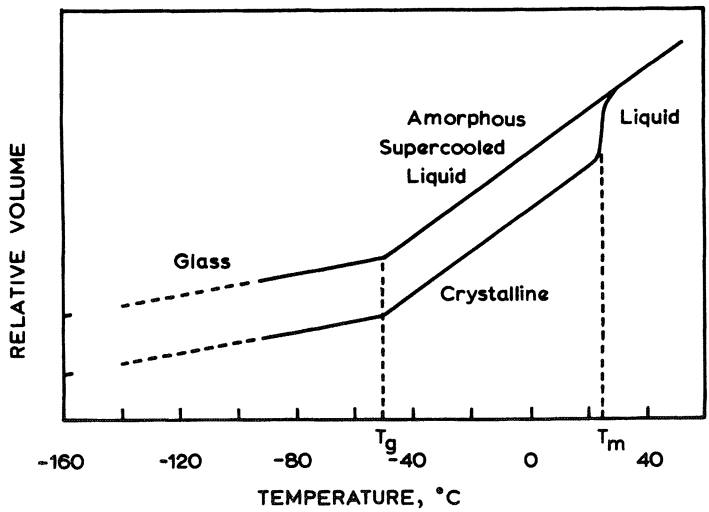

Fig. 4.1. Relationship between specific volume and temperature for a polymer which can be either amorphous or crystalline.

phous solid characteristic of a supercooled liquid takes place gradually and is not accompanied by a volume change. There is, however, a decrease in expansion coefficient to about 2×10^{-4} cm^3/°C at the *glass transition temperature* T_g, below which the polymer is in its glassy state. As it is only the first derivative of the primary thermodynamic variable (volume) which changes discontinuously with temperature, the transition is a second-order thermodynamic transition. Other physical properties which show anomalies at T_g include the dielectric constants, the refractive index, and the specific heat. However, in view of the strong strain-rate effects mentioned earlier, some authors[31] consider that it is not a true thermodynamic transition; its description as a second-order transition is nevertheless conventionally accepted.

For a crystalline material, there is a relatively sharp decrease in volume at the melting point T_m of the crystallites, and this is indisputably a first-order thermodynamic transition. In highly crystalline polymers, the volume change is of the order of 10% or more and is caused by the more efficient packing of the molecular chains when in the crystalline state. In contrast, the change of slope at the glass transition is very indistinct, while in materials of low crystallinity, the relative importance of these two transitions is reversed. Before passing on to consider the mechanisms responsible for the glass transition, it is worth pointing out the practical significance of the high expansion coefficients of polymers above these glass transition temperatures. Their expansion coefficients are considerably higher than those of most metals and this can lead to severe problems of differential contraction if both types of material have to be cooled while linked together mechanically. This topic will be reconsidered in section 6.5.3.

The physical basis for the glass transition in polymers lies in the relationship between the strength of the van der Waals-type secondary bonds which hold the molecular chains together and the thermal energy of vibration of segments of the molecular chain lying between adjacent crosslinks. At very low temperatures, the thermal energy is so low that the secondary bonds are able to hold the chain together to form a rigid structure characteristic of the glassy state. As the temperature rises above T_g the vibrational energy increases sufficiently for individual segments of the molecular chain to become mobile, although it is still too low to permit movement of the complete chains. Under the action of an applied stress, individual segments can be displaced and coiled chains can straighten; yet, when the stress is removed, the chains can coil up again, under the action of their thermal vibration and the deformation is fully recoverable. The material is thus in its *rubbery state* and T_g is often referred to as the glass–rubber transition temperature. It occurs at about one-half to two-thirds of the melting temperature and, as indicated earlier, is not strictly an invariant temperature, as its value is dependent on the method used

Table V. The Structure and Properties of Some Important Polymers

Chemical name	Normal designation	Formula of the chemical repeat unit	Technological classification[a] and physical state at room temperature	T_g, °K
Polydimethyl siloxane	Silicone rubber		R Elastomer	150–160
Polyisobutylene	Butyl rubber BR	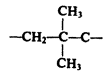	R Elastomer	205
Polyisoprene	Natural rubber	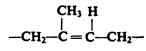	R Elastomer	203
Polychloroprene	Neoprene	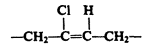	R Elastomer	230–243
Polyethylene	Polythene		TP Part crystalline	153
Polyethylene	Branched polythene		TP Crosslinked	253
Polypropylene	Polypropylene		TP Part crystalline	255
Polyvinylchloride	PVC		TP Amorphous or very slightly crystalline	353
Polystyrene	Styrene		TP Amorphous glassy	373
Polymethyl methacrylate	Acrylic, PMMA	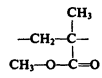	TP Amorphous glassy	380
Polyethylene terephthalate	Mylar PET	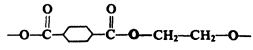	TP Part crystalline	340
Polyhexamethylene adipamide	Nylon 6.6	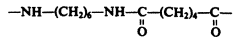	TP Part crystalline	323
Polytetrafluoro ethylene	PTFE TFE		TP Part crystalline	399
Phenol-formal-dehyde resin	Phenolics	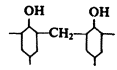	TS Glassy	—
Diglycidyl ether of bisphenol A	Epoxy resin (DGEBA)	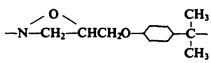	TS Glassy	—

[a] TP = thermoplastic, R = rubber, TS = thermoset.

for its determination. Furthermore, the glass–rubber transition occurs over a temperature range which is usually about 10–30° in width, but which can extend to over 100° for some rigid polymers. During the transition region, the material exhibits *viscoelastic* properties, such as creep, stress relaxation, and high damping. These phenomena will be considered in more detail in sections 4.1.1.4 and 4.1.1.5.

The temperature at which the glass transition occurs is determined by a number of factors, including the molecular weight of the polymer, the size of its side groups, the flexibility of its chains, etc. The transition temperature can be lowered by plasticizing the polymer with a polymer of low molecular weight which itself has a low glass transition temperature, while in copolymers, T_g is intermediate between those of its constituents. In partially crystalline polymers, the transition temperature is the same as that of the amorphous material but, as pointed out earlier, it is much less pronounced. Finally, it should be noted that, taking the lower limit of one-half the melting point for T_g, no polymer which is rigid at room temperature can have a glass transition much below ~150°K. Hence, this will set a lower limit to the temperature at which polymers show true elastomeric properties. The glass transition temperatures of a number of important polymers are shown in Table V together with their common designation, the formula of their chemical repeat units, their technological classification, and their physical state at room temperature.

In view of the dominant influence that crystallites exert on the mechanical properties of polymers, it is simpler to consider the properties of amorphous and crystalline polymers separately.

4.1.1.2. ***Amorphous Polymers.*** One convenient method[31] of distinguishing the three basic states of amorphous polymers is illustrated in Fig. 4.2, which shows a typical thermomechanical curve for such a material. The curve is obtained by measuring the deformation produced by a constant stress acting for a fixed time (~10 sec) while the material is heated slowly (~1–3°/min) over the requisite temperature range, which is usually somewhere between −150°C and 300–400°C. At very low temperatures, the material is in its glassy state and the deformation produced is negligibly small. As the glass transition range is entered, a measurable amount of elastic strain is developed while the stress is applied and this strain increases rapidly with temperature to give the first rise on the thermomechanical curve. At higher temperatures, the deformation saturates at a particular value which depends on the chosen values of stress and application time, this plateau corresponding to the rubbery state of the polymer. The deformation saturates because the material is able to develop its full elastic extension during the time the stress is applied, whereas at lower temperatures during the glass transition range the viscoelastic nature of the defor-

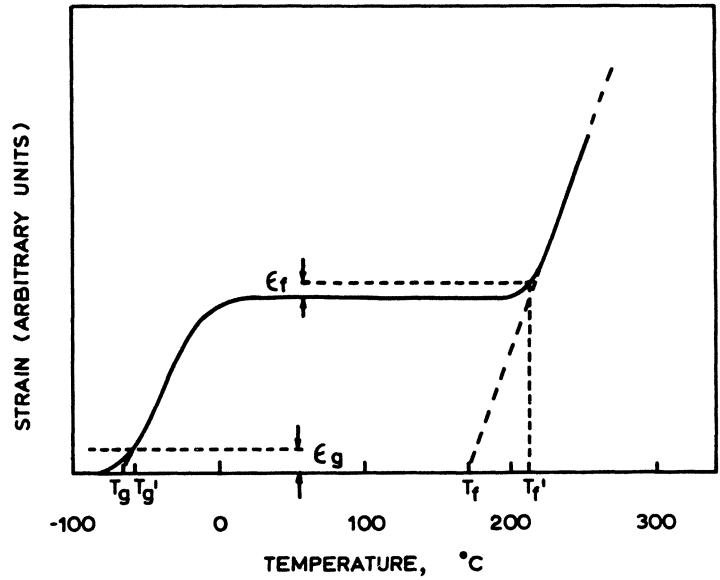

Fig. 4.2. Thermomechanical curve for a typical amorphous polymer (after Kargin and Slonimsky[31]).

mation prevents the full elastic strain from being developed in that period.

The deformation produced at temperatures corresponding to the plateau on the thermomechanical curve is fully recoverable, but at higher temperatures, large, irreversible deformation can be produced and this corresponds to the viscofluid state which exists to the right of the second rise in the curve. In this state, both the segments and the molecular chains are displaced and the deformation is partially elastic and partially by viscous flow. The existence of rubberlike deformation in the viscofluid state is of great technological importance in the production of fibers and films with oriented polymer chains (see section 4.1.2.4).

The thermomechanical curve also illustrates the importance of convention in defining the glass transition and flow temperatures. One method of specifying these temperatures is by drawing tangents to the ascending parts of the curve and defining T_g and T_f by their intersection with the abcissa (temperature axis). Other common procedures are, however, based on the temperatures at which a certain strain (ϵ_g and ϵ_f) is developed by a given combination of stress and time to produce transitions at T_g' and T_f', respectively. This procedure is similar to that used[18] to determine the "heat distortion temperature," which is of the same order as T_g'.

Finally, it should be noted that, if T_g occurs at a temperature sufficiently below ambient (~25°C), the material will be in its rubbery state in

normal use at room temperature, while if T_g is sufficiently above room temperature, the material is rigid. Polymers which have glass transitions near room temperature are usually avoided because of the large change in their properties which would be produced by seasonal variations in the ambient temperature.

When considering the mechanical properties of these polymers, the remarks made earlier about their strain-rate dependence should be borne in mind; for example, the elastic modulus used in Fig. 4.3 is that found for a particular strain rate and other testing conditions (in particular, it is the part of the modulus corresponding to the stress which is in phase with the strain; see section 4.1.1.5). The changes in modulus may be correlated with the features shown in the thermomechanical curve. In the glassy state, the modulus has a high, almost-constant value, but it drops rapidly, typically by ~3–4 orders of magnitude, during the glass transition as the material passes through its "leathery" viscoelastic state. In most polymers, the modulus decreases gradually with temperature in the rubbery state, but for those which show marked elastomeric properties, the modulus increases slightly with temperature. At higher temperatures, the viscofluid transition sets in and the modulus starts to decrease rapidly, the terms "rubbery flow" and "liquid" shown in Fig. 4.3 being commonly used to describe the viscofluid state of the material at these temperatures.

We are now in a position to consider the type of stress–strain curve found for amorphous polymers tested over a range of temperatures, noting

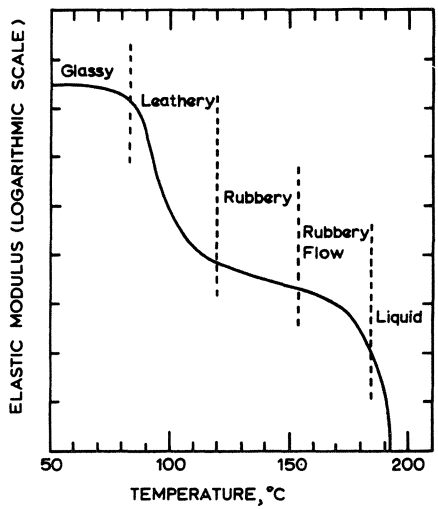

Fig. 4.3. Effect of temperature on the reversible component of the elastic modulus of a typical amorphous polymer.

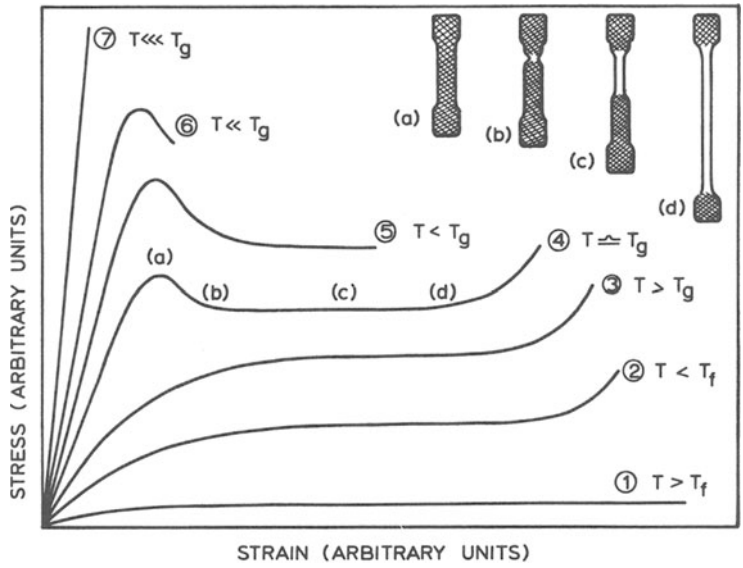

Fig. 4.4. Stress–strain curves for a typical amorphous polymer, such as polyvinylchloride, tested over a range of temperatures from below the glass transition to above the viscofluid transition.

that the family of curves illustrated for polyvinylchloride in Fig. 4.4 was obtained for one particular strain rate. The stresses and strains shown are their nominal values, that is, the load/(original cross-sectional area) and the increase in length/(original length), respectively. At temperatures above the viscofluid transition (curve 1), the material is a viscous liquid whose deformation is similar to that of a Newtonian fluid, in which the deformation stress is proportional to the imposed strain rate. At temperatures just below T_f (curve 2), the material develops large, reversible elastic strains and this behavior continues as the temperature falls toward T_g (curve 3), with larger stresses required to produce any given strain. The rapid increase in stress which is necessary to continue deformation at large strains arises because the molecular chains have finished uncoiling and a much larger stress is required to extend the straightened chains.

As the temperature drops below the glass transition (curve 4), the material undergoes forced rubbery deformation, which is commonly described as "cold-drawing." The material stretches elastically until the *yield stress* σ_y is reached, whereupon the stress decreases quite rapidly to a lower value σ_d, the *draw stress*. By examining the specimen before (a) and after (b), we see that this drop in stress reveals that the deformation has been localized and has produced a necked region. Subsequent deformation, which occurs at the draw stress, extends this neck at the expense of the

undrawn material at either side (c), and a constant ratio, the *natural draw ratio*, develops between the cross-sectional areas of the undrawn and the drawn material. Eventually, the neck draws fully through the specimen, (d), and only then is there an increase in the stress necessary to continue deformation.

X-ray diffraction studies have shown that the molecular chains in the necked region are oriented parallel to the applied stress, and in this condition the polymer is stronger than when the chains are arranged randomly. Thus, the neck is the strongest part of the specimen—a direct contrast to the more familiar situation in metals, where the neck is the weakest point. It is believed[32] that the neck develops in a region where the strain energy produces a localized rise in temperature which causes the modulus to drop. More heat is generated as the neck extends and this is conducted adiabatically through the shoulders of the neck into the undrawn material, thus lowering its modulus and allowing further drawing of the neck. As the deformation occurs at a temperature below T_g, the oriented chains remain "frozen in" and they are not able to recoil themselves when the applied stress is removed. If, however, the material is heated above T_g, the chain segments become sufficiently mobile for them to coil up again, the deformation is fully recovered, and the material returns to its original form.

At a lower temperature (curve 5), the material yields and starts to cold-draw, but in this case, fracture occurs before the neck has drawn completely through the specimen, while at a still lower temperature (curve 6), failure follows immediately after neck formation. Finally, at and below the *brittleness temperature* T_b, which is much lower than T_g, the material is completely brittle and fracture takes place on the elastic loading line. The effect of temperature on the mechanical properties of this amorphous polymer may be summarized as follows:

(1) At temperatures above T_f, it is viscofluid, deformation is unrecoverable, and the deformation stress depends on the viscosity and strain rate.

(2) Between T_f and T_g, the material is rubbery and deformation is fully recovered as soon as the applied stress is removed.

(3) Between T_g and T_b, forced rubbery deformation is produced; it is not recovered when the stress is removed but may be fully recovered if the temperature is raised above T_g.

(4) Below T_b, the material is completely brittle.

Once again, it must be emphasized that the temperatures T_b, T_g, and T_f used in this discussion are relevant to one strain rate only. At higher strain rates, the molecules would have less time to adjust themselves to the applied stress and the material would appear more rigid and brittle, and thus all three transitions would occur at higher temperatures. This is

particularly so for the glass–rubber transition region, where a material may show elastomeric properties at low strain rates but be glassy at high strain rates.

So far, we have explained the elastomeric properties of amorphous polymers above their glass transition on the basis of the coiling and uncoiling of segments of their molecular chains whose ends are held by crosslinks or mechanical entanglements. Although this model gives a qualitative explanation of many of their features, it is unable to explain a number of important properties such as the increase in modulus with temperature in the elastomeric state and the fact that an elastomer becomes warmer, not cooler, when stretched adiabatically. All these features can, however, be explained by the kinetic theory of rubber elasticity originally proposed by Meyer[33] and since refined and extended considerably. A full treatment of this topic may be found in Treloar's text,[11] while more abbreviated versions are given in many of the references cited at the beginning of section 4.1.1. Detailed consideration of such theories would be out of place in this volume; suffice it to say that during elastomeric deformation, the changes in entropy caused by the increased order of the oriented molecular chains far outweigh the normal changes in internal energy and dominate the thermodynamic functions which describe the deformation of this material.

From a practical point of view, one important use of elastomeric materials is in the form of seals, gaskets, and sealants. We have just seen that the very existence of the elastomeric state depends fundamentally on the relationship between the operating temperature and the glass transition temperature, and the use of elastomers at cryogenic temperatures will be considered further in section 4.1.2.2.

4.1.1.3 ***Crystalline Polymers.*** As we saw in Fig. 4.1, some polymers are able to crystallize when they are cooled below their melting point T_m, and the amount of crystallization which occurs is highly dependent on the chain structure of the material and the rate at which it is cooled through this transition. For example, polyethylene has a simple, symmetrical chain structure which is easy to crystallize, and it is virtually impossible to cool it rapidly enough to prevent some crystallization, while some types of nylon can be almost amorphous if quenched from the melt, but up to about 80% crystalline if cooled slowly. Their mechanical properties vary with the degree of crystallinity, highly crystalline polymers being rigid but rather brittle, and low-crystallinity ones being less rigid but tougher. As even small amounts of crystallinity cause the mechanical properties of crystalline polymers to differ fundamentally from those in the amorphous state, it is meaningful to consider their mechanical properties separately, but it should be remembered that most "crystalline" polymers

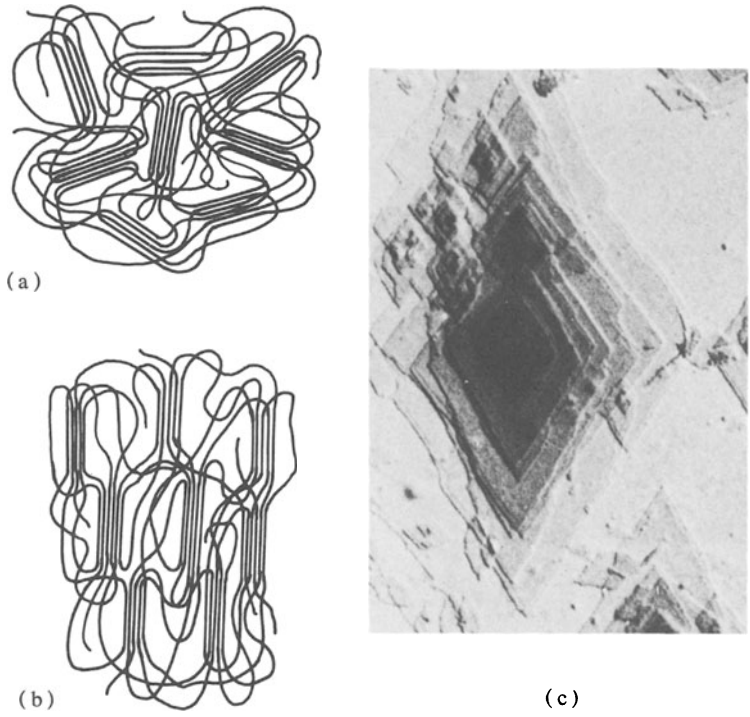

Fig. 4.5. Structure of crystalline polymers: Fringe-micelle model of (a) randomly oriented and (b) cold-drawn polymers, (c) single crystal of polyethylene (after Keller[34]); (d) schematic representation of a polyethylene spherulite, (e) proposed model of spherulite

are only partially crystalline, the remainder of the material being amorphous. One early representation of such a structure, known as the "fringed micelle" model, is shown in Fig. 4.5(a). It assumes that each molecular chain passes through a number of crystallites as well as through the amorphous region which separates adjacent crystallites. In the undeformed state, the crystallites are randomly oriented as in Fig. 4.5(a), but when deformed, they become oriented as in Fig. 4.5(b). Although able to explain many of the properties of deformed polymers, this model is unable to account for a number of their properties in the undrawn state. In particular, X-ray diffraction studies[34] on single crystals of polyethylene grown from a xylene solution showed them to be thin, diamond-shaped crystals (Fig. 4.5c) in which the polymer chains were folded back and forth in layers with a uniform thickness of about 100 Å. A similar structure is developed in the "spherulites" (Fig. 4.5d) which are characteristic of polyethylene cooled slowly from the melt. The folded chains are thought[35] to be arranged in

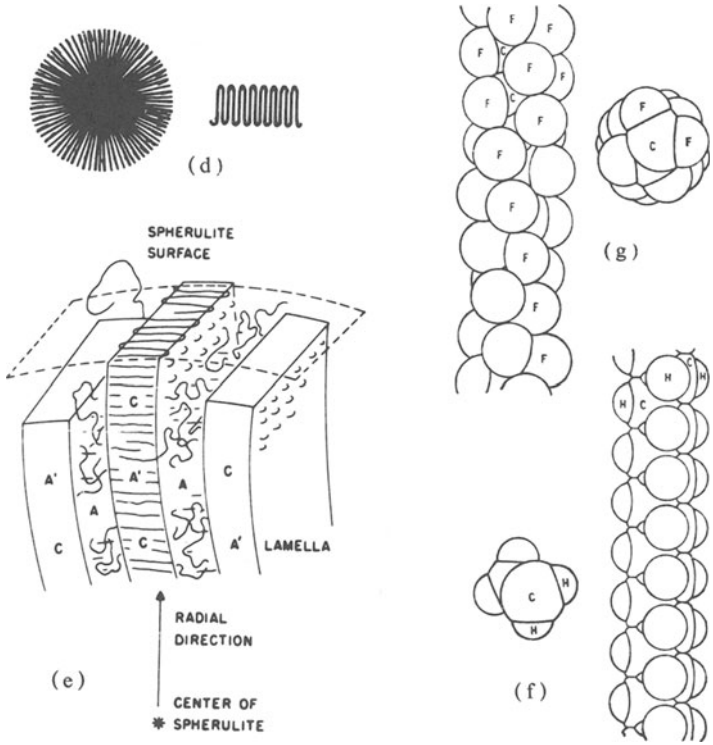

growth (after Takayangi[35]); (f) regular chain structure of polyethylene and (g) twisted zigzag structure of polytetrafluoroethylene (after Bunn and Howells[36]).

lamellae which are separated by amorphous regions and which fan out radially from the center of the spherulite (Fig. 4.5e); typical spherulites are of the order 1–100 μ in diameter and a few 100 Å thick.*

Finally, before leaving the crystal structure of polymers, it is worth noting the difference between the chain structures of polyethylene and polytetrafluoroethylene (PTFE), as this accounts for the distinctive mechanical properties of PTFE over the wide temperature range from liquid-helium temperature to its softening point of 330°C. The atomic arrangement of the polyethylene chain is shown in Fig. 4.5(f) and it can be seen that the hydrogen atoms line up one above each other to give the regular but rather knobbly section shown. This allows adjacent chains to pack tightly together when the protuberances of one chain fit into the hollows of the other, and in such an arrangement, the secondary intermolecular bonds

*One angstrom unit (Å)$\equiv 10^{-10}$ m, 1 micron (μ)$\equiv 10^{-6}$ m.

can be quite strong. When the material is cooled through its glass transition, the chains bond tightly together to make it rigid but brittle. In contrast, the larger size of the fluorine atoms makes it impossible for them to line up above one another and, in order to achieve the most efficient packing, each fluorine atom is twisted relative to the atom beneath it to give its so-called "twisted zigzag" spiral chain illustrated in Fig. 4.5(g).[36] There are 26 carbon atoms per full turn of the spiral and, when seen end on, the chain has the almost circular cross-section shown. As a result, intermolecular forces between adjacent fluorocarbon chains are very small and the excellent high-temperature properties of PTFE are derived from the packing of the atoms in the chains themselves. From a low-temperature point of view, the low intermolecular forces are important because the material does not undergo a marked change in properties as it cools through its glass transition and it still retains a useful degree of flexibility and resilience even down to liquid-helium temperatures. The properties of PTFE will be considered further in sections 2.1.1.4, 4.1.2.2, and 4.1.2.6.

Returning now to the mechanical properties of crystalline polymers, Fig. 4.6 shows typical thermomechanical curves for this type of material. The solid curve (1) represents the crystalline condition of a material such as isotactic polystyrene and it can be seen that there is only a small amount of strain developed as it passes through its glass transition at T_g because of the restraining influence which the crystallites exert on the deformation of the amorphous regions. The strain developed during the thermomechanical test remains constant until the temperature reaches T_m, at which point the crystallites melt. As curve (1) represents a polymer whose crystallite melting point T_m is higher than its viscofluid transition temperature T_f', the thermomechanical curve rises continuously above T_m. For other polymers, the viscofluid transition temperature T_f'' can be higher than T_m, and in this case, their thermomechanical curve (2) has a plateau characteristic of the rubbery state between T_m and T_f''. Now, if polystyrene is quenched rapidly from the melt, it can be prepared in the amorphous condition, and if a thermomechanical test is carried out on such a material, curve (3) is obtained. On warming through the glass transition range, it enters the rubbery state, as shown by the much larger strain developed. For most polymers, the duration of the thermomechanical test is too short to allow recrystallization to occur and hence the strain remains constant until, at T_f', it goes through its viscofluid transition. Finally, it should be noted that the lower the crystallinity of the material, the greater will be the deformation produced at temperatures between T_g and T_m and thus curve (4) is representative of a material of relatively low crystallinity.

The changes of state detected by the thermomechanical curves can also be correlated with the changes in modulus shown in Fig. 4.7 for three types of polystyrene. For the crystalline condition, there is only a

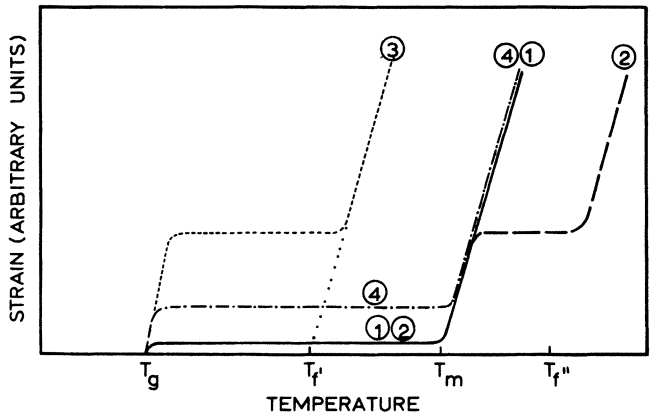

Fig. 4.6

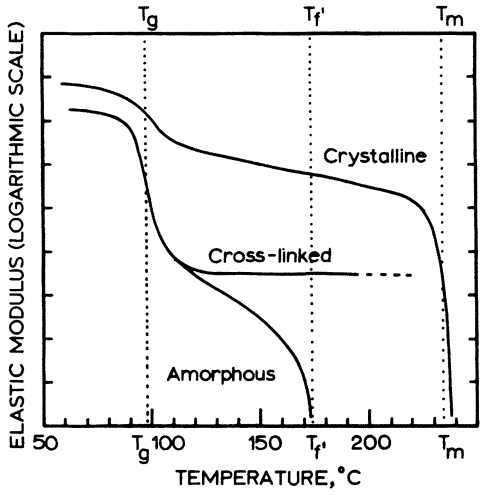

Fig. 4.7

Fig. 4.6. Thermomechanical curves for various types of crystalline polymer (after Kargin and Slonimsky[31]).

Fig. 4.7. Temperature dependence of the reversible component of the elastic modulus of polystyrene; the curve for crystalline isotactic polystyrene corresponds to thermomechanical curve (1) in Fig. 4.6 and that for amorphous atactic polystyrene to curve (3).

small change in modulus as it warms through the glass transition, this being followed by a gradual decrease in modulus until it drops rapidly at T_m when the crystallites melt. For the crosslinked polystyrene, the modulus decreases by over three orders of magnitude during the glass transition but it remains relatively constant in the elastomeric region, only decreasing again when the viscofluid transition (not shown) is reached. The amor-

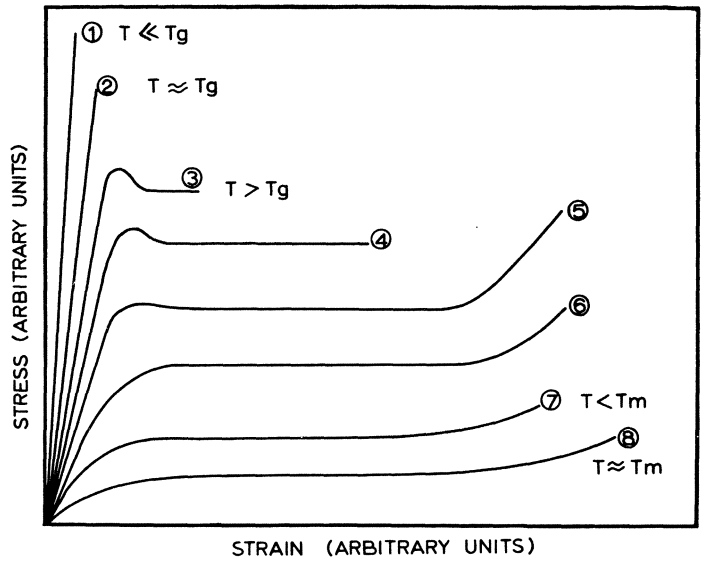

Fig. 4.8. Stress–strain curves for a typical crystalline polymer tested at temperatures ranging from its melting point to below its glass transition.

phous material also shows a large decrease in modulus as it warms through the glass transition and, with neither crystallites nor crosslinks to restrict molecular flow, the modulus continues to fall with increasing rapidity as the viscofluid transition T_f' is reached. Thus, both crystallization and crosslinking raise the upper working temperature of polystyrene by preventing its excessive softening at lower temperatures.

In Fig. 4.8, a family of stress–strain curves is illustrated for a typical highly crystalline polymer and, although at first sight they appear to have the same form as the curves shown in Fig. 4.4, for an amorphous polymer, the temperature ranges and mechanisms involved differ considerably. At temperatures much below T_g, they are both completely brittle but, whereas large amounts of forced rubbery deformation were possible at and below T_g in the amorphous polymer (curves 4 and 5 in Fig. 4.4), a highly crystalline polymer remains completely brittle up to T_g. Thus, for example, amorphous polystyrene is capable of considerable forced rubbery extension below 80°C, at which temperature it undergoes its glass–rubber transition, while the crystalline variety of the same material is completely brittle below this temperature and deformable above it. In Fig. 4.8 a yield point is visible in curve (3), which is for a temperature just above T_g, and as the temperature is increased further, neck formation and cold-drawing

take place (curve 4). At such temperatures, premature failure often occurs at a flaw before the neck draws completely through the specimen, while at higher temperatures (curves 5 and 6), cold-drawing goes to completion and the applied stress increases at high strains because the chains themselves are under load.

Thus, necking and cold-drawing take place in both crystalline and amorphous polymers, but the microscopic mechanisms involved are different. For crystalline polymers, it occurs by recrystallization of the chains along the direction of the applied stress and it is believed that the effective melting points of the crystallites oriented parallel to the stress are increased by its action, while those unfavorably oriented are lowered, thus enabling these elements to become unstable, melt, and then recrystallize in the direction of the applied stress. The details of this process are, as yet, not fully understood, but it has been shown that neither the degree of crystallinity nor the density of the material change during cold-drawing. Once cold-drawn, the material is highly anisotropic, with both high strength and high modulus occurring in the drawn direction in which the crystallites are oriented. Furthermore, there is no recovery and molecular realignment until the temperature approaches the melting point of the crystallites, and thus the process of cold-drawing crystalline polymers can be used to produce strong, uniaxially oriented fibers or biaxial films which retain their strength to a relatively high temperature. The practical aspects of the use of fibers and films at cryogenic temperatures will be reconsidered in section 4.1.2.4 It should also be noted that molecular orientation and the anisotropy it produces can occur as a result of molding or other processing treatments and that this can often be detrimental and lead to premature failure of the component.

Returning now to the stress–strain curves of Fig. 4.8, as the temperature approaches T_m (curves 7 and 8) more and more of the deformation is recoverable on removal of the stress, while above T_m, the material is a viscous fluid. The stress–strain behavior of crystalline polymers may be summarized as follows:

(1) The brittleness temperature T_b is approximately coincident with the glass transition T_g, although for low-crystallinity materials, T_b may be somewhat lower than T_g.

(2) Cold-drawing takes place over the temperature range T_g to T_m, although again for low-crystallinity materials, it is possible for this process to take place a little below T_g due to the deformation of the amorphous regions.

(3) Once cold-drawn, the strong, oriented structure is stable until the temperature is increased toward the melting point T_m.

(4) As noted earlier for amorphous polymers, the properties and

transition temperatures of crystalline polymers are highly strain-rate-dependent, the material appearing stronger and more brittle at high strain rates.

4.1.1.4. ***Viscoelastic Processes: Stress Relaxation and Creep.*** In the earlier chapters of this monograph, it was assumed that, at low strains, the elastic deformation of metals obeyed Hooke's law, and that for tensile deformation, the stress was equal to the product of Young's modulus and the strain, i.e.,

$$\sigma = E\varepsilon \tag{4.1}$$

This relationship is also valid for most amorphous and crystalline polymers at temperatures far below their glass transition, while at temperatures well above their viscofluid transition, they approximate to ideal Newtonian fluids in which the stress necessary to overcome viscous drag is equal to the viscosity multiplied by the strain rate, i.e.,

$$\sigma = \eta \, d\varepsilon/dt \tag{4.2}$$

At temperatures between these two extremes, most polymers are neither perfectly elastic nor ideally fluid and their deformation is said to be viscoelastic, or, in some circumstances, elastoviscous. Such behavior is particularly evident during the glass–rubber and rubber–viscofluid transitions and it is necessary to include both elastic and viscofluid components in the equations which describe the deformation of polymers in this state. There are two readily identifiable processes in which their mechanical properties change with time—*stress relaxation* and *creep*—and a number of models have been developed to help analyze these effects.

Stress relaxation takes place when a polymer is maintained at a given strain after being stretched rapidly to this strain. For example, if the crosshead is stopped, but not reversed, during a tensile test, the stress necessary to maintain this deformation is seen to drop, rapidly at first, but then more slowly as time proceeds. The simplest model which can be used to describe this behavior is that due to Maxwell shown in Fig. 4.9(a), in which the stress is applied to a perfect Hookean spring in series with a dashpot which contains an ideal Newtonian fluid. In this case, the stress is equal in both elements and, by solving the equations of motion, it can be shown that the stress σ_t at time t is related to the initial stress σ_0 by the equation

$$\sigma_t = \sigma_0 \, e^{-t/\tau} \tag{4.3}$$

where $\tau = \eta/E$ is the characteristic *relaxation time* of the system. Thus, the stress decays exponentially as shown in Fig. 4.9(b). The physical basis for such behavior in polymers lies in the time needed for their molecular chains and segments to slide past each other, and for a polymer above its

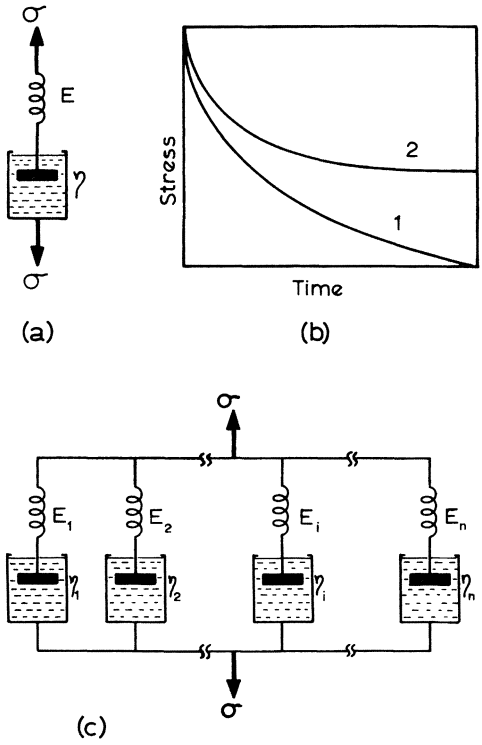

Fig. 4.9. (a) Maxwell's model for stress relaxation in an elastoviscous material; the spring has a modulus E and the viscosity of the fluid in the dashpot is η. (b) Typical stress relaxation curves for (1) an uncrosslinked amorphous polymer and (2) a crosslinked or crystalline polymer. (c) Parallel arrangement of simple Maxwell elements for a polymer with a spectrum of relaxation times.

viscofluid transition, the stress could relax to zero as the chains flow completely past each other. Similarly, given enough time, complete stress relaxation could occur in an uncrosslinked polymer in the temperature range between T_g and T_f, but for crosslinked or crystalline polymers in this temperature range, the stress will only relax partially to a value which depends on the polymer concerned, its degree of crystallinity or crosslinking, and the deformation temperature. Furthermore, a real material possesses not just one relaxation time, but a whole spectrum corresponding to the variety of micromechanisms which can contribute to the stress relaxation process. This situation can be modeled by arranging a large number of Maxwell elements in parallel as shown in Fig. 4.9(c). For n elements, the stress is given by

$$\sigma_t = \varepsilon \sum_n E_n e^{-t/\tau_n} \tag{4.4}$$

where τ_n is the characteristic relaxation time of the nth element. Further analysis can yield an expression for the stress relaxation modulus $G(t)$ for a material with a continuum of relaxation times, which are usually defined on a logarithmic basis. On addition of G_0 for the initial modulus, the expression becomes

$$G(t) = \sigma_t/\varepsilon = G_0 + \int_{-\infty}^{\infty} He^{-t/\tau}\, d(\ln \tau) \tag{4.5}$$

Further consideration of this topic is, however, beyond the scope of this text.

In the second basic viscoelastic process, creep, we are interested in the time dependence of the strain produced by the action of a constant stress,

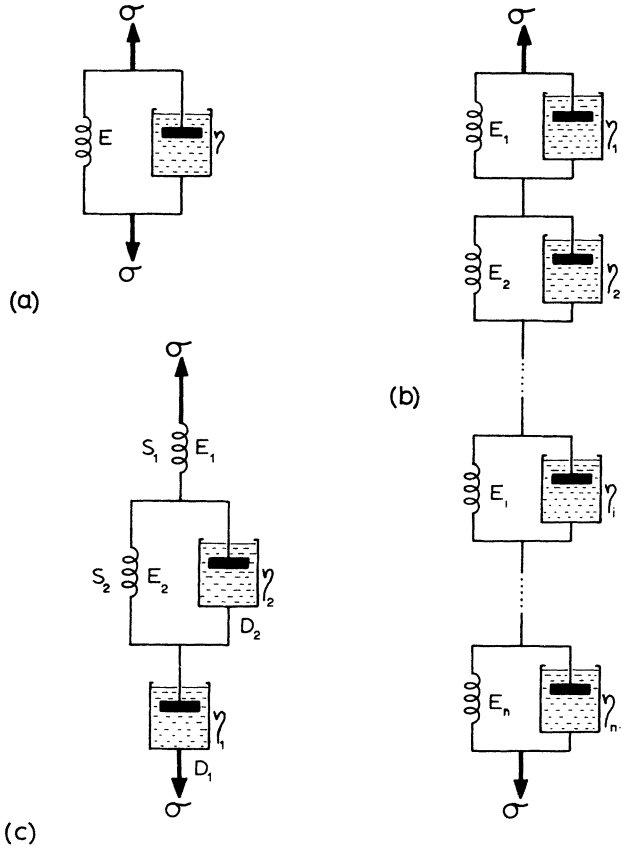

Fig. 4.10. (a) Voigt's model for creep in a viscoelastic material. (b) Series arrangement of simple Voigt elements for a polymer with a spectrum of retardation times. (c) Model of a standard linear solid which combines both Maxwell and Voigt elements and describes stress relaxation and creep.

and in this case, the basic model element is that due to Voigt and is shown in Fig. 4.10(a). The stress is applied to a parallel combination of spring and dashpot and it is now the strain which is equal in both elements. Solution of the equations of motion gives

$$\varepsilon_t = (\sigma_0/E)\ (1 - e^{-t/\tau}) \tag{4.6}$$

where once again $\tau = \eta/E$, but it is now known as the characteristic *retardation* time. As before, a real material contains a number of characteristic retardation times which may be modeled by a number of Voigt elements connected in series (Fig. 4.10 b) and the relevant equation for the strain is

$$\varepsilon_t = \sigma \sum_n (1/E_n)\ (1 - e^{-t/\tau_n}) \tag{4.7}$$

while for a continuous distribution of retardation times, the creep compliance $J(t)$ is given by

$$J(t) = \varepsilon_t/\sigma = J_0 + \int_{-\infty}^{\infty} L\ (1 - e^{-t/\tau})\ d\ (\ln \tau) \tag{4.8}$$

In reality, of course, the same material can display both creep and stress relaxation, and thus it is necessary to combine the essential features of the Maxwell and Voigt models. This can be done in a number of ways, but one of the most convenient is that illustrated in Fig. 4.10(c). This also provides a convenient model for describing the effect of temperature on the viscoelastic properties of polymers if it is assumed that the viscosity of the fluid in the dashpots varies with temperature. It has a low value at high temperature, so that the deformation is predominantly determined by dashpot $D1$ and the material is in the viscofluid state. At low temperatures, the fluid freezes, the deformation is characterized by the elasticity of spring $S1$, and the material is in its glassy state. At intermediate temperatures, both springs and dashpots are operative and the material is viscoelastic.

A more serious objection to the use of such models to describe the deformation, and especially the creep, of real polymers is that the linear viscoelastic behavior represented by the models is only found in practice for strains of up to a few per cent, while at higher strain, deformation is nonlinear. As yet, there are no simple analyses which describe nonlinear viscoelasticity and thus it has been necessary to resort to empirical expressions such as

$$\varepsilon = A \sinh B\sigma + Ct^n \sinh D\sigma \tag{4.9}$$

which has been found[37] to give a reasonable fit for data on polyethylene and polyvinylchloride, while the simpler expression

$$\varepsilon = K\sigma^n t^m \tag{4.10}$$

is followed by polypropylene and polyoxymethylene over certain ranges of time and stress.[38]

Creep is a much more serious design problem in thermoplastic polymers than it is in metals at room temperature. As might be expected, it is most serious in polymers that are above their glass transition and in general it is more pronounced in amorphous polymers than in those in the crystalline state, although slow crystallization can occur in a quenched material and cause shrinkage effects. Of particular relevance to cryogenic applications is the creep, or cold-flow, of PTFE. Although its glass transition temperature is at 399°K, we saw in section 4.1.1.3 that, due to its peculiar chain structure and consequent low intermolecular forces, its mechanical properties do not change much on cooling through the glass transition. Thus, the same molecular characteristics which enable it to remain flexible and resilient down to very low temperatures also make it excessively compliant and prone to creep. For practical applications such as seals and gaskets, it is therefore usually mixed with a filler, such as a powder, metallic particles, or glass fiber, in order to increase its stiffness and reduce cold-flow. This topic will be reconsidered further in section 4.1.2.2.

4.1.1.5. ***Dynamic Effects.*** So far, we have only considered the viscoelastic properties of polymers under static or slowly increasing stresses, but it is also possible to derive much information about their properties by conducting dynamic experiments in which the material is subjected to a sinusoidally varying stress. As the strains developed during most dynamic experiments are small, the technique has the added advantage of being compatible with the theories of linear viscoelastic deformation and it is thus possible to use the results derived in the previous section for the basic Maxwell and Voigt models. As noted earlier, viscoelastic behavior is most pronounced in a transition region and this is illustrated in Fig. 4.11 by the occurrence of the maximum in the damping curve in the middle of the glass transition. At low temperatures, when the material is in its glassy state, the applied stress and resultant strain are in phase and there is little or no loss of energy from the system. At high temperatures, where the material is in the rubbery state, the modulus is low, strains are high but fully recoverable, and again there is little energy lost. In the transition region, however, the stress and strain get out of phase and the energy of the out-of-phase component is dissipated as heat. By taking mechanical energy out of the system and turning it into heat, the material is able to damp vibrations very efficiently and polymeric components are often deliberately designed into a vibrating structure in order to dissipate its energy in the form of heat. Given a situation where a sinusoidal stress of amplitude σ_0 and frequency $\omega/2\pi$,

$$\sigma = \sigma_0 \sin \omega t \tag{4.11}$$

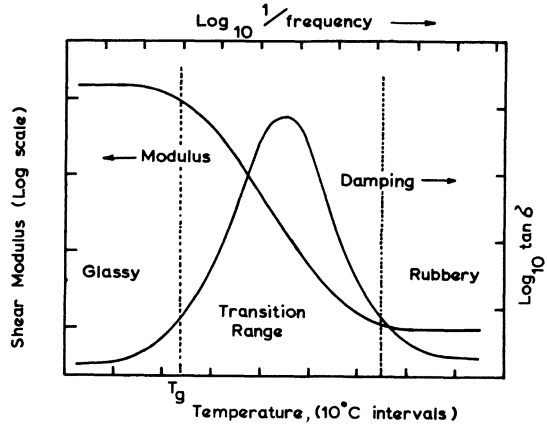

Fig. 4.11. Change in modulus and damping coefficient as an amorphous polymer undergoes its glass–rubber transition. Both temperature and time are shown as abcissas, as the transition can be induced by changing either variable.

produces a strain which is out of phase with the stress by an angle δ,

$$\varepsilon = \varepsilon_0 \sin(\omega t - \delta) \tag{4.12}$$

it is possible to define two separate moduli (which will be shear moduli if it is a torsional applied stress) such that

$$G_1 = (\sigma_0/\varepsilon_0) \cos \delta \tag{4.13}$$

is the *storage modulus*, which represents the component of the strain which is in phase with the applied stress and is proportional to the stored energy, while

$$G_2 = (\sigma_0 \sin \delta)/\varepsilon_0 \tag{4.14}$$

is the *loss modulus*, which represents the out-of-phase strain component and is thus proportional to the energy dissipated as heat in each cycle. Damping is also frequently measured in terms of the tangent of the phase angle δ and this may be obtained conveniently by measuring the logarithmic decrement of the amplitude of successive cycles of a freely oscillating specimen. Then, from equations (4.13) and (4.14),

$$G_2/G_1 = \tan \delta \tag{4.15}$$

while the total modulus is written in the complex form

$$G = G_1 + iG_2 \tag{4.16}$$

Now, if there is only one dissipative mechanism occurring and this has a characteristic relaxation time τ, the maximum energy loss per cycle will occur at resonance when

$$\omega\tau = 1 \tag{4.17}$$

In order to correlate this analysis with the type of result shown in Fig. 4.11 for a typical polymer, it is necessary to refer to the physical basis of the glass transition and rubbery deformation which was outlined in section 4.1.1.1. Rubbery deformation occurs when individual chain segments are mobile enough to be displaced by the action of an applied force. Furthermore, at a given temperature, the segments have a characteristic relaxation time τ, and if the rate at which the stress is applied is much greater than τ, the material appears to be rigid; if it is much lower than τ, it is rubbery; while the strongest viscoelastic effects are produced when the duration of the stress exactly matches the relaxation rate of the chain segments. As noted earlier, a real material has a spectrum of relaxation times and thus the resonant damping peak tends to be spread out over a range of frequencies. Experimentally, it is possible to vary the frequency of the applied stress from about 10^{-5} Hz for torsional pendulum techniques to $\sim 10^{10}$ Hz in electronic resonance experiments, and thus a wide range of possible relaxation times can be investigated.

It is also possible to obtain the same information by keeping the frequency of the applied stress constant and varying the vibrational frequency of the chain segments by changing their temperature. Thus, as noted earlier, the rate and temperature at which a polymer is deformed are interrelated, and this is usually expressed mathematically by an equation of the form

$$\tau = \tau_0 e^{H/RT} \tag{4.18}$$

or

$$\omega = \omega_0 e^{-H/RT} \tag{4.19}$$

where H is the activation energy of the mechanism concerned. Furthermore, by carrying out experiments at two frequencies ω_1 and ω_2 which produce damping peaks at temperatures T_1 and T_2, respectively, the activation energy H can be calculated from the relationship

$$\ln(\omega_2/\omega_1) = (H/R)[(1/T_1) - (1/T_2)] \tag{4.20}$$

Values so obtained can be compared with theoretical predictions to help identify the molecular mechanisms responsible for the damping.

Justification for the statement that changes in frequency can be related to shifts in temperature by equations such as (4.18) and (4.19) is provided by the fact that all the individual relaxation and retardation times τ_n of the summations in equations (4.4) and (4.7) are reduced proportionately when the temperature is raised. Similarly, all their characteristic frequencies ω_n will be increased by the same amount, and thus a single appropriate increase in the vibrational frequency is all that is required to compensate for the original increase in temperature. This is one way of stating the

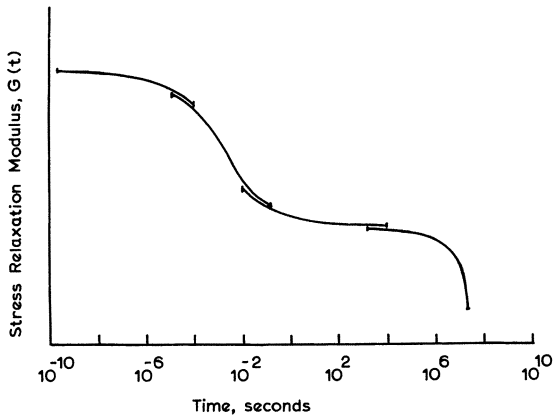

Fig. 4.12. Schematic master curve for stress relaxation (after Tobolsky[12]).

temperature superposition principle, which is a specific form of the more general Boltzmann superposition principle. It enables the curve obtained at one temperature for, say, the stress relaxation of a polymer to be superimposed on the curve obtained at a different temperature by a suitable shift along the log t axis. By such translations, Tobolsky[12] has prepared "master curves" for a number of viscoelastic, mechanical, and physical properties, that for stress relaxation being illustrated schematically in Fig. 4.12.

Williams *et al.*[39] have shown that one universal shift function (the WLF function) may be applied to a large number of organic and inorganic polymers if the deformation temperatures are related to their glass transitions by the formula

$$T = T_g - (51.6 \log_{10} a_T)/(17.44 + \log_{10} a_T) \tag{4.21}$$

or

$$\log_{10} a_T = -17.44(T - T_g)/(51.6 + T - T_g) \tag{4.22}$$

where a_T is the fractional reduction in the appropriate relaxation time caused by heating the material from its glass transition temperature to the temperature T. The glass transition temperature used as a reference is the static transition obtained by measuring the change in expansion coefficient during slow warming, and equation (4.21) can be used to correlate the static glass transition temperature with the values obtained from other methods which involve shorter deformation times. Table VI, due to Gorden,[7] makes such a comparison for the glass transition of high-molecular-weight polymethylmethacrylate as determined by its thermal expansion, a loaded needle penetrometer, and the ball-rebound technique.

Table VI

Method	Estimated time of deformation, sec	Experimental value of transition temperature, °C	Transition temperature calculated from equation 4.21, °C
Thermal expansion	10^4	110	—
Needle penetrometer	10^2	120	117
Ball-rebound	10^{-4}	160	154

The table not only shows the agreement obtained by the use of the WLF shift function, but it also provides a good illustration of the magnitude of the shift in T_g caused by a change in deformation rate of eight orders of magnitude. It should also be noted that the needle penetrometer test is a variant of the thermomechanical test described in section 4.1.1.2 and the observation that it gives a higher transition temperature than that determined by the change in expansion coefficient is also in keeping with our earlier remarks on the strain-rate dependence of transition temperatures.

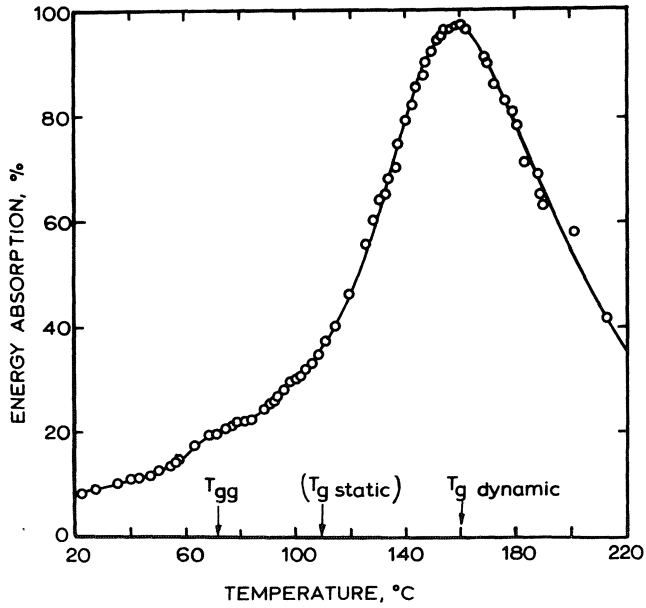

Fig. 4.13. Energy absorbed by an impacting ball as a function of temperature over the glass transition range. Also shown is the static value of the glass transition (Gorden and Grieveson[42]).

As a further point, it is perhaps worth considering the ball-rebound technique in a little detail because it provides a simple and convenient method of measuring the transition behavior of polymers. In essence, the test[40,41] measures the change in energy of a steel ball when dropped under standard conditions onto a clamped disk of the polymer concerned. By varying the testing temperature, a curve is obtained like that shown in Fig. 4.13[42] for the polymethylmethacrylate (PMMA) specimen whose results were included in Table VI. The percentage of the kinetic energy absorbed is given by $E = 100$(drop height minus rebound height)/(drop height), and this is the quantity shown in Fig. 4.13. It can be seen that E reaches a maximum at 160°C and this corresponds to the dynamic value of the glass transition temperature. Furthermore, it should be noticed that the small shoulder which can be seen at ~70°C is evidence for a "secondary" glass transition T_{gg}, which takes place at a temperature lower than that of the main transition. For PMMA, the transition is thought to be due to mobilization of the CO_2-methyl side chains, while in other polymers, mechanisms such as the rotation of chain segments have been invoked to explain the existence of these low-temperature secondary glass–glass transitions. Materials which have strong secondary glass transitions are usually tougher than those without them, and a number of workers have investi-

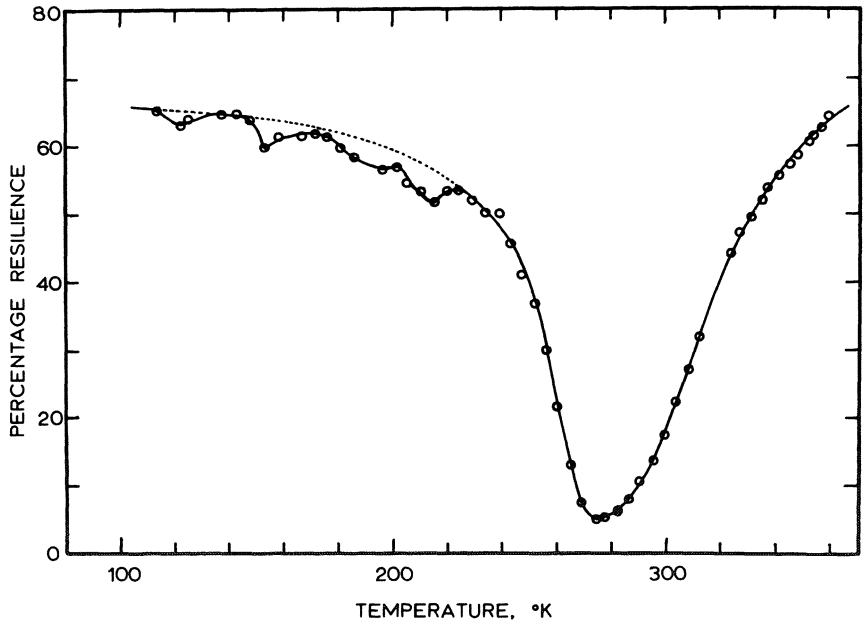

Fig. 4.14. Rebound resilience profile for a polyurethane adhesive (after Robbins[43]).

gated these transitions both for their own sake and also to aid the development of tough elastomers and adhesives for use at low temperatures. For example, Robbins[43] has used an automated ball-rebound tester to investigate the transitions in a polyurethane adhesive, and his results are shown in Fig. 4.14. In this case, the parameter measured is the "percentage resilience" defined as $R = 100$(rebound height/drop height). Thus, damping maxima show up as resilience minima and the principal resilience minimum at 270°K corresponds to the dynamic glass transition temperature, while correlation with the static glass transition determined as 235°K by dilatometric techniques was achieved by use of a suitable shift function. The secondary minimum at ~180°K was ascribed to main-chain rotation, and the low resilience and high damping produced by this secondary transition were held to be responsible for the adhesive's toughness at low temperatures.

Finally, it is worth noting that PTFE has two glass–glass transitions, $T_{gg}(3)$ at 170°K, which is thought to be due to the short-range motion of a few adjacent -CF_2- groups, and $T_{gg}(2)$ at 235°K; a normal glass transition at 393°K; and two first-order phase transformations, the first at 295°K, which is described both as an order–disorder change in its crystal structure and as the premelting and rotation of its molecular chains, and the second at 600°K, when the crystallites finally melt. A truly remarkable material!

4.1.1.6 ***Thermosetting Plastics.*** As noted in the introduction to section 4.1, the essential difference between thermoplastics and thermosets lies in their respective molecular structures. Thermoplastics are typically linear macromolecules which are held together by weaker secondary bonds, whereas thermosetting plastics consist of smaller molecules which are crosslinked together by primary bonds to form a three-dimensional molecular network. This structure produces a rigid and strong, but inherently brittle, material and once the crosslinks have been completely formed, the structure is little affected by further changes in temperature until the degradation point is reached.

It should be emphasized that thermoplastics and thermosets are distinguishable by their structure and properties rather than by their basic chemical groupings. Thus, polyesters (a generic classification for polymers produced by the condensation reaction of an acid and an alcohol) can be either thermoplastic or thermosetting. For example, ethylene glycol and terephthalic acid are both saturated and bifunctional and their resultant condensation polymer polyethyleneterephthalate (or PET) is linear and thermoplastic. In contrast, if a polyfunctional acid or alcohol is used, a thermosetting network polymer is produced. Similarly, polyurethanes, silicones, polycarbonates, and members of a number of other basic polymer families can be prepared as either thermoplastics or thermosets.

Thermosetting plastics are often grouped for convenience into three

different categories according to their typical usage: molding compounds, liquid casting resins, and reinforced plastic laminates. The molding compounds are usually supplied in a partly polymerized condition and in a convenient form for molding, such as in pellets or granules. Final polymerization and crosslinking then take place during a subsequent high-temperature molding process. The liquid casting resins are widely used for "potting" small parts, such as electronic circuits and switches, in order to keep them rigid and prevent their failure under high *g* forces. Some resins are supplied as a single component which has a reasonable shelf life at low temperatures, but which cures at high temperatures; but it is more usual for two or more components to be mixed together, with a catalyst or accelerator if needed, just before use. Epoxy resins are frequently used for potting because no reaction by-product is formed during their polymerization and hence no bubbles are produced. In contrast, the gas formed during the polymerization of polyurethane is often harnessed to blow the type of foams to be considered in section 4.1.2.5. Laminates we shall consider shortly.

As noted earlier, typical thermosets have high moduli and strengths which show little change over a wide range of temperatures. Similarly, their mechanical properties are not noticeably time- or strain-rate-dependent and they do not creep excessively under load. One relatively minor process which can lead to dimensional changes over long periods of time is the formation of further crosslinks due to oxidation or ultraviolet radiation, but the shrinkage so produced is not normally a serious problem. Their major drawback is their brittleness and in particular their low impact strength. Because of their strongly bonded structure, they are effectively organic glasses, as are thermoplastics at temperatures below their glass transition. Furthermore, due partly to their very low thermal conductivities, thermosetting plastics have a poor resistance to thermal shock and they are liable to craze if cooled rapidly, especially to cryogenic temperatures. These factors impose severe limitations on the use of unmodified thermosetting plastics, and for practical purposes, they are almost invariably used in conjunction with some type of filler.

There are a wide variety of fillers used in both thermosets and thermoplastics. At one extreme, cheap fillers such as wood flour or clay are used simply to replace the more expensive polymer and still produce a material with properties adequate for its intended use, while other fillers are employed to give the requisite color. Metallic powders are added to improve the electrical and thermal conductivities, minerals such as mica and asbestos improve the heat resistance, and paper, chopped fabric, cotton, and other natural and synthetic fibers are added to increase the toughness and shock resistance. Graphite flakes improve the frictional properties of the material to make it suitable for bearing components, while carbon black is added

to natural and synthetic rubbers to increase their stiffness. In most cases, the filler particles do not bond chemically to the resin, but in some cases, such as carbon black in rubber, chemical crosslinks are formed between them. In general, hard filler particles raise both the strength and modulus in proportion to their volume fraction but do little to improve the toughness. Fibrous fillers such as chopped glass can improve both the strength and toughness of the plastic, especially if they have a high elastic modulus. Fiber reinforcement will be discussed at some length in section 4.3.

From a low-temperature point of view, many of these fillers have a further important action in that they reduce the large expansion coefficient of the polymer to a value compatible with that of metals. This is of vital importance in applications, such as adhesives, where differential thermal contraction between unmatched components can produce fatally high stresses in the joints between them. Indeed, for maximum efficiency, the volume fractions of filler and resin should be adjusted to match the expansion coefficient of the metal concerned, and thus a range of resin/filler combinations should ideally be available to suit the many metals and alloys in common usage.

Small rubber particles are also used as fillers in both thermoplastics and thermosets and they bring about quite dramatic increases in their toughness: 50% rubber particles in polystyrene can raise its impact strength by a factor of between 5 and 10.[44] This is achieved at the cost of lowering the stiffness and strength, but on balance, the use of such fillers produces a more versatile material. It is believed that the increase in toughness is due to the ability of the rubber particles to absorb energy from rapidly moving cracks and so make their propagation more difficult. The technique, however, does not work for very low temperatures because the rubber is then below its glass transition and has therefore lost its elastomeric properties.

Finally, the third basic type of thermosetting plastic, the reinforced laminate, includes materials such as Tufnol which is commonly used for the fabrication of small parts for cryogenic equipment. Laminations of paper, cloth, asbestos, synthetic fiber, or glass are impregnated with uncured resin dissolved in a suitable solvent prior to consolidation and polymerization under pressure at the curing temperature. The resultant material is hard and rigid, but it can be machined by conventional techniques to produce the required components from the bar, rod, tube, or sheet form in which it is available.

4.1.1.7. ***Failure in Polymers.*** Within the scope of our treatment of the mechanical properties of polymers, it is not possible to give anything like the same coverage to their failure mechanisms as that given in chapter 3 for metals. There are many similarities between the failure modes of these two classes of materials, for example they undergo a ductile–brittle

transition and can fail by creep, fatigue, and stress corrosion. However, as might be expected from their fundamentally different structures, there are also significant distinctions between the detailed mechanisms involved and their relative importance in both types of material.

Referring to the stress–strain curves illustrated in Figs. 4.4 and 4.8 for amorphous and crystalline polymers, respectively, it can be seen that in both cases there is a transition from a viscous, ductile rupture type of failure at high temperatures to a completely brittle mode at very low temperatures. As noted earlier, the temperature ranges over which the material can be cold-drawn are basically below T_g for the amorphous state and above T_g for the crystalline state, but in both cases there is a transition region over which the failure strain decreases rapidly and the material goes through a ductile–brittle transition. Now, when considering similar transitions in ferrous alloys (section 3.3), we saw that the transition occurred at a higher temperature for impact loading than for lower strain rates, and, as might have been expected from the emphasis we have given to the extreme strain-rate sensitivity of their properties, a similar effect is found in polymers. At temperatures within the transition range, they can be ductile at low strain rates and brittle at high rates. Furthermore, most plastics are also notch-sensitive at these temperatures, and the stress concentrations introduced by the pressure of cracks, flaws, and notches lead to a further reduction in their impact strengths. Although notched and unnotched Charpy or Izod type specimens are used for such tests, they do not always give a good correlation with the behavior of components which have been rolled, drawn, cast, or moulded, i.e., processes which can produce a high degree of preferred orientation. Drop weight tests [18,19] are thus normally preferred, as they offer a more realistic simulation of the probable failure modes. In particular, flexural impact tests on sheet materials loaded in three-point bend, or by a point load at the center of a circularly supported sheet, are to be preferred for the evaluation of thin-gauge materials. Figure 4.15 shows the results[45] of such tests carried out over a range of temperatures for an unplasticized PVC of sheet thickness 0.060 in. It is found that the temperature range over which the toughness falls off rapidly coincides with that at which the tensile strength increases significantly, as long as the tensile tests are carried out at a strain rate comparable to that imposed during the falling-weight impact test.

A correlation between increased strength and decreased toughness similar to that brought about by a decrease in testing temperature is also found to hold for a number of other treatments which affect the strength of polymers. Thus, the yield strength of polyethylene at room temperature can be decreased by copolymerization, plasticization, and a reduction in the degree of crystallinity, and all of these processes also give an increase in toughness. In contrast, crosslinking increases the yield stress and lowers

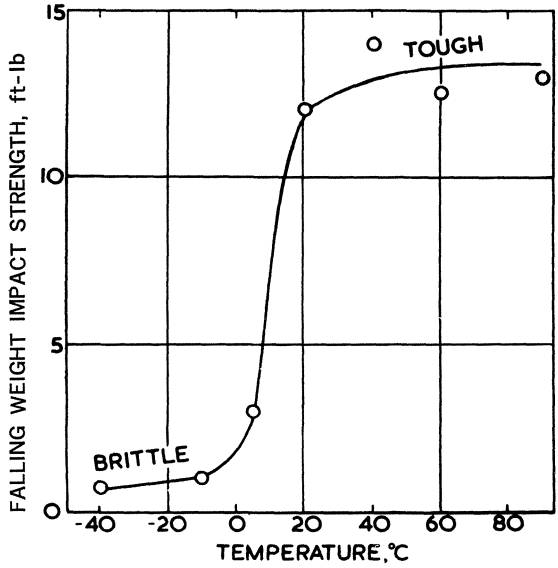

Fig. 4.15. Temperature dependence of the falling weight impact strength of unplasticized polyvinylchloride (after Horsley[45]).

the toughness. This rule is not, however, invariable, as the addition of many types of rigid nonfibrous fillers can reduce both yield stress and toughness, while fibrous fillers can improve both properties simultaneously.

When considering secondary glass transitions, we noted that polymers with pronounced transitions were tougher than those without them, and this is probably due to the side groups which are mobile at these temperatures, absorbing energy from the moving cracks and thus making their propagation more difficult. At low temperatures, the material is in the glassy state and there has been a considerable amount of work carried out to see whether the Griffith equation (3.7), which was developed from a study of the failure of inorganic glass, is also valid for organic glasses. Experiments on polymethylmethacrylate have shown[46] that the values of surface energy γ so obtained were about 100 times larger than those predicted on the basis of the primary covalent bonds. It has therefore been suggested that the effective surface energy γ is the sum of the true surface energy γ_S and a term γ_V which is a measure of the work expended in overcoming viscous flow in the region ahead of the crack tip,

$$\gamma = \gamma_S + \gamma_V \tag{4.23}$$

where $\gamma_V \simeq 10^2\gamma_S$. Thus, glassy plastics behave, in some respects, more like metals (where $\gamma_p \simeq 10^3\gamma_s$) than inorganic glasses. Confirmatory evi-

dence for the occurrence of viscous flow during failure is found in the presence of oriented regions adjacent to the fracture surfaces (in specimens broken at very low temperatures, the surfaces appear clear, but the oriented regions can be seen in polarized light; after fracture at higher temperatures, the surface sometimes appears to have a whitish color). Furthermore, fractures are found[47] to originate not only at the surface as in inorganic glass, but also at internal defects such as bubbles, voids, and impurties and in this respect they behave more like metals. In contrast, however, whereas the toughness of metals increases with temperature, the reverse is true for PMMA, which becomes tougher as the temperature falls; a fracture toughness analysis of the failure of these materials has been given recently by Vincent.[49]

So far, we have only considered the short-term aspects of failure in polymers but, as with metals, they can also fail a long time after the initial application of a static or cyclic stress. Indeed, failure due to such environmental effects has been cited as the most serious barrier which currently prevents the more widespread use of polymeric materials in structural applications. Environmental stress cracking is a term which is used to cover both the general area of delayed failure under normal operating conditions and also the particular phenomenon of stress cracking in continually loaded polymers, such as polyethylene, which takes place in the presence of certain wetting agents, soaps, and alcohols. These substances do not dissolve the polymer or attack it chemically, but nevertheless they cause it to fail under combinations of stress and time that would not lead to failure in their absence. Other chemicals can produce solvent cracking in which there is definite evidence of chemical attack, while exposure to ultraviolet light is liable to cause degradation and failure by causing the polymer chains to break down by a mechanism which starts at their ends and progresses inward. Irradiation by energetic charged particles can also cause chain breakdown, but this process can be beneficial in that it allows branching and crosslinking to occur. The phenomenon of "static" fatigue, first found in inorganic glass, is also encountered in polymers both above and below their glass transition, while thermal stress-cracking can occur if the material is subjected to a cyclic change in temperature.

Finally, polymers and elastomers can also fail by fatigue when subjected to cyclic applied stresses. It appears that there is a better correlation between their fatigue lives and the strain amplitude than there is with the stress amplitudes, this being particularly true for rubbers.[50] Some polymers seem to have a fatigue limit,[51] but the mechanism involved is not yet fully understood, while results are often complicated by the large amounts of heat generated during fatigue tests as a result of their characteristically high damping coefficients and low thermal conductivities.

4.1.2. Polymeric Materials of Particular Interest for Cryogenic Applications

Having reviewed the main factors which determine the structure and properties of polymers, we are now in a position to consider in more detail the characteristics of the relatively few materials which are used in cryogenic applications. Most of the information now available on the properties of polymeric materials at low temperatures has been generated in response to the demands of the aerospace and missile programs and in consequence it is somewhat selective, being particularly biased toward those materials which can offer the high strength/weight ratio required in these applications and also toward the development of materials which are compatible with liquid oxygen. Although the moduli and strengths of polymers increase at low temperatures, the accompanying loss of ductility and impact strength prevents the use of unmodified thermoplastics and thermosets in all but the most limited of applications. Their high thermal contraction coefficients and poor resistance to thermal shock further restrict their use, and careful design is necessary if components made from these materials are to perform satisfactorily.

One of the most pressing requirements of the space program has been the development of gaskets and seals suitable for making joints which remain leak-tight even after a large number of cycles between low and ambient temperatures, or which can act as seats for the fast-acting valves controlling the flow of liquid cryogenic propellants. As almost all hydrocarbons are more or less incompatible with liquid oxygen, the more inert silicones have been used as seals in applications where the applied stresses are static. As these materials are below their glass transition at liquid-oxygen temperatures, they cannot, however, be used where dynamic stresses are present and it has been necessary to employ fluorocarbon polymers for such applications. Polytetrafluoroethylene (TFE) and fluorinated ethylene–propylene copolymer (FEP) are normally employed for this purpose, and the use of polychlorotrifluoroethylene (Kel-F) is also quite widespread.

Probably the greatest challenge offered to polymer technologists by the needs of the space program has been the development of the structural adhesives used to bond large structural components together. For example, the common bulkhead of the Saturn IVB launch vehicle is held in place by an epoxy-phenolic adhesive which contains a glass cloth carrier, and this system is able to support the large stresses imposed during cooldown and flight. The positive expulsion bladders used to expel the fuel from these tanks are also polymers—thin films of polyethylene terephthalate—and these films are able to withstand without failure the large number of folding and unfolding cycles which occur during testing and subsequent

use. Similar films are also used for electrical insulation and for the multilayer superinsulation which minimizes heat leaks into liquid-helium storage vessels, while in less critical applications, rigid or flexible polymer foams are employed for insulation purposes. Composites made from PTFE filled with glass fibers or metal powders are able to provide bearing materials which can be used in direct contact with liquid oxygen, while the use of glass-fiber-reinforced plastics as strong, lightweight structural members is so important a topic that this and other aspects of fiber reinforcement will be considered separately in section 4.3.

The available data on the mechanical properties of polymeric materials at low temperatures are to be found in a large number of papers, conference proceedings, and reports, especially those originating from NASA, various defense agencies, and government research stations, such as the NBS–Boulder.[52,53] The Plastec report[23] on the properties of plastics and related materials at cryogenic temperatures, which appeared in 1965, gives an excellent summary of the work carried out up to that date and an almost identical version of the same report has been published in Volume 4 of the *Encyclopedia of Polymer Science and Technology*.[1] Although the latter version is probably the most accessible, the original report is to be preferred, if it can still be obtained, because of its comprehensive annotated bibliography. Further information can be obtained from the book by Serafini and Koenig[24] on the cryogenic properties of polymers, which is the proceedings of a conference held in 1967 and is thus slightly more recent.

In this section, we have attempted to summarize some of the most important aspects of the properties of molding plastics, elastomers, adhesives, films and fibers, foams, and bearing materials. It has not, however, been possible to include much actual data and the reader is referred to the reviews already cited or to the original papers for such information.

4.1.2.1. ***Molded Plastic Components.*** In contrast to their widespread use at ambient temperatures, unfilled thermoplastic moldings are very rarely employed for cryogenic applications and it is possible to identify at least three main reasons for their lack of favor: they have poor thermal shock resistance, very high thermal contractions, and low notch-toughness and impact strengths.

Many polymeric materials are liable to craze or shatter if cooled rapidly to low temperatures. Their characteristically low thermal conductivities make it possible for large temperature gradients to be set up, and the stresses produced by the resultant differential contraction can often cause failure. The effect is most serious for thick sections and it is also a problem in materials reinforced with glass fibers and other types of filler, although the greater toughness of such materials may prevent actual fracture, damage often being limited to local crazing or chipping. The use of fillers to reduce

the thermal contraction of plastics to values compatible with those of metals has already been mentioned, but even with filled materials, careful design is necessary to minimize the effect of any residual differential contraction. We have also seen that fibrous fillers normally increase the toughness of polymers, and nylon reinforced with chopped glass fiber can be used at, and below, room temperature in applications where strength and toughness are required. Similarly, PTFE filled with bronze, asbestos, graphite, or glass fiber can be used for bearings (section 4.12.6), while seals made from glass-fiber-reinforced PTFE can be used at temperatures where no elastomeric materials are available (section 4.1.2.2).

The only unfilled thermoplastics used in significant quantities for molding components for low-temperature applications are nylon, PTFE (TFE and FEP), and Kel-F. The effect of temperature on the moduli, yield strengths, elongation, and impact strengths of these materials is shown in Figs. 4.16; the properties of PET (Mylar) are also included for comparison. It can be seen that the moduli of all four materials increase strongly as the temperature is lowered, the change being most noticeable in the case of PTFE, which has a very low modulus at room temperature. The yield strengths shown in Fig. 4.16(b) give a good indication of the trends followed by these materials, but the actual strengths can differ considerably from the values shown because of the large variation in their properties caused by changes in the average molecular weight, percentage crystallinity, and, in the case of nylon, the water content. For example, an increase in water content from 0.2 to 2.5% produces about a fourfold rise in the tensile elongation of nylon at room temperature (Fig. 4.16c) due to the plasticizing action of the water, but at lower temperature, it has an embrittling effect.

The work of Mowers[54] has shown that the percentage crystallinity has a strong influence on the properties of TFE, FEP, and Kel-F at low temperatures. A range of values is shown in Fig. 4.16(b) for the strength of TFE and Kel-F, and in both cases, it is the amorphous material which is the strongest at low temperatures. It should be noted that this is a reversal of the behavior found at higher temperatures, where the higher-crystallinity material is stronger, and it would thus appear that the strength of the crystalline regions of the polymer is less affected by a decrease in temperature than is the strength of the amorphous regions. Both flexural and torsional strengths were higher in the more amorphous specimens at low temperatures, but for compressive strength, the picture is more complicated, with highly crystalline TFE being strongest, FEP remaining unaffected, and Kel-F showing a decrease in strength between 60% and 70% crystallinity.

The differences between TFE and FEP also emerge clearly from these studies, FEP having higher tensile and impact strengths as well as a greater

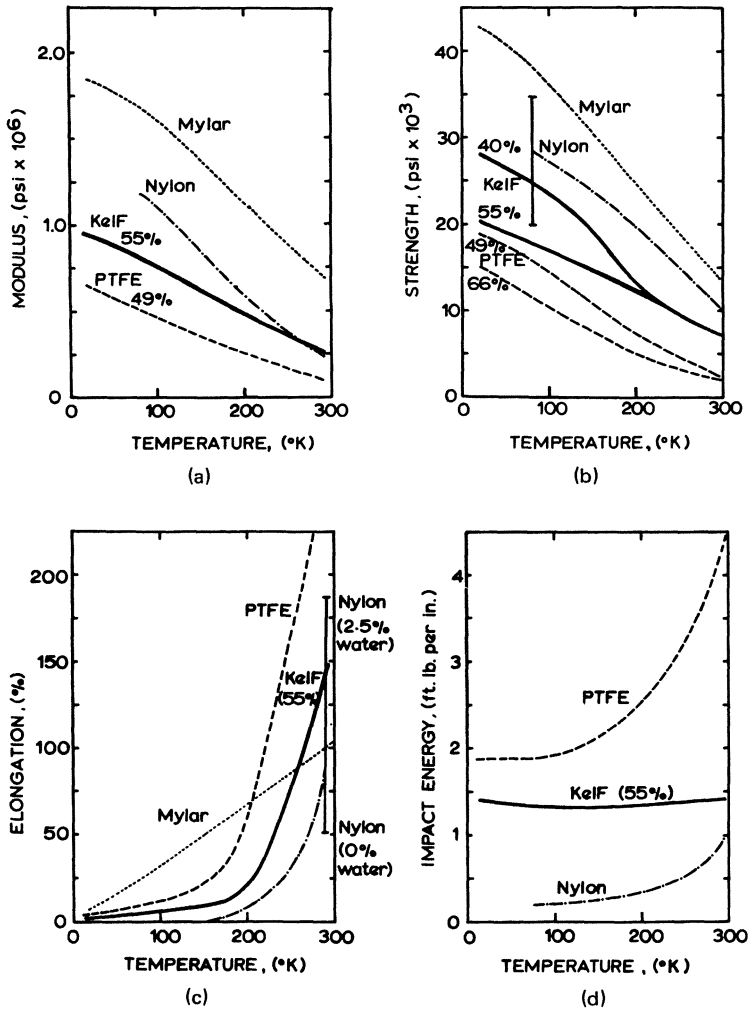

Fig. 4.16. Temperature dependence of (a) modulus, (b) yield strength, (c) elongation, and (d) impact strength of nylon, Mylar, PTFE and Kel-F (data from Ref. 55).

elongation, whereas TFE has a higher compressive strength and a considerably lower total contraction than FEP. The effect of various types of filler in TFE and FEP were also studied and it was found that, although the fillers increased the strength and wear resistance, and reduced the thermal expansion and the tendency to cold-flow, these advantages were bought at the cost of reduced elongations and impact strengths.

4.1.2.2. ***Elastomers, Seals, Gaskets, and Sealants.*** As we saw in section 4.1.1, elastomers are basically lightly crosslinked amorphous polymers which are capable of large reversible elastic strains when stressed at temperatures above the glass transition. In fact, their lowest working temperatures are about 10°K above T_g and, as no polymer has a transition temperature below ~140°K, there are no materials which have true elastomeric properties at cryogenic temperatures. As can be seen from Table V, polyisobutylene (butyl rubber) with a transition temperature of 205°K has the lowest working temperature of the hydrocarbon elastomers, while the butadiene–styrene copolymers (Buna S, BRS, SBR) have T_g values in the range 215–235°K and those of the butadiene–acrylonitrile copolymers (Buna N, Nitrile, NBR) are similar. There are also copolymers based on cis-polyisoprene (natural rubber) and polychloroprene (neoprene), but all such hydrocarbon elastomers suffer from the disadvantage of being incompatible with liquid oxygen, and even the more chemically stable polysulfides, silicones, and fluorosilicones are not completely safe for use with LOX systems. Of the polysulfides, or nitroso rubbers, Thiokol A (polyethylenetetrasulfide) is brittle below ~270°K, while the more chemically complex Thiokol ST can be used down to ~220°K. Ordinary silicone rubber, polydimethylsiloxane, has a low T_g of ~150°K and is one of the most suitable elastomers for cryogenic use. A methyl silicone + 30% vinyl copolymer has been reported[43] as having a slightly lower T_g of 146°K, but despite intensive effort,[57] no elastomers have yet been found with lower transition temperatures. The recently developed[58] poly (thiocarbonylfluoride) does, however, have a T_g of ~155°K but, although its properties appear promising, it is not yet commercially available. A number of fluorinated elastomers, in particular Viton and Fluorel (vinylidene fluoride–hexafluoropropylene copolymers) are in widespread use at somewhat higher temperatures, T_g for Viton being 218°K, and these materials have the additional advantage of being extremely fire-resistant.

Nevertheless, it is the fluorocarbon family of polymers which is most widely used for seals at low temperatures, as they are the most LOX-compatible. Although they are not elastomers, they are able to undergo enough plastic deformation to form a satisfactory seal, and TFE, FPE, and Kel-F have been used successfully in continuous operations at liquid-hydrogen temperatures and below. These materials do, however, suffer from a tendency to cold-flow under continuous load and, unless the load can be increased to compensate for this relaxation, the seal is liable to leak. To overcome this problem, PTFE/glass-fiber composites have been developed[59,60] and it is claimed that their use significantly reduces cold-flow. Seals have been made from both TFE and FEP, but the former is usually preferred.

Most seals are prepared in the form of O-rings, as it is necessary to employ a suitably designed fitting if they are to operate successfully. There

are basically two methods used for compression, confined and unconfined, and the various joint configurations, their characteristics, and the properties of the O-ring materials used in them have been reviewed[61] and discussed[62,63] in a number of papers by workers at the NBS. Further information is also available in the Design Handbook for O-rings and similar elastic seals.[64] In order to prevent the decrease in load which accompanies the contraction of elastomers below their glass transition, very large compressive strains are imposed on the O-rings so that they exert a force which will not be relaxed during contraction. As shown in Fig. 4.17, this entails compressing the material by about 80% of its cross-sectional diameter, and such seals cannot be reused, because of the compression set and material rupture produced by this treatment. The most satisfactory results are obtained with joint designs, such as that illustrated in Fig. 4.18(a),[63] which give confined compression. The O-ring in the groove is squeezed by the follower until the material completely fills the bottom of the groove and extends slightly into the clearance space between groove and follower as in Fig. 4.18(b). This type of joint also minimizes the effects of cold-flow and is thus particularly suitable for fluorocarbon seals. In unconfined compression (Fig. 4.18c), the O-ring is squeezed between two flat flanges and, as there is no restraint on its lateral expansion, these seals have a limited service life due to cold-flow. Other joint designs[64] use a combination of a

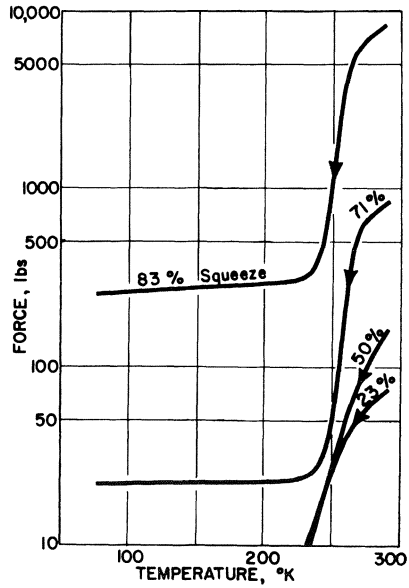

Fig. 4.17. Residual force as a function of temperature and degree of precompression (Weitzel *et al.*[63]).

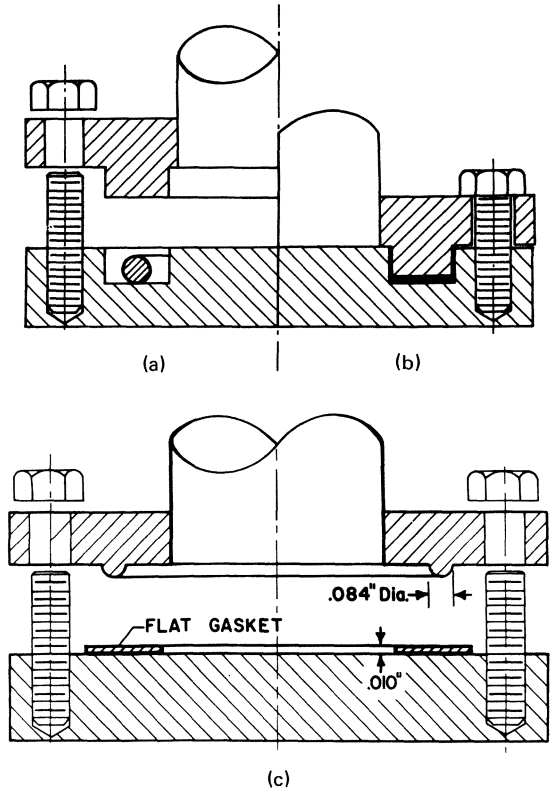

Fig. 4. 18. Joint designs for elastomeric seals. (a) Confined O-ring before compression and (b) after compression. (c) Unconfined gasket (Weitzel *et al.*[63]).

metal "C" section spring and a PTFE envelope which seals when compressed by about 10–20%, and which can be reused a number of times before cold-flow in the PTFE affects the reliability of the seal.

Other types of gasket used in cryogenic seals include those made from ductile metals such as indium, aluminum and silver, and 0.010-in.-thick films of Mylar or nylon, while the plexiglass (acrylic) window in a liquid-hydrogen bubble chamber has been successfully joined to the chamber body by the use of a complex double seal which involves the compression of both Mylar and aluminum gaskets.[65]

Finally, a number of organic sealants have been developed for use in cryogenic applications, and their properties are described in Refs. 1 and 23. As the problems associated with the use of such sealants are very similar to those encountered with adhesives, their properties will be discussed together with those of adhesives in the next section.

4.1.2.3. ***Adhesives and Coatings.*** The challenge provided by the construction of large, cryogenically fuelled rockets has encouraged not only the development of new and improved structural materials, but also the adoption of novel methods of construction and fabrication. In particular, it has led to the use of structural adhesives which can function at cryogenic temperatures without the serious problems of embrittlement and shrinkage found with most plastics. These adhesives are used to make metal–metal, metal–plastic, and plastic–plastic joints in a wide variety of applications; for example, their use allows brackets, clips, spacers, and other attachments to be bonded to the surfaces of fuel tanks without creating the stress-raisers formed by welding or other conventional techniques; tank sections can be assembled with scarf or lap joints, while corrosion-free joints between dissimilar metals can be obtained if their surfaces are kept apart by the nonconducting adhesive. Metal-to-plastic joints are made when the surfaces of metal fuel tanks are insulated with foamed plastic panels and when thin metallic liners are fixed inside glass-reinforced plastic fuel tanks to act as vapor barriers, while the thin Mylar films used to make positive expulsion fuel bladders have adhesive joints which must stand up to a large number of pressure and temperature cycles without failure (see section 4.1.2.4).

As noted earlier, adhesives can also act as sealants, and as such they are often used to provide sealed tanks and pressure-tight bulkheads in structures made from aluminum alloy. The room-temperature-vulcanizing silicones have been found[66] suitable for such applications at cryogenic temperatures and, although their strengths are much lower than those of the best structural adhesives, they are adequate for these applications, as the applied tensile and shear stresses are low. Similarly, paints and other coatings are required for the surface protection of components which are intermittently cooled to low temperatures and certain epoxy- or polyurethane-based paints have been found suitable for such applications.

Many of the problems associated with use of adhesive joints at cryogenic temperatures have been discussed by Hertz,[67] who also summarizes the results of the work carried out up to 1961. Extensive bibliographies of the earlier work are also given in Refs. 53 and 68. At room temperature, adhesives usually have much lower moduli than the adherends and the adhesive is normally able to deform sufficiently for any stress concentration to be relieved. At low temperature, however, their moduli are significantly higher, such deformation is not always possible, and crazing and cracking are likely to occur even if the bond does not fail completely. We have already noted that the expansion coefficients of polymers are much higher than those of most metals and differential contraction on cooling can cause large stresses to be built up in joints between these materials unless fillers are added to the polymeric adhesive to reduce its

expansion coefficient to match that of the metal. Shrinkage of the adhesive during curing can also produce large stress concentrations, and, where possible, room-temperature curing systems are to be preferred, while residual stresses left in the adherend when the bonding pressure is released can also lead to premature bond failure. Furthermore, most polymers have very low thermal conductivities and, unless the glue line is kept as thin as possible, large temperature gradients can be built up across a joint, thus intensifying the differential contraction problem and also encouraging failure due to thermal shock. The joint configuration and loading system can also have a strong influence on the strength at low temperature. For example, in butt joints, the main stresses induced by cooling are tensile and they are largely offset by the increase in tensile strength of the adhesive at low temperatures. In contrast, the shear stresses induced in the plane of the adhesive in a lap joint are too large to be accommodated by the increase in shear strength at low temperatures and, as a result, the joint strength decreases.

Thus, a successful adhesive system must try to minimize the adverse effects of these factors, it must also have as high a shear strength as possible, as this property represents the ultimate attainable strength of the entire bonding system, and it must be tough. In this context, toughness not only implies a high resistance to failure under impact loading, but also the ability to resist further failure in an already defective system. This is important in adhesives because a joint often contains voids, bubbles, and cracks and a tough adhesive should be able to redistribute the stress concentrations produced by these defects and even them out over a wider area. The most useful measure of toughness in adhesives is their peel strength, and various experimental tests, such as the T peel and the climbing drum peel, have been used to determine this property.

In order to meet such a specification, most structural adhesives used at cryogenic temperatures are multicomponent systems. For example, the epoxy–nylons are a mixture of a thermosetting resin and a thermoplastic, while the nitrile–phenolics contain both rubber and resin. Furthermore, they are frequently reinforced by a fabric called a "structure" or "carrier" which is normally a nonwoven, woven, or knitted structure of glass or polymer filaments. Roseland[69] has discussed the relative merits of various types of carrier and he concludes that the best results are obtained by the use of a single layer of glass mat made from unwoven single filaments; the use of multifilament threads was less efficient due to incomplete resin penetration of the multifilaments. The main action of the glass mat is to produce a uniform bond line, to even out the stresses, and to reduce the contraction of the adhesive relative to that of the substrate. For example, the differential contraction between a polyurethane adhesive and an aluminum adherend was reduced by about 50% by the inclusion of a single

layer of glass mat. A further advantage obtained by the use of this carrier was a large reduction in creep at ambient temperature, the modified adhesive showing no creep after 2000 hr in a lap shear test, whereas failure of the unmodified adhesive occurred after 600 hr in a similar test.

A large number of resin systems have been evaluated for use at cryogenic temperatures and these results are presented and discussed in papers by Hertz,[67] Kuno,[70] Kansen,[71] Smith and Susman,[72] and Roseland,[69] and are reviewed in Ref. 53 and 68. The results of a recent (1969) literature search are also available from the NBS.[73] The most widely studied systems are the epoxy–nylons, the modified epoxy–phenolics, the nitrile-modified phenolics, the epoxy–polyamides, the vinyl–phenolics, and polyurethanes. In many cases, the effects of various types of filler, carrier, fluorocarbon film, and surface treatment are also discussed. It is generally agreed that the hot curing epoxy–nylons give the highest peel and shear strengths over a wide range of temperatures, due largely to the flexibility imparted by the nylon, and these adhesives are probably the most widely used at low temperatures. Although the epoxy–phenolics have considerably lower strengths, their properties are very consistent at all temperatures below about 350°K and, because this consistency eases design problems, they were chosen for bonding the fiberglass honeycomb core to the aluminum skin that forms the common bulkhead of the liquid-hydrogen and liquid-oxygen tanks in Saturn IV. The rubber-containing phenolics have excellent peel strengths at and a little below room temperature, but their properties deteriorate rapidly at lower temperatures. The use of thin fluorocarbon films has been shown by Smith and Susman[72] to give high peel strengths, the FEP–epoxy–polyamide system being particularly attractive. Furthermore, an FEP hot melt adhesive was found to be LOX-compatible, a property shown by few other structural adhesives.

Apart from the epoxy–nylons, the other main structural adhesives are the polyurethanes, especially the more recently developed types. They are the only adhesives whose strengths increase at low temperatures and their main disadvantage lies in their rather weak room-temperature properties, in particular, they creep excessively (28 times more than the modified epoxies) unless supported by a suitable carrier. They also have the best resistance to thermal shock and can be LOX-compatible,[129] while a recently developed[74] adhesive intended for bonding thin aluminum foil to the inside of glass-fiber-reinforced plastic pressure vessels combines the advantages of both epoxy and polyurethane systems. These adducts combine the high strength and modulus of epoxy resin with the strain capability and peel resistance of the urethane to allow strains of over 2% to be developed without debonding.

It has also been reported[69] that significant improvements in adhesion may be obtained by the use of silane primers, which cause chemical bonds

to occur between adhesive and adherend, in addition to the usual intermolecular forces. The silanes are ambifunctional coupling agents, one end of which can be hydrolyzed to bond with a hydroxyl-containing substrate, while the other end reacts with the resin to form a molecular bridge between the resin and substrate. Approximately 50% improvement in joint strength was obtained when aluminum was silane-primed prior to jointing, the improvement being due to greater adhesive strength, not cohesive strength. Such treatment also produces a significant improvement in aging properties especially in mildly corrosive environments.

Finally, there are also a number of more specialized adhesive systems available or under development, for example, the polybenzimidazole resins may be used from cryogenic temperatures up to 325°K in continuous operation or up to 755°K for short periods. It has also been suggested[69] that the anaerobic adhesives, which remain liquid while air is present but cure spontaneously when it is excluded, may be suitable for carrying out repairs to spacecraft which are outside the earth's atmosphere.

4.1.2.4. ***Films and Fibers.*** As we shall see in the next section, foamed plastics can be used as a lightweight insulation for liquid-hydrogen or helium storage vessels because the gas trapped in the closed cells solidifies at these low temperatures to produce a high vacuum. If the high quality of this insulation is to be maintained, it is, however, necessary to prevent the permeation of hydrogen or helium gas into the foam. This may be accomplished by bonding a thin film on the liquid side of the foam, and the permeabilities and mechanical properties of a number of materials have been evaluated for use as vapor barriers. Bailey *et al.*[75] have measured the permeabilities of H film (polyimide), plain aluminized Mylar (PET), and thin PET/glass cloth/PET composites at a number of temperatures down to 20°K, while Caren *et al.*[76] have made similar measurements on H film, Mylar, Tedlar (polyvinylfluoride), polyethylene, FEP, and two types of Kel-F at somewhat higher temperatures. Both sets of experiments showed Mylar to have the best overall performance, especially when aluminized.

The mechanical properties of these films have been studied by a number of workers[54,76,77] and their results have confirmed the suitability of Mylar films for this type of application. In the as-received condition, Mylar is about 15% crystalline, with the crystallites preferentially oriented in the plane of the film and, as we saw in section 4.1.1.3, this accounts for the high strength of these thin films. Mowers[54] has increased the crystallinity of Mylar films to as much as 55% by a suitable heat treatment, but this did not result in improved mechanical properties. Results for H film and Kynar (polyvinylidene fluoride) are also given in this report and it is stated that H film has a higher strength than Mylar at high temperatures

and is thus more suitable for use as seals in components required to operate over a wide range of temperatures. Kynar appears to have a higher strength than Kel-F and its use would thus permit the design of thinner and more flexible seals if employed as a replacement for Kel-F.

Aluminized Mylar films are used not only as barrier layers but also as multilayer superinsulation. Although it is not quite so efficient as the aluminum foil/glass-fiber paper types because of its greater transparency to infrared radiation,[78] aluminized Mylar has the advantages of a lower density and of being a single-component system.[79] The film is often crinkled to reduce interlayer contact to a minimum by alternating crinkled and plane sheets, while woven nylon or PET fiber nets may also be used to separate the layers. Complications arise in practice, however, due to the difficulty of fitting the insulation around pipes and other connections or due to a loss of insulation if the layers are overcompressed.

In view of their success in providing barrier layers for foam insulation, attempts have been made to use thin Mylar films to provide vapor barriers for filament-wound glass-fiber-reinforced plastic pressure vessels. These attempts have not, however, met with success, due mainly to decohesion between film and GRP at its high working strains and to excessive differential contraction between the two materials. This topic will be considered in more detail in section 4.3.

Thin polymeric films are also used to produce the positive expulsion bladders needed to expel fuel from its storage tanks under "zero-g" conditions. The results of tests carried out to determine the suitability of Mylar and Kapton films with polyethylene or Nomex–nylon substrates, and the details of the tests employed, have been described by Lark.[128] "Twist-flex" tests were used to simulate the folding and unfolding experienced by a bladder during operation and it was concluded that both Mylar and Kapton had sufficient flexibility and toughness at 20°K for use in this application. Although the polymers are well below their transition temperatures, they are flexible at 20°K because their extreme thinness allows them to be bent around small radii without exceeding the elastic limit of the material. Furthermore, the use of multiple layers of thin-gauge film allows this flexibility to be retained while still providing a sufficient thickness of material to keep permeability to a minimum. It was, however, found necessary to use flexible substrates such as Nomex–nylon paper or PET fabric to increase the bend radii of the wrinkles which are formed during folding if an acceptable cycle life was to be achieved.

Both films and fibers of polymers such as Mylar have proved suitable for the insulation of electrical conductors, as their high flexibility allows them to be bent around small radii without failure. For similar reasons, they are also used to provide thermal insulation for flexible pipelines such as those used for the unloading of cryogenic liquids from road tankers.

The very low water absorption of Mylar is a particular advantage in this type of application, as water absorption causes embrittlement in other fibers such as nylon.

The strengths of a number of organic fibers have been measured[80] at temperatures down to 20°K to see whether they are suitable for use as reinforcing agents in structural materials and adhesives, and in every case except polypropylene the fiber strengths increased at low temperatures. It is suggested that organic fibers can be used to increase the peel strength of adhesives and that they might be combined with glass fibers in filament-wound composites.

4.1.2.5. ***Foams.*** Expanded plastic foams are widely used as insulants because they are cheap, convenient, lightweight, and relatively efficient. They may be made from thermoplastics such as polystrene, polyvinyl-chloride, polyethylene, and polypropylene, or from thermosetting resins like epoxies, phenolics, ureaformaldehydes, and polyurethane. Their insulating action at room temperature depends largely on the prevention of convection losses, but at lower temperatures, the thermal conductivities of "closed cell" foams decreases due to the liquefaction or solidification of residual gas in the cells. This effect is illustrated in Table VII, which shows the apparent mean thermal conductivities of a number of foams.[81]

Table VII.

Foam	Density, g/cm^3	Boundary temperature, °K	Test space pressure, Torr	Thermal conductivity, $\mu\omega$/cm/°K
Polystyrene	0.039	300–77	760	330
	0.046	300–77	760	260
	0.046	77–20	10^{-5}	81
Epoxy	0.080	300–77	760	330
	0.080	300–77	10^{-2}	168
	0.083	300–77	4×10^{-3}	130
Polyurethane	0.08–0.14	300–77	760	330
		300–77	10^{-3}	120
Rubber	0.08	300–77	760	360
Silica	0.16	300–77	760	550
Glass	0.14	300–77	760	350
Vacuum powder	—	300–77	$\sim 10^{-5}$	30–60
Superinsulation	—	300–77	$\sim 10^{-5}$	0.5–2

Thus, the thermal conductivities of foams lie between the low values of evacuated superinsulation and powders, and the considerably higher conductivities of most mineral insulants. Their use falls into two main types of applications: as a cheap and conveniently applied insulant for bulk storage tanks for the higher-boiling-point cryogenic liquids such as

liquid natural gas, and as a lightweight insulation for rockets and spacecraft.

The material used for the foam has less effect on its thermal conductivity than does the gas used to blow the foam: if the gas liquefies or solidifies at the operating temperature, it creates a vacuum in the cells and lowers the conductivity. The carbon dioxide by-product of the polymerization reaction is sometimes also employed as the blowing gas, but a better control over cell size is obtained by using fluorocarbons such as Freon, such control being desirable because the thermal conductivity increases almost linearly with the increase in cell size. As noted in the previous section, it is necessary to use vapor barrier films to prevent gas permeation into the evacuated cells if the quality of the insulation is to be maintained, and the problems which arise with internally insulated liquid-hydrogen tanks have already been discussed. There is, however, a different aspect to this problem with externally insulated tanks. In this case, it is air which permeates into the cells if no vapor barrier is provided, thus creating an explosion hazard. Helium purging is carried out to avoid this hazard, but the helium gas so introduced raises the conductivity of the foam considerably, thus largely negating its original purpose, and complex insulation systems such as that illustrated in Fig. 4.19[90] have been proposed to overcome this drawback. Data on the thermal conductivities and expansion coefficients of a number of foams suitable for cryogenic applications may be found in Refs. 81–84, 87, and 90.

The mechanical properties of most foamed plastics deteriorate at low temperatures due to the inherent brittleness of the plastic below its glass transition and also to the "internal notching" effect of the cell corners.

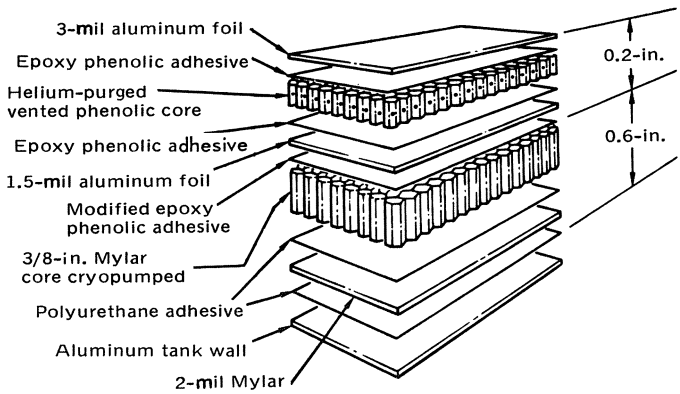

Fig. 4.19. Double-seal insulation system (Ref. 90).

Although such foams are liable to be subjected to tensile and shear stresses, the most critical loading conditions are usually compressive, and in Table VIII, the compressive properties of a number of foams are shown for tests at 20, 77, and 298°K. Tensile and shear strengths are also given in the original paper[77] from which the data for Table VIII are taken. High values of percentage set indicate that the foam has collapsed under load, and from the 20°K figures it can be seen that only Baron S. 39 and the Magnolia epoxy remain uncrushed. The Baron S. 39 would thus be suitable for internal insulation in liquid-hydrogen tanks operating at atmospheric pressure, but it would be unsuitable for pressurized tanks. However, the more dense epoxy would be suitable for pressures up to 50 psi and it has the additional advantage of good dimensional stability. Despite the rather poor showing of the rigid polyurethane in these tests, this foam system is in fact one of the most widely used for cryogenic applications. It has adequate strength for most purposes and it has the advantages of cheapness and the ability to be formed *in situ* around components with complex geometries. If the foam is required to support more than norminal loads, it is best reinforced with a suitable honeycomb structure prior to blowing, as in the system illustrated in Fig. 4.19.

Table VIII.

Foam	Yield, psi	Per cent set	Per cent compression	
			at 25 psi	at 50 psi
At 298°K				
(*a*)	—	4.0	92.0	—
(*b*)	—	2.3	93.0	—
(*c*)	—	0.6	2.3	5.0
(*d*)	31.0	19.5	3.3	54.6
(*e*)	49.0	32.3	—	4.8
At 77°K				
(*b*)	46.0	15.2	5.0	24.7
(*c*)	—	0.5	15.9	26.0
(*e*)	—	3.2	4.9	6.3
At 20°K				
(*a*)	25.0	42.0	7.0	53.2
(*b*)	—	7.6	82.6	86.9
(*c*)	25.0	67.4	10.9	82.5
(*d*)	28.0	16.7	—	30.4
(*e*)	—	2.8	4.0	6.8

[a] Baron, flexible polyester (1.9 lb/ft^3).
[b] Baron, S. 39, flexible polyester (1.6 lb/ft^3).
[c] Hexcel 14/4-2, semirigid polyester polyurethane (2 lb/ft^3).
[d] Barrett semirigid polyurethane (2 lb/ft^3).
[e] Magnolia (7015-1) epoxy (4.2 lb/ft^3).

Ebonite[85] foams are sometimes used at moderately low temperatures, as, although their strength and toughness are not particularly good, they have the advantage of possessing a very low water vapor permeability. This is particularly advantageous for exterior use and such foam has been employed to insulate liquid-methane pipelines.

In addition to the paper by Miller *et al.* already cited,[77] data on the mechanical properties of foams are available in Refs. 86–89, while both physical and mechanical properties are discussed in a recent review.[90]

4.1.2.6. ***Bearing Materials.*** Conventional organic fluid lubricants are unsuitable for use in cryogenic applications due to a combination of their incompatibility with liquid and gaseous oxygen, the need to prevent the contamination of the working fluid by impurities, and their high freezing temperatures. At ambient temperatures, it is possible to use graphite or molybdenum disulfide as lubricating agents for dry bearings because a stable graphite or MoS_2 film is formed. The presence of moisture, vapor, or oxide films is, however, essential[91] if the graphite is to bond strongly enough to the surfaces to be lubricated, but at low temperatures, these agents are not present and the film is not self-repairing. Thus, in liquid nitrogen and liquid hydrogen, wear is so rapid that very low service lives are achieved. Wisander and Johnson[92] have carried out a series of tests to find alternative bearing materials for use at low temperatures, and of the large number of combinations tried, a mixture of carbon and PTFE appeared the most promising.

Tantam and Hargreaves[93] also found that filled PTFE gave the best wear resistance in a series of tests in which journal bearings were run under load in liquid oxygen. Test bushes were made from a number of grades of carbon, metals such as 20% lead bronze, porous bronze, and aluminum zinc, and the following PTFE-containing compounds: (1) a mild-steel-backed porous bronze in which the pores were filled with PTFE and there was a 0.0005-in. overlayer of PTFE, (2) PTFE filled with a minority of graphite and bronze powder (GLACIER DQ) and, (3) a porous bronze containing 20% PTFE.

For the initial tests, the shaft material was either stainless or chromed steel and the PTFE/bronze/graphite composition (2) was found to have much the best properties. In further tests with a 20% lead bronze shaft, a tenfold reduction in wear rate was found when compared with that for either steel shaft; coefficients of friction were also lower. This difference is ascribed to the higher thermal conductivity of the bronze shaft and it illustrates the importance of good heat dissipation in bearing design. To confirm these test results, journal bearings were made from a solid bronze bush containing a number of inserts of the PTFE/graphite/bronze composition. This design allowed a free flow of liquid oxygen or nitrogen to

pass through the bearing for cooling purposes and such bearings have apparently given satisfactory service under both continuous and intermittent operating conditions. The use of inserts also facilitates repair should the bush become damaged due to overload.

A number of materials have been evaluated[94] for use as ball separators in bearing races to be employed in cryogenic applications and these tests also confirm the superiority of filled PTFE. The use of fillers also reduces the expansion coefficient of PTFE to a value low enough to avoid trouble caused by differential contraction between the ball separator and the outer bearing ring.

4.2. CERAMICS AND GLASSES

The term ceramic is used to describe the third basic class of materials as distinct from metals and polymers. Although there are a large variety of ceramic materials, they all share the characteristic of being compounds of metals and nonmetals whose atoms are held together by strong primary ionic or covalent bonds, this strong bonding accounting for their high melting points and distinctive mechanical properties. Ceramics can be either crystalline or amorphous and exist as a pure single phase or as a complex multiphase aggregate. Crystalline ceramics can have simple structures, such as the ionic face-centered-cubic structure of NaCl, and under exceptional circumstances, dislocation slip can occur and make them ductile. However, it would be a gross misrepresentation of the facts to suggest that such behavior was typical of ceramics, as the crystal structures of most ceramics are too complex for slip to be possible.

Glasses are ceramics which have been cooled too rapidly for crystallization to occur and they have an amorphous structure characteristic of a supercooled liquid. They are made up of a three-dimensional network of primary bonded units which have local order but no long-range order and plastic deformation cannot take place in such a structure. Thus, both principal types of ceramic are unable to deform plastically when loaded and hence they have characteristically high compressive and shear strengths. Theoretically, they should also have high tensile strengths, but these are rarely achieved in practice due to the premature brittle failure of the material. This is also a result of its inability to deform plastically, as such mechanisms are necessary if the stress concentrations built up at the tips of static flaws are to be relieved before the cohesive strength of the material is exceeded.

As we saw in chapter 3, the Griffith criterion for the unstable propagation of such cracks in an ideally brittle material showed that the fracture stress was proportional to the square root of the critical crack length and

that, for glasses, critical crack sizes are typically of the order of a few microns. Cracks of this magnitude are very easily produced in service and they propagate when subjected to a tensile load. Furthermore, subcritical cracks can grow slowly under lower loads when in a mildly corrosive environment (for glass, moist air is adequately corrosive) and fracture can occur at some time after the load is applied once the crack has grown to its critical length. This is known as static fatigue.

It should, nevertheless, be emphasized that tensile stresses are necessary in order for microcracks to propagate; under compressive loads, they are stable and this property is exploited in the toughening of glass by inducing compressive stresses in its surface layers. This is usually carried out by quench-cooling the surfaces in such a way as to make them rigid while leaving the interior soft enough to absorb the stresses thus induced, and then further cooling the material so that the contraction of the interior imposes the required compressive stresses in the surface layers. Cracks located in these surfaces are unable to propagate until the applied tensile stress is large enough to overcome the residual compressive stress, but deeper cracks which penetrate the surface layer can spread rapidly under the action of the residual tensile stresses which exist in the interior. This leads to rapid failure, as characteristically observed in shattered automobile windows.

Hence, residual stresses can play either beneficial or harmful roles in determining the toughness of glass components and, apart from treatments such as that described above, it is normal to give an annealing heat treatment to reduce such stresses to a minimum. If treated with suitable care, glass equipment can fulfill a useful role, as witnessed by the still-widespread use of glass Dewars in low-temperature physics laboratories. For more general use, however, bulk glass has a number of other drawbacks, for example it is prone to failure by thermal shock if cooled rapidly. This is due to the contraction stresses arising from thermal gradients built up as a result of its low thermal conductivity, but, as most glasses have relatively low expansion coefficients, this problem is not so severe as with the organic glasses (plastics) discussed earlier. Indeed, by reducing the expansion coefficient almost to zero, it has been possible to develop a type of glass, pyroceram, which is dimensionally stable over a wide temperature range and which is completely resistant to thermal shock. Pyroceram has already been used to produce mirrors for large reflecting telescopes, but the writer does not know whether its use for cryogenic applications such as bubble-chamber windows has been contemplated. It would, however, appear an attractive possibility, as at present the cooldown rates of such chambers are determined by the need to avoid thermal shock in the glass viewing windows. Another possible cryogenic application for glass in its bulk form may lie in its use as load-bearing electrical insulators for the superconducting power cables which are currently under consideration. Such applica-

tions are, however, of relatively minor importance and it is probably fair to conclude that the use of glass in its bulk form has been surpassed by its use in the form of finely divided fibers.

Freshly drawn glass fibers can have very high tensile strengths (~500,000 to one million psi) which approach the theoretical values for this material, but such strengths are only attainable when the fibers are essentially flaw-free. This high degree of perfection can be maintained if they are kept in a vacuum and their surfaces are untouched by other fibers, dust particles, or any other agent which causes microcracks to form. In commercial production, glass fibers are coated with a protective layer immediately after the drawing process, but even so, their strengths are typically reduced to about one-half of that of the virgin fiber. Most glass fibers are made from E glass, whose composition may vary but is typically SiO_2, 54%; Al_2O_3, 14.5%; CaO, 17.5%; MgO, 4.5%; B_2O_3, 8.3%; $Na_2O + K_2O + TiO_2 + Fe_2O_3 + F_2$, 1.2%. The tensile strength of the uncoated fiber is typically ~500,000 psi at room temperature, but this increases to ~820,000 psi at 77°K and probably approaches one million psi at lower temperatures. The properties of such fibers when combined with a number of thermosetting resins will be considered further in section 4.3.

Finally, it is worth noting that by far the largest use of ceramic materials is in the form of hydrolyzable silicates and oxides which constitute the cement used in concrete. This is not a material normally considered for use at low temperatures, although it is believed that there has been a proposal to use steel-reinforced concrete for the construction of above-ground storage tanks for liquid natural gas. Nevertheless, it is known that concrete mixed with ordinary Portland cement shatters when cooled to low temperatures and this can give rise to problems caused by spillage during the loading of road tankers. It has been found that such difficulties can be overcome if Ciment Fondu[95] is used instead of Portland cement, as this aluminous cement is stable down to very low temperatures.

4.3. COMPOSITES

There are two basic requirements which have to be fulfilled by an engineering material: it must be able to support a load and it must be tough and not brittle. In most applications, loads have to be carried with the minimum amount of deflection and hence a high modulus is also preferred. Most common engineering materials are metals. They have reasonably high moduli due to their primary type of bonding and quite good strengths, although the observed strengths are between 10 and 1000 times lower than their theoretical values. As we have seen in chapters 1 and 2, this de-

ficiency is due to the presence of dislocations, and all the conventional methods of increasing the strength of a metal—work-hardening, grain-size refinement, alloying, and precipitation- or dispersion-hardening—depend for their action on restricting the movement of these dislocations. However, they all suffer from a common drawback in that the more a metal is strengthened, the harder it becomes for it to deform. Not only is its ductility lessened, but its toughness is also reduced and it is less able to withstand impact loads, especially in the presence of stress-raisers such as notches. Thus, as we saw in chapter 3, very high strengths and good toughness are basically incompatible in conventional metals and alloys.

Ceramics—in particular, the oxides, carbides, and nitrides of the light elements—are potentially very attractive materials because they are covalently or ionically bonded and have high theoretical strengths, moduli, and melting points combined with low densities. However, like glasses, they are brittle in the bulk form because small (micron-sized) cracks can propagate through them in a low-energy mode, but in the form of finely divided fibers or small single crystals, called whiskers, strengths can be achieved which approach the theoretical values of the materials. The concept of fiber reinforcement allows these high strengths to be developed in such a way as to avoid the brittleness which is characteristic of the bulk form while producing materials which are suitable for engineering use. Essentially, this approach is based on the principle of "not putting all one's eggs in one basket" so that the failure of one fiber does not automatically lead to the failure of the whole structural member. There is, of course, nothing new in this concept, which is exploited by nature to produce strong and tough materials such as bone, bamboo, etc. It is, however, only in the last 25 years that man-made composites such as glass-fiber-reinforced plastic (GRP) has been in widespread use, while fiber-reinforced metals have yet to progress out of the development laboratory and into service. In particular, fiber-reinforced metals have no obvious cryogenic applications; they are being developed for use at high temperatures as possible replacements for existing superalloy turbine blades and these materials will not be considered further except where it is relevant to point out where the theory of metallic matrices differs from those of nonmetallic ones.

Fiber-reinforced plastics, on the other hand, are already in use in a number of low-temperature applications. The matrices are usually thermosetting resins such as the polyesters, epoxies, phenolics, and silicones, as they are easy to apply, have good fiber-wetting characteristics, and may be cured either in one operation or two, the intermediate stage then being a so-called "pre-preg" which can be shaped prior to final curing. Thermoplastics are also employed as matrices, but their use is less widespread, due to the more complex fabrication techniques involved. However, as noted

earlier in this chapter, nylon reinforced with chopped glass fiber has a high impact strength, while PTFE/glass-fiber composites are useful as O-ring seals.

There are a large number of potentially attractive types of reinforcement which can be used to make fiber composites, and the mechanical and physical properties of some of the most important are given in Table IX. It can be seen that they may be grouped into three basic types: whiskers, nonmetallic fibers, and metal wires. Although whiskers have the highest strengths and moduli, the problems involved in producing whisker-reinforced composites on a commercial basis are so enormous that it is extremely doubtful whether it will be attempted in the foreseeable future. The use of high-strength wires for reinforcement is much more straightforward, especially as wires made from, for example, steel are relatively easy and cheap to produce. Composites have been made from these wires but it is unlikely that they would be used for cryogenic applications, one reason being that steel has a high density and the resulting composite would have a poor strength/weight ratio. For practical purposes, this leaves us with the nonmetallic fibers, silica, glass, and carbon. Although silica fibers have good high-temperature properties, and the recently developed carbon fibers offer the combination of a relatively high strength, low density,

Table IX. Properties of Selected Whiskers, Wires, and Filaments

Material	Tensile strength σ, 10^6 lb/in.^{2}	Young's modulus E, 10^6 lb/in.^{2}	Specific gravity, ρ	σ/ρ, 10^5 lb/in.^{2}	E/ρ, 10^6 lb/in.^{2}
Al_2O_3 whisker[a]	2.2	76(max)	4.0	5.5	19
Si_3N_4 whisker[a]	2	55	3.1	6.5	18
SiC whisker[a]	3	100(max)	3.2	9.4	31
Asbestos fiber[a]	0.85	27	2.5	3.4	11
Drawn silica fiber[a]	0.86(mean)	10.5	2.5	3.5	4.2
E glass fiber[b]	0.5 (max)	10.5	2.5	2.0	4.2
RAE type I[c] carbon fiber	0.27	50	2.0	1.35	25
0.9% C steel wire[a] (0.004 in.)	0.6	30	7.8	0.8	3.9
Tungsten wire[d] (0.005 in.)	0.4	50	19.3	0.21	2.6
Molybdenum alloy[d] TZM wire (0.010 in.)	0.3	53	10.2	0.29	5.2
Boron[e]	1.0	64	2.3	4.35	28

[a] Ref. 97.
[b] Ref. 26, p. 281.
[c] Ref. 126.
[d] Ref. 127.
[e] Ref. 98

and a very high modulus, by far the most widely used reinforcing agent is glass fiber. For most purposes, E glass is used to make these fibers, but other types are available for special applications, i.e., C glass has a higher chemical resistance, M glass a higher modulus, and S glass better high-temperature properties. Glass fiber is available in a large variety of forms, such as continuous filaments, woven or unwoven fabrics, and chopped strand or felted mats, the continuous filaments being of particular interest as they permit the construction of spherical, cylindrical, and other simple shapes by the technique of filament winding. The precision and control obtainable using this technique enables the strength of the glass fibers to be fully exploited, thereby producing materials with high strength/weight ratios. Filament-wound GRP's are finding application as fuel tanks and other lightweight pressure vessels, not only in rockets, but also in a number of less esoteric situations where weight-saving is important. One drawback with these vessels is, however, their porosity, and it has been found necessary to bond impermeable liners to the interior of fuel tanks intended for cryogenic fluids.

Glass-fiber-reinforced plastics have a further attraction for cryogenic use in that their high strength and low thermal conductivities combine to give very high strength/thermal conductivity ratios. This property is of vital importance in load-bearing supports to storage vessels and other equipment in which heat leaks must be reduced to a minimum, and GRP's are already in use for such applications. The low-temperature mechanical and physical properties of glass-fiber-reinforced plastics and, to a lesser extent, carbon-fiber-reinforced plastics will be discussed at some length in section 4.3.2, but first, in section 4.3.1, a brief summary will be given of the theory which underlies the properties of fiber-reinforced composites.

A comprehensive work on most aspects of composite materials has been edited by Broutman and Krock[26] and there are also a number of other texts available,[27,28] some of which cover more limited topics such as fiber-reinforced metals[97-99] in more detail, while others deal with the more practical aspects of glass-reinforced plastics.[30,119] Other reviews and original papers will be cited below, as will the much more limited number of papers which deal specifically with the cryogenic properties of composites.

4.3.1. Basic Theory

In all practical fiber-reinforced composites, the fibers have higher strengths and moduli than the matrix, which has three main functions: (1) to bind the fibers together and protect their surfaces from damage, (2) to separate the fibers and prevent continuous crack propagation between them, and (3) to transfer applied stresses effectively from the weak matrix to the

stronger fibers. This point is particularly important, as in an efficient composite, the matrix is not required to carry a high stress itself but simply to transfer the stress to the fibers, which are better able to support it.

The simplest analysis of the properties of composites is obtained by assuming that the fibers are continuous, aligned parallel to the direction of the applied stress, uniformly stressed, and identical in size and strength, and that there is a perfect bond between fiber and matrix. Having carried out this analysis, the effect of relaxing the various constraints can be evaluated to consider discontinuous fibers, misorientation, and the effect of interfacial bond strength on the toughness of a composite.

4.3.1.1. ***Continuous Fibers.*** For the idealized system defined above, the principle of combined action requires that equal strains are developed by both components,

$$\epsilon_{\text{comp}} = \epsilon_{\text{matrix}} = \epsilon_{\text{fiber}} \tag{4.24}$$

If both matrix and fibers deform elastically, it follows that

$$\sigma_f/\sigma_m = (E_f/E_m)(V_f/V_m) \tag{4.25}$$

where σ_f and σ_m are the stresses, and E_f and E_m the tensile moduli of fiber and matrix respectively, while V_f is the volume fraction of fibers and $V_m = (1 - V_f)$ is the volume fraction of the matrix.

As Young's modulus for glass fiber is about 10^7 psi, while that of resins such as epoxy or polyester is $\sim 3\text{–}4 \times 10^5$ psi, the fiber stress in a 50 vol.% composite will be about 30 times that in the matrix, and significant stress transfer is also possible at much lower volume fractions of fiber. Furthermore, while deformation is elastic, the modulus of the composite is given by

$$E_c = E_f V_f + E_m V_m \tag{4.26}$$

This is, in fact, a minimum value which is only obtained if Poisson's ratio is the same for both fiber and matrix; if not, E_c is larger.[100] Furthermore, as $E_f \gg E_m$ this equation simplifies to

$$E_c \simeq E_f V_f \tag{4.27}$$

For metal matrices, plastic deformation of the matrix occurs under load and thus the stress transfer mechanism is different but the approximation given in equation (4.27) is still valid.

The strength of a fiber-reinforced composite is largely determined by the failure strain of the fibers, as illustrated in Fig. 4.20. As we have assumed that the fibers are loaded uniformly, the composite breaks at the failure strain of the fibers and the stress carried by the matrix at this instant is given by σ'_m. Once a certain critical volume fraction V_{crit} is exceeded, the strength of the composite is given by the law of mixtures,[101]

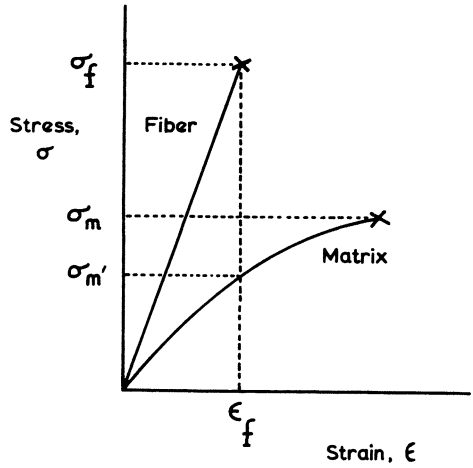

Fig. 4.20 Distribution of stresses in a composite at failure.

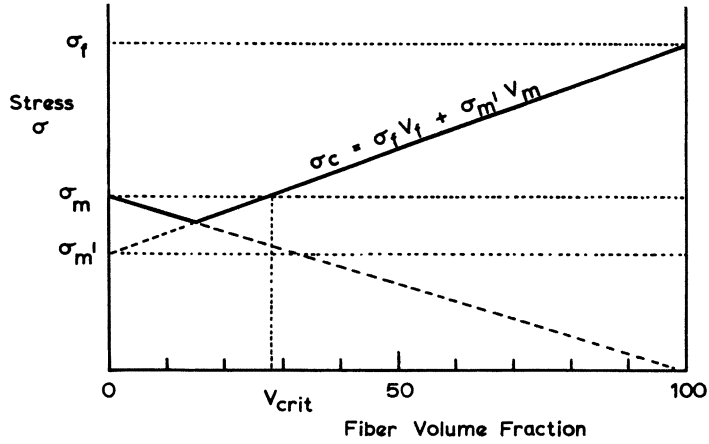

Fig. 4.21. Composite strength as a function of fiber volume fraction showing the derivation of the critical volume fraction.

$$\sigma_c = V_f\sigma_f + V_m\sigma'_m \qquad (V_f > V_{crit}) \tag{4.28}$$

The significance of V_{crit} is illustrated in Fig. 4.21, which shows the composite strength as a function of the volume fraction of fibers. At low volume fractions, the fibers are too far apart for stress to be transferred from fiber to fiber via the matrix, the fibers effectively act as holes, and the strength drops linearly with increase in the volume fraction of these holes. As more fibers are added, there comes a point at which stress transfer begins and reinforcement commences. It is not, however, until V_{crit} is exceeded

that the strength of the composite σ_c is greater than that of the unreinforced matrix σ_m. The value of V_{crit} can be obtained by applying similar triangles to Fig. 4.21, and one gets

$$V_{crit} = (\sigma_m - \sigma'_m)/(\sigma_f - \sigma'_m) \tag{4.29}$$

As for most resins $\sigma'_m \ll \sigma_f$, V_{crit} is small for these systems, but in metals, the matrix can have quite a high strength and critical volume fractions can be so high that most of the fibers in the composite are necessary to make good the degradation in matrix strength caused by their presence!

The equations developed so far have been confirmed experimentally and, although most of the work has been performed in metal wire–metal matrix systems,[98,101-103] they are generally valid for most other systems, especially at low strains. At high strains, the measured moduli of fiber-reinforced plastics usually fall further and further below the theoretical values as the strain increases and this is thought to be due to the premature failure of weaker fibers or those which may have buckled as a result of resin shrinkage in curing.

4.3.1.2. ***Discontinuous Fibers.*** A significant degree of reinforcement can also be achieved in most systems by the use of discontinuous fibers. Under the influence of an applied load, shear strains develop in the fibers due to the difference in moduli of the two components and these strains provide a mechanism by which a tensile stress can be transferred from the matrix to the fibers, the maximum rate of stress transfer being governed by the failure stress of the matrix or of the fiber–matrix interface. It is found that the stresses are not carried uniformly over the length of the fibers but, to a first approximation, they are distributed as illustrated in Fig. 4.22. The stress builds up from zero at the fiber ends to a constant

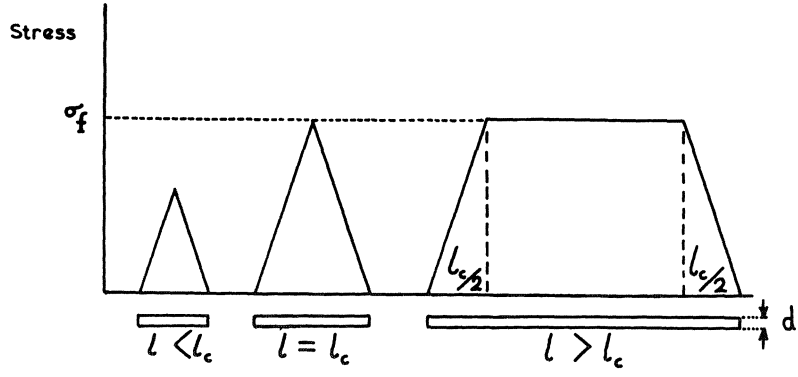

Fig. 4.22. Stress distribution in fibers of various lengths, showing the origin of the critical transfer length.

maximum value of σ_f at distances greater than $l_c/2$ from either end. The distance l_c is known as the *critical transfer length* because a fiber of length $l < l_c$ can never be stressed enough for the stress at its center to reach σ_f. It is in fact more usual to consider the critical aspect ratio l_c/d rather than just l_c, and it can be shown that this is given by

$$l_c/d = \sigma_f/2\tau_y \tag{4.30}$$

where τ_y is the shear yield stress of the matrix. For fibers well bonded to a metal matrix, critical aspect ratios are typically of the order 10, while for resin matrices, they are about one or two orders of magnitude larger. Not all of this difference can be ascribed just to the lower shear yield stresses of the matrix and it is worth considering in a little more detail what happens when a composite containing discontinuous fibers in a resin (e.g., Al_2O_3 in epoxy) is stressed.[104]

Initially, at very small strains, the shear stress in the resin is below its yield stress and the measured modulus corresponds quite closely to that given by equation (4.26). However, at higher strains, the shear yield stress of the resin is exceeded and failure occurs near the end of the fiber where the shear stresses are greatest. As this region can no longer contribute effectively to the reinforcement, the composite modulus drops below its theoretical value and the more the resin is strained, the larger the area of the failed region of the resin and the lower the modulus. Thus, as the stress increases, the modulus decreases continuously and the stress–strain curve becomes concave toward the strain axis. Outwater[105] has pointed out that, once the bond between the fiber and matrix is broken, the fiber pulls through the resin and further stress transfer takes place due to friction between the resin and the matrix. The force acting on the fiber is thought to be that produced when the resin contracts around the fiber during cooling, and good agreement has been achieved between calculated values of the frictional forces and those found experimentally. Furthermore, this theory also explains the deleterious effect that moisture has on the properties of such composites, as its presence lowers the coefficient of friction between resin and fiber. Despite the change in mechanism, the critical aspect ratio is still given by an equation of the form of (4.30), but with the shear yield stress τ_y replaced by a term which represents the frictional forces involved. One important difference between the behavior of discontinuous fibers in metallic and resin matrices is that the metal is able to flow completely around the ends of the fibers, but in resins, this is not possible and hence voids are formed behind the fiber. This complicates the calculation of the stresses at the ends of fibers and it has been found that the actual shear stresses can be considerably higher than those predicted by the simple theory.

The strength of composites containing discontinuous fibers can be calculated once the distribution of shear stresses along the length of the

fiber is known. For the simple system shown in Fig. 4.22 the average stress carried by the fiber is

$$\bar{\sigma} = \sigma_f[1 - (l_c/2l)] = \sigma_f[1 - (1/2\alpha)] \tag{4.31}$$

where $\alpha = l/l_c$. If this average stress is substituted into equation (4.28) for the composite strength, we get

$$\sigma_c = \sigma_f V_f[1 - (1/2\alpha)] + \sigma'_m V_m \tag{4.32}$$

This formula has been experimentally verified for a number of metal wire–metal matrix systems. If $l/l_c = 3$, then strengths of about 80% of those for continuous reinforcement can be achieved, while l/l_c ratios of ~10 permit the realization of 95% perfect reinforcement. For glass fibers in resin, lengths of the order of $\frac{1}{4}$ in. give l/l_c ratios high enough to achieve significant reinforcement to typical resin matrices and this value can be checked by the use of equations (4.30) and (4.32). Putting $\sigma_f = 500{,}000$ psi for glass fibers 0.0004 in. in diameter and $\tau_y = 8000$ psi for typical resins gives critical lengths of the order 0.013. Allowing for the known deficiencies of this formula and increasing l_c to 0.050 in. gives $\alpha = 5$ for fibers 0.250 in. long and hence reinforcement is 90% of that obtainable from continuous fibers.

4.3.1.3. ***Orientation Effects.*** If a composite made from continuous fibers is stressed so that the fiber direction makes an angle ϕ with the tensile axis (Fig. 4.23a), there are three factors which influence the failure stress of the composite and whose effect varies with the orientation ϕ. The applied stress necessary to cause *tensile failure* of the fibers is given by the relationship

$$\sigma_T = \sigma_C \sec^2 \phi \tag{4.33}$$

shear failure parallel to the fibers requires an applied stress

$$\sigma_S = 2\tau_u \operatorname{cosec} 2\phi \tag{4.34}$$

where τ_u is shear failure stress of the matrix in the presence of fibers, while *tensile failure* perpendicular to the fibers requires a stress

$$\sigma_P = \sigma_u \operatorname{cosec}^2 \phi \tag{4.35}$$

where σ_u is either the ultimate tensile stress of the matrix or the failure stress of the fiber–matrix interface under such loading conditions. Kelly[27] has shown that the relative importance of these three mechanisms varies with ϕ as illustrated in Fig. 4.23(b) while Tsai[106] has considered the similar case of alternate layers of fibers cross-plied at angles of $+\phi$ and $-\phi$ to the tensile axis. In both cases, the failure stress of composites with resin matrices falls off rapidly as ϕ is increased, due to the low interlaminar shear

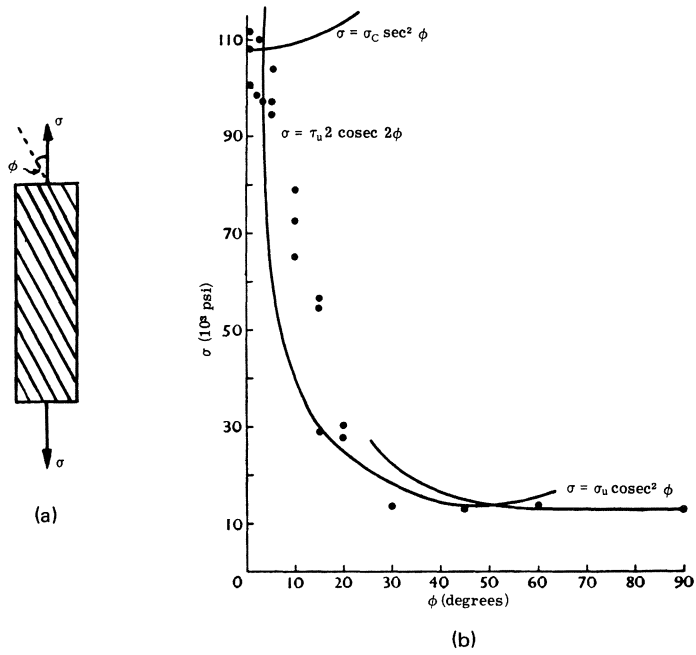

Fig. 4.23. (a) Composite with fibers oriented at an angle ϕ to the tensile axis. (b) Variation of tensile strength with fiber orientation, showing degree of agreement between measured values and theoretical predictions for three different failure modes (Kelly[27]).

strengths of the resin–fiber interfaces, although the decrease is less rapid for the cross-plied composite. For metallic matrices, shear strengths are higher and the failure stress does not start to decrease rapidly until ϕ is about 30°.

Although cross-plied laminates can be prepared with the plies arranged in any desired combination, probably the most commonly used unwoven laminates are those made with alternate plies oriented at 90°, while in woven cloths, the warp and woof threads are also mutually perpendicular. In both types of material, the stress–strain curve shows a characteristic knee, such as that illustrated in Fig. 4.24, at which the modulus drops from its initial value to a lower, secondary value. In unwoven laminates, it has been shown[107] that the knee occurs due to the tensile failure of the fiber–matrix interface of plies oriented at 90° to the tensile axis, and both the stress and strain at which the transition takes place agree with those found in tests on a single ply oriented at 90° to the tensile axis. For woven cloth, such as the type 181 cloth used in the composite considered in Fig. 4.24, this mechanism is probably responsible for the initial knee found at low strains, but a further transition which occurs at higher strains is thought[108]

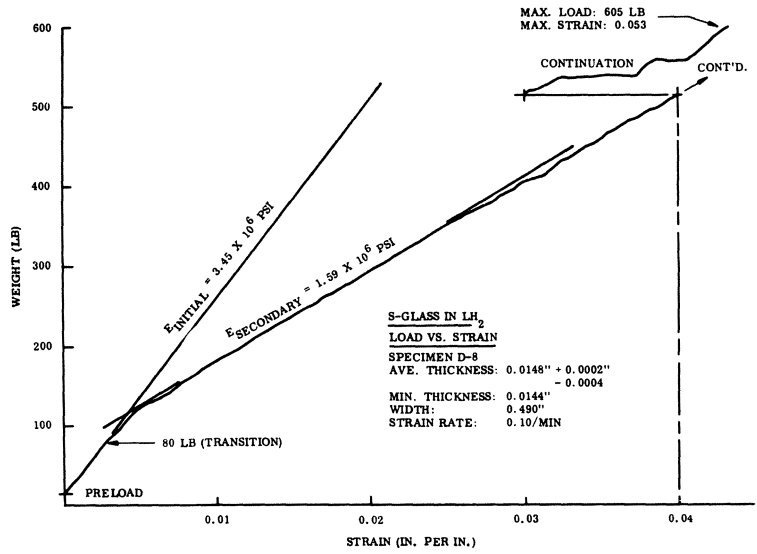

Fig. 4.24. Stress-strain curve for epoxy-glass cloth composite tested at 20°K, showing initial and secondary moduli (Caren *et al.*[76]).

to be due to microcracking in the resin caused by the straightening of the crumpled fibers under load.

Once the matrix has failed, the secondary modulus is that due to the volume fraction of fibers that are oriented parallel to the applied stress and it is these fibers which carry the load until complete failure takes place. The material is, however, excessively porous once the transition stress has been exceeded and it is for this reason that barrier layers are required if the composite is to be used to contain liquids or gases. The barrier layer problem will be considered in more detail in the next section.

The stress-strain curve illustrated in Fig. 4.24 was obtained by Caren *et al.*[76] for a single ply of type 181 S glass cloth impregnated with epoxy resin, and in Table X, their results are given in more detail, as they provide a good illustration of a number of important points, as follows.

1. For both types of glass cloth and for the quartz stressed parallel to either warp or woof, the initial modulus and ultimate stress both increase as the temperature is lowered and this is a reflection of the higher strength and modulus of the glass fiber which was noted earlier.

2. In contrast, the secondary modulus and the transition stress both fall at low temperatures, an indication of the decrease in shear strength of the resin matrix or the matrix-fiber interface.

3. The maximum failure strains are high for all types of cloth and at all testing temperatures.

Table X. The Mechanical Properties of Epoxy-Impregnated Type 181 Single-ply Quartz and Fiberglass Cloths As a Function of Tensile Orientation and Testing Temperature[a]

Material type and direction of pull	Test temperature	Initial modulus, $\times 10^{-6}$ psi	Ultimate stress, $\times 10^{-3}$ psi	Maximum strain ($\Delta l/l$)	Secondary modulus, $\times 10^{-6}$ psi	Transition stress, $\times 10^{-3}$ psi
Fiberglass (E-series)	Room	3.14(6.4%)	31.4(7.0%)	0.013(17.0%)	2.10(11.0%)	10.1(21%)
	LN_2	4.25(3.5%)	51.0(1.6%)	0.024(8.3%)	1.78(9.5%)	11.3(7.1%)
	LH_2	5.02(11.6%)	52.4(4.6%)	0.023(8.7%)	1.77(13.0%)	8.0(10%)
S-glass (D-series)	Room	2.83(4.2%)	58.9(12.0%)	0.12 (8.5%)	2.25(9.3%)	17.7(13%)
	LN_2	3.92(8.2%)	92.0(1.4%)	0.045(8.9%)	1.97(6.6%)	16.0(13.1%)
	LH_2	3.60(4.7%)	85.6(1.9%)	0.052(77.7%)	1.73(6.4%)	12.6(12.7%)
Quartz warp (A-series)	Room	2.71(3.3%)	44.6(3.6%)	0.037(3.0%)	2.06(6.8%)	13.0(13.0%)
	LN_2	2.78(8.6%)	73.3(2.3%)	0.040(10.0%)	1.85(1.6%)	11.2(15.2%)
	LH_2	3.87(14.5%)	71.4(8.0%)	0.034(8.0%)	1.97(8.8%)	11.1(12.6%)
Woof (C-series)	Room	2.52(4.4%)	45.5(9.0%)	0.023(8.7%)	1.89(4.8%)	9.7(1.0%)
	LN_2	2.82(2.1%)	57.2(4.5%)	0.038(10.5%)	1.48(5.4%)	6.3(17.5%)
	LH_2	2.99(6.4%)	68.5(16.8%)	0.041(5.0%)	1.59(12.6%)	6.6(16.7%)
45° to Warp (B-series)	Room	1.62(14.0%)	15.0(4.7%)	0.029(15%)	—	—
	LN_2	2.51(9.2%)	21.2(30%)	0.019(88%)	—	—
	LH_2	2.88(11.8%)	19.2(2.1%)	0.014(28.6%)	—	—

[a] Percentage values are the maximum deviation from average of three tests.

4. In the case of the cloth tested with the stress of 45° to the warp, the moduli, ultimate stress, and failure strain were all considerably lower than for the cloths tested at 0° or 90° to the warp direction. Furthermore, both ultimate stress and failure strain fell at low temperatures, giving a further indication of the poorer shear strengths at low temperatures. Finally, there was no transition from initial to secondary modulus, as for this orientation no fibers are oriented perpendicular to the applied tensile stress.

Despite the lower values of strength and modulus obtained when the stress is not applied parallel to the fibers, the technique of bonding together sheets of uniaxially aligned fibers at varying orientations is the most efficient method of producing composites which have isotropic properties in the plane of the sheet. The only other method of obtaining isotropic properties is to use a random two- or three-dimensional arrangement of fibers to give a mat or felt, respectively. Cox[109] has shown that the strengths of such composites are proportional to their moduli and that, for a planar mat of randomly oriented, continuous fibers, the modulus is given by

$$E_c = E_f V_f/3 \tag{4.36}$$

while for a solid mat,

$$E_c = E_f V_f/6 \tag{4.37}$$

As it is difficult to achieve a high volume fraction of fibers in such random arrangements, the properties of these composites, as compared to those made from uniaxially oriented fibers, are even worse than is suggested by equations (4.36) and (4.37).

Finally, the compressive properties of composites loaded parallel to the fibers have been shown[110,111] to be as good as, or better than, their tensile properties. Failure, when it occurs, is by buckling of the fibers, but for typical fiber/resin composites, failure stresses can be of the order of 400,000 psi and thus these materials are highly suitable for use under compressive loading conditions.

4.3.1.4. ***Notch-Toughness and Failure Modes.*** As we saw in chapter 3, the notch-toughness, or more specifically, the fracture-toughness, of a material is a measure of its ability to resist the low-energy propagation of a crack. Fibrous materials are generally tough and not notch-sensitive and there are a number of possible reasons for this behavior. Firstly, Cook and Gorden[112] have shown that if the bond between the fiber and matrix has an adhesive strength that is about one-third to one-fifth of the cohesive stress of the matrix, the stress concentrations ahead of a crack advancing normal to the fiber can cause the interface to fail. When the crack reaches the

fiber, it is then diverted along the cracked interface and blunted. In order for the crack to propagate, it must then be reinitiated and large amounts of energy can be absorbed if this process can be repeated many times as the crack spreads. This is believed to be the principal mechanism responsible for the toughness of glass-fiber-reinforced plastics and natural materials such as wood, bone, and bamboo. As the strength of the bond between fiber and matrix can be increased by the use of coupling agents or decreased by the use of coatings with low shear strengths, it is possible to exercise some control over the toughness of the composite. If there is a very strong bond between fibers and matrix, the stress concentrations set up by the failure of one fiber nucleate a crack in the next so that progressive failure occurs. Nevertheless, the work required to nucleate a crack in each fiber contributes to the total work of failure of the composite and, in consequence, its toughness will be higher than that of an equivalent volume of bulk material.

Secondly, high toughness can be obtained if either the fiber–matrix interface or the matrix itself has a low shear strength. In this case, the critical transfer length l_c is large and if a fiber fails the stress cannot be concentrated because the fiber is partially relaxed over a distance equal to l_c. Failure can then only occur if the stress is high enough to break all the fibers simultaneously. Furthermore, if a composite is made from discontinuous fibers of length approximately equal to l_c, failure can only take place if fibers are pulled out from the matrix. In some composite systems, e.g., tungsten wires in copper, large amounts of work are done in pulling fibers from the matrix and hence tough composites are obtained.

Two other failure modes for composite materials should also be noted and both are often referred to as fatigue. Static fatigue can take place in glass-reinforced composites as well as in bulk glass and the stresses required to cause such failures are often considerably below their short-term strengths. Environmental effects can also be serious under certain circumstances, for example, water is a plasticizer for polyester resins, and quite severe decreases in strength can be caused in composites with polyester matrices when they are exposed to moisture.

Conventional fatigue due to alternating applied stresses can also be a serious problem in fiber/resin composites. In particular, large amounts of heat are generated during cyclic tests as a result of the high internal friction and low thermal conductivity of the resin, and this complicates the interpretation of the results. In general, the fatigue lives of glass-reinforced composites decrease continuously as the number of cycles increases and, although some curves show a change of slope, none appear to have a true fatigue limit. Fatigue in composites is reviewed in Ref. 26, while in section 4.3.2, we will consider further the cryogenic aspects of the problem.

4.3.2. Cryogenic Properties of Composites

4.3.2.1. ***The Effect of Temperature on the Basic Mechanical Properties.*** Some of the most important compilations of data on the mechanical properties of fiber-reinforced plastics at cryogenic temperatures are to be found in the reports[113,114] written by Chamberlain and his co-workers at the Narmco Research and Development Corporation. The conclusions drawn from this work have also been published in a more accessible form[115] and they are summarized in Figs. 4.25–4.29. Although some tests were carried out using stainless steel mesh, and fluorocarbon and cellulose fabrics as reinforcement, the majority of the work was with type 181 glass cloth (probably E glass, but this is not specifically stated in Ref. 115, nor is the value of volume fraction used). All the materials tested showed increased strengths and moduli at temperatures down to 77°K, with little or no further increase on cooling to 20°K. As may be seen from Fig. 4.25, the epoxies had the highest tensile strengths and moduli, and a similar superiority is also shown in Figs. 4.26, 4.27, and 4.28, for compressive, flexural, and bearing strengths, respectively. In these static tests, the two next most promising materials were the polyesters and the phenolics, but when the program was extended to include fatigue tests, the polyesters gave consistently lower fatigue lives at both room and liquid-hydrogen temperatures (Fig. 4.29). Further details of the results of fatigue tests on composites

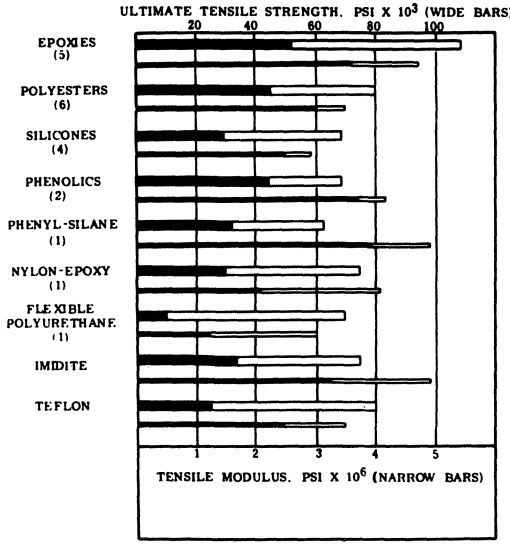

Fig. 4.25. Average ultimate tensile strength and modulus of laminates at room temperature and at 20°K (Chamberlain[115]). (Shaded bars indicate room-temperature values.)

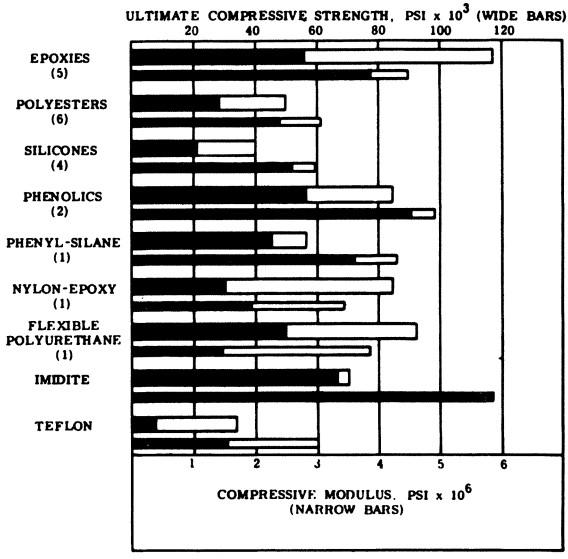

Fig. 4.26. Average ultimate compressive strength and modulus at room temperature and at 20°K (Chamberlain[115]). (Shaded bars indicate room-temperature values.)

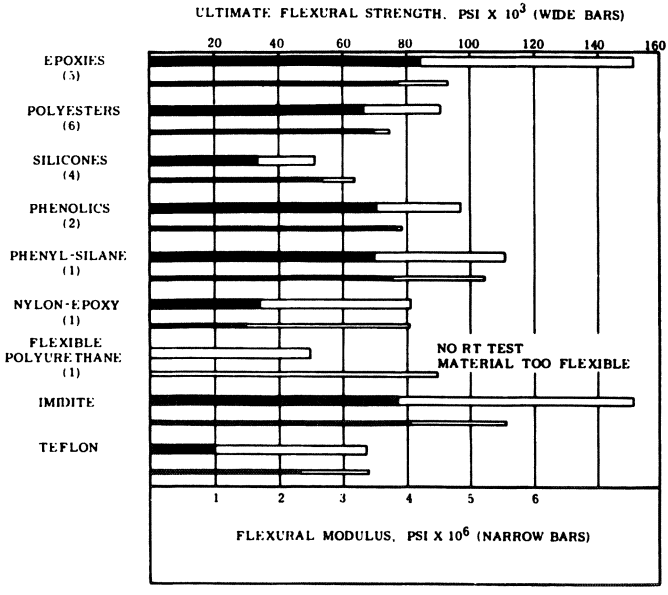

Fig. 4.27. Average flexural strength and modulus at room temperature and at 20°K (Chamberlain[115]). (Shaded bars indicate room-temperature values.)

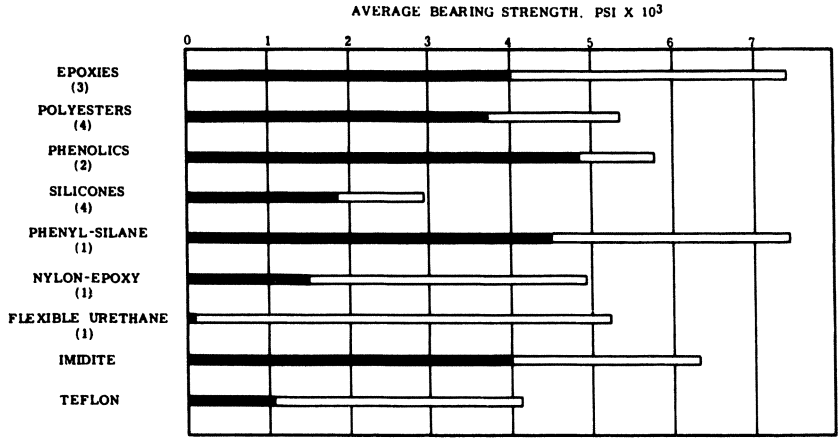

Fig. 4.28. Average bearing strength of $\frac{1}{8}$-in.-thick laminates and a $\frac{3}{16}$-in.-diameter pin at room temperature and at 77°K (Chamberlain[115]). (Shaded bars indicate room-temperature values.)

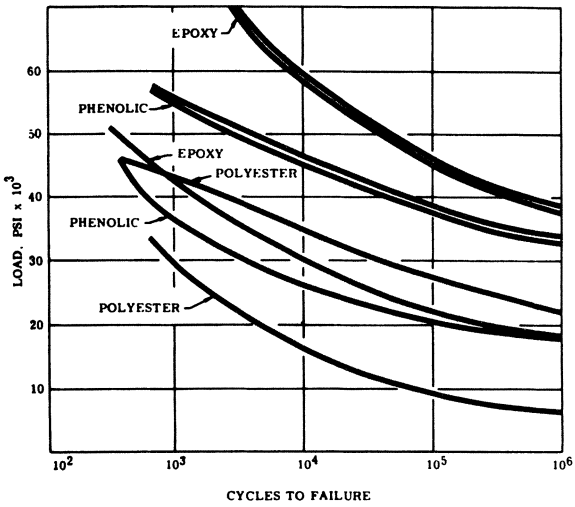

Fig. 4.29. Composite S–N curves derived from average fatigue strength values at room temperature and at 20°K (Chamberlain[115]). (Shaded bars indicate room-temperature values.)

with epoxy matrices, together with details of the testing techniques, are given in Ref. 116.

A further extensive testing program has been carried out at the Martin Co., and the main results of this work are summarized in Ref. 117. Epoxy, phenolic, polyester, and polyimide resins were used as matrices in these

tests, which confirmed the superiority of epoxy resins for cryogenic applications. Both E-glass and S-glass cloths were used to reinforce the epoxy matrices and, as might be expected, the composites reinforced with the stiffer S glass had higher moduli at all temperatures; there was, however, little difference in their strengths. Tensile, flexural, and compressive tests were carried out on these glass-cloth-reinforced specimens using a series of ingenious cryostat attachments which permitted a number of specimens to be tested during one cooldown period. These devices will be considered further in chapter 5.

A further series of tests was carried out on filament-wound specimens in the form of $\frac{1}{4}$-in. standard Naval Ordnance Laboratory (NOL) rings strained in a conventional split-D ring test fixture, and once again, the epoxy-bonded specimens were superior. In an interesting extension to these tests, static fatigue experiments were carried out at ambient temperature and at 77°K to see whether static fatigue occurred at low temperatures. It was found that a load equivalent to the average tensile strength of the composite could be maintained for long periods without failure at 77°K, but that failure at room temperature occurred within 1–10 min under a load equivalent to 80% of the average tensile strength. No failures at room temperature were obtained if the specimens were kept in vacuum or in dry air, thus identifying water vapor as the probable cause of degradation in atmospheric air. At low temperatures, of course, the water would not be in the liquid or vaporized states.

Having seen from both these sets of results that the epoxy resins gave the best low-temperature performance, it might be expected that experiments would be undertaken to find the most suitable type of epoxy. Such work has, in fact, been carried out by Soffer and Molho,[118] who have investigated the properties of four modified epoxy resins (which were chosen from screening tests on 41 candidate resin systems) and composites made from these resins. Measurements carried out included the tensile strength, modulus, and elongation, notch-toughness, and impact strength, as well as the thermal contraction coefficient and thermal shock resistance. The two most successful resin systems were a hybrid epoxy/polyurethane and a highly modified bisphenol-A epoxy, but the short pot life and high viscosity of the epoxy/polyurethane ruled it out for use in filament-wound applications. The effect of the different resin matrices on the mechanical properties of the composites was shown most clearly by the results from interlaminar shear strength tests on sections cut from standard NOL rings. The influence of void concentration on the shear stresses was also clearly shown for all systems, with the highest shear stresses being given by the resins with the lowest void concentrations. Finally, the thermal shock resistance of the composites was also found to depend on the type of matrix, the modified bisphenol-A epoxy having the best thermal shock resistance.

4.3.2.2. ***Filament-Wound Composites and the Barrier-Layer Problem.*** The technique of filament winding offers one of the most promising methods of fabricating pressure vessels and other components with extremely high strength/weight ratios and it is already used extensively to produce rocket motor cases, pressure vessels, and other structures which operate at ambient or slightly elevated temperatures. The topic has been covered in depth in the work by Rosato and Grove[29] and the practical aspects are also discussed in Refs. 30 and 119. In section 4.3.1.3 it was noted that cross-plied laminates of parallel continuous fibers gave the most efficient method of obtaining two-dimensional reinforcement, and filament-winding allows this technique to be extended to form simple three-dimensional structures which are usually solids of revolution. The continuous filament, which may be wound longitudinally, circumferentially, at a helix angle, or in any combination of these three directions depending on the loading requirements, is normally coated with resin as it is wound onto a rotating mandrel where it cures *in situ*. For closed shapes, the mandrel is typically made from a water-soluble salt or a low-melting-point alloy which can be easily removed once the component has cured.

In view of the success obtained with such structures at room temperature, it was to be expected that they would be evaluated for cryogenic applications, particularly liquid-oxygen and liquid-hydrogen fuel tanks in rockets, and the cryogenic properties of a number of laminates have been reviewed by Hertz.[120] The initial experiments revealed, however, that there were serious problems associated with this concept. In essence, the cause lay in the relatively low modulus of the glass-reinforced plastic and the consequent high strains developed when the material was stressed to anywhere near its ultimate. As we saw earlier, failure strains of the order of 5% are typical for these materials, but matrix failure and excessive porosity sets in at much lower strains, in the region of ~1–2%. In order to circumvent this difficulty, it is necessary to use a liner or vapor barrier on the inner surface of the vessel, and a number of candidate materials have been evaluated for this purpose. As noted earlier, polymeric films such as Mylar have proved[121] to be of limited use because of their high differential contraction with respect to GRP and their low failure elongations, but more promising results have been obtained with thin electrodeposited nickel coatings[122] and adhesive-bonded aluminum foils with longitudinal lap seams.[124] Furthermore, electrodeposited nickel gives a seamless, contoured liner which can be flared out to accommodate sealing flanges or other leadouts without having to make joints in the liner. Although the metal liner has to deform plastically to remain in contact with the GRP vessel, cycling tests using $7\frac{1}{2}$-in.-diameter biaxial cylinders lined with 0.005 in. of electrodeposited nickel have shown[122] that the liner was able to withstand a large number of 0.8% strain cycles at 20°K without failure.

The use of biaxially wound cylinders for the burst tests also carried out in these studies gives a realistic representation of the conditions likely to be found in use, i.e., resin cracks and strains in two directions, and they are thus to be preferred to the more widely used NOL rings where possible.[123] Both NOL rings and biaxial cylinders were in fact used in the later work reported by Hanson[124] in which the properties of graphite- and boron-filament-wound composites were compared with those reinforced with glass filaments. As noted earlier, the tensile strengths and moduli of glass-reinforced plastics increase by about 30% on cooling from room to cryogenic temperatures, due to the enhanced low-temperature strength of the glass filaments. No such increase is found for either boron- or graphite-reinforced composites because there is no marked change in the properties of the fibers at low temperatures. The composite tensile strengths at room temperature of NOL rings of glass, boron, and graphite (Thornel 25) filaments were found to be 290,000 psi, 174,000 psi, and 87,000 psi, respectively, but it was noted that the boron and graphite fibers did not appear to develop their full strengths when in the composites. As both boron and graphite fibers have much higher tensile moduli than glass, their use can offer distinct advantages in pressure-vessel fabrication and it is worth considering the implications of these results in more detail.

We saw earlier that the need for liners and vapor barriers arose from the high strains developed by glass-reinforced composites when stressed to their ultimate. Glass fibers have a modulus of about 12 million psi, while the moduli of boron and RAE* high-modulus carbon fibers are ~60 million psi and ~55 million psi, respectively. Thus, the strain developed in reaching a given stress is a factor of five lower for boron and carbon than for glass and, although the tensile strength of carbon fiber is only ~250,000 psi compared to ~500,000 psi for glass (see Table IX), its use would allow pressure vessels to be designed with much lower working strains, and hence with much less severe barrier layer problems, than those encountered with glass-reinforced composites.

In view of the apparent potential of carbon fiber composites for cryogenic applications, their basic mechanical properties have been evaluated at temperatures down to 77°K and the main results of this work are summarised in Table XI. Both epoxy and polyester matrices were used for these composites and in all cases their strengths and moduli were found to follow the law of mixtures given in equations (4.26) and (4.28); thus, the full fiber strengths are realized by these composites. In contrast, those used by Hanson[124] in the experiments discussed earlier did not realize the full fiber potential and this was ascribed to low interlaminar shear strengths, the presence of voids, and to inherent flaws in the low-modulus Thornel 25

* Royal Aircraft Establishment, Farnborough, U.K.

Table XI. Typical Mechanical Properties for RAE Type I High-Modulus Carbon-Fiber-Reinforced Epoxy Composites

	50 vol.% fiber		30 vol.% fiber	
	295°K	77°K	295°K	77°K
Tensile strength,[a] psi × 10^3	110	—	63	65
Tensile modulus,[a] psi × 10^6	26	—	16.0	16.8
Failure strain,[b] %	0.45	—	—	—
Impact energy,[b]	5.8 ±0.3	5.7 ±0.5	4.0 ±0.3	—

[a] Tensile speciments with 1 in. parallel gauge length, 0.1 in. square section.
[b] Standard 55 by 10 by 10 mm Charpy bars with 2 mm deep V-notch.

filaments or defects produced during fabrication. As the RAE carbon-fiber composites were prepared by leaky mold techniques and not by filament-winding, further comparisons between these two sets of results is not possible.

It can be seen that strength, modulus, and impact energy increase with fiber content up to at least 50 vol.% fibers and that there is virtually no change in these properties on cooling from room temperature to 77°K. The low failure strain of ~0.45% is only slightly larger than that predicted for elastic failure, and hence fracture was essentially due to tensile rupture of the fibers. One possible disadvantage of carbon fibers for cryogenic applications lies in their high thermal conductivities as compared to glass fibers, and this effectively rules out their use for load-bearing insulating supports. It does, however, partially account for the excellent fatigue characteristics of carbon-fiber-reinforced composites, as the combination of high modulus (and hence low strain) and good thermal conductivity allows the material to run without the large temperature rise associated with glass-fiber-reinforced plastics. Furthermore, the material has a high damping capacity and other favorable dynamic properties. Further details of the ambient temperature properties of carbon-fiber-reinforced plastics are given in a report by Phillips[126] of RAE, and more up-to-date information can be obtained from the same source.

REFERENCES

Textbooks and Reference Works

1. H. Mark (Ed.), *Encyclopedia of Polymer Science and Technology*, John Wiley and Sons, New York, Vol. 1 (1964) to latest Vol. 11 (1969).
2. E. H. Andrews, *Fracture of Polymers*, Oliver and Boyd (1968).
3. F. W. Billmeyer, *Textbook of Polymer Science*, Interscience, New York (1962).
4. F. Bueche, *Physical Properties of Polymers*, Interscience, New York (1962).
5. J. D. Ferry, *Viscoelastic Properties of Polymers*, John Wiley and Sons, New York (1961).

6. P. J. Flory, *Principles of Polymer Chemistry*, Cornell University Press, Ithaca, New York (1953).
7. M. Gorden, *High Polymers*, Iliffe, London (1963).
8. G. F. Kinney, *Engineering Properties and Applications of Plastics*, John Wiley and Sons, New York (1957).
9. L. E. Nielsen, *Mechanical Properties of Polymers*, Reinhold, New York (1962).
10. G. R. Palin, *Plastics for Engineers*, Pergamon Press, Oxford (1967).
11. L. R. G. Treloar, *The Physics of Rubber Elasticity*, Clarendon, Oxford (1958).
12. A. V. Tobolsky, *Properties and Structure of Polymers*, John Wiley and Sons, New York (1960).
13. L. H. Van Vlack, *Elements of Materials Science*, Addison-Wesley, Reading, Mass. (1964).
14. J. Wulff (Ed.), *The Structure and Properties of Materials*, Vol. 1 ("Structure") and Vol. 3 ("Mechanical Behavior"), John Wiley and Sons, New York (1965).
15. E. Gillam, *Materials Under Stress*, Newnes-Butterworths, London, (1969).
16. *Plastics Engineering Handbook of the Society of the Plastics Industry*, 3rd ed., Reinhold, New York (1960).
17. *Plastics Year Book*, Iliffe, London. (1966).
18. "ASTM Standards on Plastics," Am. Soc. Testing Mat., Philadelphia (1964).
19. "B. S. Methods of Testing Plastics," British Standards Institution, London (1963).
20. A. S. Tetelman and A. J. McEvily, Jr., *Fracture of Structural Materials*, John Wiley and Sons, New York (1967).
21. B. Rosen (Ed.), *Fracture Processes in Polymeric Solids*, Interscience, New York (1964).
22. R. M. Ogorkiewicz, *Engineering Properties of Thermoplastics*, John Wiley and Sons, London (1970).
23. A. H. Landrock, "Properties of Plastics and Related Materials at Cryogenic Temperatures," PLASTEC Rept. No. 20, CDC Accession No. AD 469126 (1965).
24. T. T. Serafini and J. L. Koenig (Eds.), *Cryogenic Properties of Polymers*, Marcel Dekker, New York (1968).
25. K. D. Timmerhaus (Ed.), *Advances in Cryogenic Engineering*, Plenum Press, New York, latest annual volume 16 (1971).
26. L. J. Broutman and R. H. Krock, *Modern Composite Materials*, Addison-Wesley, Reading, Mass. (1967).
27. A. Kelly, *Strong Solids*, Clarendon, Oxford (1966).
28. G. S. Holister and C. Thomas, *Fibre Reinforced Materials*, Elsevier, Amsterdam, (1966).
29. D. V. Rosato and C. S. Grove, *Filament Winding: Its Development, Manufacture, Application and Design*, John Wiley and Sons, New York (1964).
30. P. Morgan, *Glass Reinforced Plastics*, Iliffe, London (1961).

Other References

31. V. A. Kargin and G. L. Slonimsky, "Mechanical Properties (of polymers)," in H. Mark (Ed.), *Encyclopedia of Polymer Science and Technology*, Vol. 8, John Wiley and Sons, New York (1968), p. 455.
32. I. Marshall and A. B. Thompson, *Proc. Roy. Soc.* **A221,** 541 (1954).
33. K. H. Meyer, C. von Susich, and E. Valko, *Kolloid.* **59,** 208 (1932).
34. A. Keller, in R. H. Doremus *et al.* (Eds.), *Growth and Perfection of Crystals*, John Wiley and Sons, New York (1958), p. 499.
35. M. Takayangi, *Mem. Fac. Sci. Kyush Univ.* **D23** (I), 41 (1963), quoted in Ref. 24, p. 173.
36. C. W. Bunn and E. R. Howells, *Nature* **174,** 549 (1954).
37. W. N. Findley and G. Khosla, *J. Appl. Phys.* **26,** 821 (1955).
38. H. G. Gibbs and D. W. Saunders, *Contemp. Phys.* **8,** 529 (1967).
39. M. L. Williams, R. F. Landel, and J. D. Ferry, *J. Am. Chem. Soc.* **77,** 3701 (1955).
40. E. Jenckel and E. Klein, *Z. Naturforsch.* **7a,** 619 (1952).

41. L. Mullins, *Proc. Inst. Rubb. Ind.* **20,** 235 (1947).
42. M. Gorden and B. M. Grieveson, *J. Polymer. Sci.* **29,** 9 (1958).
43. R. F. Robbins, "Behavior of Polymeric Materials at Cryogenic Temperatures," Rept. on NASA Contract H-92120 to N.B.S. Boulder, Colorado (1968).
44. R. N. Haward and J. Mann, *Proc. Roy. Soc.* **A282,** 120 (1964).
45. R. A. Horsley, *Trans. Plastics Inst.* **30,** 164 (1962).
46. J. P. Berry, *J. Appl. Phys.* **34,** 62 (1963); also, in *Fracture Processes in Polymeric Solids*, Interscience, New York (1964), p. 195.
47. O. K. Spurr and W. D. Niegisch, *J. Appl. Polymer Sci.* **6,** 585 (1962).
48. F. C. Frank, *Proc. Roy. Soc.* **A282,** 9, (1964).
49. P. I. Vincent, "Fracture (of polymers)," in H. Mark (Ed.), *Encyclopedia of Polymer Science and Technology*, Vol. 7, John Wiley and Sons, New York (1967), p. 292.
50. A. G. Thomas, "Fracture of Rubber," in "Proc. Int. Conf. on Physical Basis of Yield and Fracture," Inst. Phys. and Phys. Soc., London (1966), p. 134.
51. B. J. Lazan and A. Yorgiadis, "ASTM Symposium on Plastics," STP 59, Am. Soc. Testing Mat. Philadelphia, (1944).
52. "Bibliography of References—Low-Temperature Properties of Plastics," Cryogenic Data Center, N.B.S. Boulder, Colorado (February 1964).
53. "Bibliography of References—The Properties of Adhesives at Low Temperatures," Cryogenic Data Center, N.B.S. Boulder, Colorado (January 1963).
54. R. E. Mowers, Final Report, "Program of Testing Nonmetallic Materials at Cryogenic Temperatures," Rocketdyne Division of North America Aviation, Contracts No. RTD-TDR-63-11, OTS-AD. 294 772, CEL-NBS 17404 and 15840.
55. "Cryogenic Materials Data Handbook," N.B.S. Boulder, Colorado. Last updating (December 1961). Now superseded by Ref. 56.
56. F. R. Schwartzberg, S. H. Osgood, R. D. Keys, and T. F. Kiefer (Eds.), *Cryogenic Materials Data Handbook*, The Martin Co., Denver, ML-TDR-64-280 (August 1964); available from OTS as PB 171809 (revised).
57. P. D. Schuman, E. C. Stump, and G. Westmoreland, in Ref. 24, p. 263.
58. V. Englehardt, *Chem. Eng. News* **43,** 80 (1965).
59. R. B. Gosnell, in Ref. 25, Vol. 9 (1964), p. 139.
60. F. M. Wilson, in Ref. 25, Vol. 10 (1965), p. 145.
61. R. F. Robbins and P. R. Ludtke, *J. Spacecraft Rockets* **1** (3), 253 (May–June 1964).
62. R. F. Robbins, D. H. Weitzel, and R. N. Herring, in Ref. 25, Vol. 7 (1962), p. 343; paper R. 320 CDC N.B.S. Boulder, Colorado.
63. D. H. Weitzel, R. F. Robbins, and W. R. Bjorkland, in Ref. 25, Vol. 6 (1961), p. 219; *Rev. Sci. Instr.* **31** (12), 1350 (1960).
64. W. R. Walker, "Design Handbook for O-rings and Similar Elastic Seals," Dept. WADC TR 59-428, Part II Boeing Airplane Co. (April 1961).
65. K. B. Martin, T. H. Fields, E. G. Pewitt, and J. G. Fetkovitch, in Ref. 25, Vol. 9 (1964), p. 146.
66. F. A. Schreihaus and D. E. Robinson, in "Proc. 7th Natl. Symp. Adhesives and Elastomers for Environmental Extremes," Soc. Aerospace Mat. Process Eng. (SAMPE), Los Angeles, California (May 20–22, 1964).
67. J. Hertz, *Adhesives Age* **4** (8), 30 (1961); Rept. ERR-AN-032, General Dynamics, San Diego, California (January 25, 1961).
68. T. I. Bell, "The Low and Cryogenic Temperature Properties of Adhesives," Bibliography No. 233, RAE Farnborough (January 1963).
69. L. M. Roseland, "Adhesives for Cryogenic Applications," in Ref. 24, p. 17.
70. J. K. Kuno, in "Proc. 7th Natl. Symp. Adhesives and Elastomers for Environmental Extremes," Soc. Aerospace Mat. Process Eng. (SAMPE), Los Angeles, California (May 20–22, 1964).
71. R. C. Kansen, in "Proc. 7th Natl. Symp. Adhesives and Elastomers for Environmental Extremes," Soc. Aerospace Mat. Process Eng. (SAMPE), Los Angeles, California (May 20–22, 1964).

72. M. B. Smith and S. E. Susman "Development of Adhesives for Very Low Temperature Application," Final Report on NASA Contract 1565 Narmco R. & D. Division (May 1963); also, in Ref. 25, Vol. 8 (1963), p. 300.
73. "Adhesives for Cryogenic Applications," N.B.S. C.D.C. Boulder, Paper No. B-479 (August 1969).
74. Brief announcement in *Cryogenics* **10,** 77 (1970); details from Lewis Research Center, Cleveland, Ohio.
75. C. D. Bailey, W. D. Holland, and J. Hulsebos, SAE Paper No. 7460, Natl. Aeronautics and Space Eng. and Mfg. Meeting, Los Angeles, California (September 23–27, 1963).
76. R. P. Caren, R. M. Colston, A. M. C. Holmes and F. Dubus, in Ref. 25, Vol. 10 (1965), p. 171.
77. R. N. Miller, C. D. Bailey, R. J. Beall and S. M. Freeman, in Ref. 25, Vol. 8 (1963), p. 417.
78. S. T. Stoy, in Ref. 25, Vol. 5 (1960), p. 216.
79. J. S. Light, "Proc. Int. Conf. Materials ASTM-RILEM Philadelphia," (February 1964).
80. L. M. Roseland, Paper No. 1666, Natl. Aeronautics and Space Eng. and Mfg. Meeting, Los Angeles, California (September 23–27, 1963).
81. R. H. Kropschot, "Low-Temperature Insulation," in R. W. Vance and W. M. Duke (Eds.), *Applied Cryogenic Engineering*, John Wiley and Sons, New York (1962), Chapter 5.
82. J. Hertz, in Ref. 25, Vol. 11 (1966), p. 287.
83. J. F. Haskins and J. Hertz, in Ref. 25, Vol. 7 (1962), p. 353.
84. L. R. Stoeiker, in Ref. 25, Vol. 5 (1960), p. 273.
85. A. Cooper, *J. Plastics Inst.* **29** (80), 40 (1961).
86. R. M. McClintock, in Ref. 25, Vol. 4 (1958), p. 132.
87. R. N. Miller, C. D. Bailey, B. T. Beale, S. M. Freeman and E. F. Coxe, *Ind. Chem. Eng.* **1**, (4), 257, (1962).
88. D. J. Doherty, R. Hurd, and G. R. Lester, *Chem. Ind.* (*London*) **1962,** 1340.
89. J. D. Griffin and R. E. Skochdopole, "Plastic Foams," in E. Baer (Ed.), *Engineering Designs for Plastics*, Reinhold, New York (1964).
90. Article in *Cryogenic Engineering News*, **1969** (May), 20.
91. E. E. Bisson, R. L. Johnson, and W. J. Anderson, "Friction and Lubrication with Solid Lubricants at Temperatures to 1000°F with Particular Reference to Graphite," Proc. Inst. Mech. Eng. (London), Conf. Lubrication and Wear (1957), p. 348.
92. D. W. Wisander and R. L. Johnson, Ref. 25, Vol. 6 (1961), p. 210; Vol. 4 (1960), p. 71; Vol. 3 (1960), p. 390.
93. D. H. Tantam and R. Hargreaves, in Ref. 25, Vol. 6 (1961), p. 228.
94. W. A. Wilson, K. B. Martin, J. A. Brennan, and B. W. Birmingham, in Ref. 25, Vol. 6 (1961), p. 245; Vol. 7 (1962), p. 262.
95. The Lafage Aluminous Cement Co. Ltd., Lafage House, 207 Sloane St., London S.W.I.
96. L. Holiday (Ed.), *Composite Materials*, Elsevier, Amsterdam (1966).
97. A. Kelly, "Fibre Reinforcement of Metals," H.M.S.O., London (1965).
98. A. Kelly and G. J. Davies, *Met. Revs.* **10,** 1 (1965).
99. D. Cratchley, *Met. Revs.* **10,** 79 (1965).
100. R. Hill, *J. Mech. Phys. Solids* **11,** 357 (1963).
101. D. L. McDanels, R. W. Jech, and J. W. Weeton, *Metal Prog.* **78** (6), 118 (1960).
102. D. L. McDanels, R. W. Jech, and J. W. Weeton, *Trans. Am. Inst. Min. Metall. Petrol. Engrs.* **233,** 636 (1965).
103. A. Kelly and W. R. Tyson, in V. F. Zackay (Ed.), *High-Strength Materials*, John Wiley and Sons, New York (1965), p. 578.
104. W. H. Sutton, B. W. Rosen, and D. G. Flom. *SPE J.* **20,** 1 (1964).
105. J. O. Outwater, *Mod. Plastics* **33,** 156 (1956).
106. S. W. Tsai, NASA Rept. DR-224 (1965), quoted in Ref. 27, p. 153.

107. J. W. Davis and N. R. Zurkowski, Tech. Rept. Minnesota Mining and Mfg. Co., Reinforced Plastics Div., quoted in Ref. 26, p. 370.
108. F. J. McGarry and M. B. Desai, "Failure Mechanisms in Fibreglass Reinforced Plastics," Proc. 14th Conf. SPI Reinforced Plastics Div., Section 16-E (1959).
109. H. L. Cox, *Brit. J. Appl. Phys.*, **3**, 72 (1952).
110. B. W. Rosen, in "Fiber Composite Materials," Am. Soc. Metals, Cleveland, (1965), p. 37.
111. H. Schuerch, NASA Rept. CR-202 (1965).
112. J. Cook and J. E. Gorden, *Proc. Roy. Soc.* **A282,** 508 (1964).
113. N. O. Brink, "Determination of the Performance of Plastic Laminates under Cryogenic Temperature," ASD-TDR-62-794, Narmco Res. and Dev., San Diego, California (August 1962).
114. D. W. Chamberlain, *Ibid.*, Part II (March 1964).
115. D. W. Chamberlain, in Ref. 25, Vol. 10 (1965), p. 117.
116. D. W. Chamberlain, in Ref. 25, Vol. 9 (1964), p. 131.
117. R. D. Keys, T. F. Kiefer, and F. R. Schwartzberg, in Ref. 25, Vol. 11, (1966), p. 470.
118. L. M. Soffer and B. Molho, in Ref. 24, p. 87.
119. S. S. Oleesky and J. G. Mohr, *Handbook of Reinforced Plastics*, Reinhold, New York (1964).
120. J. Hertz, "The Effect of Cryogenic Temperatures on the Mechanical Properties of Reinforced Plastic Laminates," *SPE J.* **21,** (2), 181, (1965).
121. J. M. Toth, Jr., in Ref. 25, Vol. 9 (1964), p. 537; also Douglas Aircraft Co. Santa Monica, Rept. SM-42594 (1962).
122. J. M. Toth, Jr., and J. R. Barber, in Ref. 25, Vol. 10 (1965), p. 134.
123. L. M. Roseland, "Filament Winding Materials for Cryogenic Application," Eng. Paper No. 1666, Douglas Missile and Space Systems Div. (September 1963).
124. M. P. Hanson, "Glass-, Boron-, and Graphite-Filament Wound Resin Composites and Liners for Cryogenic Pressure Vessels," in Ref. 24, p. 29.
125. D. A. Wigley, R. A. Heaver, R. J. Robinson, and J. F. Harper, unpublished work.
126. L. N. Phillips, Royal Aircraft Establishment Farnborough Tech. Rept. 67088 (April 1967).
127. A. Burwood-Smith, "Mechanical Properties of Refractory Metal Wires for High-Temperature Reinforcement," N.G.T.E. Note 739, National Gas Turbine Establishment, Pystock, Hants, U.K. (December 1968).
128. R. F. Lark, in Ref. 24, p. 1.
129. L. M. Roseland, "Evaluation of Structural Adhesives for Potential Cryogenic Use," in Section 7 of "Proc. 7th Natl. Symp. Adhesives and Elastomers for Environmental Extremes," Soc. Aerospace Mat. Process Eng. (SAMPE), Los Angeles, California (May 20–22, 1964).

Chapter 5

Testing Methods and Techniques

Although it is not possible to give a detailed account of the variety of equipment used to test the mechanical properties of materials at low temperatures, a brief description is given here of some of the main types of apparatus that have been employed in obtaining the results discussed in the earlier chapters. As noted in section 1.1, the uniaxial tensile test is the technique most widely used for obtaining both fundamental and design data and a large number of different tensile cryostats have been employed for this purpose.[1] Apart from the natural preference of most experimentalists to design their own equipment, there is a more fundamental reason for the development of such a variety of cryostat systems. It is, in most cases, desirable to have a machine which is as "stiff" as possible in order to observe the sharp yield and serrated stress–strain curve phenomena which were discussed in section 2.4. To achieve such stiffness, relatively massive pull-rods are needed to transmit the applied stresses, but this requirement contradicts the other basic necessity of any piece of cryogenic equipment, namely the need to minimize the heat leak into the cryogenic fluid. Thus, each design represents a compromise between these factors in addition to the usual optimization of the conflicts between initial costs and running costs, simplicity and versatility, etc. In consequence, many tensile cryostats for use at 4°K have a much restricted load capacity in order to keep the liquid-helium consumption down to a reasonable level and this in turn means that specimen sizes have to be reduced accordingly. For fundamental research, this is not usually too serious a limitation, but care has to be taken if such results are to be used for design purposes, as such small specimens do not always give a true indication of the properties of larger sections of the same materials.

In writing this chapter, the emphasis has been placed on describing the basic types of tensile cryostat, their cooling systems, and some of the more commonly used attachments, as it is thought that these topics are likely to be of most general interest. It is recognized that the more specific and complex tests, such as the biaxial tensile test,[2] are often needed for the

generation of design data, but it is considered that such equipment is outside the scope of this text. Similarly, the main types of strain-measuring equipment are discussed, but here again it has been necessary to restrict the coverage to a general survey of the basic principles involved.

The techniques used in testing mechanical properties at low temperature have been reviewed by Rosenberg,[3] Schwartzberg,[4] Klajvin,[5] and Arsenault,[2] while most workers have described their own techniques in detail either in internal reports or in the open literature. It should be noted that the examples used in the following section have been chosen to illustrate the basic principles involved and are thus not necessarily the most up-to-date or efficient models available.

5.1. BASIC TYPES OF CRYOSTAT AND COOLING SYSTEMS

Although much of the equipment used by the early research workers was purpose-built for their experiments, most cryostats are now designed

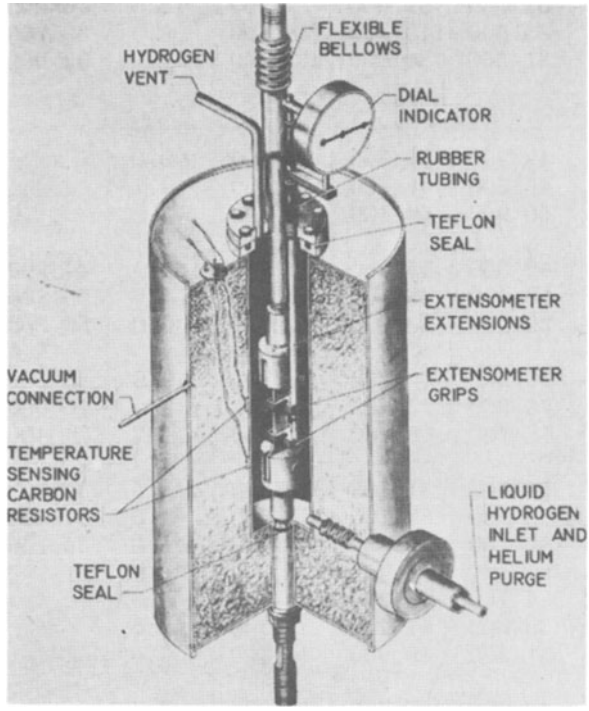

Fig. 5.1. Simple foam-insulated cryostat capable of use down to 20°K (Hanson *et al.*[6]).

for use with one of the many testing mechines which are produced commercially. In many of these machines, a tensile specimen is strained between a fixed upper crosshead, which also supports the load cell, and a downward-moving lower crosshead. For testing at temperatures above ambient, it is common practice to surround the specimen with a furnace or an oven which can produce the desired temperature and it is a logical extension of this concept to replace the furnace by a cryostat for testing at low temperatures. Many of the facilities built to obtain engineering design data at 77 and 20°K were of this type, a typical example being that used at NASA—Lewis Research Center[6] and shown in Fig. 5.1. This very simple foam-insulated cryostat is more than adequate for use with liquid nitrogen and could be used at 20°K, although it has a rather excessive liquid-hydrogen consumption of about 30 liters per test! This figure can be improved considerably by the use of the more efficient vacuum and liquid-nitrogen insulation, and more sophisticated cryostats of this type have been built.[7,8] For example, the Battelle[9] equipment had a capacity of 200,000 lb and was able to fracture high-strength steel specimens with diameters in excess of 0.5 in., yet it only used about 6–7 liters of hydrogen per test. However, such cryostats are not really suitable for use with liquid helium, due to the high heat leaks along the pull rods (especially the lower pull rod, as it is not cooled by the cold evaporated gas as is the upper rod). McClintock and Warren[10] have attempted to overcome this problem by designing a cryostat in which the force on the lower end of the specimen is transmitted through a stack of thin, stainless steel washers which have a very low net thermal conductivity, especially under zero-load conditions. Their cryostat had a capacity of 5000 lb and used $2\frac{1}{2}$ liters of liquid hydrogen or 3 liters of liquid helium per test; one possible disadvantage of this arrangement is, however, the loss of machine stiffness which results from the use of the stack of washers.

Most cryostats used for tensile testing in liquid helium are of the type illustrated in Fig. 5.2, which employs a compression cylinder and load cup to transmit the force to the lower grip. This arrangement obviates the need for a lower pull rod and specially modified Dewars, thus allowing standard glass or metal Dewars to be used. Furthermore the large surface area of the load cylinder facilitates efficient cooling by the cold, evaporated gas and thus minimizes the heat leak into the liquid helium. The NBS cryostat shown in Fig. 5.2 has a load capacity of 10,000 lb and uses between 2 and 5 liters of liquid hydrogen or 3 and 7 liters of helium, depending on the time taken to carry out the test. Axial loading is ensured by the use of spherically seated connections to the load cell at the top of the straining frame and to the compression cup at the bottom of the cryostat; the axiality may be checked by using a specimen which has strain sensors on opposite sides, thus allowing any bending to be detected. Similar

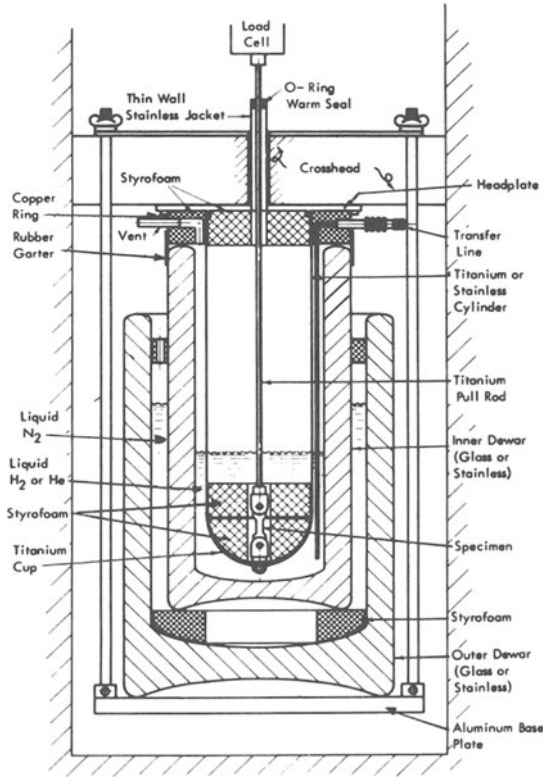

Fig. 5.2. Typical tensile cryostat for testing at 4°K (Reed[24]).

cryostats have been described by Hull and Rosenberg,[11] Basinski,[12] Klajvin,[5] Arsenault,[2] and many others.

One feature common to both types of cryostat considered so far has been the cooling technique, which entails simply filling the Dewars surrounding the specimen with the appropriate cryogenic fluid. The range of available testing temperatures can be extended somewhat by pumping over the liquid to reduce its temperature, but even so, this still leaves the temperature intervals between 5 and 14°K, 20 and 60°K, and above 90°K inadequately covered. In Basinski's cryostat, intermediate temperatures are attained by using helium (or nitrogen) gas to achieve heat exchange between the specimen and an electrically heated copper cylinder which surrounds it, but this technique is unable to cope adequately with the heat generated adiabatically during a tensile test (see section 2.4). A more satisfactory system is that developed by Wessel[13] and illustrated in Fig. 5.3. The central part of the equipment is the "helium distributor and tempera-

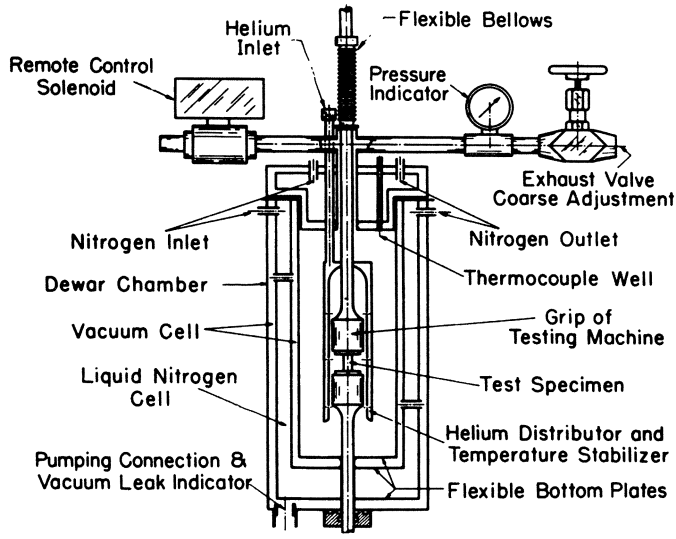

Fig. 5.3. Tensile cryostat for testing at temperatures in the range 4° to 77°K (Wessel[13]).

ture stabilizer" which surrounds the specimen and directs a continual stream of atomized liquid helium onto the specimen and the heads of its grips. In this way, the latent heat is evolved where it is most needed and the enthalpy of the cold gas is then used to cool the remainder of the cryostat before it is pumped off through the solenoid valve at the top. Sensing thermocouples placed on the specimen are used to control the duty cycle of the solenoid valve (and thus the rate at which liquid helium is supplied) to hold the required temperature constant to better than ±1°C. Discaloy (25 Ni, 13.3 Cr, 2.75 Mo, 2.25 Ti, 0.81 Mn, 0.72 Si, 0.07 Al, 0.076 C, Bal Fe) is used for the grips, as this alloy has the desired combination of high strength and toughness and low heat capacity and thermal conductivity at low temperatures. The net result was a machine with a capacity of 20,000 lb, yet which used only 2 liters of liquid helium for cooldown and for a 30-min test at 4°K, while at 50°K, the consumption dropped to 0.75 liter per test. In view of its economical performance it is, perhaps, surprising that relatively few cryostats of this type seem to have been built. One possible reason could be that, for engineering purposes, it is usually sufficient to interpolate between the results obtained at 4, 20, and 77°K using the simpler cryostats described earlier. One modification of the basic Wessel technique worth noting is that of Behrsing and Lucas,[14] in which epoxy-coated Styrofoam is used as an insulant, sections of which may be removed from the side to allow access to the specimen without removing the rest of

the cryostat. The less efficient insulation does, however, raise the helium consumption to about 4–6 liters per test at 4°K.

5.2. MODIFICATIONS, VARIATIONS, AND SPECIAL-PURPOSE ATTACHMENTS

5.2.1. Multiple-Specimen Testing

There are two basic and interrelated drawbacks to the type of cryostat described so far: the length of time taken to complete each cycle of cool-down, test, and warmup to ambient, and the cost of the liquid hydrogen or helium used to cool the apparatus prior to each test. The obvious solu-

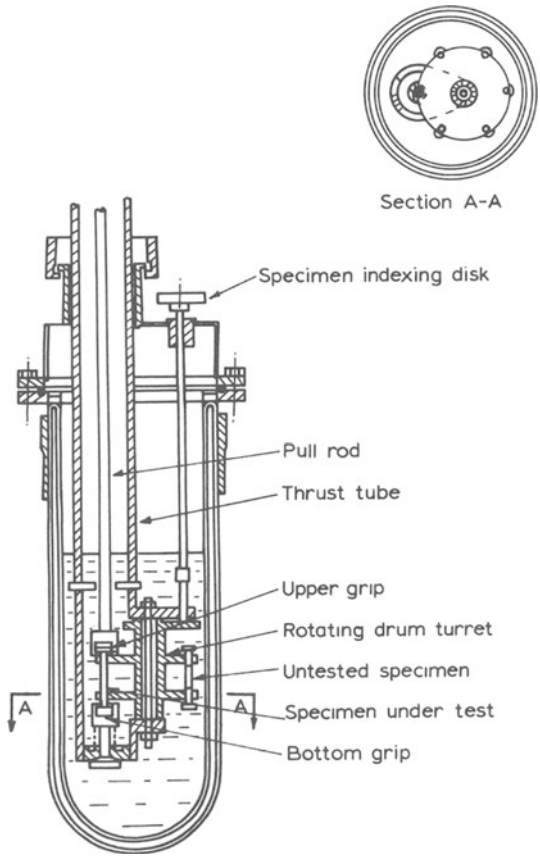

Fig. 5.4. Device for changing tensile specimens while at low temperatures (Gindin *et al.*[15]).

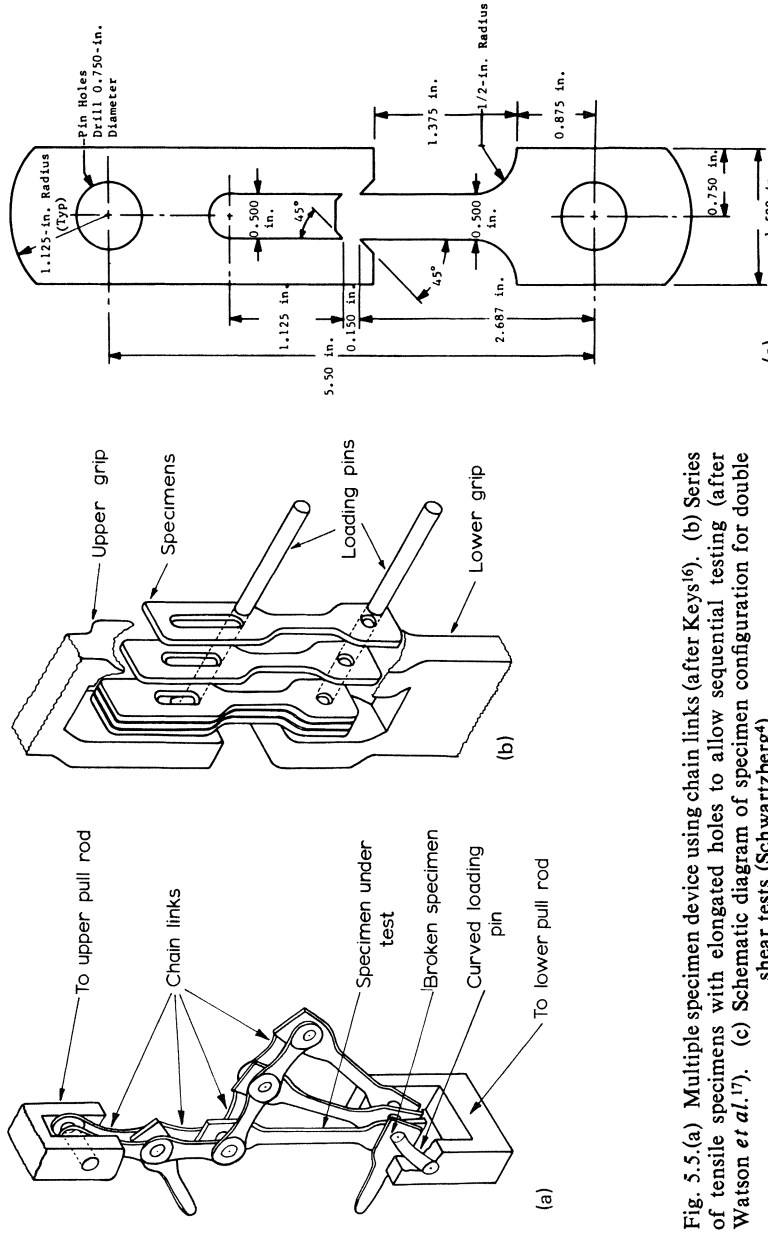

Fig. 5.5.(a) Multiple specimen device using chain links (after Keys[16]). (b) Series of tensile specimens with elongated holes to allow sequential testing (after Watson *et al.*[17]). (c) Schematic diagram of specimen configuration for double shear tests (Schwartzberg[4]).

tion to this problem is to construct a device which allows a number of specimens to be loaded at room temperature, cooled, and then tested sequentially at low temperature; various mechanisms have been developed which achieve this aim more or less successfully. One example developed by Gindin *et al.*[15] is shown in Fig. 5.4. Six cylindrical specimens are stored in a drum-turret which can be rotated so that each specimen in turn is brought into line with the tensile axis. The grips are tapered in such a way that the fracture halves may be removed and retained in the drum so that the next specimen may be tested. It is claimed that the use of this device improves productivity by about a factor of five and reduces the consumption of liquefied gas to about one-seventh of its previous value. Not all multispecimen devices would produce such a reduction in refrigerant costs, as they tend to be more massive than single-shot machines and hence to use more liquid during cooldown.

Two methods for testing multiple specimens which are in the form of thin sheets are shown in Fig. 5.5(a, b). That of Fig. 5.5(a) is due to Keys[16] and employs a system of chain links to couple together the "top ends" of the specimens and also to serve as their loading pins. Once the first specimen has been fractured, further upward movement of the pull rod brings the next specimen into a vertical position ready for testing and the sequence continues until all the specimens have been tested. Axial loading is achieved by curving the lower loading pin, onto which all the specimens are loaded, so that each specimen will be at the top of the pin when it is tested.

In the method of Fig. 5.5(b) due to Watson *et al.*,[17] the specimens are all loaded side by side in the upper and lower pins and the use of successively more elongated holes at the top of each specimen enables them to be tested sequentially. Universal joints below the grips permit axial alignment of the specimens during test. In both of these systems, there is very little lateral pressure on the specimens at the loading pins and it is normal for doublers to be bonded to the ends of the specimens to spread the load and to prevent buckling or fracture beneath the loading pin.

One further point worthy of note is that both these devices are suitable for use with the double-shear sheet specimen[4] illustrated in Fig. 5.5(c). This configuration enables shear tests to be carried out in a tensile cryostat without the modifications needed for other techniques such as the double-pin shear test.[18]

Extensometry is a problem with most multitest devices and the most common solution is to use strain gauges bonded directly to each specimen. Although care has to be taken to protect the electrical connections to the gauges from mechanical damage, this technique has been used successfully by Keys and his co-workers[16] in the device shown in Fig. 5.5(a).

5.2.2. Compression Testing

Values of the compressive strengths of materials are often required for design purposes and in many cases it is possible to obtain such data by direct measurement. As, however, it is rarely possible to test ductile metals

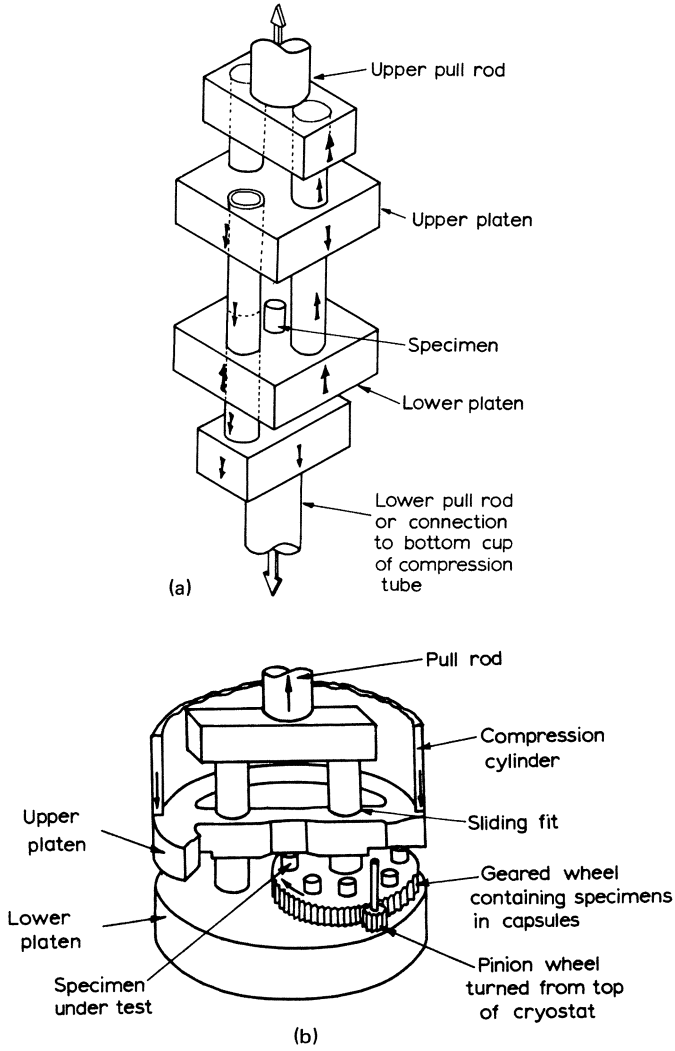

Fig. 5.6.(a) Fixture to allow compression testing in a tensile cryostat. (b) Device to enable compression specimens to be tested sequentially at low temperatures (after Taylor[20]).

satisfactorily in compression (due to difficulties encountered with compression instability and frictional restraint by the platens), most work has been concentrated on high-strength, low-ductility alloys and composites such as glass-reinforced plastic.[19] From a more fundamental point of view, many of the research groups working on the mechanical properties of bcc metals at low temperatures have employed compression tests because they not only utilize small, easily machined specimens but also allow tests to be carried out at loads in excess of the tensile failure stress of the metal.

The equipment used for compression testing at room temperature often consists simply of a pair of flat, hardened-steel platens attached to each crosshead, but for low-temperature use, a compression cage such as that shown schematically in Fig. 5.6(a) is normally attached to an existing tensile cryostat. The two rods fixed to the upper pull-rod exert an upward force on the lower platen, while the upper platen is restrained by the rods attached to the lower grip. The rods and platens are accurately machined to give a good sliding fit between them and thus keep the platens accurately parallel to each other during testing. Furthermore, all components are usually made from the same material in order to avoid any possible trouble with binding caused by differential contraction between dissimilar metals.

Once again, there are large advantages to be gained if a multitest capability is designed into the apparatus, and one such device[20] is illustrated schematically in Fig. 5.6(b). A gear wheel rotates about one of the two rods which support the lower platen, and holes are drilled in the gear to take the ten specimens, which are contained in separate capsules each fitted with a plunger. The bottom of the gear is cut like a ratchet so that it can only be turned freely in one direction; when it is turned back, it engages on a stop positioned so as to locate the specimen to be tested accurately on the loading axis. One additional advantage of such an arrangement is that it permits the specimens to be retrieved after straining so that they may be examined or retested if required, as, for example, in temperature-change experiments.

Other multispecimen devices for compression testing have been designed: that developed by the Martin Co.[4] also employed a rotating plate to change the specimens, while Altshuler's[20] used a pawl mechanism.

5.2.3. Flexural, Torsional, and Other Tests

A further important type of test is the flexural test, which is usually carried out with either the three-point bending configuration illustrated schematically in Fig. 5.7(a) or the four-point of Fig. 5.7(b). The three-point configuration is simpler, but the four-point one has the advantage of imposing a constant radius of curvature in the section of the specimen between the central knife-edge supports, and this simplifies both measurement

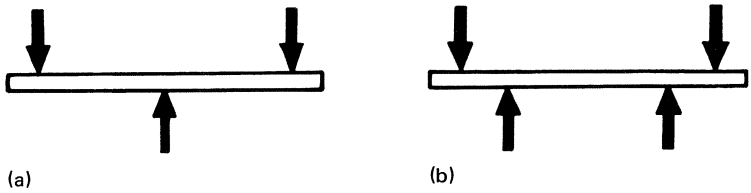

Fig. 5.7. Schematic representations of a) 3 point and b) 4 point bend test configurations.

of the strain developed and also calculation of the tensile and compressive stresses involved. As specimens used in flexural tests do not need the complicated machining required for tensile specimens, flexural tests are often used for preliminary investigations and the results converted to tensile strengths using the formulas which describe the tensile stresses developed in a bent beam. A further advantage of the four-point geometry is that the load on the central portion of the specimen is applied through two knife edges and there is thus less likelihood of localized fracture than with the three-point geometry, in which the whole load is applied through a single knife edge. The span-to-depth ratio of the specimens is usually specified by the relevant standards; for example, the ASTM recommendation for glass-reinforced plastics is that the span-to-depth ratio should be 16 plus 4 or minus 2, while short bend tests are used to measure the interlaminar shear strengths of composite materials.

As before, three- or four-point bending rigs are usually made to fit on to existing tensile cryostats. Thus, in the examples shown in Fig. 5.7(a, b), it would be quite simple to arrange that the load on the outer knife edges was supported by the compression tube while the upward force was applied via the central pull-rod. Furthermore, the advantages of multispecimen testing devices still hold for flexural testing and the use of such a device has been reported by the Martin Co.[4]

Other attachments which are sometimes fitted to a tensile cryostat include those for measuring bearing strength,[19] the shear or tensile strength of adhesive joints,[19] and other, more specialized requirements. Hardnesses can be measured by using similar fitments, but Battelle[21] found it easier to fit an extension to the indenter of a standard Vickers machine so that the impressions could be made at cryogenic temperatures on specimens clamped to a small stage suspended in an open-mouthed Dewar. In this case, the indentations were measured subsequently at room temperature, but Hull and Rosenberg[22] have shown that it is possible to carry out optical metallography at low temperatures using a cryostat in which the specimens are mounted on top of a cold finger to bring them up into the focal plane of the microscope.

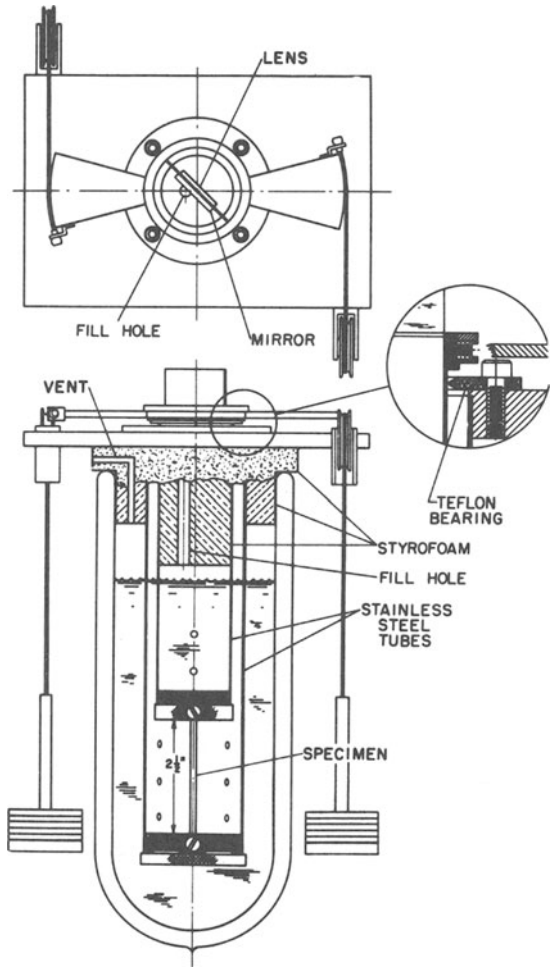

Fig. 5.8. Cryostat for testing specimens in torsion (Mikesell and McClintock[23]).

Torsional properties are best measured in purpose-built cryostats such as that developed by Mikesell and McClintock[23] and shown in Fig. 5.8. A static couple is applied to the specimen by the rotation of the inner stainless steel tube relative to the outer tube, which remains stationary. An optical lever is used to measure the strain developed by the specimen, and to avoid hysteresis effects, the shear modulus is taken as the average of the values measured during loading and unloading.

5.2.4. Fatigue Testing

As we saw in section 3.4.1, fatigue failure is of interest both from a fundamental point of view and because it is a frequent mode of failure in engineering structures. The equipment used to carry out fatigue tests reflects this spread of interests, ranging from the simple arrangements used for fundamental studies on small specimens of pure metals to the complex rigs used to reproduce the type of stresses likely to be developed in real structures. Thus, in their studies on pure copper, aluminum, silver, gold, etc., McCammon and Rosenberg[25] used a Goodman's vibration generator to apply an alternating axial compressive–tensile stress to small specimens with a minimum diameter of 0.5 mm. On a larger scale, flexural tests on thin sheets were carried out by Battelle[26] using cantilevered specimens shaped in such a way as to keep the outer fiber stress constant, the vertical deflection being produced by drive shaft connected to a conventional cam-operated reverse bending fatigue machine.

Although bend tests are relatively simple to perform, the stress applied varies from tensile in the outer fiber through zero on the neutral axis to compressive on the inner fiber, and this is not representative of the stress system likely to be found in aerospace structures such as fuel tanks. Here, stresses are much more likely to be of the alternating tension–compression mode and thus a number of fatigue cryostats have been developed to reproduce this type of loading in reasonably large specimens. Keys and Schwartzberg[27] have designed a cryostat which operates in conjunction with a commercial axial loading fatigue machine, the entire cryostat vibrating at the machine speed of 1800 Hz. Very precise fitting is, however, essential, as a misalignment of 0.001 in. in a sheet specimen 0.100 in. thick would induce a bending stress of the same magnitude as the applied stress. Nachtigall *et al.*[28] have also performed axial fatigue tests on both notched and unnotched sheet specimens using a cryostat which fitted onto a modified Krouse machine. As the maximum cycling rate used was 33 Hz, particular attention had to be paid to minimizing heat leaks into the cryostat so as to keep refrigerant consumption to a minimum. Chamberlain's[29] cryostat differs from the two previously mentioned not only in being designed for use with nonmetallic materials, but also in using a load-carrying cylinder to avoid the need for the lower grip to be taken out through the bottom of the cryostat. Dynamic seals were thus at room and not cryogenic temperatures, but even so, it was found necessary to use PTFE O-rings, as Neoprene rings coated with silicone grease did not always last through the 12 or so hours needed to complete a test to 10^6 cycles. Finally, as we saw in section 3.4.1, high-stress, low-cycle fatigue tests are of particular interest, as they reproduce the type of loading experienced by heat exchangers and

other periodically cooled equipment. Such tests have been carried out by General Dynamics/Astronautics[30] at temperatures down to 20°K using a hydraulically operated machine which had a period of 6 cycles per minute. Tests were carried out on sheet specimens of a number of alloys both in the as-received and welded conditions.

5.2.5. Impact Testing

The advantages and disadvantages of impact tests, particularly those using Charpy V-notch specimens, are discussed at some length in chapters 3 and 6 and the main conclusion drawn is that they are of most use with ferrous alloys which undergo a shear-to-cleavage fracture transition at low temperatures. No ferrous alloys are, as yet, approved for use below 77°K and this rather conveniently happens to be the lowest temperature at which it is easy to test specimens by the technique of rapidly transferring them from the refrigerant to the anvils of the impact machine. If the specimens are fractured within about 4–5 sec of leaving the refrigerant, it is found that the temperature rise is limited to a maximum of about 5°C and this is accurate enough for most applications. If greater precision is required, it is possible to limit the temperature rise by surrounding the specimen with a thin paper boat or by sticking pieces of foam or other absorbent material to those faces of the specimen that do not come into contact with the anvil or the pendulum striker; in this way, some refrigerant is kept in contact with the specimen for a few seconds. This technique has even been used by some workers to carry out impact tests down to 20°K, but more sophisticated arrangements are necessary if accurate control is to be obtained over the specimen temperature, due to the low specific heats of metals at these low temperatures. As two of the main sources of heat input are by convection and by condensation of air onto the specimen, De Sisto[31] placed a complete impact machine into an evacuated enclosure to prevent heating due to these two mechanisms. A storage and cooling system was used which could handle 105 specimens without reloading and the whole testing cycle could be controlled from outside the enclosure. A similar, but less elaborate, approach to this problem was adopted by Kiefer *et al.*,[32] who fitted a tent around their testing machine and purged it with hydrogen or helium gas to prevent air condensing on the specimens. Yet another approach was adopted by Eash,[33] who designed a sophisticated device which used pressurized helium gas to transfer miniature Izod-type specimens from a cryostat to the anvil only a fraction of a second before they were fractured by the striker.

Materials tested at and below 20°K in these machines include a number of stainless steels, aluminum and titanium alloys, and other nonferrous alloys of interest for potential low-temperature applications. As few of

these materials fail by cleavage and the transition from low-energy shear to high-energy shear does not show up very clearly on standard Charpy or smaller-sized specimens, doubts have been raised as to the suitability of impact testing at temperatures below 77°K. Indeed, as experience with fracture toughness and crack opening displacement techniques builds up, it appears that these more rigorously based approaches to the problem of fracture are likely to take precedence over the cruder impact tests.

5.3. EXTENSOMETRY

When a load is applied in a tensile test, the crossheads move apart, this motion is transferred to the specimen via the pull rods and grips, and the extension so produced may be converted to a strain if the specimen has a suitable parallel gauge length. This sequence of events also describes, in ascending order of accuracy, the ways in which extension or strain are commonly measured: thus, the simplest and least accurate technique is to measure the crosshead displacement, subtract from this the displacement due to the machine itself, and then ascribe the resultant to the specimen. The machine correction is usually measured by replacing the specimen with a stiff link and a large part of this deflection is commonly found to be due to the load cell. If greater precision is required, some form of extensometer is needed. In some cases, such as when using very soft specimens, the extensometer is attached to the shoulder of the specimen or even to its grips, but whenever possible, it is preferable to clamp it over the gauge length of the specimen itself, as the extension produced can then be converted directly to strain.

Extensometers for use at room temperature are normally relatively massive and complex devices in which the extension is read off from a dial gauge or through a telescope, but for high- or low-temperature use, these systems are usually impracticable, as access to the hot or cold zone is too restricted. There are two basic ways of overcoming this difficulty; in one, a system of mechanical links is used to transmit the deflection from the cold zone to the measuring device mounted at room temperature (the simplest such example being an accurate dial gauge), in the other, the extension is converted into a change in electrical resistance, voltage, or capacitance, etc., which can be taken out of the cold zone through thin leads. As an electrical output is most convenient for feeding directly into recording devices such as strip or X–Y recorders, many workers have combined these two approaches by using extension arms with one end clamped to the specimen and the other end activating an externally mounted transducer.

With the exception of directly bonded strain gauges (which have their own disadvantages), all other forms of extensometer suffer from the major

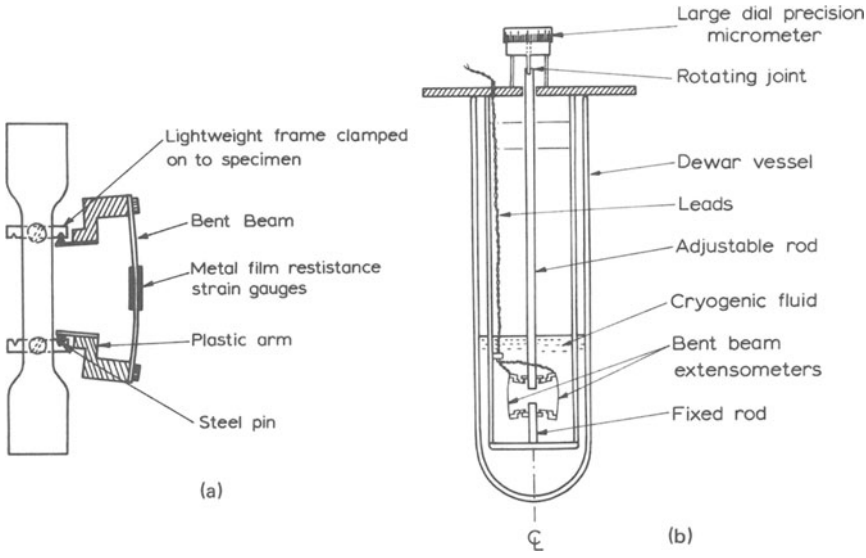

Fig. 5.9.(a) Technique used for attaching extensometers to tensile specimens.
(b) Device for calibrating extensometers for low temperature use.

drawback of needing to be attached mechanically to the specimen. This almost invariably leads to the introduction of stress-raisers which influence the plastic deformation or fracture mode of the specimen. For example, most extensometers rotate about knife edges or needle points, which tend to dig into soft materials or to form microcracks which nucleate fracture in the more brittle ones. There are a number of techniques which have been tried, more or less successfully, in an attempt to overcome this problem, perhaps the most common being the use of lightweight clamps attached to the specimen so that they spread the load placed on it while providing a firm support for the extensometer needles or knife edges (Fig. 5.9a)[34]. Another method which is most suitable for sheet materials is to shape the specimens so that they have "pips" on their sides which enable the extensometers to be attached without digging into the specimen proper.

For most purposes, accurate extensometry is needed for the initial stages of deformation only. Thus, for reliable determination of the 0.1 or or 0.2% proof stress, British Standard 18 (1962) recommends that the accuracy should be within $\pm 0.005\%$ of the gauge length; this limit is reduced to $\pm 0.001\%$ if Young's modulus is required, and a similar accuracy combined with high sensitivity is desirable for measurement of Poisson's ratio because of the small magnitude of the transverse strain. Once these quantities have been obtained, such accuracy is rarely needed, except perhaps for fundamental studies on the mechanisms involved in plastic deformation,

and most extensometers would be damaged if they had to operate over the full strain range developed by many ductile materials. Accordingly, it is usual to design their attachments so that they fall off, or can be taken off, as the extension exceeds a certain value, and Fig. 5.9(a) shows such an arrangement used in conjunction with a bent-beam extensometer. As the total plastic deformation (ductility) is usually only required to be measured to the nearest 1%, it is sufficient to obtain this from the movement of the crossheads or by fitting together the fracture halves and measuring between prescribed gauge length markers.

Most extensometers are made for use at room temperature and are calibrated accordingly. To recalibrate for low temperatures, or to obtain periodic checks on this calibration, it is normal to employ some simple device such as that illustrated schematically in Fig. 5.9(b). This is built around a precision micrometer whose large dial enables accuracies of the order of 1×10^{-5} in. to be obtained over a 2-in. range. A stainless steel extension is used to transmit the micrometer deflection to the extensometer at the bottom of the cryostat, care being taken to prevent rotation of the rod and to minimize any backlash. Thus, the extensometer is effectively mounted across two halves of a dummy specimen, whose separation can be varied as required to give a direct calibration of the extensometer output.

Extensometers which have been used in measurements at low temperatures fall into one of three basic categories: those based on resistive strain gauges, on capacitance gauges, and on transducers such as the linearly variable differential transformer.

5.3.1. Resistive Strain Gauges

Although some strain gauges are still made from thin metal wires, those used for cryogenic purposes are almost exclusively of the evaporated metal foil type with an integral polymeric backing. They are attached to a specimen by using one of the adhesives discussed in section 4.1.3, such as the polyurethanes or epoxy–nylons, and one of the most important factors in the successful use of such gauges lies in choosing a suitable adhesive and applying it in as thin a layer as possible. The fundamental assumption underlying the use of these gauges is that the adhesive and substrate transmit accurately the strain ϵ developed by the specimen to the resistance element, the resultant change in resistance then being given by the equation $\Delta R/R = K\epsilon$, where K is the gauge factor (sometimes also known as the strain sensitivity). As K is temperature-dependent, it is necessary to calibrate the gauges before use at low temperatures. Suitable devices have been described by Chiarito,[35] McClintock,[36] and others, most of them being based on a bent beam which enables a known strain to be applied to the gauge under test. One aspect not always emphasized is that usually

only one or two samples are tested from a given batch of gauges and it is then assumed that the other gauges have similar characteristics. In practice, this assumption is normally adequate, but it does demand that a consistent technique be used for attaching the gauges. The most suitable types of gauge are usually those whose K factor is least temperature-sensitive over the range to be covered by the required tests, and Armour D and Nichrome V have been widely used down to 20°K.

Although integrally bonded strain gauges are convenient and simple to use, most suitable types of gauge are relatively expensive (of the order of 5–25% of the total cost of the test) and they cannot normally be reused. Many investigators therefore prefer to use strain gauges mounted on some form of bent beam extensometer, in which one or more gauges are attached to a thin beam which is mounted on a specimen in the manner described in the previous section. The sensitivity of such a device depends on a number of factors, such as the length and thickness of the beam, its height above the specimen, etc., and once constructed, it is most conveniently calibrated using the type of cryostat described in Fig. 5.9(b). The applied displacement can then be correlated directly with the output from the a.c. bridge or whatever circuitry is used to detect the resistance changes. One practical point worthy of note is that it is most convenient to have both active and passive gauges at cryogenic temperature in order to minimize adverse temperature effects, while adequate protection and waterproofing of the gauges are necessary, as good electrical insulation is required if maximum sensitivity and reliability are to be achieved.

Warren and Reed[37] have described a more elaborate version of the basic bent beam device which is able to operate reproducibly up to strains of about 85%, but the penalty paid for this extended range is an increase in weight and complexity which may not always be acceptable. Yet another variation on the same theme is provided by the compliance gauges which are used in the K_{Ic} fracture toughness or COD tests described in chapter 3, these being basically bent beam devices designed to operate with high sensitivity over a limited strain range.

5.3.2. Displacement Transducers

There are two main types of displacement transducer; the linearly variable differential transformer, in which a movable ferromagnetic armature varies the coupling between the primary winding and two secondary windings connected in series opposition, and the linearly variable differential inductance, in which the armature varies the inductive coupling between two coils connected in the active arms of an ac bridge circuit. Both types are designed primarily for room-temperature operation and are normally adapted for low or high temperatures by using extension arms as described

earlier. This technique has, however, a number of drawbacks; there is an additional heat leak down the extension rods or tubes and care has to be taken to prevent water vapor or air condensing in them and causing blockages, while the weight of the assembly can cause bending, especially in thin sheet specimens. Backlash and stickslip in the transducer or the rod linkage can also be troublesome, but Arsenault[2] has overcome this problem by mounting a small solenoid vibrator on the transducer and thus allowing it to operate satisfactorily at its full sensitivity of a few multiples of 10^{-6} in. Furthermore, in his apparatus, the zero can be adjusted either mechanically or electrically by using a micrometer head or suitable electronic circuitry, respectively.

Other workers[20,29,38] have avoided using extension rods by simply immersing the transducer in the cryogenic liquid and recalibrating it if necessary. Not all transducers can be treated in this manner; in particular, those in which the core is potted in epoxy or another type of thermosetting resin are usually unsuitable, as the resin tends to craze. Immersed transducers have proved particularly successful for use with compression testing equipment because they can be activated by the platens and the weight of the transducer does not have to be supported by the specimens themselves.

5.3.3. Capacitance Gauges

These gauges offer a higher sensitivity than any of the previous types. For example, the parallel plate device developed by Brown and his coworkers[39] has a sensitivity of 10^{-8} in., but it suffers from two major drawbacks: the change in capacitance is a hyperbolic function of the plate separation, and it has a limited useful range. These deficiencies are overcome, however, by the use of the type of overlapping cylinder device designed by Reed and Durcholz.[40] The sensitivity of their gauge was limited to about 3×10^{-6} in. by the noise level in the measuring circuit, but they expect that considerable improvement will be achieved once the circuitry has been refined.

REFERENCES

1. K. D. Timmerhaus (Ed.), *Advances in Cryogenic Engineering*, Plenum Press, New York.
2. R. J. Arsenault, "Low Temperature Deformation Techniques," in H. Herman (Ed.), *Advances in Materials Research*, Vol. 1 (1967), p. 215.
3. H. M. Rosenberg, *Met. Revs.* 3, (12); 357 (1958); "The Measurement of Mechanical Properties," in F. E. Hoar, L. C. Jackson, and N. Kurti (Eds.), *Experimental Cryophysics*, Butterworths (1961).
4. F. R. Schwartzberg, in Ref. 1, Vol. 8 (1963), p. 608, and in the Preface to the Cryogenic Materials Data Handbook, ML-TDR-64-280 (1964), and later supplements.

5. O. V. Klajvin, *Industrial Lab.* **29**, 473 (1963).
6. M. P. Hanson, G. W. Stickley, and H. T. Richards, Am. Soc. Testing Mat., Special Tech. Pub. No. 287 (1960), p. 3.
7. Yu. E. Andrianov, D. V. Lebedev, and B. M. Ovsyannikov, *Industrial Lab.* **32**, 1077 (1966).
8. J. F. Watson and J. L. Christian, *Mat. Res. Standards* **1**, 87 (1961).
9. J. E. Cambell and L. P. Rice, Am. Soc. Testing Mat., STP 287, (1960), p. 158.
10. R. M. McClintock and K. A. Warren, *Mat. Res. Standards* **1** (2), 95 (1961).
11. D. Hull and H. M. Rosenberg, *Phil. Mag.* **4**, 303 (1959).
12. Z. S. Basinski, in G. K. White (Ed.), *Experimental Techniques in Low-Temperature Physics*, Oxford Univ. Press (1968), p. 164.
13. E. T. Wessel, *Bull. ASTM* **1956** (January), 40.
14. G. U. Behrsing and L. R. Lucas, *Rev. Sci. Instr.* **36** (5), 617 (1965).
15. I. E. Gindin, Ya. D. Starodubov, and G. G. Chechel'nitskii, *Industrial Lab.* (*USSR*) **32** (7), 1079 (1966).
16. R. D. Keys, in Ref. 1, Vol. 7 (1962), p. 455.
17. J. F. Watson *et al.*, "A Study of the Effects of Nuclear Radiation on High Strength Aerospace Vehicle Materials at the Boiling Point of Hydrogen (−423°F)," ERR-EN-085, General Dynamics/Astronautics (September 1961).
18. W. Weleff, W. F. Emmons, and H. S. McQueen, in Ref. 1, Vol. 10 (1965), p. 50.
19. D. W. Chamberlain, "A Cryostat, Accessories, and System for Mechanical Properties Testing at Temperatures down to 4°K," Application Series SA-4, Instron Corp., 2500 Washington Street, Canton, Mass.
20. G. Taylor, Metallurgy Dept., Oxford University, private communication.
21. R. L. McGee, J. E. Cambell, R. L. Carlson, and G. K. Manning, "The Mechanical Properties of Certain Aircraft Structural Metals at Very Low Temperatures," WADC TR-58-386 (November 1960).
22. D. Hull and H. M. Rosenberg, *Cryogenics* **1**, 27 (1960).
23. R. P. Mikesell and R. M. McClintock, Ref. 1, Vol. 7 (1962), p. 509.
24. R. P. Reed, in Ref. 1, Vol. 7 (1962), p. 448.
25. R. D. McCammon and H. M. Rosenberg, *Proc. Roy. Soc.* **A242**, 203 (1957).
26. R. J. Favor, D. N. Gideon, H. J. Grover, J. E. Heyes, and G. M. McClure, "Investigation of Fatigue Behavior of Certain Alloys in the Temperature Range from Room Temperature to −423°F," WADD TR-61-132 (June 1961).
27. R. D. Keys and F. R. Schwartzberg, *Mat. Res. Standards* **4**, 222 (1964).
28. A. J. Nachtigall, S. J. Klima, and J. C. Freche, *J. Mat. JMLSA*, **3** (2), 425 (June 1968); and NASA Tech. Note D-4274 (December 1967).
29. D. W. Chamberlain, in Ref. 1, Vol. 9 (1964), p. 131.
30. J. L. Christian, "Physical and Mechanical Properties of Pressure Vessel Materials for Application in a Cryogenic Environment," ASD-TDR-62-258 (March 1962).
31. T. S. De Sisto, "Automatic Impact Testing to 8°K, WAL-TR-112/93, Watertown Arsenal Laboratory (July 1958).
32. T. F. Kiefer, R. D. Keys, and F. R. Schwartzberg, in Ref. 1, Vol. 10 (1965), p. 56.
33. D. T. Eash, in Ref. 1, Vol. 11 (1966), p. 401.
34. R. P. Reed and V. D. Arp, *Cryogenics* **9**, 362 (1969).
35. P. T. Chiarito in Ref. 1, Vol. 7 (1962), p. 433.
36. R. M. McClintock, *Rev. Sci. Instr.* **30** (8), 715 (1959).
37. K. A. Warren and R. P. Reed, N. B. S. Monograph 63 (1963).
38. G. V. Aseff, R. F. Callaway, and A. M. Liebschutz, in Ref. 1, Vol. 8 (1963), p. 624.
39. J. M. Roberts and N. Brown, *Trans. AIME* **218**, 454 (1960); *Acta Met.* **10**, 1101 (1962).
40. R. P. Reed and R. L. Durcholz, in Ref. 1, Vol. 15 (1970), Paper J3.

Chapter 6

Design and Materials Selection Criteria

In the foregoing chapters, we have discussed the mechanical properties of materials at low temperatures from a relatively fundamental point of view in order to show the ways in which a change in temperature can influence their deformation and fracture characteristics. For many workers, a study of these properties, or even certain aspects of them, provides a full and sufficient outlet for their talents. To others, however, the justification of such a study is to be found in the application of such knowledge to the more efficient use of materials in the construction of apparatus and equipment operating at low temperatures. In sympathy with this viewpoint, we attempt to indicate in this chapter some of the factors which have to be considered when selecting materials for low-temperature applications. Within the context of this work, a rigorous coverage of such a complex subject is not possible, nor has it been attempted. Rather, we have tried to draw together some of the points made in the earlier chapters and to correlate them with the constraints imposed by the need to produce equipment which is both economically viable and technically adequate for its intended use.

In many respects, the fact that a piece of equipment is intended for use at low temperatures may be considered as just an additional constraint to be added to those normally applied to the design of any article. One could, in fact, go even further and say that the most important consequence of the need to operate at low temperatures is an intensification of the normal requirement that an item shall be able to withstand safely any load or stress which may be applied to it, i.e., that it can withstand not only the static and dynamic stresses which can be predicted for normal operation, but also the thermal shocks and thermal cycles and the accidental overstresses or impact loads to which it may occasionally be subjected. As we have seen, this implies that the item, and hence the material from which it is made, must possess adequate toughness. Hence, it is the effect of low temperatures on the toughness of materials, and in particular on the notch-toughness of materials which contain flaws and other stress-raisers, that

constitutes the most important additional factor to be taken into consideration when designing equipment or selecting materials for cryogenic use.

The most difficult aspect of applying this constraint usually lies in deciding what is an *adequate* level of toughness for the item under consideration. As we saw in chapter 3, there are a number of criteria, some of which are more scientifically based than others, which may be applied to determine the toughness of a material. In some cases, the required criterion is specified by the relevant code of practice; in others, the designer has greater freedom of choice. In most instances, however, it is the designer who is left with the task of balancing the risks involved in the use of smaller safety factors against the penalties of increased costs, lower efficiencies, etc. incurred by the provision of overgenerous safety margins.

The other almost mandatory requirement to be satisfied by a piece of equipment is that it shall be compatible with its working environment. From a cryogenic point of view, this is most important in the case of liquid oxygen and the less common oxidizing agents such as liquid fluorine and chlorine trifluoride. Under certain conditions, the more chemically reactive metals such as titanium, magnesium, beryllium, and even aluminum can ignite and burn spontaneously in liquid oxygen, while mild and stainless steels can be ignited by high velocity impact in Lox.[11] Furthermore, virtually all hydrocarbon-based nonmetals are also incompatible with liquid or gaseous oxygen, and hence it is necessary to find substitute materials for use as gaskets and seals in oxygen-containing equipment. It is equally important that an item is compatible with its external environment, even though this may on first sight appear innocuous. There have been, for example, a number of premature failures in air separation plants constructed from aluminum alloys due to corrosion caused by chemical effluents from nearby petrochemical works or salt spray from the sea.

The constraints of compatibility and adequate toughness are usually the two most important technical requirements to be satisfied, although in some cases, other mechanical or physical properties are of major importance. Apart from strength, the mechanical property most frequently required of an item is rigidity, and hence a high-modulus material is often called for. Of the physical properties, thermal conductivity is possibly the most important, with high-conductivity materials required where temperature gradients have to be minimized and low-conductivity materials needed where they are to be maximized. Thermal expansion must be considered where dissimilar materials are used together, while a low specific heat is advantageous in a situation where an item has to be cooled down frequently. Density is also of extreme importance in aerospace applications, where weight is so critical, and it is usually specific strength (strength/density) which determines a material's usefulness, not its absolute strength. Similarly, in the case of thermal conductivity, a high strength is often required in conjunction with a low thermal conductivity and here it is the strength/thermal conductivity ratio which is important.

It is, however, rare for an item or piece of equipment to be designed or specified purely on technical considerations. Apart, perhaps, from items intended for military or advanced scientific applications, the manufacture of most cryogenic equipment is subject to the same economic constraints as any other merchandise; hence, it must be made in the most practicable and economical way possible. Although these two factors are highly interrelated—in the limit, most things being practicable if the economic constraint is removed—it is more convenient for the purposes of this chapter to treat them separately.

When evaluating the relative merits of various candidate materials for a particular application, it is necessary to consider whether they are all available in the size, form, or quantity required, many materials being only available in a number of stock sizes which may not conform to those required by the initial design study. Furthermore, in countries other than the U.S. it is frequently found that suitable low-temperature design data are not available for domestically produced materials and the designer is faced with the problem of having to secure such data or to obtain materials which conform to American standards. Adequate facilities must also be available for forming and processing the materials, and in most cases, it is also necessary to have access to the appropriate equipment and skills required to join subcomponents together. These are some of the factors which have to be optimized when evaluating the practicability of various materials for a given application.

Finally, in most cases, the decisive factors are economic. When assessing the cost of a job or process, it is necessary to consider not only the price of the raw materials, but also the additional expense of forming components, joining them together, inspecting them, carrying out any necessary reworking, and finishing the job to the required standards, such as cleanliness, moisture, content, etc.

In short, it may be stated that there is no unique formula for the successful design of cryogenic equipment. Each different job has its own priorities and constraints and a formula which proved successful in one instance might well be a failure in the next. In most cases, however, the exercise reduces to one of finding the most practicable and economical method of producing a finished item which is technically adequate for its intended duty.

6.1 COMPATIBILITY

6.1.1. Compatibility with Liquid Oxygen and Other Process Fluids

Liquid oxygen is used in large quatities in rocket systems because it is a powerful oxidizing agent. It is, however, so powerful that, given suitable ignition conditions, a number of important structural metals will burn in

it in a highly exothermic reaction. As such materials are obviously unsuitable for use in contact with liquid oxygen, screening tests have been developed to measure their "LOX compatibility." The most widely used is the compressive impact LOX compatibility test, in which a known weight is dropped from a variable height on to a striker resting on the sample which is immersed in liquid oxygen. In Table XII, the fraction of such tests in which a reaction occurred is shown for stainless steel type 301, aluminum alloy type 2024 and for coated and uncoated samples of a titanium alloy.[12] Also given are the results from a less severe type of test in which rapid fracture of a pressurized diaphragm was produced by a drop-weight penetrator.

Table XII. Reaction Ratios for Two Types of LOX Compatibility Test

Material	Compressive impact test	Diaphragm puncture test
Stainless steel type 301	0/20	0/10
Aluminum alloy type 2024	10/16	0/14
Titanium alloy	10/10	12/15
Coated titanium alloy	50/60	8/10

It can be seen that no reactions were obtained with the stainless steel in either test, while in a high proportion of both types of test, the titanium alloy showed extensive reactions. Both Ti–6Al–4V and Ti–5Al–2.5S alloys were used, but no significant differences in their LOX compatibilities could be detected. The coatings applied to the titanium alloy were generally oxidation inhibitors, but electroless nickel and copper platings have also been tried, with limited success. Reactions were only obtained with the 2024 aluminum alloy in the compressive impact test, not the diaphragm puncture test, but these were much less severe than in the case of titanium. Aluminum alloys are, in fact, generally considered to be compatible with liquid oxygen and are widely used for the construction of fixed and mobile storage tanks.

Analysis of these results and those from other tests showed that the titanium–oxygen reaction was only initiated by rapid fracture, not by slowly propagating or fatigue failures. It was postulated that initiation was caused by the spontaneous ignition of small metal particles which flaked off the fracture surfaces or by the adiabatic heating which accompanies rapid fracture in some metals. Some support for this hypothesis is provided by the lack of reaction obtained with copper, where it is known that, due to the high thermal conductivity of copper, heat is conducted away from the ignition site too rapidly for the reaction to become self-supporting. The other main factors shown by this work to influence the LOX compatibility of metals are their surface condition and cleanliness.

Data on the ignition of materials in high-pressure oxygen are given in Refs. 13 and 14.

As it is relatively easy to find alternatives for titanium and other reactive metals in oxygen-containing systems, their lack of LOX compatibility is not too serious a problem. It is, however, less easy to replace the wide range of hydrocarbon-based nonmetals which have also been found to be incompatible with liquid and gaseous oxygen. Their degree of LOX sensitivity was originally determined by the same type of compressive impact test as used for metals, but Hauser and Rumpel[15] have now increased its resolution by measuring the intensity and duration of the light flash using a photocell and the pressure of the sound pulse with a microphone. These improvements have removed much of the subjective nature of the original test and made it possible for the LOX-sensitive components to be identified. In general, it was found that pure polymers and elastomers were much less sensitive than their compounded forms, the plasticizers and antioxidants being the sensitive components. The LOX compatibility of polymers can be increased by replacing the hydrogen atoms (whose weak C–H bonds may be easily broken to allow the oxygen to react with both the carbon and hydrogen fragments) with more strongly bonded groups such as halogen atoms. It is, therefore, not surprising that polytetrafluoroethylene (PTFE) and polychlorotrifluoroethylene (Kel-F), in which the hydrogen atoms are replaced by four fluorine atoms and one chlorine and three fluorine atoms, respectively, are the most LOX–compatible polymers known. As discussed in chapter 4, they also have the most advantageous low-temperature mechanical properties and thus are widely used for gaskets, seals, etc.

A number of other plastics and elastomers are only mildly LOX–sensitive and they are considered by many to be usable in applications where there is little chance of impact. For example, Mylar is used in expulsion bags and as a diaphragm in high-pressure LOX regulators. Viton and Nitroso rubber are also reputed to have reasonable LOX compatibility, as have the silane and polyurethane elastomers; at liquid-oxygen temperatures, however, their elastomeric qualities are virtually nonexistent and seals need to be designed so that they do not have to operate dynamically while at low temperature.

The other main group of cryogenic fluids which have materials compatibility problems are the fluorine-based oxidizers: liquid fluorine, chlorine trifluoride, oxygen difluoride (OF_2) and a mixture of liquid oxygen and liquid fluorine known as FLOX. They are even more potent oxidizers than liquid oxygen and have been evaluated for use in upgrading the specific impulse of existing LOX–burning rocket engines. As might be expected, they are incompatible with titanium, and are most compatible with Monel and similar alloys. The 300 series stainless steels are reasonably compatible as long as they are properly cleaned, although some doubts

have been expressed[16] as to their suitability for parts subjected to flowing liquid-fluorine compounds, because of the possible erosion of the passivating film.

The importance of cleanliness has been underlined by the experience of North American Aviation, as reported by Zeilberger.[17] They found that properly cleaned stainless steel was compatible with liquid fluorine and therefore this material was used for a prototype liquid-fluorine transfer system. After a short period of time, however, loosely adhering red and green corrosion products 1/16 in. thick were found on the walls of pipes and valves. These "stainless steel fluorides," which caused numerous blockages in valves and other equipment downstream, were found to have been caused by minute traces of moisture from the helium pressurant combining with residual propellant to attack the stainless steel. Despite the rather exotic nature of this example, it does serve to emphasize at least three points which have wider implications: that minute traces of a third component can have a marked influence on the compatibility between materials and cryogenic fluids; that, although the reaction itself may not have immediate serious consequences, the reaction products can have; and, finally, that all compatibility testing should be carried out under conditions which simulate as closely as possible the actual operating conditions in service.

6.1.2. Compatibility with the External Environment

In many respects, the compatibility of a piece of cryogenic equipment with its external environment may be considered as outside the scope of this text, as it is not specifically a low-temperature problem. Thus, although this is a rather short-sighted attitude to adopt, we do not intend to discuss the topic in detail in this section and the reader is referred to any of the standard engineering texts on this subject. Suffice it to say that any of the mechanisms discussed in chapter 3 by which cracks in metals may enlarge, sharpen, or propagate—corrosion, stress corrosion, corrosion fatigue, oxidation, hydrogen embrittlement, etc.—may all cause failures which could lead to the loss of a piece of cryogenic equipment. Correct design procedures are therefore important if such losses are to be avoided. Most failures of metallic equipment can usually be traced to one of the mechanisms listed above; if, however, nonmetals, and in particular polymeric materials, are used, there are a few further possible causes of failure. As we saw in chapter 4, stress relaxation is a frequent problem with parts which are continuously loaded. Other mechanical properties of polymers are also time-dependent due to aging effects caused by atmospheric oxygen, water vapor, or sunlight. Relatively small concentrations of airborne impurities can accelerate these processes and hence cause the premature failure of polymers and elastomers used as valve diaphragms and other components exposed to such pollution.

Although there are not many applications in which cryogenic equipment has to operate in a radiation environment—bubble chambers, other high-energy physics apparatus, and prototype nuclear propulsion systems being a few current examples—such combinations can lead to compatibility problems and work is in hand to evaluate these effects. Both the problem and initial results on metals are well summarized by Lombardo *et al.*,[18] who show that many structural alloys exhibit small but significant adverse changes in one or more of their mechanical properties after exposure to moderately high radiation fluxes.

Finally, to return briefly to the compatibility problems of more conventional cryogenic equipment, there are occasions on which the specification of an item asks for certain cleaning or drying procedures to be followed. For example, it is common to require complete moisture removal prior to start up in order to prevent heat-exchanger plugging. As this is commonly achieved by purging with pressurized dry nitrogen at $\sim 120°C$, and as ASME 8 design codes limit the use of some aluminum alloys to below 70°C, such a requirement would weigh against the use of aluminum for this plant. Similarly, the need for periodic caustic washing in some chemical plants means that aluminum has to be replaced by stainless steel in the affected components.

6.2. TOUGHNESS

6.2.1. The Basic Problem

Failure mechanisms were discussed at length in chaper 3 and at this point it is only necessary to reiterate some of the more important conclusions which affect the design of equipment intended for use at low temperatures. In section 3.2.4, materials were classified generally into high-, medium-, and low-strength types. As high-strength alloys have low fracture toughnesses at all temperatures, it was concluded that the only safe basis for design was that given by fracture mechanics, i.e., the operative stress to be calculated from the fracture toughness of the material concerned and the size of the largest flaw it was likely to contain.

Medium-strength materials have adequate toughness at and above room temperature, but in some cases, the toughness decreases at lower temperatures due to the increase in their yield strengths. In these cases, it is also necessary to design according to the concepts of fracture mechanics and the tests used both to screen materials for possible loss of toughness and to measure the appropriate K_c value were described in section 3.2. In practice, the use of high- and medium-strength alloys has largely been restricted to aerospace and other sophisticated equipment where the strength/weight ratio of materials is so critical, fracture toughness criteria having

been shown to give a satisfactory basis for the design of equipment such as fuel tanks and pressure vessels intended for use at cryogenic temperatures. Such criteria are, however, not as yet accepted as a basis for the design of pressure vessels and other commercial equipment which has to satisfy the requirements of the British Insurance Inspection Company in the U.K. or the national inspection authorities in other countries. As most of the materials used in commercial applications come into the low-strength category, having toughnesses which are too large for fracture mechanics analyses to be valid, this is not in fact too serious a limitation, but it does prevent the efficient use of the stronger alloys which could occasionally be employed advantageously.

Most low-strength materials have high toughnesses at all temperatures and hence they do not fail in a low-energy mode. The only exceptions are those alloys that are susceptible to cleavage fracture, and from a practical point of view, this means the plain-carbon and low-alloy steels. The criteria used to determine the lowest temperatures at which these materials may operate safely have already been discussed at length in section 3.3, and they also form an integral part of the codes of practice which have to be followed in designing pressure-containing equipment.

6.2.2. Codes of Practice for Pressure-Containing Equipment

In essence, these codes define the minimum temperature at which a given material may operate when subjected to a certain design stress. This stress is derived by multiplying the room-temperature proof or tensile stress by an agreed safety factor, usually $\frac{2}{3}$ in the case of proof stress codes such as BS 1515 and $\frac{1}{4}$ in the case of tensile stress codes such as BS 1500 and ASME VIII. As it is the proof or tensile stress *as measured at room temperature* which is used in these codes, no benefit can be gained from the considerable increase in strength shown by most metals at low temperatures. There is, however, some justification for this apparently inefficient procedure, as it is most convenient to proof-test vessels at ambient temperature, and hence they must be able to withstand such stresses at this higher temperature.

The design codes lay down minimum operating temperatures for each type and grade of material approved for the construction of pressure vessels, pipelines, or whatever equipment is covered by the relevant code. These temperatures are obviously related to the temperature at which the toughness becomes unacceptably low, but, as we saw in chapter 3, there are a number of different criteria which can be used to define this tough-brittle transition. In general, minimum operating temperatures are usually at least 25°C above the nil ductility temperature in ferrous alloys, but this varies somewhat from metal to metal. Furthermore, as we saw in chapter

3, there are a number of factors, such as plate thickness, residual tensile stresses, grain size, etc., which can affect the tough–brittle transition temperature of a metal. In order that these factors can be taken into consideration, most codes require some form of test to be carried out on both the parent metal and weldment samples to ensure that the material is up to specification. The most common type of test used is the impact test, usually Charpy V-notch, but sometimes with other notch geometries. We have already discussed at some length the various limitations of this type of test, yet it must be admitted that in many cases, and especially for ferritic steels, it is a very convenient and reliable method of quality control. Providing that a *meaningful* value of impact energy is chosen for the grade and thickness of material under consideration, it gives a simple "go–no go" criterion. Its value in checking the toughness of weldments is possibly open to a little more criticism. It is capable of detecting gross deficiencies in toughness, as brought about perhaps by a bad batch of filler rods, but it is less likely to show up the nonsystematic type of flaw which could still lead to vessel failure. Here again, though, it could be argued that any type of test which relies on checking a small sample of test pieces is open to the same criticism and that only full-scale tests on the completed vessel would eliminate this type of defect.

The most serious limitation of the conventional impact test is, however, its use with fcc metals, which do not undergo cleavage failure. As stated earlier, it is necessary to employ the more sophisticated type of test, such as the drop weight tear test or notched tensile test, to give a reliable indication of lack of notch toughness in these metals. The situation is at its most unsatisfactory in the case of the aluminum alloys. Most of the alloys in widespread use for the construction of cryogenic equipment will not absorb more than about 20 ft lb of energy in a Charpy V-notch impact test, yet there are codes which demand that aluminum alloy weldments be rejected if they are unable to pass a 15-ft lb impact test. This would appear to many to be an unjustifiable use of such a test and cases are known where cryogenic pressure vessels made from welded aluminum alloy have been rejected by one inspection authority on this basis, yet have subsequently proved entirely reliable in service elsewhere.

Care has to be taken to ensure that a piece of equipment has been designed to comply with all the codes operative in its intended location. For example, most American insurance companies accept the ASME code in its entirety, but only about half the states in the U.S. do likewise. Furthermore, some states are less lenient than the insurance companies in accepting some of its more controversial parts such as heat-exchanger tubesheet designs. Similarly, some European code authorities not only have to approve the design of a pressure vessel, but also require that its material conforms to one of their national specifications and that it is obtained

from an approved supplier. This can sometimes involve considerable time and expense and is one of the factors to be considered when costing a vessel.

There are in fact only a limited number of design codes that govern the construction of vessels for operation at low temperatures and some of the most important of these are listed below. It should be noted that the following remarks are for guidance only and that *the codes themselves must be consulted for design purposes.*

6.2.2.1. ***Tensile Stress Codes.***[2] The *ASME code on unfired pressure vessels, (1965), Section VIII* deals with vessels intended for operation at temperatures below −29°C (−20°F).

Subsections UCS, 65, 66, and 67 cover most carbon and low-alloy steels and require nearly all vessels to be stress-relieved and to absorb at least 15 ft lb in a Charpy V-notch impact test carried out at the minimum operating temperature. The only exceptions to this rule are those vessels which have low operating pressures (UCS-66).

Subsection UNF 65 covers wrought aluminum and its alloys down to −254°C, and copper, nickel, and cast aluminum alloys down to −198°C with no special requirements other than the normal design stress of $\frac{1}{4}$UTS. For lower temperatures, however, satisfactory impact energies are required.

Subsection UHA-51 covers wrought stainless steel types 304, 304L, and 347 down to −254°C, only requiring impact tests for even lower temperatures. Similar types in cast form, and types 309, 310, 316 in the form of deposited weld metals, need, however, to be impact-tested if used below −20°C. Most other austenitic stainless steels (including those with high carbon contents and those whose analysis is outside standard AISI composition ranges) and the ferritic chromium stainless steels, also require satisfactory impact testing before use.

ASME code case 1308–4, special ruling (1962) covers the use of 9% nickel steel in the quenched and tempered or double normalized and tempered form down to −196°C. A series of full-scale bursting tests were carried out[19] at −196°C on welded 9% nickel steel pressure vessels made from 2-in. sheet to prove that this material failed in a ductile manner even without thermal stress relief after welding. A minimum impact energy of 25 ft lb is, however, required in a Charpy V-test at −196°C. It was this special ruling, the first for a non-stress-relieved ferritic metal at −196°C, which gave rise to the rapid increase in the use of 9% nickel steel for large cryogenic storage tanks.

BS 1500, (1958), part 1, Appendix C[3] covers the use of plain carbon steels, carbon manganese steels, and chromium molybdenum steels down to −60°C and the impact-tested LT steels down to −190°C. The effects of plate thickness and thermal stress relieving are taken into consideration

and impact tests are required. These conditions may, however, be relaxed if the pressure is due solely to the vapor pressure of its contents and where low temperatures are only coincident with low pressures. (Table 21).

6.2.2.2. ***Proof Stress Codes.*** *BS 1515, (1965), part 1, Appendix C* covers the use of plain carbon steels, carbon manganese steels, chromium molybdenum steels, and $3\frac{1}{2}\%$ nickel steel. None of these steels may be used below $-60°C$ and many of them have higher minimum operating temperatures. It also covers the use of the impact-tested LT steels, one of which, LT 100, may be used down to $-100°C$. As before, the effects of plate thickness and stress relief are taken into consideration and satisfactory impact energies are required.

A. D. Merkblätter,[5] *Data Sheet W. 10 (Draft, December 1963), Section 3* considers the intended duty of the pressure vessel and then defines three separate minimum working temperatures for each of the three classes: heavy, lesser, low. For example, a certain killed steel may be used down to $-10°C$ for heavy-duty, $-50°C$ for lesser, and $-100°C$ for low-duty applications. For heavy-duty purposes, construction must be in accordance with AD data sheet Hl and stress-relieving must be carried out if the wall thickness is over 30 mm. For lesser duties, lower temperatures are allowed, but the safety factors used to calculate the design stress are increased as much as fourfold in some cases, and stress-relieving has to be carried out for thinner wall sections.

6.2.3. Some Economic Implications of Designing to Pressure Vessel Codes

If a designer has the choice of working to either a proof stress code or a tensile stress code, it is necessary to ascertain whether there are economic advantages to be gained by use of the proof stress code. Adoption of these codes can sometimes result in considerable savings on material costs for metals with high proof/tensile stress ratios such as 9% nickel steel or the hi-proof stainless steels, but these savings are sometimes partially offset by the additional costs incurred by the more sophisticated design, fabrication, and inspection techniques required for these thinner-walled vessels. When evaluating candidate materials for use in these circumstances, it is normal to consider the cost of providing a given level of available proof or tensile stress and, as shown in the following calculation, this is given by the cost multiplied by the density divided by the design stress.

Consider a right cylindrical pressure vessel of length L, shell radius R, wall thickness t, and design pressure P. Neglecting the end plates, tubes, etc. and assuming that the design stress of the material is S and that the joint efficiency is E, then the wall thickness is related to the design pres-

sure by the formula

$$t = PR/SE \tag{6.1}$$

If the material has a density ρ, its mass is given by

$$M = \rho \cdot 2\pi RLt \tag{6.2}$$

and if the cost per unit mass of material is c, substituting for t, we obtain the total cost of the shell C as

$$C = c\rho \cdot (2\pi R^2 LP/SE) \tag{6.3}$$

Assuming for simplicity that the joint efficiency does not vary from material to material, it follows that the total cost C of a shell of constant dimensions is proportional to

$$c\rho/S \tag{6.4}$$

In Table XIII, two such indices, one based on ASME VIII design stresses and the other on BS 1515, are given both in absolute terms and relative to carbon steel, which is often considered as a baseline for such calculations. Also shown are the corresponding weight indices and the various data necessary for these calculations. As the relative costs of the different materials have varied considerably during 1968 and 1969, two sets of prices are included, one for January 1968 and the other for November 1969.

In order to examine some of the points that arise from these indices, let us assume that a large storage tank is to be constructed to contain liquid natural gas. Four of the most suitable materials available are type 5083 aluminum alloy, types 304L and 304 + N_2 stainless steel, and 9% nickel steel. Consider first the situation in January 1968. If the tank is for use in a location where BS 1515 is operative, the relevant cost indices are those in lines (g) and (h). It can be seen that 9% nickel steel with a relative index of 2.43 is the obvious choice, and even allowing for the fact that most vessels would have to be welded, thus making the relevant index value 3.36, the material has a clear advantage over aluminum at 5.67, nitrogen-bearing stainless steel at 6.25, and ordinary 304L at 10.7.

If the vessel has to be designed to ASME VIII, the relevant cost indices are those in lines (n) and (o). The 9% nickel steel still comes out best even in the welded condition, with a relative index of 3.62, but the aluminum alloy, at 4.38, is now a much more serious rival, with the stainless steels lagging somewhat at 5.90 and 7.18 for the nitrogen-bearing and low-carbon alloys, respectively. As the cost for the 9% nickel steel does not include the cost of the expensive electrodes needed for welding, the choice between it and the aluminum alloy is even closer than these figures suggest.

Consider now the construction of a similar vessel in November 1969.

Table XIII. Design Indices for Some Common Construction Materials[a]

	Carbon steel A201B	Aluminum NP8 ASA 5083 (O)	Stainless steel 304L (annealed)	Stainless steel 304+N_2	Normalized and tempered 9% nickel steel, ASTM code case 1308	9% Nickel steel welded with Nicrex 9 electrodes	Phosphorous-deoxidized copper SB 11
(a) Cost, £/ton, January 1968	46	378	380	(380)[b]	260	(260+)[b]	610
(b) Cost, £/ton, November 1969	62	500	525	(527)[b]	420	(420+)[b]	857
(c) Density ρ, g/cm^3	7.8	2.7	7.9	7.9	7.9	7.9	8.9
(d) 0.2% Proof stress, psi	32,000	16,000	25,000	42,600	75,000	55,000	10,000
(e) Design Stress to BS 1515, 2/3(d)	21,200	10,650	16,650	28,400	50,000	36,200	6,000
(f) 2/3 Proof stress/density, (e)/(c)	2,718	3,944	2,107	3,595	6,330	4,582	748
(g) Cost Index, BS 1515, January 1968 (a)/(f)	16.9	95.8	180	106	41.1	56.7	815
(h) (g) Relative to carbon steel	1	5.67	10.7	6.25	2.43	3.36	48.2
(i) Cost Index to BS 1515, November 1969 (b)/(f)	22.8	126.8	249.1	146.6	66.35	91.66	1145
(j) Relative to carbon steel	1	5.56	10.9	6.43	2.91	4.02	50
(k) Ultimate tensile stress, psi	60,000	39,000	70,000	85,200	100,000	95,000	26,800
(l) Design stress to ASME VIII, 1/4(k)	15,000	9,750	17,500	21,300	25,000	23,750	6,700
(m) 1/4 UTS/density, (l)/(c)	1,923	3,611	2,215	2,696	3,165	3,006	753
(n) Cost index to ASME, VIII, January 1968 (a)/(m)	23.9	104.7	171.6	140.9	82.15	86.49	810
(o) (n) Relative to carbon steel	1	4.38	7.18	5.90	3.44	3.62	33.9
(p) Cost index to ASME, VIII, November 1969, (b)/(m)	32.2	138.5	237.0	195.5	132.7	139.7	1138
(q) (p) Relative to carbon steel	1	4.30	7.36	6.07	4.12	4.34	35.3
(r) Weight index to BS 1515 $1/(f)\times10^{-4}$	3.68	2.54	4.75	2.78	1.58	2.18	13.36
(s) (r) Relative to carbon steel	1	0.69	1.29	0.76	0.43	0.59	3.63
(t) Weight index to ASME, VIII, $1/(l)\times10^{-4}$	5.20	2.77	4.51	3.71	3.16	3.33	13.28
(u) (t) Relative to carbon steel	1	0.53	0.87	0.71	0.61	0.64	2.55

[a]Prices are for guidance only and may vary considerably depending on the quantity and form of the metal involved. Prices for November 1969 contain a surcharge on all nickel-containing alloys.

[b]Costs in parentheses are approximate and probably underestimate the true values. This is particularly true for welded 9% nickel steel, where electrode costs are high.

Due to a rapid rise in nickel prices, the cost of the 9% nickel and stainless steels has risen faster than that for the aluminum alloy. Reworking the example first for a vessel constructed to the proof stress code BS 1515, the relevant indices are those in lines (i) and (j). The 9% nickel still has definite advantage, with a relative cost index of 4.02 in the welded condition compared to 5.56 for the alminum alloy. Even allowing for electrode costs, the 9% nickel probably still has the edge on the aluminum alloy, with the nitrogen-bearing hi-proof stainless not far behind at 6.43.

If, however, the vessel has to be constructed to comply with ASME VIII, the picture changes, as may be seen from the indices in lines (p) and (q). The aluminum alloy type 5083, with a relative cost index of 4.30, is marginally superior to the welded 9% nickel, index 4.34. As it stands, this difference is not significant, as these indices are not accurate to the third figure. Nevertheless, once the high cost of welding 9% nickel steel is taken into consideration, it is probable that the superiority of the aluminum alloy would be confirmed. Similarly, the performance of both stainless steels is worse in 1969 than it was in 1968.

Those with any experience of costing the design of such vessels will be painfully aware that this example is a gross oversimplification of the problem ; further analysis is, however, outside the scope of this text. Nevertheless, there are one or two further points which may be drawn from Table XIII. Copper was once the preeminent material for the construction of cryogenic apparatus and equipment. Now, however, it is a complete nonstarter except for one or two specialist applications in which its high thermal and electrical conductivities or its good forming and brazing characteristics are of paramount importance.

In some applications, the total weight of a vessel is an important design consideration, and from the indices shown in lines (t) and (u), it may be seen that, as might have been expected, the aluminum alloy is most attractive if design is to a tensile stress code. Yet, if a proof stress code can be used, lighter vessels may be constructed from 9% nickel steel even if they have to be welded. Although the two types of stainless steel used as examples in Table XIII do not look attractive on a strength/weight basis from the figures given, it should be pointed out that cryogenic fuel tanks for rockets have been made form cold-worked stainless steel sheets. The construction of these "flying pressure vessels" is not, however, covered by the commercial design codes we have been considering.

6.3 PRACTICABILITY

6.3.1. Availability of Materials

There are so many factors which can affect the availability of a ma-

terial that it is only possible to note here a few of the commonest. Short-term factors, such as strikes in the mines or processing works, sudden large demands due to military requirements, or the influence of the quota system on vendors' stocks, are most likely to affect the availability of copper and nickel. Recent increases in the price of copper have further encouraged its replacement by aluminum in a large number of applications, while the effects of the current (1969) nickel shortage on the price of stainless steels and 9% nickel steels have already been discussed. In contrast, most aluminum alloys are readily available and the price of the basic metal is not subject to the uncertainties which influence copper and nickel.

A further factor which can influence the availability of some materials is the size of the organization employing the designer. If he has the backing and purchasing power of a large company, he is more likely to be able to order in quantities sufficient to encourage a vendor to supply material in the required form. This is particularly noticeable in the case of 9% nickel and other recently developed alloys such as the "hi-proof" grades of stainless steel, which are virtually unobtainable in the quantities needed by some of the smaller companies in the U.K.

Most materials are produced in a number of preferred sizes, and where possible, it is best to design to these sizes and thus avoid the additional expense of either rerolling sheets and drawing tubes to nonstandard sizes, or using sections thicker than those necessary to satisfy the design code. Such additional constraints often have a marked influence on materials selection; to illustrate this point, consider the construction of three pressure vessels to the specifications given in Table XIV. Using the same simplifying assumptions as in the previous example, the wall thickness is again given by equation (6.1), $t = PR/SE$. For the low-pressure vessel 1, the calculated wall thicknesses are 0.050 in. for type 304L stainless steel and 0.090 in. for 5083 aluminum. If such a vessel were to be operated as part of an air separation plant, it is probable that a vessel of diameter 30 in. made from 0.050-in. sheet would be considered insufficiently rigid, and thus thicker material would be required. Under such conditions, the alumi-

Table XIV. Comparative Wall Thicknesses for Three Pressure Vessels Made of Aluminum Alloy and Stainless Steel[a]

		Vessel 1	Vessel 2	Vessel 3
Diameter, in.		30	30	72
Operating pressure, psi		50	500	500
Aluminum alloy	t calculated, in.	0.090	0.900	2.18
type 5083:	t actual, in	0.125	0.969	—
Stainless steel	t calculated, in.	0.050	0.502	1.21
type 304L:	t actual, in.	0.125	0.531	1.25

[a]Design stresses are to ASME VIII. Joint efficiencies of 0.85 have been assumed throughout.

num alloy would be a more appropriate choice, with sheet of thickness 0.125 in. being the most likely selection. Low-pressure distillation columns are also designed for structural rigidity rather than pressure containment, and under these conditions, aluminum alloys offer considerable cost advantages over stainless steels. If, however, shell bending is a design limitation (as, for example, in a column subjected to lateral wind loading), then the higher modulus of stainless steel (30×10^6 psi compared to 10×10^6 psi for aluminum) can restore the balance in favor of stainless steel.

Returning to the example of the pressure vessels, the calculated wall thicknesses for the small high-pressure vessel (No. 2) are 0.900 in. and 0.502 in., respectively, for aluminum and stainless steel. As the nearest stock sizes are 0.969 in. for the aluminum and 0.531 for the stainless steel, the use of aluminum would result in more excess metal than if stainless steel were specified. The aluminum vessel would, however, still be cheaper [see lines (o) or (q), Table XIII] on material costs alone and more detailed costing would be needed before making a final decision.

In the case of vessel 3, there is no doubt that it would be made of $1\frac{1}{4}$ in. stainless steel plate. The calculated thickness of 2.18 in. for the aluminum alloy would be too thick for welding, $1\frac{1}{2}$ in. being virtually the maximum thickness possible using high-current, automatic, double-pass welding techniques.

Finally, the ready availability of standardized fittings such as bends, joints, connectors, reducers, flanges, etc. virtually excludes the use of nonstandard size tubes for the majority of commercial low-temperature equipment.

6.3.2. Availability of Reliable Design Data

Much of the impetus for the recent growth in cryogenic engineering has come from the nuclear and space programs undertaken by the U.S. and the U.S.S.R. The demands of these programs have led to the generation of many valuable design data on the properties of materials at cryogenic temperatures, but inevitably, the majority of these data are for materials which conform to the relevant national specifications. Furthermore, a considerable fraction of the data refers to the more sophisticated aerospace materials, which have only a limited relevance to the manufacture of most cryogenic equipment intended for commercial use. Without the incentive provided by such programs, there has not been any comparable effort applied to the testing of materials produced to British or European specifications, and in consequence, there is only a limited amount of data available on the mechanical properties of these materials at low temperatures. It is not uncommon for a designer in the U.K. to be faced with

the choice of using a British standard material for which he has inadequate design data or of ordering from the U.S. a similar material for which the relevant data exist. The problem of finding suitable equivalents to American standard materials is made more difficult by two main factors. First, the permissible composition ranges of many British alloys are wider than those allowed by the ASTM and this has particularly serious consequences for the 300 series stainless steels, where, as we saw in chapter 3, small differences in composition can have a large influence on the stability of the austenite–martensite transformation. Second, the lack of a standardized numbering system for British steels and aluminum alloys makes it impossible to achieve a systematic basis for finding equivalent types of these materials.

Faced with these difficulties, a significant proportion of designers take the easy way out of this problem and automatically specify materials to ASTM or similar standards.

6.3.3. Availability of Suitable Forming Equipment and Techniques

There are many factors which influence the ease with which a material may be formed into components. Some of these factors are determined by limitations on the type of equipment available, while others are a more direct consequence of the mechanical properties of the material itself. For example, one of the principal advantages of 9% nickel steel is its high proof stress, but this also makes it difficult to cold-form, and hot-forming techniques are used for the production of dished ends for pressure vessels. The limited availability of such facilities can in turn create supply problems with such components, especially if small quantities are required. Furthermore, a tenacious scale can be formed if the hot-forming is not carried out correctly and this can create problems if the material has subsequently to be welded.

Some aluminum alloys also have a limited ability to be cold-formed. The higher-strength alloys in particular have a relatively small elongation before fracture and can crack if bending radii are too small, e.g., a 4-in. radius is the minimum for $\frac{1}{2}$-in. plate of 5083. These limitations do not, however, apply to many of the softer alloys, such as the 3000 series, and these alloys are widely used for pipes, pipe fittings, flanges, etc. and other applications which require good forming characteristics. Furthermore, it is easy to produce accurate high-quality extrusions from commercial-purity aluminum and its low-strength alloys and it is possible to use such extrusions to form edge seals for distillation column trays and thus avoid the need for complicated machining operations. Two further attributes possessed by the softer aluminum alloys are their ability to be cut with

roller cutters or other simple shearing equipment and the ease with which well-defined, burr-free holes can be punched in sheets to form, for example, sieve-type trays for distillation columns.

The 300 series stainless steels are generally considered easy to form when in the annealed condition. They have the additional advantage of requiring minimal finishing or cleaning, and this, together with their corrosion resistance, makes them suitable for use in many types of cryogenic equipment.

As we saw earlier, copper is now almost prohibitively expensive for use in large cryogenic plants, but there are still a number of specialist applications where it is employed. It is, for example, widely used for small-bore cryogenic piping, where stresses are low and ease of assembly to valves and other fittings is important. Another application is in coil-wound heat exchangers, where tubes for different streams have to be pair- or triple-wound to improve heat transfer and a large number of permanent, leak-free joints have to be made between tubes and tube-plate. Copper and its alloys, the most important of which is α-brass, are also still widely used for the construction of small, laboratory-scale cryogenic apparatus, where their ease of jointing and good forming characteristics outweigh their higher costs.

6.3.4. Jointing Techniques

One of the most important factors which must be considered in the manufacture of cryogenic equipment is the provision of strong, reliable, leak-free joints between components. Apart from the relatively few occasions where a faulty weld may lead to the catastrophic failure of pressure-containing equipment, there have been countless less serious failures which have caused leakage of process fluid or the loss of an insulating vacuum, and whose repair has necessitated a long and costly shutdown of expensive equipment. In order to minimize such losses, welded joints are used wherever possible, although brazed or soldered joints are sometimes employed. Special transition pieces have been developed to join together dissimilar metals such as stainless steel and aluminum alloy and these joints have now achieved a high standard of reliability. The use of flanged and bolted joints is restricted where possible to the connection of valves and other auxiliary equipment which may require periodic removal for maintenance purposes.

6.3.4.1. ***Welding Processes and Techniques.*** Detailed consideration of this topic is outside the scope of this text and we will restrict ourselves to an indication of some of the points which affect the welding of the three metals most widely used in the construction of cryogenic equipment, aluminum, stainless steel, and 9% nickel steel.

The aluminum alloys most widely used in the construction of cryo-

genic equipment, the aluminum–manganese 3000 series and the stronger aluminum–magnesium 5000 series alloys, are readily welded by either of the inert-gas shielded arc techniques. The metal inert gas (MIG) process, in which the arc is struck between the filler wire and workpiece, is normally used for plate thicknesses in excess of 3/16 in. However, a modification of this basic technique, pulsed arc welding,[20,21] allows sheets 1/16 in. thick to be welded routinely in all positions, and thicknesses down to 0.030 in. are weldable under closely controlled conditions. Thin sheets are normally welded by the tungsten inert gas (TIG) process, in which the arc is struck between a nonconsumable tungsten electrode and the workpiece, with the filler wire fed in separately. The TIG process offers complete control for all welding positions, but distortion is greater and welding speeds are two to three times slower than those obtained by the newer pulsed arc technique.

In order to obtain consistently high-quality, leak-free welds that will pass X-ray acceptance tests, it is important to ensure that the edges to be joined are well prepared and scrupulously clean. It is also important that the welder performing the job has the necessary qualification for welding aluminum, as it has been found that higher skills are required for welding these alloys than, for example, for stainless steel.

The grade of stainless steel most frequently used for the construction of cryogenic equipment is the low-carbon-content 304L, and this alloy is readily welded by both MIG and TIG processes if the correct type of filler metal is used. Compositions which leave about 5% free ferrite in the weld deposit are favored if hot-cracking is to be avoided; some of the other metallurgical problems associated with welding this type of alloy have already been discussed in chapter 2. Two other techniques can also be employed to weld these alloys, the submerged arc technique, which can give good-quality welds at high speeds and low cost, and the shielded metal arc process with flux-coated electrodes. As these electrodes can absorb water vapor from the atmosphere, they are best stored in a drying cabinet at about 120°C if porous weld deposits are to be avoided.

We have already found that welds made in 9% nickel steel lower its design stresses and increase the overall cost of the completed equipment. These problems arise from the fact that electrodes of composition similar to that of the parent metal produce welds of unacceptably low toughness at low temperatures. Two basic types of electrode are used to circumvent this problem. The Inconel type Ni/Cr compositions form tough welds and have thermal expansion coefficients which match that of the parent metal. In general, however, the welds have low proof and tensile stresses which lower the allowable design stresses to those shown in Table XIII. To overcome this loss of strength, complex austenitic-type electrodes are sometimes used, but their thermal expansion coefficients do not match those of the

parent metal and this can lead to the development of dangerously high stresses if the vessels are thermally cycled. Furthermore, both types of electrode are very expensive and the inclusion of their cost has an adverse effect on the otherwise favorable economics offered by 9% nickel steel. Electrodes have been produced which go some way toward satisfying the technical deficiencies of the above-mentioned electrodes, but they are usually even more complex and expensive than the Inconel or stainless steel types. The development of a cheap, but technically adequate, electrode for welding 9% nickel steel would undoubtedly remove a barrier which at present curtails the further use of this alloy.

Both manual arc welding with flux-coated electrodes and inert-gas shielded techniques can be used without preheat for sections less than about 1.5 in. In general, electrodes are used for on-site construction of, for example, large storage tanks for liquid gases, while the increased rate of weld deposition achieved by MIG techniques is largely responsible for its preference for factory fabrication. Nickel-base electrodes are difficult to use in a vertical position and welding in this position can result in porous weld deposits. This problem can, however, be partially overcome by the use of the fine-wire process,[22] which utilizes filler wires of ~0.030 in. diameter. Finally, cleanliness is again essential if sound weld deposits are to be achieved. Mill and flame cutting scale should be removed from the weld area by grinding, blasting, or power-brushing and flux should also be removed between weld passes.

6.3.4.2. ***Brazing and Soldering.*** Copper can be welded using inert-gas shielded arc techniques, although difficulties are encountered both with heavy sections and thin sheets. Its traditional use for cryogenic equipment stems, however, from the ease with which it and its alloys may be brazed and soldered. Hard solders are mainly based on a copper-zinc brazing alloy with additional silver, and a range of solders with melting points between 600 and 1000°C are obtained by varying the relative proportions of these three metals. Boric acid or borax is normally used as a flux and elaborate joint preparation is not so necessary as with the low-melting-point solders. These soft solders are generally tin–lead alloys of various compositions and melting points which vary from 327°C for pure lead to 183°C for the eutectic composition 63% Sn, 37% Pb. Careful cleaning and pretinning are necessary to produce reliable leak-free joints and these procedures are well described by Croft[23] and White.[6] The flux used depends on the metals concerned, zinc chloride being suitable for copper alloys, but phosphoric acid giving better results with stainless steel. *As all fluxes are corrosive, some highly so, joints must be thoroughly washed after soldering in order to preclude subsequent corrosion and leakage.*

The low-melting-point solders allow joints to be made at temperatures

below 100°C. They are mainly alloys of bismuth, lead, tin, cadmium, and indium–Woods metal, for example, containing 50% Bi, 25% Pb, 12.5% Sn, and 12.5% Cd and melting between 65 and 70°C. There are also special solders used for making joints in cryogenic apparatus, e.g., 60% Bi–40% Cd does not become superconducting above 0.8°K, the 70% Cd–30% Sn alloy has a very low thermoelectric force with respect to copper, while pure indium readily wets most metals and also some nonmetals like glass. Details of these alloys are given in Refs. 1, 6, and 23.

Before leaving this subject, it is worth mentioning that a complicated research cryostat will probably contain joints made using a large number of different solders. The highest-melting-point solders are usually employed for making permanent joints in the core of the apparatus, soft solder for those joints which need occasional remaking, and the low-melting-point alloys for the outermost vacuum jackets, which need frequent removal.

Aluminum alloys can be soft-soldered if the correct fluxes and solders are used, but such techniques are rarely, if ever, used for cryogenic apparatus. Dip brazing is, however, widely used for the construction of extended plate heat exchangers. Alternate flat and corrugated alloy plates are assembled into blocks together with the aluminum–silicon brazing alloy and brazing is carried out in a large bath of molten salt which acts both as a heating medium and a flux. Alloys such as the aluminum–manganese type 3003 are preferred for this process, as they contain little or no copper or magnesium to inhibit the brazing action. Modified versions of this process such as the "Al-Fin" technique are used to produce transition pieces between aluminum alloy and stainless steel or aluminum fins on stainless steel tubes. Basically, the stainless steel is prepared with a special flux and then immersed in a bath of molten aluminum–silicon to form a thin layer of the intermetallic $FeAl_3$. Once this layer has been formed on the surface of the stainless steel, it can be wetted by the aluminum alloy, which is subsequently cast around it in the desired shape.

6.3.4.3. ***Transition Pieces.*** As both aluminum alloy and stainless steel have advantages and disadvantages for use in the construction of cryogenic equipment, there are numerous occasions in which both types of alloy are used in the same equipment. In such circumstances, the need arises for reliable leak-free joints between them and it has been found that the most satisfactory way of making such joints is to use special transition pieces, the aluminum end of which is easily welded to the aluminum component or pipe, while the stainless steel end is similarly welded to the stainless steel component. Thus, during assembly, welding is only between similar metals and should be a trouble-free process.

Such transition pieces are usually made by one of three main processes: friction welding, diffusion bonding, or coextrusion, although the

brazing processes described earlier are also used for certain applications. Friction welding techniques were pioneered by Chedekov in the U.S.S.R. and have been developed extensively at the British Welding Research Association. These joints are made by rotating the two components in contact until sufficient heat has been developed to enable a bond to be formed when they are forced together under pressure. Once all the variables involved have been ascertained, such joints may be made on a routine basis with a high standard of reliability. Failure in a tensile test is almost invariably by ductile fracture in the aluminum half, with the bond-line remaining sound, while in other tests, thermal cycling under pressure between ambient and liquid-nitrogen temperatures did not produce any detectable leakage. As, however, the joint can be destroyed by temperatures in excess of 400°C, a thermal shunt is necessary to prevent overheating during subsequent welding operations. (This precaution is necessary for most types of transition joint.) At the time of writing, friction-welded joints are not readily available in sizes exceeding about 6 in.

Diffusion-bonded joints are in more widespread use in the U.S. than in the U.K. and Europe, where friction-welded joints are most commonly used. The joint is made by clamping the two components together and heating the assembly in a furnace for long enough for sufficient interdiffusion to occur and produce the bond. Both these and the coextruded[24] joints are claimed by their manufacturers to be as reliable as the friction-welded joints described earlier and it would probably be necessary to evaluate each type to find the most suitable transition piece for a given application.

6.3.4.4. ***Flanged and Bolted Joints.*** As mentioned earlier, such joints are primarily used for coupling in components which might subsequently need to be removed for repair or routine servicing. When the two flanges are made from the same metal, the bolt should also be made from this material in order to prevent differential contraction from changing the tension during thermal cyling. If, however, the flanges are made from dissimilar metals such as aluminum alloy and stainless steel, greater care is necessary. Should, under such circumstances, an aluminum alloy bolt be tightened enough to obtain the required sealing load at room temperature, there would be a distinct risk of its failure on subsequent cooling to low temperature. Conversely, if a stainless steel bolt were used, it would be necessary to apply a bolt load at room temperature, which could overstress the aluminum flange, in order to prevent leakage at low temperatures. These troubles may be avoided by use of a compensated sleeve joint similar to that illustrated in Fig. 6.1. As the expansion coefficient of monel is lower than that of stainless steel, which is in turn lower than that for aluminum, the length of the monel sleeve can be calculated so that the tension

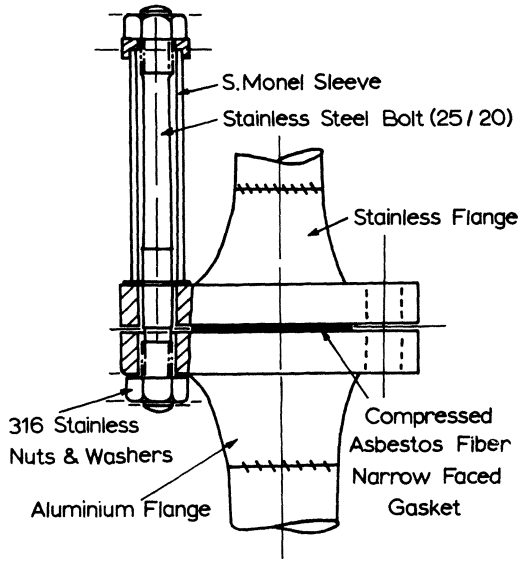

Fig. 6.1. Compensated sleeve joint between stainless steel and aluminum alloy (after Halford[25]).

in the stainless steel bolt is independent of the temperature. Similar joints have been made between aluminum alloy and 9% nickel steel flanges by using an Invar (Nilo 36) sleeve to compensate for the contraction in the 9% nickel steel bolt.

6.4. ECONOMIC CONSIDERATIONS

We have already examined some of the factors which have to be taken into account when selecting the most economical material for a particular application, namely the cost of the material on an allowable stress basis, the restrictions imposed by the availability of standard size plates or the rigidity of low-pressure containers, and the upper limit on plate thicknesses imposed by current welding techniques. There are so many other factors which enter into consideration that we cannot in this section do more than note a few of the more important ones. To the cost of the basic material must be added that of forming the components and joining them together, inspecting the joints and carrying out any necessary rework, and finally, testing the completed equipment and finishing it to the required standards of cleanliness or moisture content, etc. In general, the cost of the basic

material is the largest single factor, but there are wide variations in the relative magnitudes of these items. One estimate[7] for pressure vessels and other similar cryogenic equipment gives material costs in the range 30–75%, forming costs between 8 and 15%, welding and its associated expenses between 10 and 20%, inspection costs from 2–7% and other expenses, such as cleaning, testing, fittings, etc., amounting to between 5 and 25%. One factor which has a considerable influence on the cost of large tanks for the storage of cryogenic liquids is whether the vessels are to be entirely shop-fabricated before dispatch or whether the components formed in the works are to be erected and joined in the field. The larger storage vessels are almost inevitably field-erected and it is possible that some materials are more suitable for this method than others that may require, for example, more closely controlled conditions for satisfactory welding. Furthermore, although most field-erected vessels are built to comply with ASME or API design codes, these codes are not, in fact, strictly applicable to many of the types of tank used for bulk liquid storage. In such tanks most of the strength is required to support the hydrostatic head of the stored liquid, not to withstand a uniformly distributed pressure as in the examples considered earlier in this chapter. Another constraint encountered with this type of vessel is the need for internal stiffeners to help support the weight of the insulation between the inner and outer vessels, and, for a certain design, it is possible that such stiffeners would be required if aluminum alloy were used, but that they might not be needed for a similar vessel made of steel.

Yet another factor to be considered is the shape of the vessel and its optimum length/diameter ratio; this in turn depends on the capacity of the vessel and its operating pressure. For cryogenic service, there is a further complication in that high length/diameter (and hence surface area/volume) ratios lead to higher heat leaks. Therefore, the optimum L/D ratio will have to be a compromise between that necessary to minimize the initial cost of the storage vessel and that which will give the lowest liquid loss rate due to evaporation. This is, of course, but one example of yet another fundamentally important compromise to be reached when costing equipment: the question of initial costs versus running costs.

One further general point to note on materials costs is that the figures given in the earlier examples were for comparative purposes only and that the actual costs depend on the form and quantity in which the materials are required. Forming costs are also subject to similar variations. As regards the cost of welding components together, it should be noted that, apart from the more obvious sources of expense such as welding rods, fluxes, shielding gas, power, labor, and normal overheads, it is usually also necessary to include the costs of performing a 100% X-ray inspection of the weld and of carrying out any reworking necessary to bring it up to the re-

quired standards. Reworking costs are in general higher for nonferrous metals than for steels because of the increased probability of encountering porous welds in nonferrous metals.

Most pressure containing equipment has to be proof-tested before its final acceptance by the insurance inspectors and the cost of performing these tests is usually borne by the manufacturer. Although this expense is not likely to vary from metal to metal, it is one further item to be considered in assessing the final cost of such equipment.

Detailed examples of costing exercises on pressure vessels, storage tanks, and other typical items of cryogenic plant have been prepared by Arthur D. Little, Inc. and United States Steel and are given in the latter's "Cryogenic Materials Manual."[7] Although other interested parties such as the major aluminum producers would probably contest some of the detailed points involved, most designers would agree with the conclusions that aluminum alloys appear most suitable for the construction of small-capacity and low-pressure equipment, while stainless and 9% nickel steels are superior for large capacities and high pressures. Where the actual crossover points occur for the numerous vessels, tanks, and other pieces of cryogenic equipment which lie between these extremes is; however, a much more contentious issue.

6.5. OTHER TECHNICAL CONSIDERATIONS

In this volume on the mechanical properties of materials at low temperatures, the main emphasis has been on the variation with temperature of the basic mechanical properties, strength and toughness, and also of associated factors such as impact strength, modulus, fatigue life, shear strength, etc. Although any extensive consideration of the physical properties of materials is outside the scope of this text, these properties can have an important influence on the selection of materials and a brief mention of some of their most relevant aspects is thus considered appropriate.

6.5.1. Density

A large number of items of cryogenic equipment are manufactured for inclusion in rockets, satellites, and other aerospace applications. As weight minimization is of critical importance for this type of equipment, much effort has gone into the development of materials having high strength/weight ratios, and some aspects of this problem have already been discussed in chapters 1, 2, and 4. Similar, but less critical, considerations also apply to the construction of less sophisticated equipment such as road-haulage trailers for the transportation of liquefied and/or compressed gases. Although

the low-density aluminum alloys are strong contenders for all these applications, final selection is usually based on strength/weight ratios, and this enables the stronger but more dense ferrous alloys such as stainless steel to be competitive, especially if they can be cold-rolled or stretch-formed for additional strength.

6.5.2. Specific Heat

The amount of heat which has to be extracted to cool down a material can have important economic consequences, particularly if the equipment concerned has to undergo a large number of heating and cooling cycles. The major contribution to the specific heat, and hence heat capacity, of most materials arises from the crystal lattice, although there are also small contributions from the conduction electrons in metals, from phase and order–disorder transformations, and from other minor sources. The variation with temperature of the specific heat of crystalline materials is well-described by the Debye theory, in which the specific heat at constant volume C_v is given by

$$C_v = aD(\theta_D/T) \tag{6.5}$$

where a is a constant and θ_D is the Debye characteristic temperature of the solid, which, to a first approximation, may be considered independent of temperature. Similarly, for temperatures less than ambient, C_v is virtually equal to the specific heat measured at constant pressure, C_p. The specific heats of some representative materials are shown as a function of temperature in Fig. 6.2, and it may be seen that C_p for metals and other crystalline solids is relatively constant at high temperatures but that it drops off rapidly as the temperature falls. The temperature at which this steep drop occurs is approximately equal to the Debye temperature θ_D, and metals with low values of θ_D still have high heat capacities at relatively low temperatures. This may be seen by comparing the values of, say, lead, aluminum, copper, and iron at 77 or 20°K. At 20°K, the specific heat of lead is about an order of magnitude higher than that of copper, and hence, small lead spheres are used in regenerators for very-low-temperature cooling cycles. It can also have important consequences where, for example, soft solder with a high lead content is used to make joints in a copper cryostat. Furthermore, as the amount of lead used is normally determined by the volume of the fillet concerned, it will be appreciated that the position is even more serious for a high-density material like lead than that indicated in Fig. 6.2, where the specific heat is shown in joules per gram per degree. On the other hand, a similar consideration shows that, although aluminum has a higher specific heat per unit mass than, say, iron (and hence steel), they have similar specific heats when considered on a volumetric basis.

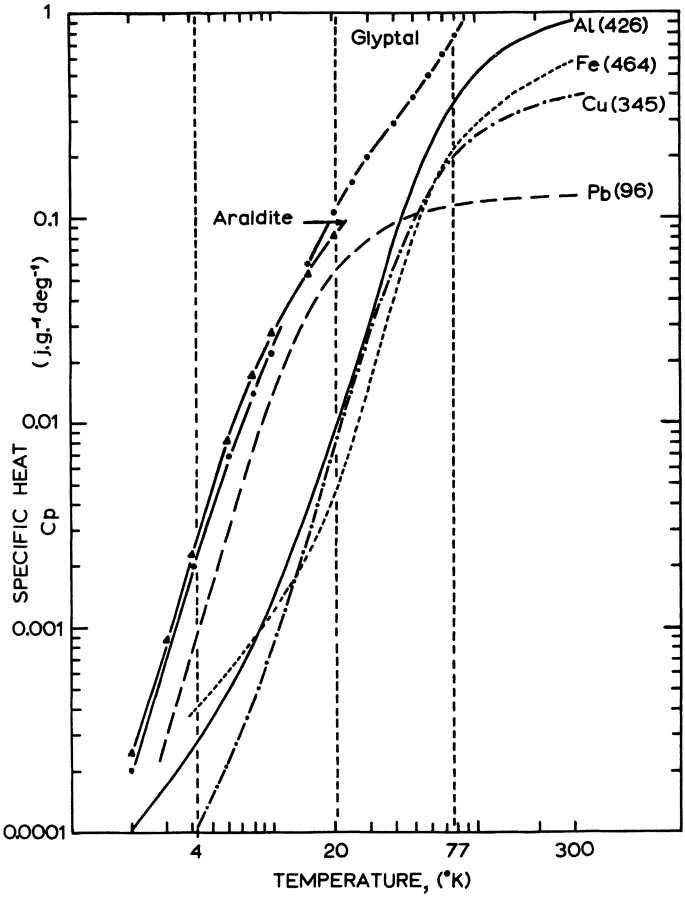

Fig. 6.2. Temperature dependence of the specific heat of some common materials. (Debye temperatures are shown in parentheses for the pure metals.)

It is also worth noting that the specific heats of most metals are relatively unaffected by their physical condition, although cold-work has been shown to cause a slight decrease in heat capacity. Therefore, for most practical purposes, it is safe to use published values for specific heat and enthalpies (the enthalpy $H = \int C_p \, dT$).

Finally, it should be noted that the Debye theory is not applicable to noncrystalline materials such as resins, polymers, and elastomers. As may be seen from the behavior of Araldite and Glyptal in Fig. 6.2, their specific heats generally rise continuously to the melting point. In addition, most polymers and elastomers go through "glass" transitions which are accompanied by specific-heat anomalies which can be very sharp. Further-

more, it can also be seen from Fig. 6.2 that the specific heats of common resins and varnishes can be considerably larger than those of metals at low temperatures, and hence their excessive use should be avoided. It should also be noted that their specific heats are more likely to vary from the published values than are those of metals because of variations in their processing history. Data on the specific heats of many pure and technical substances are given in NBS Monograph 21,[9] a monograph by Gopal,[8] in the same series as this volume, and also many textbooks on low-temperature physics.[6]

6.5.3. Thermal Expansion

It can be shown that the linear expansion coefficient α of a crystalline solid is related to its specific heat C_v by the Grüneisen expression,

$$\alpha = \tfrac{1}{3}\gamma \mathrm{X}(C_v/V) \tag{6.6}$$

where X is the isothermal compressibility, C_v/V the specific heat per unit volume, and γ is the Grüneisen coefficient, which is, to a first approximation, constant. As the isothermal compressibility is only slightly temperature-dependent, it follows that the expansion coefficient α is proportional to the specific heat C_v, and hence it too is almost constant at high temperatures, but drops off rapidly at temperatures below θ_D to a negligibly small value below $\sim\theta_D/5$. As most metals have a θ_D of between 200 and 400°K, they have all virtually finished contracting at or just below liquid-nitrogen temperature. Hence, if an item of equipment remains sound on cooling from 300 to 77°K, it is unlikely to be damaged by contraction on further cooling to lower temperatures. The proportionality between expansion coefficient and specific heat may also be used to provide approximate low-temperature values for one where only values for the other are available. The relationship

$$\alpha(T)/\alpha(293) \approx C_v(T)/C_v(293) \tag{6.7}$$

should, however, be used with care in case either specific heat or expansion coefficient show anomalous behavior at low temperatures.

In many references,[10] data are presented in terms of the total linear contraction between a temperature T and some reference temperature (usually 293 or 300°K) relative to the length at this temperature, i.e.,

$$(L_{293} - L_T)/L_{293} \tag{6.8}$$

This quantity is shown in Fig. 6.3 for a number of materials commonly used at low temperatures. We have already remarked upon the low values shown by Invar (Nilo 36) and its consequent use for the construction of long runs of cryogenic transfer line in order to reduce the number of ex-

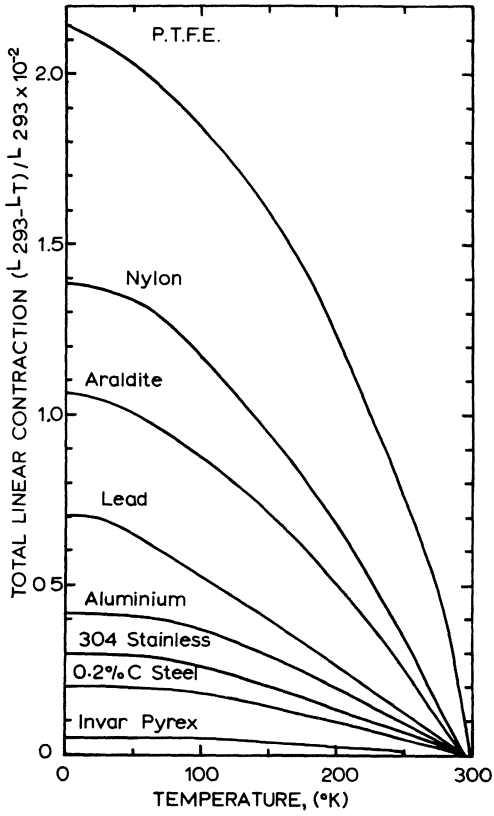

Fig. 6.3. Total linear thermal contraction as a function of temperature for some materials used in cryostat construction.

pansion joints required. Similarly, the high contractions shown by polymers and resins were mentioned in chapter 4, together with the use of glass fiber and other fillers to reduce these contractions to values which are compatible with those of metals.

Finally, it should be noted that many failures are due to differential contraction between two components and that these can usually be traced to one of two basic types of design fault, as follows.

a. *One Material, Different Temperatures.* This is illustrated in Fig. 6.4(a), where coaxial vessels are joined at either end and the space between them is thermally insulated. If the inner vessel is cooled, it contracts relative to the warmer outer vessel and large, often fatal, stresses are imposed on the joints. Such difficulties can be overcome by the inclusion of expansion members or by suitable redesign.

b. *Different Materials Cooled to the Same Temperature.* This type of

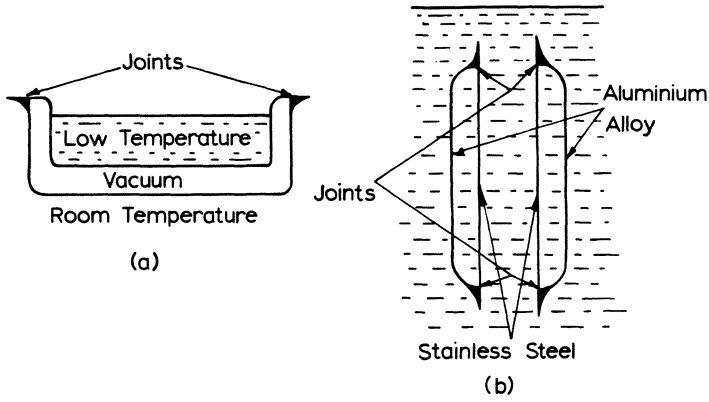

Fig. 6.4. Schematic illustrations of two types of design fault which can cause failure by differential contraction: (a) same material with a temperature differential, (b) dissimilar materials at the same temperature.

design fault is illustrated schematically in Fig. 6.4(b), where coaxial tubes made from dissimilar metals are again joined at both ends. If the whole assembly is cooled, one metal contracts more than the other to leave one tube in tension and the other in compression. If, for example, one tube were made from aluminum alloy and the other from stainless steel, a differential contraction of $\sim$0.1% would be set up by cooling from 300 to 77°K. Assuming Young's modulus of aluminum to be $\sim$10 million psi, the tensile stress developed in the aluminum tube would be 10,000 psi. This stress exceeds the yield stress of pure aluminum and some of its alloys, and repeated temperature cycling could lead to buckling if joint failure did not occur first.

6.5.4. Electrical Conductivity

The electrical resistance of a metal is due to the scattering of electron waves by two basic mechanisms: thermal vibrations of the lattice, and static defects such as impurity atoms. For most purposes, these two mechanisms may be considered separately and their contributions to the total resistivity added by Matthiessen's rule,

$$\rho = \rho_0 + \rho_i(T) \tag{6.9}$$

where ρ_0 is the temperature-independent "residual" resistivity and $\rho_i(T)$ the "ideal" resistivity, which is a function of the temperature and which drops off rapidly at low temperatures for many metals to less than 10^{-8} ohm-cm at or below 20°K. At these temperatures, the measured resistivity is then equal to the residual resistivity and is determined by the purity of

the metal concerned. Measurement of ρ_0, or, more often, of the resistance ratio $\rho(293°K)/\rho(4°K)$, gives a convenient and accurate determination of the purity of a metal and, as we shall see, this in turn allows its thermal conductivity to be deduced.

6.5.5. Thermal Conductivity

There are two basic mechanisms of heat conduction in metals: by the conduction electrons and by quantized lattice vibrations (called phonons). In pure metals, the electronic conductivity is dominant and the phonon conductivity may be neglected. The conduction electrons are again scattered by both lattice vibrations and static defects, and the thermal analog of Matthiessen's rule may be written as

$$1/K_e = w = w_i + w_r \tag{6.10}$$

where w_i, the "ideal" thermal resistance due to the scattering of electrons by phonons, is proportional to T^2, and w_r, the resistance due to impurity scattering, is proportional to $1/T$, i.e.,

$$w = \alpha T^2 + (\beta/T) \tag{6.11}$$

At high temperatures, phonon scattering is strong, the thermal resistance large, and the conductivity small. As the temperature drops, the scattering is reduced and the conductivity rises, as shown by the pure metals in Fig. 6.5. Eventually, scattering by the static defects limits the rise in conductivity with decrease in temperature and the thermal conductivity goes through a maximum before falling at very low temperatures. The purer the metal, the higher the conductivity maximum and the lower the temperature at which it occurs. This has important practical consequences in the case of copper, as the conductivity of commercially available coppers at 20°K ranges from about 25 W cm^{-1} deg^{-1} for very pure annealed metal, through ~6 W cm^{-1} deg^{-1} for free cutting tellurium copper, to only 0.4 W cm^{-1} deg^{-1} for phosphorous-deoxidized copper, the variety used for most copper tubing and some plate and sheet. It is, therefore, important to know which grade of material is being used if an accurate value of its low-temperature thermal conductivity is required. Direct measurement is, of course, the most accurate, if rather inconvenient, solution to this problem, but White[6] has shown that it is possible to estimate the thermal conductivities of many metals from measurements of their electrical resistivities.

The basis for this technique lies in a comparison of equation (6.9) for the electrical resistivity and (6.11) for the thermal resistivity. If the same scattering mechanism is responsible for both the electrical resistivity

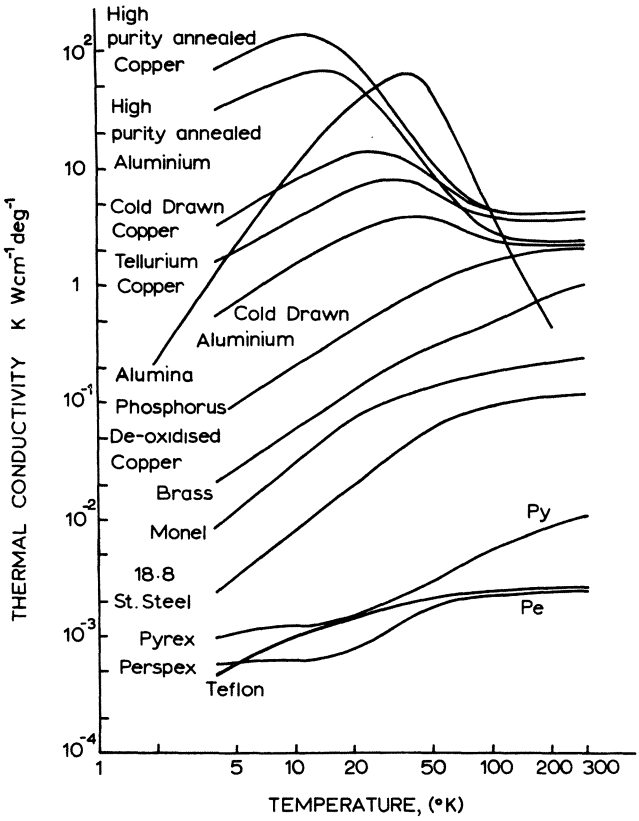

Fig. 6.5. Temperature dependence of the thermal conductivity of a number of materials used in cryogenic equipment.

ρ and the thermal resistivity w, then the Wiedemann–Franz law says that $\rho/wT = L$, the Lorenz ratio, which has the value 2.45×10^{-8} W ohm deg^{-2}. Such a situation often exists at very low temperatures (e.g., 4.2°K) where impurity scattering is dominant, and hence

$$K_{4.2} = L(4.2/\rho_{4.2}) \tag{6.12}$$

This relationship is, for most practical purposes, accurate enough for the thermal conductivities of a range of available metals to be ranked by simple measurement of their resistivities at 4.2°K. Selection on the basis of their spectrographic purities would be a far less reliable guide, as some impurities are more effective than others, their scattering efficiencies being dependent on the electronic band structures of host and impurity atoms. Furthermore, the metallurgical structure of the alloy influences its conductivity, as impurities in solid solution in the lattice have a much greater effect than

those which are segregated at grain boundaries. Lastly, it is difficult to estimate the degree of cold-work which has been received by a metal and, as can be seen from Fig. 6.5, this can have a strong influence on its thermal conductivity at low temperatures.

The above relationship between the electrical and thermal conductivities of metals does not, however, hold for complex alloys, such as stainless steels, which contain such high concentrations of impurities that the thermal conduction due to electrons is reduced to the same order of magnitude as that due to lattice vibrations. The measured thermal conductivity is then due to a combination of both mechanisms and it is not proportional to the electrical conductivity. This is particularly unfortunate, as alloys like monel, german silver, and stainless steel are frequently used for reducing heat leaks into cryogenic equipment and it is thus usually necessary to rely upon tabulated data for the thermal conductivity values necessary for design purposes.

Although certain nonmetallic crystals such as diamond and alumina can have extremely high thermal conductivities at low temperatures, the technologically significant nonmetals, such as glass, polymers, elastomers, resins, and varnishes, all have low thermal conductivities, as typified by the values shown for Pyrex, perspex, and PTFE in Fig. 6.5. This is because these materials have little or no long-range order and their thermal conductivity is determined by scattering from the "boundaries" of the small regions of local order. It should be noted that the conductivities shown in Fig. 6.5 are for guidance only, since variations in density, percentage crystallinity, and the degree of molecular orientation can alter their thermal conductivities by about an order of magnitude.

Even lower thermal conductivities are obtained from the resin-bonded glass-fiber composites discussed in chapter 4. Not only do their constituents have intrinsically low conductivities, but the large number of fiber–matrix interfaces further reduces the total conductivity. Boundary and contact resistances are, in general, very important when considering the thermal conductivities of materials at low temperatures. Very low effective conductivities can be obtained from stacks of thin disks of materials such as stainless steel because of the large contact resistances between successive layers. Furthermore, this configuration has the added advantage of being able to support considerable compressive loads.

Finally, there are numerous applications in which a low thermal conductivity is required in combination with a high tensile or compressive strength. This is usually a relatively easy combination to achieve, as most metallurgical processes—such as alloying, precipitation-hardening, cold-working, and reduction in grain size—which are used to increase the strength automatically lower the thermal conductivity. Similarly, treatments which strengthen glasses and plastics usually also decrease their

Table XV. Strength/Thermal Conductivity Ratios for Various Solids[a]

Material	σ_y, $\times 10^3$ psi	K, mW cm^{-1} deg^{-1}	σ_y/K	σ_y/K_{rel}
Stainless steel, type 304 annealed	35	109	0.32	1
Stainless steel type 304, cold-drawn to 210,000 psi	150	104	1.44	4.5
Titanium alloy, type Ti-5Al-2.5Sn	130	45	2.89	9.0
Polytetrafluoroethylene (PTFE, Teflon)	2	3	0.66	1.9
Nylon	10	2.8	3.6	11.2
Epoxy-glass-fiber laminate	75	3.5	21.4	67

[a] σ_y is the yield stress at 300°K, K is the average thermal conductivity between 20 and 300°K.

thermal conductivities. It is, however, the glass-fiber-reinforced plastics which are undoubtedly outstanding on a strength/thermal conductivity basis, as may be seen from Table. XV. Hence, the ratio σ_y/K (the yield stress at 300°K divided by the average thermal conductivity in the temperature range 300–20°K) is shown both in absolute terms and relative to that of annealed stainless steel.

In contrast, the combination of high mechanical strength and good thermal and/or electrical conductivity is much more difficult to achieve. Although some increase in the strength of copper has been achieved by light cold-rolling or certain precipitation- and dispersion-hardening treatments, a better compromise is probably that currently used for the windings in large superconducting magnets. A multiple composite of superconductor–copper–stainless steel is formed in which the superconductor carries the current for most of the time, the copper conducts both current and heat during the rare occasions when part of the magnet windings go normal, and the hoop stresses are contained by the strength of the stainless steel.

6.5.6. Other Physical Properties

There are a number of other physical properties which sometimes influence the selection of materials for the construction of cryogenic equipment. We have already dealt at some length with the undesirability of ferromagnetic materials in bubble chambers and other apparatus which have to operate in a magnetic field, particularly with reference to the stability of 18/8 type stainless steels with respect to martensitic transformations. A further problem encountered with this type of equipment is the generation of eddy currents in electrically conducting components subjected to a changing magnetic field. For example, epoxy-fiber-glass bellows are being

developed for use as a compliant vacuum seal on the expansion piston for the large liquid-hydrogen bubble chamber under development at the Rutherford Laboratory. Other specific electrical, magnetic, or nuclear properties are also occasionally called for in particular applications.

Another, more frequent requisite, is for high reflectivity and/or low emissivity to improve the insulation of cryogenic equipment by a reduction in radiative heat transfer. Stainless steel is particularly useful in such circumstances, as its high polish does not tarnish as rapidly as that of copper and, to a lesser extent, aluminum. For very critical applications, gold plating is, however, the most satisfactory, if expensive, solution to this problem.

REFERENCES

Textbooks and Reference Works

1. *American Society for Metals Handbook*, 8th ed., Metals Park, Cleveland, Ohio.
2. "ASME Code on Unfired Pressure Vessels (1961)," Section VIII, Am. Soc. Mech. Eng.
3. "Steels for Use in Chemical, Petroleum and Allied Industries. Low Temperatue Supplementary Requirements to British Standards," 1500, British Standards Institution (1958).
4. K. D. Timmerhaus (Ed.), *Advances in Cryogenic Engineering*, Plenum Press, New York, latest annual volume 16 (1971).
5. A. D. Merkblatt, W.10, German Standards Institution.
6. G. K. White, *Experimental Techniques in Low Temperature Physics*, 2nd ed., Clarendon Press, Oxford (1968).
7. "Low Temperature and Cryogenic Steels," United States Steel Materials Manual, 3rd ed., U.S. Steel, New York (1968).
8. E. S. Raja Gopal, *Specific Heats at Low Temperatures*. Plenum Press, New York (1966).
9. R. J. Corruccini and J. J. Gniewek, "Specific Heats and Enthalpies of Technical Solids at Low Temperatures," NBS. Monograph 21, (1960).
10. R. J. Corruccini and J. J. Gniewek, "Thermal Expansion of Technical Solids at Low Temperatures," NBS Monograph 29 (1961).

Other References

11. W. Keeping, British Oxygen Co., Morden, private communication.
12. J. L. Christian, J. E. Chafey, J. F. Watson, and W. E. Witzell. *Metal Progress* **1963** (April), 100.
13. M. Güter "Ignition of Materials in High Pressure Oxygen," S and T Memo 13/50 (1950), available from H.M.S.O. (London).
14. G. R. Allen, Royal Aircraft Establishment Farnborough Tech. Report, to be published.
15. R. L. Hauser and W. F. Rumpel, in Ref. 4, Vol. 8 (1963), p. 242.
16. N. A. Tiner in Ref. 4, Vol. 12 (1967), p. 771.
17. E. J. Zeilberger, "Compatibility of Materials," Chapter 6 in *Materials for Missiles and Spacecraft*, McGraw-Hill (1963), p. 122.

18. J. J. Lombardo, C. E. Dixon, and J. A. Begley, "Effects of Radiation on Structural Metals," ASTM STP 424, Am. Soc. Testing Mat. (1967), p. 625.
19. "Operation Cryogenics Demonstrates Toughness of 9% Ni Steel," *INCO Nickel Topics* 14 2 (January 1961).
20. P. Boughton and J. A. Lucey, *Brit. Weld. J.* **1965** (April), p. 159.
21. L. M. Laydon, *Metal Progr.* **1969** (July), p. 60.
22. D. E. Jordan and D. J. Heath, *Brit. Weld. J.* **1964** (January), p. 2.
23. A. J. Croft, "Materials and Methods for the Construction of Low Temperature Apparatus, "in F. E. Hoar, L. C. Jackson, and N. Kurti (Eds.), *Experimental Cryophysics*, Butterworths (1961).
24. Co-Bond Joints Data from Spembly Technical Products, Sittingbourne, Kent, U. K.
25. P. Halford, private communication.

Appendix I

A Brief Summary of the American Aluminum Association Alloy and Temper Designation System

1000 Series are unalloyed and non-heat-treatable. Commercially pure aluminum is typical member, having low strength and good ductility. Can be cold-worked for higher strength. Easily welded.

2000 Series. Copper is major alloying addition, heat-treatable to reasonably high strengths. Weldability varies from alloy to alloy.

3000 Series. Manganese is major alloying addition, solution-hardens to raise strength above that of 1000 series without loss of good forming and welding characteristics. Non-heat-treatable.

4000 Series. Silicon is major alloying addition, most alloys being used in the as-cast, not wrought, state.

5000 Series. Magnesium is major alloying addition and solution-hardens more efficiently than the manganese of the 3000 series. Readily weldable with correct fillers. Non-heat-treatable.

6000 Series. Magnesium and silicon are major alloying additions; can be heat-treated to give moderately high strengths while still remaining easily worked and readily weldable.

7000 Series. Zinc is major alloying addition and alloys can be heat treated to give the highest strengths of any aluminum alloy, but ductilities are often low and welding difficult. The copper-free members of this series are, however, tougher and more weldable.

TEMPER DESIGNATIONS

The four basic tempers are represented by the letters O (annealed), F (as-fabricated), H (strain-hardened), and T (heat-treated). Additional information is given by the digits which follow the basic letter. Some of the most common designations are as follows:

O: Annealed and recrystallized.

H1: Strain-hardened only; the second digit indicating the degree of strain hardening on a scale which runs from 1 to 8, e.g., H18 ≡ full, H14 ≡ half, H12 ≡ quarter hard, etc.

H2: Strain-hardened and partially annealed, the second digit indicating the degree of residual hardening.

H3: Strain-hardened and then stabilized. Used for magnesium-containing alloys only.
W: Unstable condition following solution heat-treatment.
T3: Solution-treated and cold-worked, naturally aged to substantially stable condition.
T4: Solution-treated and then naturally aged to substantially stable condition without prior cold-work.
T5: Artificially aged only.
T6: Solution-treated and then artificially aged; the second digit indicates whether aged by user (T62) or producer (T63).
T8: Solution-treated, cold-worked, and then artificially aged.

For further details, see Ref. 7 or 56 of Chapter 2.

Appendix II

Conversion Table for the Units Most Commonly Used to Measure Stress or Pressure*

	10^3 psi (1 ksi)	1 kg/mm^2	1 ton/in.^{2}	1 MN/m^2	1 dyne/cm^2	1 bar	1 atm
10^3 psi (1 ksi)	1	0.7031	0.4464	6.895	68.95×10^{6}	68.95	68.03
1 kg/mm^2	1.422	1	0.6349	9.807	98.07×10^{6}	98.07	96.81
1 ton/in.^{2}	2.240	1.575	1	15.44	154.4×10^{6}	154.4	152.4
1 MN/m^2	0.1450	0.1020	64.75×10^{-3}	1	10×10^{6}	10	9.869
1 dyne/cm^2	14.50×10^{-9}	10.20×10^{-9}	6.475×10^{-9}	0.1×10^{-6}	1	10^{-6}	0.9869×10^{-6}
1 bar	14.50×10^{-3}	10.20×10^{-3}	6.475×10^{-3}	0.1	10^{6}	1	0.9869
1 atm	14.70×10^{-3}	10.33×10^{-3}	6.562×10^{-3}	0.013	1.013×10^{6}	1.013	1

* 1 psi ≡ 1 lb/in.^{2} ≡ one pound force per square inch; 1 kg/mm^2 ≡ one kilogram force per square millimeter; 1 ton/in.^{2} ≡ one ton force per square inch; 1 MN/m^2 ≡ one meganewton per square meter; 1 dyne/cm^2 ≡ one dyne per square centimeter; 1 atm ≡ one standard atmosphere (≡ 760 mm Hg at 0°C, ≡ 29.92 in. Hg at 0°C).

Appendix III

Some Important Cryogenic Temperatures

Cryogen	Fixed point	Temperature		
		°K	°C	°F
Water	M.P.	273.15	0	+32
Ammonia	B.P.	239.8	−33.3	−27.9
Freon 22 ($CHClF_2$)	B.P.	232.5	−40.6	−41.0
Carbon (dioxide)	Sublimation	194.6	−78.5	−109.3
Xenon	B.P.	164.0	−109.1	−164.4
Krypton	B.P.	121.3	−151.8	−241.2
Methane	B.P.	111.7	−161.4	−258.5
Oxygen	B.P.	90.1	−183.0	−297.4
Argon	B.P.	87.4	−185.7	−302.3
Fluorine	B.P.	86.0	−187.0	−304.6
Nitrogen	B.P.	77.3	−195.8	−320.4
Neon	B.P.	27.2	−245.9	−410.6
Tritium	B.P.	25.1	−248.0	−414.4
Deuterium	B.P.	23.6	−249.5	−417.1
Hydrogen	B.P.	20.4	−252.7	−422.9
Helium-4	B.P.	4.2	−268.9	−452.1
Helium-3	B.P.	3.2	−269.9	−453.8

Author Index

Subject Index